THE UNIVERSITY *of* EDINBURGH

CHARACTERISATION AND FUNCTIONAL ANALYSIS OF A NOVEL MSP DOMAIN – CONTAINING PROTEIN, MOSPD1

MADINA KARA

THESIS PRESENTED FOR THE DEGREE OF DOCTOR OF PHILOSOPHY

UNIVERSITY OF EDINBURGH

2011

To my family, who took every step of this journey with me.

I declare that the work presented in this thesis is my own, unless otherwise stated.

Madina Kara

Acknowledgements

I would like to thank my supervisors, Lesley Forrester, Martin Denvir and Carl Tucker for all their support and guidance throughout my PhD as well as Matthew Sharpe for contributing to my PhD committee. Special thanks to the late Katrin Buerger who was involved in the project before me and who taught me everything I needed to know about the *Mospd* gene family. Many thanks go to my colleagues, both past and present, in the John Hughes Bennett Laboratory for providing a wonderful atmosphere to work in and making my time in the lab enjoyable. Thanks also to Katherine Hamilton-Smith for her advice with the zebrafish experiments and John Pound for his advice and assistance with antibody production. My heartfelt appreciation goes to the British Heart Foundation for providing my PhD studentship, which made this work possible. I would also like to thank my family, especially my father, for all the love, support and patience they have provided.

Abstract

MOSPD1 belongs to a class of proteins that have a major sperm protein (MSP) domain at the N terminus and two transmembrane domains at the C terminus and are thought to act as membrane adaptor proteins. Previous work in the laboratory indicated that the closely related, mammalian-specific, *Mospd 3* plays a role in the development and function of the heart as homozygous *Mospd 3* gene trap neonates displayed a right ventricle defect characterised by a thinning of the right ventricle wall. The function of *Mospd 1* is not known. Whilst *Mospd 3* is mammalian specific *Mospd 1* is conserved in all vertebrates including *Danio rerio* (zebrafish).

The aims of this thesis were to investigate the possibility of genetic redundancy between *Mospd 1* and *Mospd 3* by identifying the sub-cellular localisation of MOSPD1 and MOSPD3 in both cells and tissues and to investigate the function of MOSPD1. Mouse monoclonal antibodies specific for MOSPD1 and MOSPD3 were generated and tested to ensure they did not cross react. MOSPD1 was found to be localised to the nucleus whilst MOSPD3 was located in the nucleus and cytoplasm. The sub-cellular localisation of these proteins changes during the cell cycle as they were localised to the cytoplasm during cell division, possible due to the breakdown of the nuclear membrane during cell division.

To investigate the function of *Mospd 1* during early development *Mospd 1* gene expression was knocked down using morpholino anti-sense knockdown technology. A morpholino was generated against the splice-site between exons 2 and 3 of the zebrafish *Mospd 1* gene and injected into early embryos. At doses that significantly reduced the level of *Mospd 1*, to below 50 %, the embryos developed normally and did not exhibit any gross morphological phenotypes when compared to both non-injected and 5 mispair control morpholino-injected embryos. A morpholino targeted to the start site of the *Mospd 1* gene confirmed the lack of a gross morphological phenotype. In conjunction with the zebrafish functional tests the tools were generated to assess the role of *Mospd 1* in a mammalian system. A conditional allele of *Mospd*

1 was generated in mouse embryonic stem (ES) cells which could be used to generate a conditional *Mospd 1* mouse. The electroporation of a *Cre recombinase* plasmid into the conditional *Mospd 1* ES cell line resulted in the generation of *Mospd 1* null ES clones which could be used for functional studies both *in vitro* and *in vivo*. The *Mospd 1* null ES cells were able to self-renew, expressed ES cell specific markers and were able to differentiate into cardiomyocytes. However, *Mospd 1* null cells showed a reduced ability to differentiate into osteoblasts compared to wild type cells and showed changes in the expression of genes involved in Epithelial to mesenchymal transition (EMT) indicating *Mospd 1* may be involved in this process.

CONTENTS

LIST OF FIGURES

LIST OF TABLES

ABBREVIATIONS

α	anti
ALS	Amyotrophic Lateral Sclerosis
ARVC	Arrhythmic Right Ventricular Cardiomyopathy
BAC	bacterial artificial chromosome
bp	base pair
bet	*pairing protein Beta*
BSA	Bovine serum albumin
C	carboxy
C	Celcius
Cdh1	*cadherin 1* (*E-cadherin*)
Cdh11	*cadherin 11* (*osteo-cadherin*)
CDTA	1,2-cyclohexylenedinitrilotetraacetic acid
C elegans	*Caenorhabditis elegans*
cmcl2	*cardiac myosin light chain 2*
cm	centimetre
cm^2	centremetre squared
CNS	central nervous system
CO^2	carbon dioxide
CRAL-TRIO	Cellular retinaldehyde binding/ triple function
Cre	*Cre recombinase*
DAB	3, 3'-Diaminobenzidine
DAPI	4', 6-diamidino-2-phenylindole
dCTP	deoxycytidine triphosphate
^{o}	degree
DMSO	dimethyl sulfoxide
DNA	deoxyribonucleic acid
dNTP	deoxyribonucleotide triphosphate
DP	desmoplakin
dpf	days post fertilisation
Drosophila	*Drosophila melanogaster*

DSC	desmocollin
DSG	desmoglein
E	embryonic day
E	eosin
EB	embryoid body
ECL	enhanced chemiluminescence
E. coli	*Escherischia coli*
EDTA	ethylenediaminetetraacetic acid
Ef1α	*Elongation factor 1 alpha*
EMT	epithelial to mesenchymal transition
ENU	ethylnitrosourea
ER	endoplasmic reticulum
ES	Embryonic stem
et al	*et alia*
exo	*exonuclease*
5’	Five prime
5MP	five mispair
F	Phenylalanine
FACS	Fluorescence Activated Cell Sorting
FITC	fluorescein isothiocyanate
fli1	*friend leukaemia integration 1*
FRT	flipase recognition site
FSC	fetal calf serum
g	g- force
G418	geneticin antibiotic
GAPDH	Glyceraldehyde 3-phosphate dehydrogenase
GFP	green fluorescent protein
GMEM	Glasgow Minimum Essential Medium
Golgi	Golgi apparatus
HACAT	human keratinocyte cells
H	haematoxylin
HIFI	High Fidelity

hpf	hours post fertilisation
HRP	Horseradish peroxidase
HUVEC	human umbilical vein endothelial cell
ICC	immunocytochemistry
ICM	inner cell mass
IDP	inner dense plaque
IgG	Immunoglobulin G
IHC	immunohistochemistry
IMDM	Iscove's modified Dulbecco media
Jsap	*c-JUN NH_2-terminal kinase (JNK)/ stress-activated protein kinase-associated protein 1*
K	lysine
kb	kilobase
KCl	potassium chloride
kDa	kilo Daltons
KIF	keratin intermediate filament
kV	kilovolt
L	leucine
lac Z	*β-galactosidase*
LB	Luria-Bertani bacterial culture broth
LIF	Leukaemia inhibitory factor
LV	left ventricle
MBT	mid-blastula transition
MET	mesenchymal to epithelial transition
$MgCl_2$	magnesium chloride
$MgSO_4$	magnesium sulphate
MHC	myosin heavy chain
µF	microfarad
µg	microgram
µl	microlitre
µm	micrometre
µM	micromolar

ml	millilitre
MLC-2V	myosin light chain 2V
mm	millimetre
mM	millimolar
MO1	Start morpholino
MO2	Splice-site morpholino
Mospd	*Motile sperm domain-protein*
MSC	mesenchymal stem cell
MSP	Major Sperm Protein
N	amino
N	asparagine
NaCl	Sodium chloride
NaOH	Sodium hydroxide
NEAA	nonessential amninoacids
neo	neomycin
NES	nuclear export signal
ng	nanogram
NLS	nuclear localisation signal
nm	nanometre
NP-40	nonyl phenoxypolyethoxylethanol
ODP	outer dense plaque
P	proline
PAGE	polyacrylamide gel electrophoresis
PBS	phosphate buffered saline
PBST	phosphate buffered saline triton X-100
PCR	Polymerase chain reaction
%	percent
PFA	paraformaldehyde
PFAM	protein family database
PG	plakoglobin
π	*pi*
PI	propidium iodide

PKP	plakophilin
PM	plasma membrane
PMT	photomultiplier tube
poly A	polyadenylation
qPCR	quantitative Polymerase chain reaction
R	arginine
r	radius
R124	*Mospd 3* gene trap
RA	retinoic acid
RIPA	Radioimmunoprecipitation assay
RNA	ribonucleic acid
rpm	revolutions per minute
RT	reverse transcription
RV	right ventricle
SDS	sodium dodecyl sulphate
snRNP	small ribonucleoprotein particles
S.O.C.	Super Optimal broth with Catabolite repression
SSC	saline-sodium citrate
T	threonine
TBE	Tris Borate
TBST	Tris Buffer Saline Tween-20
TE	Tris-EDTA
TM	transmembrane
Tx-100	Triton X-100
3D	Three dimensional
3’	Three prime
U	units
UPR	Unfolded Protein Response
V	valine
V	volt
VAP	VAMP-associated proteins
v/v	volume/volume

WISH	whole mount *in situ* hybridisation
w/v	weight/ volume
YFP	yellow fluorescent protein
YSL	yolk synctial layer

CHAPTER 1:
INTRODUCTION

1.1. Why study *Mospd 1*?

Motile sperm domain-protein (Mospd) 1 is a member of the *Mospd* gene family. There is very little information about the localisation of MOSPD1 in the literature. It has recently been suggested that *Mospd 1* may play a role in Epithelial-Mesenchymal Transition (EMT) (Thaler *et al*., 2010). The only other clue to the function of *Mospd 1* is evidence that the closely related *Mospd 3* gene is involved in cardiac development (Pall *et al*., 2004). MOSPD1 has a Major Sperm Protein (MSP) domain and two transmembrane domains. The MSP domain is predicted on the secondary protein structure and conservation of important residues from the MSP protein found in nematodes.

1.1.1. MSP in Nematodes

Major Sperm Protein (MSP) (NCBI Accession AAA28115.1) is a 14.5 kDa cytoskeletal protein that gets its name from the fact that it is the most abundant protein in nematode sperm, making up 17 % of the total protein content (Klass and Hirsh, 1981). More than 60 % of all MSP domain proteins, identified to date, are found in nematodes (Tarr and Scott, 2005a). MSPs are involved in male reproduction as the expression of many of these proteins is up-regulated in the male germ line (Tarr and Scott, 2004). Nematode sperm use a crawling motion, rather than a flagellum based motion used by mammalian sperm. Instead of using an actin-based system for motility nematode sperm depend exclusively on the cytoskeletal protein, MSP, which acts in a cyclical and pH dependent manner (Italiano *et al*., 1999). MSP deficiency results in infertility in the organism (Nelson and Ward, 1981). In *Caenorhabditis elegans* (*C. elegans*) it has also been found to be involved in signalling pathways that promote oocyte meiotic maturation, ovulation and sheath cell contraction (Miller *et al*., 2001). MSP binds to the membranes of oocytes and sheath cells via the VAB-1 Ephrin receptor protein-tyrosine kinase resulting in the activation of the MAPK signalling pathway (Miller *et al*., 2003).

MSP is composed of a 7-stranded β-sandwich (Figure 1.1 A) made up of a 3-stranded sheet opposing a 4-stranded sheet (Bullock *et al*., 1996; Tarr and Scott, 2005b). Through the sheet structure of the IgG-like domain MSP can interact with other proteins as the IgG domain is involved in protein-protein interactions (Bork *et al*., 1994). MSP belongs to the Immunoglobulin (IgG) superfamily based on its IgG-like fold and is similar in structure to the amino terminal of PapD, a bacterial chaperonin. In solution MSP dimerizes (Haaf *et al*., 1996) and these dimers polymerize to form helical microfilaments. These microfilaments coil around each other to form filaments which then coil around each other to form larger macrofibers (Figure 1.1 B) (King *et al*., 1994).

1.1.2. Vesicle Associated Proteins (VAPS)

MSP domain-containing proteins are found in a wide range of organisms including yeast (Kagiwada *et al*., 1998), plants (Laurent *et al*., 2000), insects (Pennetta *et al*., 2002) and mammals (Nishimura *et al*., 1999). A family of MSP domain-containing proteins, called VAMP-associated proteins (VAPs), have been identified and their functions studied. VAPs have an N terminal MSP domain and a C terminal transmembrane domain making them similar to the MOSPD family. The first VAP that was identified was in the sea slug *Aplysia* and it was named VAP-33 due to it binding to VAMP (synaptobrevin), a synaptic vesicle protein, and its 33 kDa size (Skehel *et al*., 1995). VAP33 was localised to the central nervous system (CNS) and gills of *Aplysia* and was important for synaptic transmission. The VAP33 homolog in *Drosophila melanogaster* (*Drosophila*), DVAP-33, is expressed at neuromuscular junctions in larvae and is involved in mediating the interactions between the pre-synaptic membrane and microtubules (Pennetta *et al*., 2002).

A

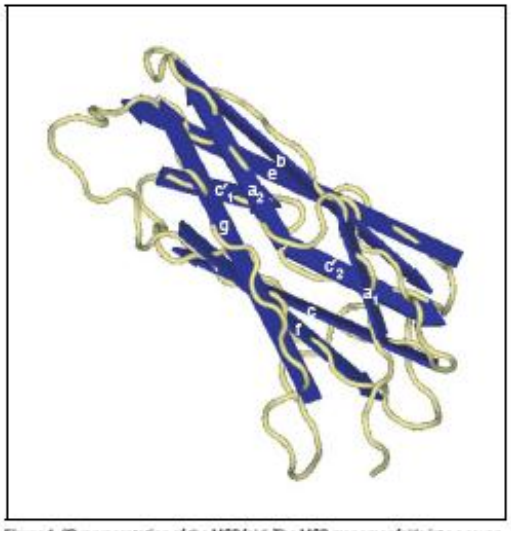

B

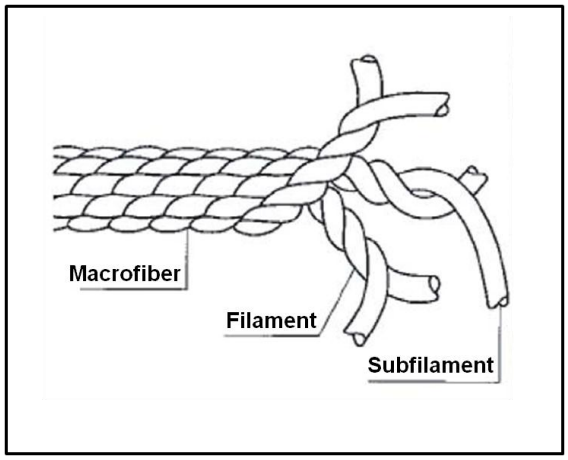

Figure 1.1: Structure of MSP. A: 3-dimensional (3D) representation of the MSP fold. The MSP monomer is comprised of seven β-strands, each designated by a letter, that fold to form a sandwich. B: The coiling of MSP. MSPs polymerize to form subfilaments. Two subfilaments coil around each other to form filaments which then further coil around each other to form macrofibers. (Images taken from Tarr and Scott, 2005b (A) and King *et al*., 1994) (B)).

VAPs are widely expressed in mammalian tissues (Nishimura *et al*., 1999); (Soussan *et al*., 1999); (Skehel *et al*., 2000) and mammalian homologs of VAP33 are called VAPA, VAPB and VAPC (Nishimura *et al*., 1999). The rat homolog of VAPB was termed ERG30 when it was first discovered as it was localised to the endoplasmic reticulum (ER) and Golgi apparatus (Golgi) (Soussan *et al*., 1999). Inhibition of ERG30 (rat VAPB) resulted in an inhibition of intra-Golgi transport and an accumulation of vesicles due to this inhibition. Mouse VAP is localised to the ER and microtubules (Skehel *et al*., 2000).

A mutation in VAPB has been identified that causes some forms of the neurodegenerative disease amyotrophic lateral sclerosis (ALS) (Nishimura *et al*., 2004). ALS is characterised by the loss of motor neurons from the brain stem, spinal cord and motor cortex. The P56S mutation in the MSP domain was identified in families with autosomal dominant ALS. The alteration of this conserved proline residue was due to a cytosine to thymine ($C_{166}T$) mutation in exon 2 of the VAPB gene. Other patients with this mutation suffer from spinal muscular atrophy (SMA), another neurodegenerative motor disease (Nishimura *et al*., 2004). The MSP domain of wild type VAPB forms a seven stranded IgG-like beta sandwich and the P56S mutation results in loss of the secondary structure of VAPB (Shi *et al*., 2010). This misfolding of the VAPB protein leads to the protein becoming insoluble and forming aggregates in the ER. This mutated VAPB interferes with the ER's unfolded protein response (UPR) which is important for preventing the accumulation of misfolded proteins in the ER (Kanekura *et al*., 2006). Studies using *drosophila* VAP have found that the N terminal of VAP (the MSP domain) is cleaved, secreted and binds to EPHRIN (EPH) receptors in the same way as MSP in nematodes. This indicates a conserved role for the MSP domain in EPH receptor binding and cell signalling. When the human P56S mutation is introduced into drosophila VAP it inhibits the secretion of the MSP domain resulting in aggregation of the protein (Tsuda *et al*., 2008). The fact that both MSP in nematodes and VAPs bind EPH receptors may provide a further clue to a possible role of the MSP domain in MOSPD proteins.

1.1.3. Major Sperm Protein (MSP) domain-containing proteins

The *Mospd* gene family actually belongs to a much larger MSP domain-containing family which is found in a wide range of organisms and evidence suggests the MSP domain plays a role in protein-protein interactions (Bork *et al*., 1994). The MSP domain consensus sequence was built from 171 sequences of MSP-domain containing family members from a wide range of species. The MSP domain consensus sequence has four invariant (P7, N29, K40 and P51) and eight highly conserved residues (L3, R34, F37, K38, V39, T42, 69R and 79N) that are important for MSP domain folding (Tarr and Scott, 2004).

Overall sequence similarity between the MSP domain in proteins and MSP from nematodes is only 35 % (Figure 1.2 A). However, the presence of an MSP domain is predicted based on secondary structure and conservation of important residues (Tarr and Scott, 2004). This secondary structure is the IgG-like fold important for protein-protein interactions. The MSP domain in mouse VAP shares 48 % sequence identity with the MSP domain consensus sequence and has all four invariant residues as well as six of the eight highly conserved residues (Figure 1.2 B).

843 proteins that contain at least one MSP domain are currently found in the Pfams database (Bateman *et al*., 2004) and these are divided into Types I-V based on the relative position of the MSP domain. Type II MSP domain proteins are between 150 and 350 amino acids in length and contain the MSP domain in the N terminus. They can be subdivided by the absence (IIa) or presence of one (IIb) or two (IIc) transmembrane domains in the C-terminus (Tarr and Scott, 2005b). *Mospd 1* falls into the Type IIc category. The MSP domain in MOSPD1 shares 33 % sequence homology with the MSP domain consensus sequence (Tarr and Scott, 2004). It has three of the four invariant residues and five of the eight highly conserved residues important for secondary structure of the MSP domain (Figure 1.2 C).

A: MSP (*C. elegans*) and MSP domain (MSPD)

```
MSP     GDIQTQPNAKIVFNAPYDDKHTYHIKVINSSARRIGYGTKTTNMKRLGVDPPCGVLDPKE
        G     P    VF  P D   T      N S  RI    KTTN KR  V PP G L P E
MSPD    GELKLDPPVTVVFPNPFDKQGTSTLTLKNPSDKRIAFKVKTTNNKRYRVRPPYGILEPGE

MSP     AVLLAVSCDAFAFGQEDTNNDRITVEWTNTPDGAAKQFRREW-FQGDGMVRRKNLPIEY
         V LA     F  G    N D   V  T  P GAA   R    FQ    V     P
MSPD    SVNLAIT-QRFK-GLPKKNKDKFAVQYTEAPSGAADKAREAFKFQAQAGVGETKIPVVF
```

B: MSP domain of VAPA and MSP domain (MSPD)

```
VAPA     LVLDPPSDLKFKGPFTDVVTTNLKLQNPSDRKVCFKVKTTAPRRYCVRPNSGIIDPGSIV
         L LDPP    F  PF    T  L L NPSD    FKVKTT   RY VRP  GI  PG  V
MSPD     LKLDPPVTVVFPNPFDKQGTSTLTLKNPSDKRIAFKVKTTNNKRYRVRPPYGILEPGESV

VAPA     TVSVMLQPFDYDPNEKSKHKFMVQ
               Q F   P  K K KF VQ
MSPD     NLAIT-QRFKGLP-KKNKDKFAVQ
```

C: MSP domain of MOSPD1 and MSP domain (MSPD)

```
MOSPD1             PVFFVFPTELIFYADDQSTHKQVLTLYNPYEFALKFKVLCTTPNKYVVV
                   P   VFP       D Q T    LTL NP      FKV  T    Y V
MSPD         GELKLDPPVTVVFPNPF----DKQGTS--TLTLKNPSDKRIAFKVKTTNNKRYRVR

MOSPD1     DAAGAVKPQCCVDIVIRHRDVRSCHYGVIDKFRLQVSEQSQRKALGRKEVIAT
             G   P   V   I  R          DKF  Q  E     A    E
MSPD       PPYGILEPGESVNLAITQR-FKGLPKKNKDKFAVQYTEAPSGAADKAREAFKFQAQA

MOSPD1
MSPD       GVGETKIPVVFE
```

Figure 1.2: Protein sequence alignment between the MSP domain consensus sequence and MSP (*C. elegans*), mouse VAPA and MOSPD1 MSP domains. Letters in red correspond to identical sequence, residues highlight in green are invariant and residues highlighted in yellow are highly conserved.

1.1.4. *Mospd* gene family

Mospd 1 belongs to the *Mospd* gene family which is characterised by encoding an N terminus Major Sperm Protein (MSP) domain and a transmembrane (TM) domain in the C terminus. There are four *Mospd* gene family members in the mouse including *Mospd 1* (NM_027409), *Mospd 2* (NM_029730), *Mospd 3* (NM_030037) and *Mospd 4* (NM_028086) (Figure 1.3). *Mospd 2* also encodes a Cellular retinaldehyde binding/ triple function (CRAL-TRIO) domain and a nuclear localisation signal (NLS). *Mospd 1* and *Mospd 3* are the most similar family members as they encode the MSP domain in the N terminal and two C terminus TM domains. Although MOSPD1 (NP_081685) and MOSPD3 (NP_084313) only share 38 % overall protein sequence identity the majority of the shared sequence is located in the MSP and TM domains (Figure 1.4). The similarity of *Mospd 1* and *Mospd 3* could indicate the two may be genetically redundant.

Mospd 1 is located on the X chromosome in mice and humans. MOSPD proteins are highly conserved as there is a high sequence homology between mouse *Mospd 1* (NM_027409.4) and human *Mospd 1* (NM_019556.1) of 87 %. *Mospd 3* is located on chromosome 5 and is thought to be mammalian specific. Mouse *Mospd 3* (NM_030037.1) and human *Mospd 3* (NM_001040097) have a high sequence similarity of 87 %. This conservation in sequence between species indicates these genes could be functionally important.

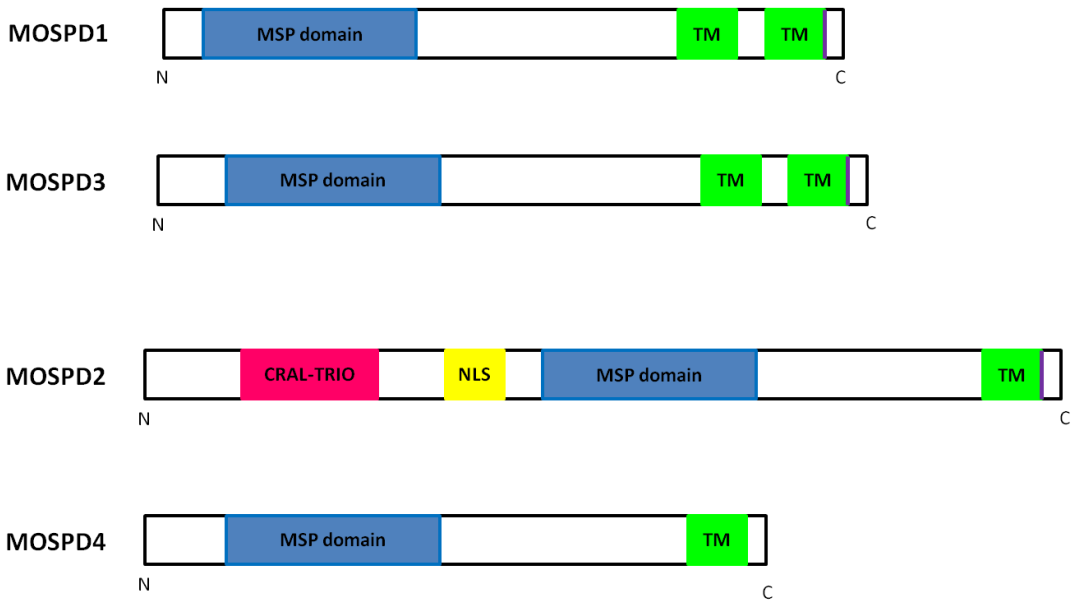

Figure 1.3: Schematic representation of members of the *Mospd* gene family. The four members of the *Mospd* gene family encode a Major Sperm Protein (MSP) domain (blue) and at least one transmembrane (TM) domain (green) at the C terminus. MOSPD2 also encodes a Cellular retinaldehyde binding/ triple function (CRAL-TRIO) domain (pink) and a nuclear localisation signal (NLS) (yellow). MOSPD1 and MOSPD3 are the most similar in protein structure.

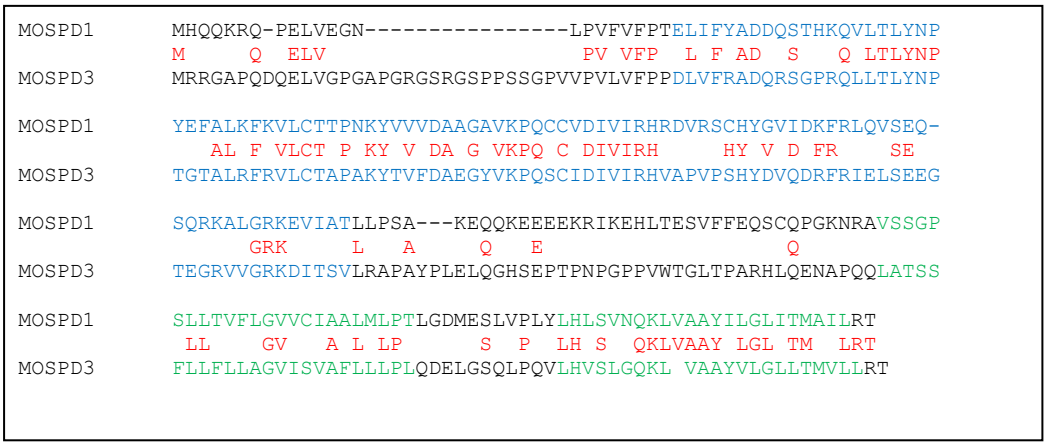

Figure 1.4: Protein sequence alignment between mouse MOSPD1 and MOSPD3. MOSPD1 and MOSPD3 (NCBI accession NP_081685 and NP_084313, respectively) share 38 % sequence identity. Letters in red correspond to identical sequence, letters in blue represent the MSP domains and letters in green represent the transmembrane domains.

1.1.5. Discovery of *Mospd 3*

The only clue for the function of the *Mospd* gene family came from a gene trap integration into the *Mospd 3* gene (McClive *et al*., 1998; Pall *et al*., 2004). Gene trapping in ES cells has been used to perform large scale mouse mutagenesis (Hansen *et al*., 2003; Skarnes *et al*., 2004). The vector used in the gene trapping screen contained a promoter-less *β-galactosidase* (*lac Z*) reporter gene immediately downstream of a splice acceptor site and a termination sequence (poly A tail). The vector also contains a selection cassette (Forrester *et al*., 1996). The trapped gene regulates the *lac Z* expression and due to the stop signal, downstream sequences of the trapped gene are prevented from being transcribed resulting in a mutant gene transcript being generated. The biological role of the trapped gene can be identified after germ line transmission.

The gene trap screen, in which *Mospd 3* was discovered, identified twenty genes that were responsive to retinoic acid (RA) treatment in a study to identify genes involved in embryonic development (Forrester *et al*., 1996). Retinoic acid is known to affect the patterning of tissues during embryogenesis. Nine of the gene trap integrations were found to be induced by RA whilst eleven were found to be repressed. One of these genes repressed by RA, the R124 integration, chimeras showed lacZ staining in the heart, branchial arch and dorsal hindbrain (Forrester *et al*., 1996). Using 5' RACE-PCR it was shown that the gene trap vector had integrated into the 5' UTR of the *Mospd 3* gene. The insertion was mutagenic and mice homozygous for the gene trap did not express *Mospd 3* in their tissues indicating a null allele had been generated. The expression of the neighbouring genes, *S7* and *Polce*, was not affected and, therefore, any phenotype observed was most likely due to the lack of *Mospd 3* (Pall *et al*., 2004).

1.1.6. Phenotype of *Mospd 3* gene trap mice

There were significantly fewer mice homozygous for the gene trap integration observed due to a neonatal lethality in these animals (Pall *et al*., 2004). 50 % of these homozygotes died within 24 hours of birth due to a right ventricle defect. The neonates showed dilated right ventricles and a thinning of the right ventricular parietal wall (Figure 1.5). The myocardium did not show any obvious fatty or fibrous replacement which is often seen in hearts with cardiomyopathies. Overall there was a 37 % reduction in the right ventricular wall and a 56 % increase in right ventricle volume when homozygotes were compared to wild type and heterozygous littermates. The compact myocardium was narrowed and the number and size of the trabeculae carnae was reduced resulting in the thinning right ventricular wall *(Pall et al*., 2004). This cardiac phenotype in a closely related family member of *Mospd 1* may provide a clue to the function of *Mospd 1* and could indicate that *Mospd 1* may also be involved in cardiac development. To investigate a possible mechanism for a thinning of the right ventricular wall a literature search to look for similar cardiac phenotypes was carried out.

1.1.7. Comparable right ventricle phenotypes

Similar right ventricle defects to that observed in the mice homozygous for the gene trap integration into *Mospd 3* have been found in several genes coding for desmosome components. Desmosomes are large protein complexes that are important in maintaining cell adhesion. They are important for providing mechanical strength by forming a 3D structure, as they anchor intermediate filaments to the cytosolic membrane. They play a vital role in maintenance of tissue integrity and are concentrated at the junctions of epithelia and cardiac muscle, tissues requiring high strength. Desmosomal proteins form a complex (or plaque) that links intermediate filaments of cells. Desmosomes span the intercellular space between adjacent cells and they are less than 1 μm in diameter (Figure 1.6). Desmosomes are made up of three areas including an extracellular core with the transmembrane proteins desmocollin (DSC) and desmoglein (DSG) (Delva *et al*., 2009).

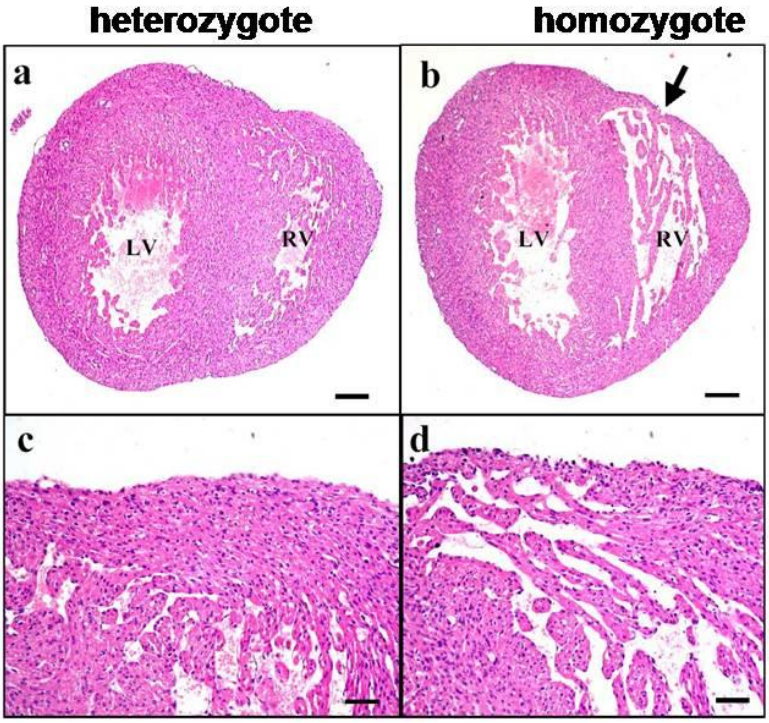

Figure 1.5: Transverse sections from E19 *Mospd 3* gene trap mice. Heart section from a mouse heterozygous for the *Mospd 3* gene trap (a & c) and a homozygous null heart section (b & d). The homozygote heart (b) shows a thinning of the right ventricle wall, indicated by the arrow, compared to the heterozygote heart (a). LV: left ventricle; RV: right ventricle. Scale bar for a & b = 100 µm and for c & d = 25 µm. Sections were stained with H & E. (Figure taken from Pall *et al*., 2004).

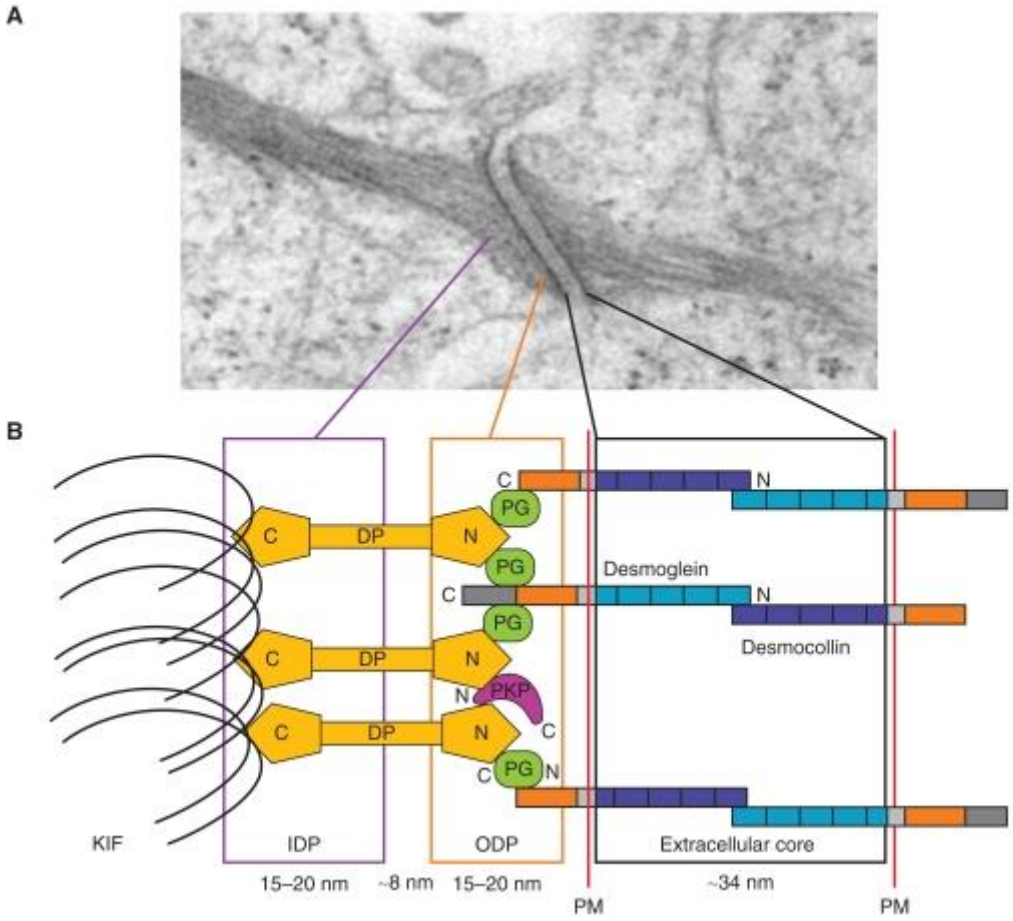

Figure 1.6: Structure of a desmosome. A: A desmosome on an electron micrograph. B: Schematic of a desmosome showing the components and the relative distances from the plasma membrane (PM). DP: desmoplakin; PG: plakoglobin; PKP: plakophilin; KIF: keratin intermediate filaments; IDP: inner dense plaque; ODP: outer dense plaque. (Figure taken from Delva *et al*., 2009.)

The outer dense plaque (ODP) of desmosomes has the C terminal of DSC and DSG linked to plakoglobin (PG) which is in turn linked to the N terminal of desmoplakin (DP). Plakophilin (PKP) is bound to PG to further stabilize the plaque. The inner dense plaque (IDP) contains the C terminal of DP which bind keratin intermediate filaments (KIFs) (Garrod and Chidgey, 2008; Delva *et al*., 2009).

Like the *Mospd 3* gene trap mice the majority of *Plakoglobin* (*Pg*) null mice die at mid-gestation due to cardiac defects. E10.5 PG null mice hearts had a thin ventricle wall and the ventricular trabeculae, atria and endocardial cushions were not well developed. There was further evidence of cardiac dysfunction due to blood pooling within the heart and surrounding area. Null embryos that lived past E10.5 died at birth and in addition to the cardiac phenotype also showed skin blistering and detaching epidermis (Bierkamp *et al*., 1996). Ruiz *et al*. (1996) also generated PG null mice with a similar cardiac phenotype. Between E12 and E16 most PG null mice died due to cardiac rupture resulting in the pericardium being filled with blood. There were no desmosomes present in the intercalated discs between cardiomyocytes in the nulls. Mice heterozygous for PG were normal at birth. However, they developed cardiac defects and dysfunction by 10 months and this was exacerbated by exercise (Kirchhof *et al*., 2006).

Another desmosome component that when deficient shows a similar cardiac phenotype to the *Mospd 3* gene trap homozygote nulls is *Desmoplakin* (*Dp*). Homozygous targeted disruption of the *dp* gene in mice results in death at E6.5 shortly before implantation (Gallicano *et al*., 1998). Tissue -specific *dp* deletion in cardiac tissue results in embryonic lethality in the majority of the mice. Those that survived at birth died within approximately two weeks due to cardiac defects. The hearts of these mice were less well developed, the chambers enlarged and there was fatty and fibrous replacement of the cardiomyocytes. The cytoskeleton was unorganized and there was blood within the pericardial sac. Mice heterozygous for

dp in the heart developed cardiac defects only after birth as they aged, with 20 % dying within 6 months with the same phenotype as the homozygous animals (Garcia-Gras *et al*., 2006).

Mice null for plakophilin 2 (PKP2) died at mid-gestation (E110.5-E11) and their hearts showed thinning of the chamber walls, reduced trabeculae in the ventricles and perforations in the heart resulting in leakage of blood into the pericardial sac. The cytoskeleton was disorganized and there was a change of DP localization from adhering junctions to cytoplasmic aggregates (Grossmann *et al*., 2004).

As mutations in genes encoding desmosome components result in similar thinning of the right ventricle wall to that of mice homozygous for the gene trap integration into *Mospd 3* it may be that *Mospd 3* is required for desmosomes. If this association with desmosomes is true for *Mospd 3* it may also be for *Mospd 1* due to their similar structure. There is a human condition with a similar cardiac phenotype to that of homozygous *Mospd 3* gene trap mice.

1.1.8. Arrhythmic Right Ventricular Cardiomyopathy

Mutations in desmosome components in humans result in a disease known as Arrhythmic Right Ventricular Cardiomyopathy (ARVC) which is characterized by dilatation and dysfunction of the right ventricle and thinning of the right ventricle wall. A loss of cardiomyocytes which are replaced by fatty and fibrous tissue (Fontaine *et al*., 1999) occurs. It is an inherited disease that causes ventricular arrhythmias, cardiac failure and sudden death, especially in young adults *(Thiene et al*., 1988). The disease affects approximately 1 in 5000 individuals and is a familial disease with incomplete penetrance and variable expressivity (Nava *et al*., 1987; Nava *et al*., 1988). Mutations in the desmosome components *Plakoglobin (McKoy et al*., 2000), *Desmoplakin* (Norgett *et al*., 2000), *Plakophilin 2* (Gerull *et al*., 2004),

Desmoglein 2 (Awad *et al*., 2006; Pilichou *et al*., 2006) and *Desmocollin 2* (Heuser *et al*., 2006; Syrris *et al*., 2006) have been identified in ARVC patients.

The first mutation in desmosomes that was implicated in the pathogenesis of ARVC was in the *Plakoglobin* (*Pg*) gene. Individuals that carried a mutation in *Pg* demonstrated ARVC as well as skin abnormalities and woolly hair *(Protonotarios et al*., 1986). This disease, also known as Naxos disease, is an autosomal recessive syndrome, characterized by a two base pair deletion in the *Pg* gene (McKoy *et al*., 2000). It is completely penetrant by adolescence in individuals homozygous for the mutant PG protein (Protonotarios *et al*., 2001).

A disease similar to Naxos disease was identified in which individuals had woolly hair, skin abnormalities and cardiomyopathy. This disease, known as 'Carvajal Syndrome' (Rao *et al*., 1996) was found to be an autosomal recessive disease and was the result of a mutation in the *Desmoplakin* (*Dp*) gene. This mutation was a deletion in exon 24 which results in a truncated protein being formed due to the introduction of a premature stop codon (Norgett *et al*., 2000).

The majority of cases of ARVC show mutations in the *Plakophilin 2* (*Pkp2*) gene. 25 *Pkp2* mutations were identified which included nonsense mutations, splice site mutations, missense mutations, insertion and deletion mutations (Gerull *et al*., 2004). These mutations were located throughout the gene but there were higher incidence in the C- terminal coding region. *Pkp2* is the only *Plakophilin* expressed in cardiomyocytes (Klymkowsky, 1999).

Similarly to *Pkp2 Desmoglein 2* (*Dsg2*) is also the only *desmoglein* expressed in cardiomyocytes (Schafer *et al*., 1994). Individuals with mutations in *Dsg2* exhibit ARVC but do not show the hair and skin abnormalities associated with mutations in *plakoglobin* and *desmoplakin* (Awad *et al*., 2006; Pilichou *et al*., 2006). Pilichou *et*

al. (2006) identified nine mutations in *Dsg2* with seven of these mutations located in the extracellular domains which are important for adhesion. Awad *et al*. (2006) identified a further 5 mutations in the *Dsg2* gene implicated in ARVC. Mutations in another desmosomal cadherin, *Desmocollin 2* (*Dsc2*), have also been identified. Two mutations which both resulted in truncated DSC2 protein were identified by Syrris *et al*. (2006) and a mutation in a splice acceptor site of the *Desmoglein 2* gene resulted in the introduction of a premature termination codon and reduced levels of transcript (Heuser *et al*., 2006). The complete loss of DSG2 is lethal in mice. *Dsg2* null mice die just after implantation (Eshkind *et al*., 2002). The desmosomal genes that are involved in ARVC are listed in Table 1.1.

The human ARVC disease has a similar phenotype to the homozygous *Mospd 3* gene trap mice as they both show a thinning of the right ventricular wall. This could indicate that the loss of *Mospd 3* could result in ARVC or a similar condition. If *Mospd 1* has a similar function to *Mospd 3* then a mutation in the *Mospd 1* gene may also result in a similar human disease. 50 % of ARVC cases are due to a mutation in a known desmosome component (den Haan *et al*., 2009; Bhuiyan *et al*., 2009) and the cause of the other 50 % of cases is unknown. It is possible that mutations in *Mospd 1* and *Mospd 3* could be responsible for some of these cases.

Gene	Gene abbreviation	Mouse phenotype	Human disease	References
Plakoglobin	*Pg*	Nulls: embryonic lethality at E10.5 due to ventricular defects; skin blistering Hets: ARVC by 6 months	ARVC with skin defects and woolly hair	Bierkamp *et al*., 1996 Kirchhof *et al*., 2006 McKoy *et al*., 2000
Desmoplakin	*Dp*	Nulls: embryonic lethality at E6.5 Hets: ARVC by 6 months	ARVC with skin defects and woolly hair	Gallicano *et al*., 1998 Garcia-Gras *et al*., 2006 Norgett *et al*., 2000
Plakophilin 2	*Pkp2*	Nulls: die at midgestation due to cardiac defects	ARVC	Grossman *et al*., 2004 Gerull *et al*., 2004
Desmoglein 2	*Dsg2*	Nulls: Embryonic lethal	ARVC	Eshkind *et al*., 2002 Awad *et al*., 2006; Pilichou *et al*., 2006
Desmocollin 2	*Dsc2*	Mouse knockout not reported to date	ARVC with skin defects and woolly hair	Heuser *et al*., 2006 Syrris *et al*., 2006

Table 1.1: Desmosome components implicated in ARVC and the phenotypes associated with mutations in these proteins.

1.1.9. A link between *Mospd 1* and EMT

A recent study found that *Mospd 1* expression was higher in mesenchymal-derived cells and increased during the differentiation of osteoblastic, myoblastic and adipocytic cells, all of which are mesenchymal cell types. *Mospd 1* expression increased in dense (confluent) cell cultures compared to sparse cell cultures (Thaler *et al*., 2010).

siRNA knockdown of *Mospd 1* gene expression in the MC3T3-E1 osteoblastic cell line resulted in the down regulation of numerous osteoblastic and mesenchymal genes and a shift to more epithelial gene expression. Osteoblastic genes, such as *Runx 2* and *Osteocalcin* were down regulated as well as mesenchymal genes such as *Vimentin* and *Smooth muscle actin*. *Runx 2* is a transcription factor required for osteoblast formation whilst *Osteocalcin* is a marker of osteoblast differentiation. Up regulation of epithelial genes such as *E-cadherin* (*Cdh1*), *Emp1* and *Trp63* (Thaler *et al*., 2010) occurred in cells when *Mospd 1* expression was knocked down. EMP1 is a protein localised to epithelial membranes and can be used as a marker for epithelial cells. TRP63, which is also known as P63, is a transcription factor that is a homolog of the tumour suppressor P53. P63 is required for the formation of the epidermis as demonstrated by the lack of epidermis in mice with a targeted disruption of the *p63* gene. This loss of epidermis results in their death shortly after birth due to dehydration (Mills *et al*. ,1999; Yang *et al*., 1998). P63 serves as the switch for the initiation of epithelial stratification during epidermal development (Koster *et al*., 2004). The loss of P63 also results in craniofacial and limb defects (Yang *et al*., 1998; Wolff *et al*., 2009). The *cadherin* found in osteoblasts, *Cdh11*, was down regulated in cells treated with *Mospd 1* siRNA. Expression of genes involved in EMT was also found to be altered in *Mospd 1* knockdown cells. There was a down regulation of the *E-cadherin* repressor genes *Snai1* and *Snai2* (Thaler *et al*., 2010). This suggested a reduction in *Mospd 1* could result in the down regulation of *Snai1* and *Snai2* leading to the up regulation of *E-cadherin* and resulting in MET. Therefore, it could be hypothesised that *Mospd 1* may be involved in regulation of *Snail* and *Snai2* and thus be involved in controlling EMT during osteoblast differentiation.

1.1.10. Epithelial- Mesenchymal Transition (EMT)

Epithelial cells show plasticity and can change into mesenchymal cells through a process known as Epithelial- Mesenchymal Transition (EMT) (Greenburg and Hay, 1982). During normal development cells that arise in one area of the embryo need to move to other areas of the embryo. Epithelial cells do not have migratory properties and, therefore, need to change into mesenchymal cells which are more mobile (Hay, 1968). EMT is required during embryogenesis to form the three germ layers beginning during gastrulation. When EMT is disrupted an organism cannot proceed past the blastula stage as it fails to undergo gastrulation. During EMT the characteristics of epithelial cells change to those of mesenchymal cells and this switch is governed by complex signalling and transcription factor networks.

Epithelial cells have adherens junctions, tight junctions, gap junctions and desmosomes at their cell junctions. Epithelial cells form layers of cells with a basal lamina and have an apical-basal polarity. Whilst epithelial cells can be motile they remain within the epithelial layer. Mesenchymal cells differ in that they do not form layers of cells, do not have a basal lamina and the actin cytoskeleton polarised and these cells can easily migrate. They also differ in morphology as mesenchymal cells are more spindle-like whereas epithelial cells usually grow in clusters with cell-cell contacts always maintained and are more regular in shape (Greenburg and Hay, 1982).

During EMT cell adhesion molecules are down regulated allowing tight junctions, adherens junctions and desmosomes to dissociate. This allows cells to lose cell-cell contacts and become more mobile and thus change into mesenchymal cells (Figure 1.7). The reverse process whereby mesenchymal cells can change into epithelial cells is known as Mesenchymal- Epithelial Transition (MET). During embryogenesis several rounds of EMT and MET are required for proper development.

Mutations in desmosome components have been described in previous sections and result in a similar phenotype to that of the homozygous gene trap *Mospd 3* mice (Pall *et al*., 2004) indicating a possible link between desmosomes and *Mospd* genes. Given this possible link and the loss of desmosomes due to down regulation of *E-cadherin* during EMT it is possible that MOSPD proteins are involved in EMT and, therefore, disruption of them may result in desmosome disruption and a cardiac phenotype.

1.1.11. *E-Cadherin* (*Cdh1*) involvement in EMT

Cadherins are a family of calcium-dependent cell adhesion molecules. *E-cadherin* (*Cdh1*) was the first *cadherin* identified and is the form found in epithelial cells where it is important for cell adhesion (Takeichi, 1988) as well as for apical-basal polarity of epithelial cells (Gumbiner, 1988). E-CADHERIN is located in adherens-junctions at cell junctions.

E-cadherin is expressed in the ectoderm and epithelial regions derived from the endoderm of the developing mouse embryo (E7.5 to E9.5) but is absent from regions undergoing EMT and mesoderm (Cano *et al*., 2000). *E-cadherin* is essential as *E-cadherin* null mice are embryonic lethal, do not develop past the 32 cell stage and die around implantation as they do not form normal blastocysts (Larue *et al*., 1994; Riethmacher *et al*., 1995). Due to this early embryonic lethal phenotype it was difficult to assess the role of *E-cadherin* in development past this point in mice. Morpholino knockdown of *E-cadherin* in zebrafish embryos resulted in a 60 % reduction in embryo survival as well as defects in cell movements resulting in inhibition of epiboly and gastrulation. Cell cleavage patterns and compaction were also disrupted in morpholino-injected embryos (Babb and Marrs, 2004).

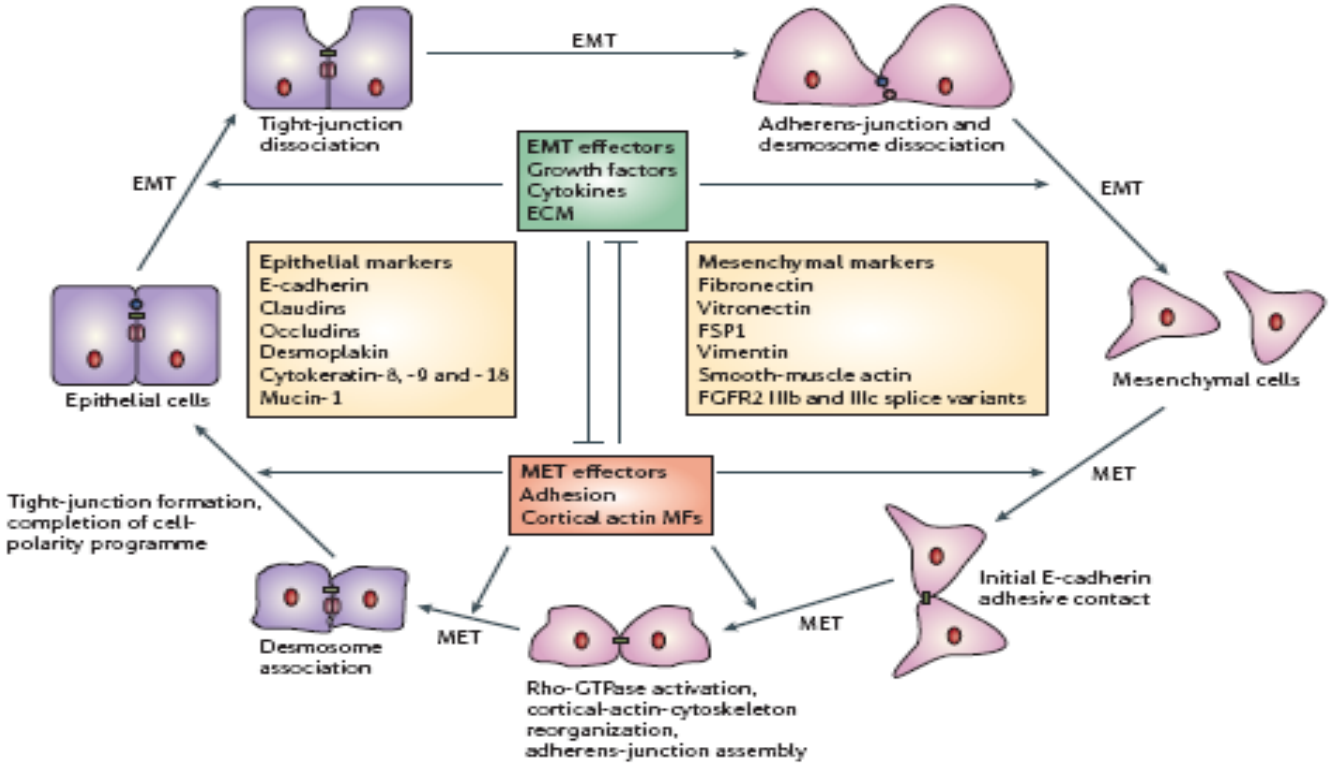

Figure 1.7: Epithelial -Mesenchymal Transition (EMT) and Mesenchymal -Epithelial Transition (MET). Epithelial and mesenchymal cells show plasticity and can interchange by the processes of EMT and MET. Epithelial cells and mesenchymal cells have different markers. During EMT tight junctions, adherens-junctions and desmosomes dissociate and epithelial cells change into mesenchymal cells. During the reverse process, MET, these junctions and desmosomes associate and epithelial cells form. Various transcription factor and signalling networks control EMT and MET. (Figure taken from (Thiery and Sleeman, 2006).

The *E-cadherin* promoter has an E-pal regulatory element consisting of a palindromic sequence (Behrens *et al*., 1991). This E-pal element, containing two E boxes, is a site that can bind transcription factors, resulting in changes of *E-cadherin* expression. *E-cadherin* expression is repressed by the transcription factors *Snai1* (Cano *et al*., 2000) and *Snai2* (*Slug*) (Bolos *et al*., 2003) by binding of SNAI1 and SNAI2 to the E-pal element.

1.1.12. *Snai1* and *Snai2* (*Slug*) transcription factors

The *Snail* family are zinc finger transcription factors that are essential regulators of EMT. *Snail* is expressed in the primitive streak pre-migratory and migrating neural crest cells of the developing mouse embryo as well as other regions undergoing EMT and in the mesoderm (Smith *et al*., 1992; Cano *et al*., 2000). Loss of *Snai1* is embryonic lethal as *Snai1* null mice fail to undergo gastrulation due to defects in EMT (Carver *et al*., 2001). *Snai2* (*Slug*) is expressed during early embryonic development during organogenesis with high expression in mesenchyme and organs from the mesoderm (Oram *et al*., 2003).

Snai1 and *Snai2* have high homology at the N terminal as they both have a SNAG transactivation domain and at the C terminal where they have 4-5 zinc fingers. The intermediate region of the *Snai2* gene has a *Slug* domain which is 29 amino acids in length and its function is not known (Manzanares *et al*., 2001).

Snail transcription factors bind to the E box (CAGGTG) in the E-pal element. *Snai1* is a repressor of *E-cadherin* and results in a down regulation of epithelial genes such as desmosome components and up regulation of mesenchymal genes such as *Vimentin* and *Fibronectin* (Cano *et al*., 2000). The up regulation of *Snai1* results in decreased cell–cell contacts through a reduction in desmosomes and adherens junctions. This dissociation of cell junctions results in cells becoming more migratory and, therefore, mesenchymal through EMT. *Snai2* also has the ability to

repress *E-cadherin* expression and induce EMT. An increase in mesenchymal marker gene expression and migratory cells is observed when *Snai2* is expressed. *Snai2* binds the E-box of *E-cadherin* but with a lower affinity to that of *Snai1* (Bolos *et al*., 2003). Increase in *Snai2* expression by transfection resulted in the loss of *Desmoglein* and *Desmoplakin* expression indicating a loss of desmosomes. These changes were accompanied by a loss of epithelial properties and a gain of mesenchymal properties (Savagner *et al*., 1997). Increased *Snai1* and *Snai2* repress *E-cadherin* expression resulting in less cell-cell attachment and an increase in mesenchymal properties and markers.

1.1.13. EMT in cancer

Whilst EMT has an important role to play during embryogenesis there is less requirement for the process in adult tissues. In fact EMT in certain circumstances is involved in pathological processes such as cancer. EMT has been implicated in tumour progression of epithelial tumours. Tumour cells express high levels of *Snail* and can reduce their cell adhesion properties resulting in a decrease in cell-cell contacts (Cano *et al*., 2000). Cells can then cross the basement membrane and have mesenchymal characteristics such as migration properties. This allows the cells to migrate from the primary tumour location to secondary locations and thus EMT is involved in metastasis of tumours. Many of the same transcription factors and signalling molecules are involved in this tumour progression through EMT as during normal development. The loss of *E-cadherin* has been shown to be involved in tumour progression (Perl *et al*., 1998) and *Snai1* repression of *E-cadherin* has been implicated in tumour progression (Battle *et al*., 2000).

1.2. Functional study of genes

As described in the previous sections there are possible clues to the function of *Mospd 1* from the structure and function of MSP in nematodes and other MSP domain- containing proteins, such as VAPs even *Mospd 3*, as well as the recent finding that *Mospd 1* may be involved in EMT in osteoblast cells (Thaler *et al*., 2010). Models are required to investigate the function of *Mospd 1 in vivo* and *in vitro*. To study the function of *Mospd 1 in vivo* a model organism like *Danio rerio* (zebrafish) is an option due to the presence of a *Mospd 1* gene in its genome.

1.2.1.1. *Mospd 1* expression in zebrafish

The zebrafish genome only has one copy of the *Mospd 1* gene (NCBI accession 007878.1) located on chromosome 14. As no gene duplications of *Mospd 1* have occurred in the zebrafish genome *Mospd 1* can be studied in this organism without the complications of a duplicate. As there is no *Mospd 3* gene found in the zebrafish genome the possibility of genetic redundancy between *Mospd 1* and *Mospd 3* in zebrafish is not an issue.

However, whilst *Mospd 3* is not found in the zebrafish genome *Mospd 2* is expressed and is located on chromosome 9. Whole mount *in situ* hybridisation (WISH) on zebrafish embryos has demonstrated that *Mospd 2* is ubiquitously expressed in pre-gastrula embryos. This expression is observed from the 2 cell stage to 64 cell stage indicating maternal expression of *Mospd 2* in zebrafish embryos (Hong *et al*., 2010). There is 28 % sequence identity between zebrafish MOSPD1 and MOSPD2 and, therefore, there is the possibility that MOSPD2 may compensate for the loss of MOSPD1. There is no information reported in the literature about the expression of *Mospd 2* in embryos past 8 hpf or the function of *Mospd 2*.

WISH performed in a high throughput screen to investigate the expression patterns of zebrafish genes in zygotic embryos (0-0.75 hours) to the hatching pec fin developmental stage (60-72 hours) revealed that *Mospd 1* RNA was expressed

throughout the embryo (Figure 1.8) and was not localised to a particular region of the developing embryo (Thisse *et al*., 2004) from www.zfin.org). It is not known whether the *Mospd 1* mRNA expression reflects the protein expression. MOSPD1 is highly conserved between mouse (NCBI accession NP_081685.1) and zebrafish (NCBI accession NP_998534.1) as the proteins share 77 % sequence identity (Figure 1.9).

1.2.1.2. Zebrafish as a model organism

Zebrafish are an excellent model organism to examine developmental processes as they possess many advantages. They are easy and inexpensive to maintain and large numbers of embryos can be accessed from the earliest developmental stages as zebrafish have high fecundity and eggs are externally fertilised. The transparency of the embryos facilitates the observation of organ development *in vivo* by light microscopy. The entire zebrafish genome has been sequenced (www.sanger.ac.uk/Projects/D_rerio) aiding genetic studies in this organism.

Zebrafish provide advantages over the use of classical model organisms, such as *C. elegans* and *Drosophila*, as zebrafish are vertebrates and, therefore, are evolutionarily closer to mice and humans. Many biochemical and biological processes are conserved from zebrafish to humans allowing processes specific to vertebrates to be investigated. Zebrafish embryos do not require normal blood circulation during early development as they acquire sufficient oxygen through diffusion (Burggren and Pinder, 1991). This allows embryos that have cardiovascular defects to survive and develop and facilitates phenotypic assessment of these fish (Chen *et al*., 1996). This is advantageous compared to using mice as a model organism as it allows mutations that act at early stages of development and are embryonic lethal to be assessed which would be difficult to study in mice as mouse embryos are dependent on normal blood circulation for survival.

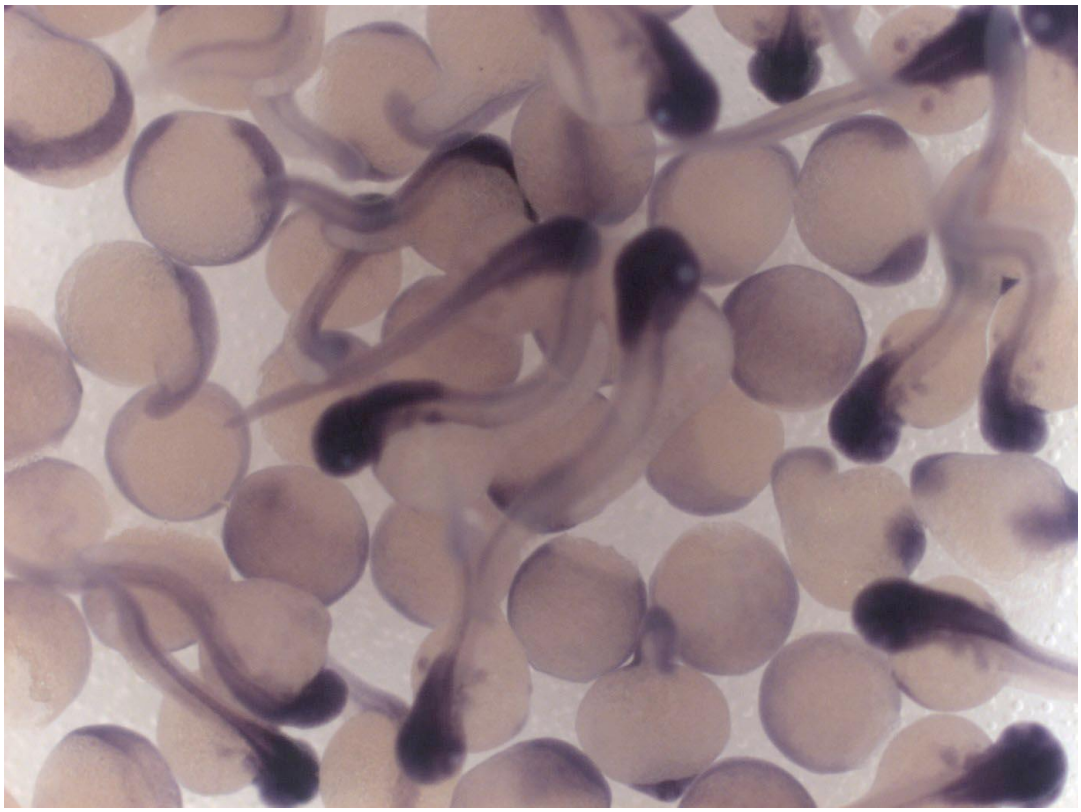

Figure 1.8: Expression of *Mospd 1* RNA in developing zebrafish embryos. Whole mount *in situ* hybridisation of *Mospd 1* in zebrafish embryos from the one cell stage to the hatching pec fin stage was performed and *Mospd 1* was found to be expressed throughout the embryo (Thisse *et al*., 2004; image from www.zfin.org).

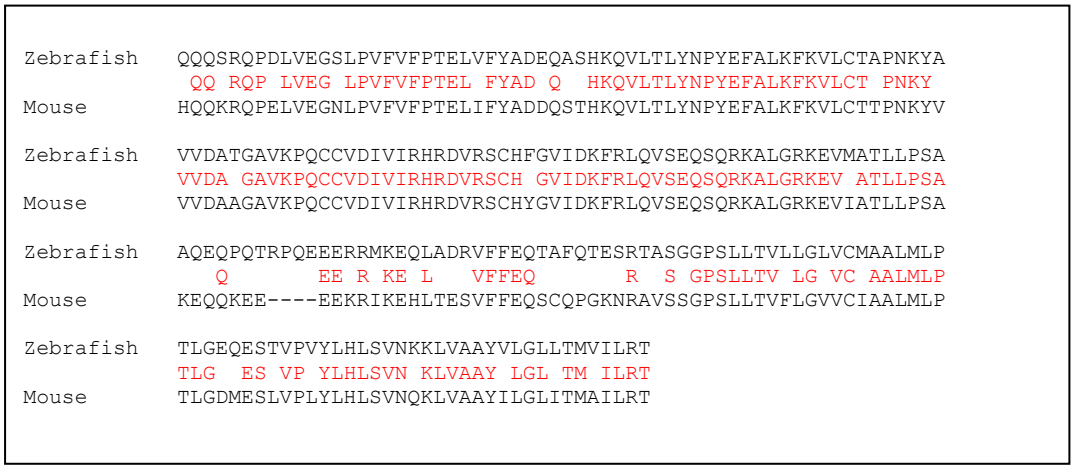

Figure 1.9: Protein sequence alignment between zebrafish MOSPD1 and mouse MOSPD1. Zebrafish MOSPD1 and mouse MOSPD1 (NCBI accession NP_998534.1 and NP_081685.1, respectively) share 77 % sequence identity. Letters in red correspond to identical sequence.

1.2.1.3. Zebrafish development

Zebrafish embryos develop through periods, from a one cell embryo to an embryo with well developed organs by 72 hours post fertilisation (hpf,) when the embryos are kept at 28.5 ℃ (Figure 1.10). The developmental period from a one cell newly fertilised zebrafish egg until the first cleavage occurs is known as the zygotic period and it lasts from 0-0.75 hpf. During this time the cytoplasmic movement is activated and cytoplasmic streaming occurs. This is followed by the cleavage period (0.75-2.25 hpf) where cells divide every 15 minutes until there are 128 cells and this marks the beginning of the blastula period (2.25-5.25 hpf) (Kimmel *et al*., 1995). Mid blastula transition (MBT) occurs during this period which is characterised by lengthening of the cell cycle and the onset of zygotic gene expression (Kane and Kimmel, 1993). This is followed by the beginning of epiboly which is when the yolk syncytial layer (YSL) and the blastoderm spread around the yolk cell.

The gastrula period (5.25-10 hpf) begins at 50 % epiboly and the primary germ layers and embryonic axis are formed at this time. There are two germ layers formed during gastrulation, namely the epiblast (definitive endoderm) which will give rise to the epidermis, central nervous system and neural crest and the hypoblast which gives rise to the mesoderm and endoderm structures (or mesendoderm). Following gastrulation is the segmentation period (10-24 hpf) in which the primary organs, such as the heart and pronephric kidneys, begin to develop as well as the eye. Tail morphogenesis occurs resulting in the elongation of the embryo and the yolk extends. The somites develop in the trunk and tail of the embryo during this period from 3 somites (at 11 hpf) to 26 somites (at 22 hpf). These somites later form the myotome. Neuromeres, develop which give rise to the brain structures such as the midbrain and hindbrain (Kimmel *et al*., 1995).

The pharyngula period (24-48 hpf) is characterised by the continuous lengthening of the embryo and the straightening of the head.

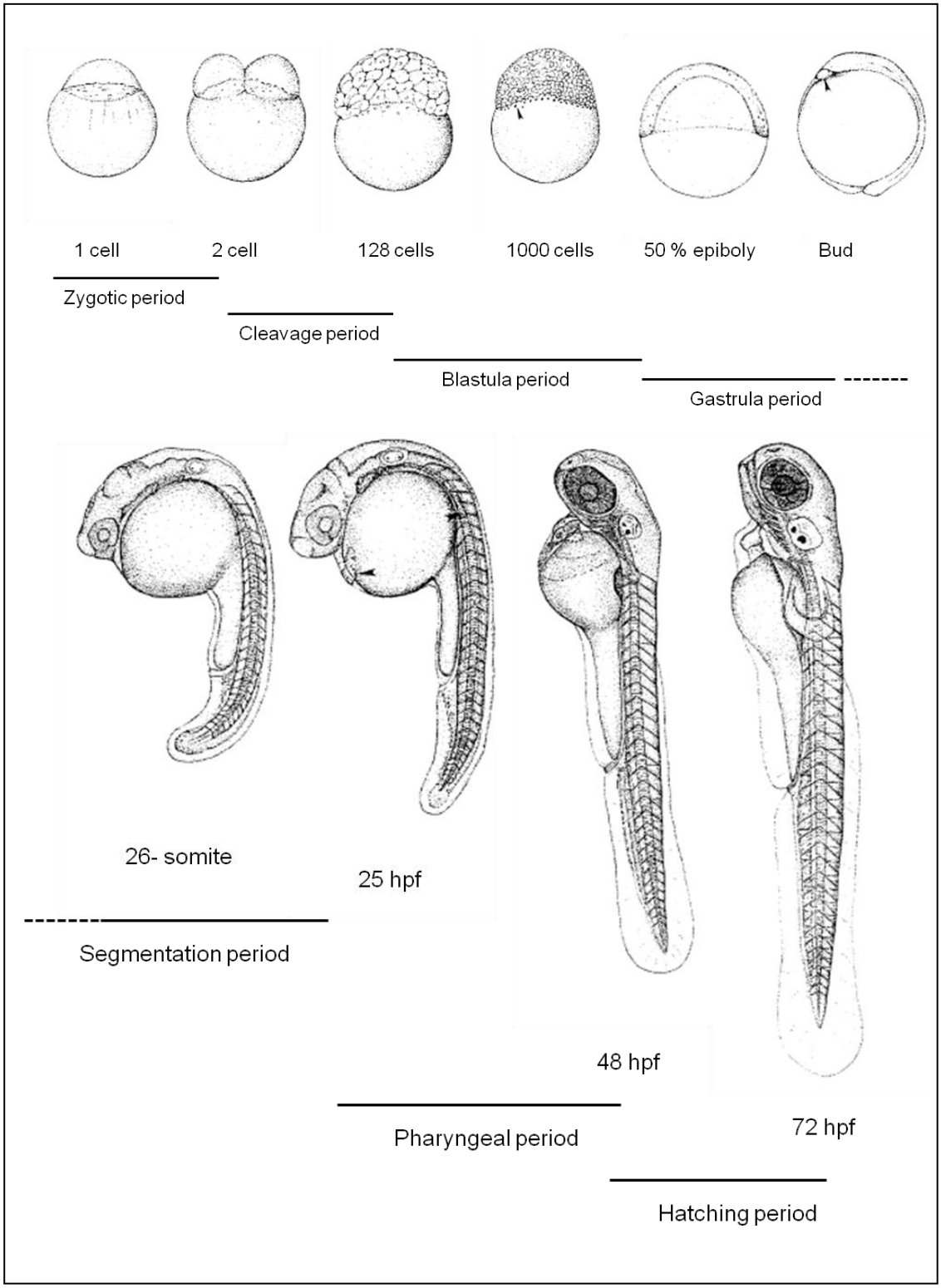

Figure 1.10: Stages of zebrafish development. Sketches of zebrafish embryos at different stages showing the periods of development (from zygotic to hatching) are shown. Image adapted from sketches in Kimmel *et al*. (1995).

The pharyngeal arches develop which gives rise to structures such as the jaw and gills. Pigmentation commences, the fins begin to develop and the embryo becomes sensitive to touch and is able to swim when freed from the chorion. The embryos hatch from the chorion during the hatching period (48-72 hpf) allowing them to swim freely. The embryos have a protruding mouth and show behavioural traits such as avoidance and food seeking from this time. From 72 hpf onwards embryos continue to develop rapidly (Kimmel *et al*., 1995).

1.2.1.4. Zebrafish heart development

The heart is the first organ to develop in zebrafish embryos and is comparable to the early human heart. At approximately 22 hpf heart tube contraction begins which is followed by circulation by 24 hpf. By 36 hpf the heart tube has looped and there are co-ordinated contractions of the chambers. There are two chambers, the atrium and the ventricle, separated by valves and an outflow tract called the bulbous arteriosis (Stainier *et al*., 1993). The heart beats at about 140 beats/ minute by 48 hpf (Denvir *et al*., 2008) and by this time there is also strong blood circulation in the head and tail.

1.2.1.5. Zebrafish Resources

ZFIN (the Zebrafish Model Organism Database (www.zfin.org)) is an online database of information about zebrafish research that allows the zebrafish research community access to a wide range of protocols, gene information and zebrafish research findings. The Zebrafish International Resource Centre (ZIRC) is able to provide zebrafish lines and WISH probes to the scientific community. These resources facilitate research and are another advantage when using zebrafish as a model organism.

Transgenic zebrafish lines have been generated that assist in the study of various developmental processes. For example, a transgenic line with GFP under the control of the *Cardiac myosin light chain 2* (*Cmlc2*) promoter has been developed which

shows fluorescence in myocardial cells (Huang *et al*., 2003). The fli1-GFP zebrafish transgenic line has the GFP gene fused to the *Friend leukaemia integration 1* (*Fli1*) gene and is used to visualise the vasculature during embryogenesis (Lawson and Weinstein, 2002). In Gata-1-GFP transgenic zebrafish the GFP is under the control of the erythroid-specific *Gata 1* promoter and this allows visualisation of blood cells in circulation to be monitored (Long *et al*., 1997).

1.2.1.6. Mutagenesis studies in zebrafish

Large-scale mutagenesis studies have been carried out on zebrafish to identify genes involved in zebrafish development (Driever *et al*., 1996; Haffter *et al*., 1996). Zebrafish have been exposed to ethylnitrosourea (ENU) which is a powerful mutagen that introduces point mutations into the genome (Bode, 1984). This allows the identification of the gene causing the phenotype to be determined by sequencing. Haffter *et al*. (1996) isolated mutant embryos displaying a visible phenotype when assessed by light microscopy and characterised 1163 mutants. By using complementation crosses they assigned 894 mutants to 372 genes which were involved in morphogenesis, organogenesis, pattern formation and differentiation. Another ENU screen was carried out on zebrafish in the same year and 577 mutants were identified which were involved in embryogenesis (Driever *et al*., 1996).

Large-scale mutagenesis screens of the zebrafish genome have identified many mutations that affect the cardiovascular system (Stainier *et al*., 1996; Chen *et al*., 1996). Stainier *et* a*l*. (1996) identified 58 mutations and Chen *et al*. (1996) identified 53 cardiovascular mutations. Mutations that have been identified have been subdivided into those that affect cardiac morphogenesis and those that affect cardiac function. Most heart mutants show oedema that progressively worsens, being observed firstly in the pericardial sac and the majority of these mutants die by 7 dpf. Mutations that affect the vasculature have been identified that result in haemorrhaging (blood pooling) after circulation begins (Stainier *et al*., 1996). However, these large-scale ENU mutant screens have limits such as genes with

subtle phenotypes could go undetected. They are time-consuming and redundancy in identification of genes occurs.

1.2.1.7. Morpholinos antisense oligonucleotides

Morpholino gene knockdown is an established technology in zebrafish and is used for functional genomics. Morpholinos are designed and manufactured by Gene Tools (www.gene-tools.com) and are able to knockdown gene expression allowing the characterisation of the function of genes during early development. They are short antisense oligonucleotides that are comprised of the standard nucleic acid bases (A, C, G and T). However, morpholine rings replace ribose rings and phosphorodiamidate linkages are present instead of phosphodiester bonds found in DNA and RNA resulting in a net neutral charged oligonucleotide (Summerton and Weller, 1997) (Figure 1.11). This results in morpholinos being stable as they are resistant to nuclease activity (Hudziak *et al*., 1996). Morpholinos do not induce an immune response and have a high affinity for RNA. Morpholinos are most effective for the first two to three days post fertilisation (dpf) and as most organ systems develop during this time morpholinos are excellent tools for developmental research.

Morpholinos are injected into embryos between the 1-16 cell stages and the development of the embryos monitored. A 3'carboxyfluorescein tag on the morpholino allows the injected embryos to be monitored for successful uptake and even distribution in the cells. 5 mis-pair morpholinos are used as a negative control as they are highly similar to the specific injected morpholino but should not cause knockdown of the gene of interest due to the 5 base pair changes. These controls are used to monitor for possible off target effects and morpholino toxicity.

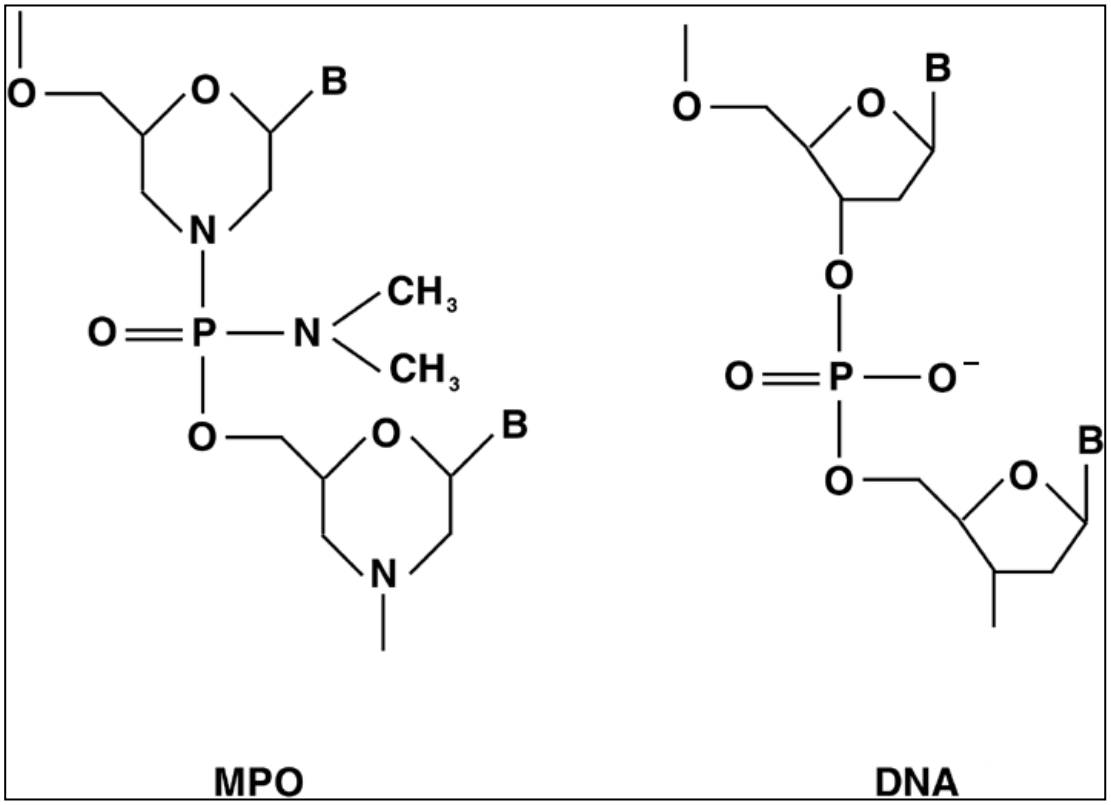

Figure 1.11: Comparison of the structure of a morpholino (MPO) and DNA. Morpholinos are comprised of the standard nucleic acid bases (B). Morpholine rings and phosphorodiamidate linkages in morpholinos replace the deoxyribose rings and phosphodiester bonds found in DNA. Morpholinos have a net neutral charge. (Figure taken from Sumanas and Larson, 2002).

Morpholinos can act either by blocking translation in the cytosol or by blocking pre-mRNA splicing in the nucleus depending where they are targeted to. Translational blocking morpholinos can be targeted anywhere from the 5'cap through to about 25 bases 3' to the translational start site. Therefore, morpholinos targeted to the 5' untranslated region (UTR) or morpholinos targeted to the start site of the mRNA can be used to block translation. It is hypothesised that binding of the morpholino hinders the scanning of the 5' UTR by the small ribosomal unit (40S) so it cannot identify the start codon. Therefore, the large ribosomal unit (60S) is not recruited and as the full ribosomal complex is not formed translation of the mRNA is blocked (Figure 1.12 A) (Summerton, 1999; Hardy *et al*., 2010).

Small ribonucleoprotein particles (snRNP) form the spliceosome which binds to pre-mRNA at specific binding sites. This is required for normal splicing of pre-mRNA where introns are removed resulting in the formation of mRNA. Morpholinos targeted to snRNP binding sites (splice junctions) of genes can alter pre-mRNA splicing by blocking the recognition of the spliceosome (Figure 1.12 B). This can result in the targeted exon being excluded (exon skipping) or inclusion of an intron in the mRNA). Quantitative real-time PCR can be used to determine the level of knockdown using splice-site morpholinos.

1.2.1.8. Morpholinos to knockdown expression in zebrafish

Morpholinos targeted to the start site of genes have been used to demonstrate the effectiveness of morpholinos in blocking translation. A morpholino targeted to the start site of the *Green fluorescent protein* (*Gfp*) gene was injected into GFP transgenic zebrafish embryos and the reduction in GFP expression monitored by fluorescent microscopy and measured by western blotting (Nasevicius and Ekker, 2000). Injection of 4.5 ng of the GFP morpholino into embryos resulted in inhibition of GFP expression and a reduction of GFP activity by 80 %. This inhibition of expression was sequence-specific as the 4 base pair mis-pair morpholino injected as a control at the same dose only resulted in a 15 % reduction in GFP activity.

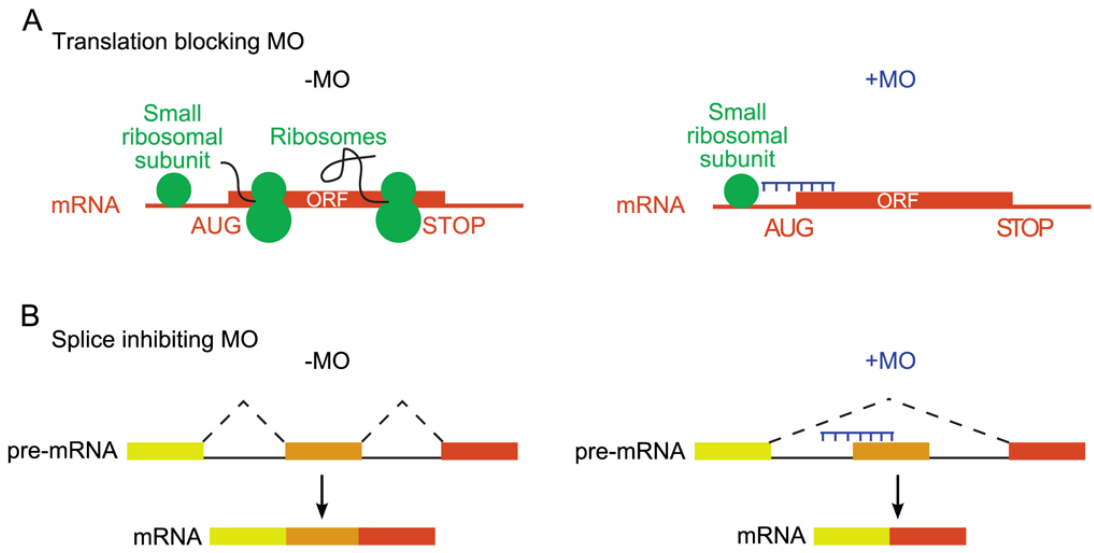

Figure 1.12: Mechanism of action of morpholinos. The mechanism for a translational blocking morpholino (A) and a splice-inhibiting morpholino (B) are shown. (Figure taken from Hardy *et al*., 2010.)

The knockdown was also dose-dependent as an increase in the dose resulted in a further reduction in GFP activity. However, at an increased dose non-specific defects were observed (Nasevicius and Ekker, 2000).

Morpholinos have been used to phenocopy zebrafish mutants identified in large scale mutagenesis studies. Table 1.2 shows examples of phenocopies of known zebrafish mutants. As the zebrafish genome has undergone partial duplication some genes have duplicates and, therefore, studying their function can be complicated by genetic redundancy. Morpholinos can also be co-injected against 2 different genes to knock down these functionally redundant genes thus facilitating the assessment of the function of genes (Bahary *et al*., 2007; Cermenati *et al*., 2008).

1.2.1.9. Zebrafish to model human diseases

Many of the mutants identified in the mutagenesis screens displayed phenotypes that corresponded to particular human disorders. Zebrafish are now widely used as a model for human diseases. For example, mutations in the desmosomal gene, *Desmocollin 2* are associated with the human arrhythmic right ventricular cardiomyopathy (ARVC) due to cellular junction defects and a thin right ventricle wall. Morpholino mediated knockdown of *Desmocollin 2* in zebrafish embryos results in contractility defects and reduced desmosome plaque area (Heuser *et al*., 2006) modelling ARVC. Another example is *Bicaudal C* (*Bicc1*) whose morphants have kidney cysts which are similar to those observed in polycystic kidney disease where mutation in *Bicc 1* gene have been identified (Bouvrette *et al*., 2010). Zebrafish models of muscular dystrophy have been used to study the disease. Morphants of the *Fukutin-related protein* (*Fkrp*) display altered somatic structures, muscle fibre organisation and a reduction in alpha-dystroglycan glycosylation which is a feature of muscular dystrophy (Kawahara *et al*., 2010). There are many more diseases that are being modelled in zebrafish and this allows the function of genes involved in the pathogenesis of disorders to be studied as well as possible treatments.

Gene name	Mutant name	Phenotype	Reference
Chordin	Dino	U-shaped somites, abnormal tail fin, blood island	Hammerschmidt *et al*. (1996) Nasevicius and Ekker, 2000
BMP7	Snailhouse	Dorsalisation	Lele *et al*. (2001)
Protein kinase Cλ	Heart and soul	Heart patterning defects	Peterson *et al*. (2001)
Sox 10	Colourless	Pigment defects	Dutton *et al*. (2001)
Synaptojanin (synj1)	No optokinetic response c (nrc)	Unanchored cone photoreceptor ribbons and abnormal synaptic transmission	Van Epps *et al*. (2004)
Fibrillin-2	Puff daddy^{gw1}	Disruption of notochord and vascular development	Gansner *et al*. (2008)
Protoporphyrinogen oxidase (ppox)	montalcino	Deficient in haemoglobin, anaemic and porphyric	Dooley *et al*. (2008)

Table 1.2: Phenocopies of known zebrafish mutations.

1.2.2. Functional study of genes using Embryonic Stem (ES) cells

1.2.2.1. ES cells as a tool for mammalian development

Embryonic stem (ES) cells are pluripotent cells derived from the inner cell mass (ICM) of the developing blastocyst that can differentiate into all cell types (Evans and Kaufman, 1981; Martin, 1981). They can be maintained *in vitro* in an undifferentiated state by culturing them in the presence of Leukaemia Inhibitory Factor (LIF) (Smith *et al*., 1988). ES cells can give rise to all three germ layers and when differentiated can form three dimensional aggregates of cells known as embryoid bodies (EBs). These EBs show a mixed population of different cell types (Doetschman *et al*., 1985).

ES cells provide a useful tool to study development as they can be made to differentiate into any cell type depending on culture conditions. The addition of different growth factors or drugs or co-culturing ES cells with other cell types can direct differentiation towards a particular lineage. ES cells have been differentiated into various types of cells *in vitro* including cardiomyocytes (Doetschman *et al*., 1985), haematopoietic cells (Nakano *et al*., 1994), neuronal cells (Fraichard *et al*., 1995), adipocytes (Dani *et al*., 1997), chondrocytes (Kramer *et al*., 2000) and osteoblasts (Buttery *et al*., 2001). In this way ES cells provide a useful *in vitro* model to study differentiation and development as well as the gene expression changes that accompany different lineage specification.

1.2.2.2. *In vitro* ES cell differentiation into cardiomyocytes

When ES cells differentiate, by the formation of EBs, they form different types of cells including spontaneously beating cells (Doetschman *et al*., 1985). These beating regions are made up of different types of cardiomyocytes such as sinus nodal (pace-maker-like), atrial-like and ventricular-like cells (Maltsev *et al*., 1993). These ES-

derived cardiomyocytes have similar morphology to cardiomyocytes *in vivo* and show intercalated disks and myofibrillar Z bands (Doetschman *et al*., 1985; Hescheler *et al*., 1997). They express cardiac specific genes such as *α*- and *β-cardiac myosin heavy chain* (*α-mhc* and *β-mhc*) which are expressed during cardiac development in 9 day (E9) embryos (Robbins *et al*., 1990). As ES-derived cardiomyocytes continue to differentiate they show different electrophysiological properties, as measured by patch clamp studies on isolated cardiomyocytes, and the presence of different ion channels (Maltsev *et al*., 1994) due to the presence of the different types of cardiomyocytes present. As these ES-derived cardiomyocytes share properties of early cardiomyocytes *in vivo* they provide a tool to study early cardiac development.

Within an EB only about 5 % of the cells are beating cardiomyocytes and as there is no known cell surface marker specific to cardiomyocytes isolation of a pure population of cardiomyocytes is challenging. Transgenic ES cell lines have been established to increase the numbers of cardiomyocytes able to be made and purified. (Klug et al., 1996) generated an ES cell line with the *α-cardiac myosin heavy chain* (*α-Mhc*) gene, which is expressed in all types of cardiomyocytes, linked to a neomycin resistance gene. When these ES cells were differentiated and selected with G418 only cardiomyocytes survived. Another transgenic ES cell line was established with GFP under the control of the *α-actin* promoter which resulted in all cardiomyocytes expressing GFP allowing FACS analysis of ES cell derived cardiomyocytes (Kolossov *et al*., 1998). To isolate ventricular cardiomyocytes a transgenic ES cell line with GFP under the control of the *ventricular specific myosin light chain 2V* gene (*Mlc-2v*) was established (Muller *et al*., 2000). Percoll purification and FACS resulted in a 97 % level of purification allowing subsequent analysis of these ventricular cardiomyocytes. Only about 0.2 % of the cells in the EBs were GFP positive ventricular cardiomyocytes.

ES cells have been used to study the role of genes thought to be essential in cardiac development such as the *c-JUN NH_2-terminal kinase (JNK)/ stress-activated protein kinase-associated protein 1* (*Jsap 1*). *Jsap 1* null ES cells have impaired cardiomyocyte differentiation ability as there is a significant reduction in the percentage of beating EBs formed by these null cells compared to wild type ES cells. These *Jsap 1* null ES cells also show a reduction in *Nkx 2.5* expression as well as cardiac structural genes (Sato *et al*., 2005).

1.2.2.3. *In vitro* ES cell differentiation into bone

An alternative to using Mesenchymal Stem Cells (MSCs) isolated from bone marrow to generate osteoblasts is differentiating ES cells into cells of the osteoblast lineage using the appropriate culture conditions. Media supplemented with β-glycerophosphate, ascorbic acid and dexamethasone has been shown to enhance osteoblast formation (Buttery *et al*., 2001) as well as being required for bone mineralization. ES cells co-cultured with fetal osteoblasts show enhanced osteoblast formation indicating other factors may be involved in bone formation (Buttery *et al*., 2001).

It has been reported that *Mospd 1* expression is high in mesenchymal cell types including osteoblastic MC3T3-E1 cells (Thaler *et al*., 2010) and that siRNA knockdown of *Mospd 1* in these cells results in changes in expression of genes involved in EMT. However, Thaler *et al*. (2010) did not investigate the role of *Mospd 1* in other mesenchymal cell types. ES cells can be differentiated along the osteoblastic lineage to investigate the role of *Mospd* from earlier time points. This is the advantage of using ES cells to investigate the function of genes *in vitro*.

1.2.2.4. Gene targeting using ES cells

In order to introduce changes into the genome of a cell a DNA vector and an endogenous gene can undergo homologous recombination if there is sufficient

homology between the two DNA sequences. Homologous recombination and, therefore, genetic modification in mammalian cells is possible (Smithies *et al*., 1985). Gene targeting in ES cells has the advantage of allowing functional analysis of the gene of interest. Genetically modified ES cells can be transplanted into a developing blastocyst to produce germ-line chimeric animals which when crossed can result in homozygous transgenic animals (Robertson *et al*., 1986; Gossler *et al*., 1986). This can be useful to studying the function of genes. However, sometimes the loss of a gene can be embryonic lethal and, therefore, the role of this gene at later stages cannot be studied using this system. In order to study genes such as these ES cells carrying a conditional allele are generated which are then injected into blastocysts resulting in the generation of chimaeras. Crossing of these chimaeras can then result in the generation of conditional knockout animals *in vivo* using systems such as *Cre recombinase.*

1.2.2.5. *Cre recombinase* mediated excision of a gene

Cre recombinase (*Cre*), from the bacteriophage P1 can cause site-specific recombination at lox P sites (Sauer and Henderson, 1989). Lox P sites are 34 bp sequences made up of two palindromic 13 bp sequences surrounding an asymmetric 8 bp sequence. A conditional allele is an allele where lox P sites are inserted flanking the region of the DNA sequence that is to be removed. These loxP sites are placed in a region that will not affect normal transcription of the gene, normally in an intron. These conditional alleles should express the gene of interest until exposed to *Cre* at which time recombination occurs and the lox P flanked sequence is deleted. CRE forms a dimer at lox P sites and as a tetramer it induces recombination (Figure 1.13). Upon introduction of *Cre* the lox P flanked sequence is irreversibly removed.

The deletion of the lox P flanked sequence can be done *in vitro* by electroporation of a plasmid with the *Cre* gene. Alternatively ES cells carrying the lox P flanked allele can be injected into blastocysts and transgenic mice with the floxed allele in their genome can be generated.

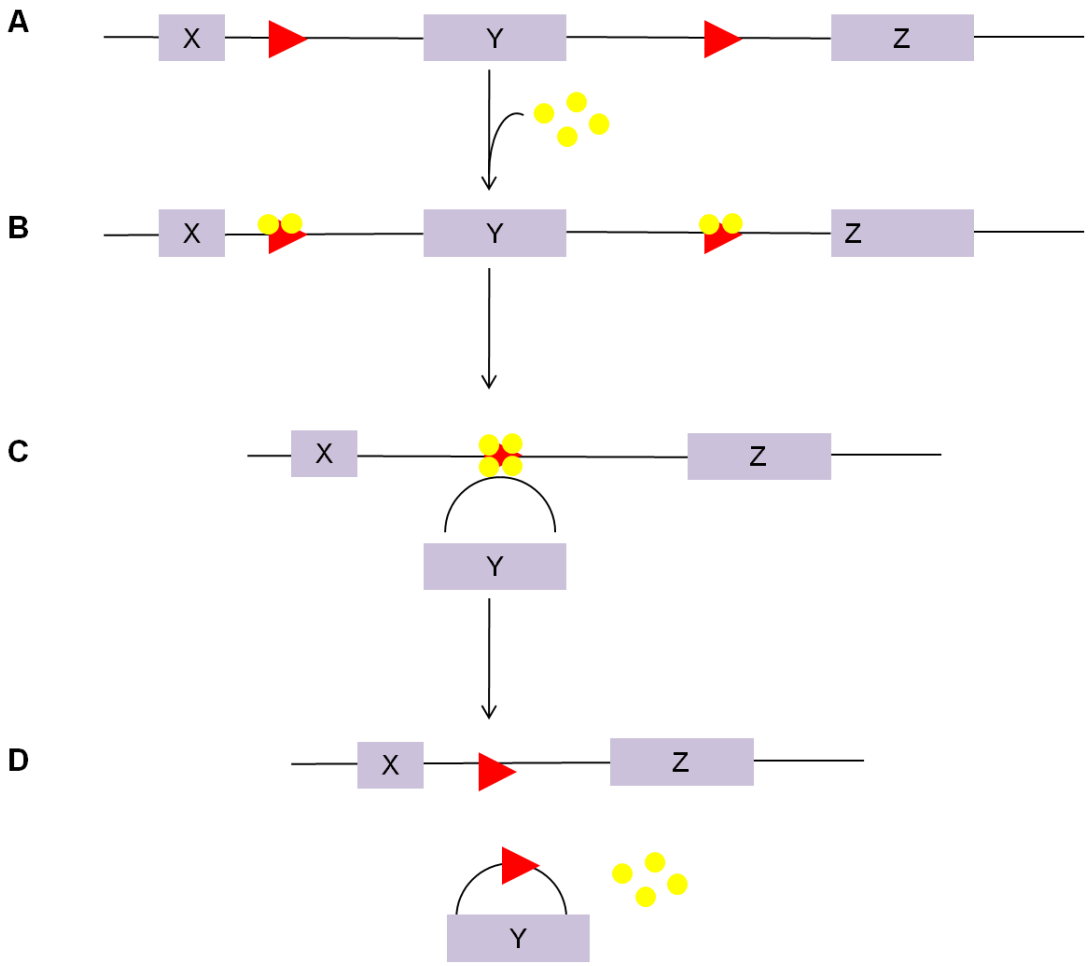

Figure 1.13: Schematic of *Cre recombinasel* loxP recombination. A: A conditional allele with lox P sites in the intron of the gene on either side of exon Y. B: Two Cre recombinase molecules bind to each lox P site. C: Exon Y is removed and D: Recombined allele showing that exon Y has been removed. Purple boxes = exons, red triangle = lox P sites, yellow circles= Cre recombinase. (Figure adapted from Cvetkovic and Sigmund, 2000).

When these mice are crossed with *Cre* expressing mice recombination at the lox P sites results in the deletion of the lox P flanked sequence resulting in offspring lacking that DNA sequence and allowing the function of the gene of interest to be studied. If the mice express *Cre* in a specific tissue it results in a deletion only in that tissue allowing the function of the gene to be studied for that specific tissue (Gu *et al*., 1994).

Inducible *Cre*-lox systems are available allowing *Cre* to be expressed at a particular time point during development. *Cre* has been shown to be able to be controlled temporally by a tetracycline responsive promoter (St-Onge *et al*., 1996). For example, to investigate the temporal requirements for the *Vascular endothelial growth factor* (*Vegf*) gene in the development of the vasculature of the retina and choroid of the eye an inducible conditional transgenic mouse line was established (Le *et al*., 2010). Tetracycline- induced mice with *Cre* under the control of the Retinal Pigment Epithelium (RPE)-specific gene *Vitelliform macular dystrophy 2* (*Vmd2*) promoter (Le *et al*., 2008) were crossed with mice carrying a conditional knockout of *Vegf*. Upon feeding doxycycline (in sucrose) to the pregnant mice *Vegf* was knocked out. This resulted in the finding that loss of VEGF at E10 or E13 resulted in the reduction of vascular density of the choroid and reduced photoreceptor function. However, loss of VEGF after E15 did not affect choroid vasculature indicating that VEGF is important prior to this time point (Le *et al*., 2010).

Another *recombinase* capable of site-specific recombination in mammalian cells is *Flp recombinase* (*Flp*) from *Saccharomyces cerevisiae* (yeast) (O'Gorman *et al*., 1991). *Flp recombinase* recognises FRT sites which consist of an 8 bp core sequence flanked by two 13 bp repeated sequences (Andrews *et al*., 1985). FRT sites can be introduced into alleles to generate conditional alleles. Both FRT and lox P sites can be introduced into DNA when generating a conditional allele to allow removal of a selection marker. For example a conditional allele of the histone methyltransferase *Smyd1* gene was generated which had an frt-neo-frt cassette in intron 1 and lox P

sites flanking exon 1 of the gene (Diehl *et al*., 2010). *Flp recombinase*- mediated deletion of the selection marker was carried out *in vivo* and the mice then crossed with mice expressing *Cre* under the control of the cardiac specific *Nkx 2.5* promoter resulting in the deletion of exon 1 of *Smyd 1* in cardiomyocytes only (Diehl *et al*., 2010).

Even though there is little knowledge of the localisation and function of MOSPD1 there are clues provided by the structure and function of MSP in nematodes and the MSP domain-containing proteins such as VAPs as well as the phenotype of the *Mospd 3* gene trap mice. The recent finding indicating a possible role in EMT in osteoblasts for *Mospd 1* (Thaler *et al*., 2010) provides another clue to the function of *Mospd 1* and this thesis aims to build on these clues to investigate both the sub-cellular localisation and function of MOSPD1 using both *in vivo* and *in vitro* systems.

1.3. Aims

- **Expression analysis**
    - Generate and test the tools required for expression analysis (specific monoclonal antibodies)
    - Assess the sub-cellular localisation of MOSPD1 and MOSPD3 to determine whether they localise to the same sub-cellular compartments
        - *in vitro* using immunocytochemistry (ICC) on human keratinocytes (HaCaTs).
        - *in vivo* using immunohistochemistry (IHC) on mouse tissue sections including ear, heart, kidney and skeletal muscle

- **Assess the function of *Mospd 1***
    - *In vivo* using zebrafish embryos
        - Assess the phenotype of embryos injected with morpholinos to knockdown *Mospd 1*
        - Measure knockdown of *Mospd 1* expression using qPCR
    - *In vitro* using ES cell differentiation
        - Generate the tools to assess the function of *Mospd 1*
            - Generate a *Mospd 1* conditional allele by targeting *Mospd 1* in ES cells
            - Generate a *Mospd 1* null ES cell line by expressing *Cre recombinase* in targeted *Mospd 1* null ES cells

- Phenotypically characterise the *Mospd 1* null clones to assess whether:
    - *Mospd 1* plays a role in ES cell proliferation and/or self renewal
    - *Mospd 1* is required for differentiation either in early differentiation, cardiomyocyte or osteoblast differentiation.
    - *Mospd 1* is involved in EMT by measuring genes involved in EMT such as *Snail, Snai2* and *Cdh11*.

CHAPTER 2:
MATERIALS AND METHODS

2.1. Molecular biology techniques

2.1.1. Transformation of bacterial cells

50 µl (1 vial) of One Shot® Chemically Competent *E. coli* (Invitrogen) was thawed on ice and 1 µl of DNA was added to the cells and gently mixed. The samples were incubated on ice for 30 minutes, heat shocked for 30 seconds at 42 ℃ and transferred back to ice for a further 2 minutes. 250 µl room temperature Super Optimal broth with Catabolite repression (S.O.C.) medium (Invitrogen) was added and the mixture was shaken at 200 rotations per minute (rpm) at 37 ℃ for 1 hour. 10- 50 µl of the transformation reaction was plated on Luria-Bertani (LB) agar -containing specific antibiotic (such as 100 µg/ml ampicillin or 50 µg/ml kanamycin) plates and incubated at 37 ℃ overnight.

2.1.2. Plasmid preparation (Minipreps and Maxipreps)

A single bacterial colony was picked and cultured in 5 ml (for minipreps and starter cultures) LB containing antibiotic or 250 ml LB (for maxipreps) containing antibiotic (such as 100 µg/ml ampicillin or 50 µg/ml kanamycin) and incubated at 37 ℃ overnight at 200 rpm in an orbital shaker. The cells were harvested by centrifugation at 6000 x g at 4 ℃ and DNA extracted using either a miniprep kit or a HiSpeed plasmid maxi kit (Qiagen).

2.1.3. DNA preparation for electroporation into ES cells

20 µg of the targeting vector was linearised with *Pme I* overnight at 37 ℃ and the digestion was subsequently phenol/ chloroform purified. An equal volume of 50:50 phenol: chloroform solution was added to the digest and the sample centrifuged at 13 000 rpm for 3 minutes in a Biofuge 13 bench-top centrifuge (Heraeus Sepatech) and the aqueous phase transferred to a fresh eppendorf. An equal volume of chloroform was added and the solution re-centrifuged. The aqueous phase was transferred to a fresh eppendorf and the DNA precipitated using ammonium acetate and isopropanol.

The pellet was washed with 70 % ethanol, dried and resuspended in 20 µl tissue grade Phosphate Buffered Saline (PBS) and stored at 4 ℃, ready for electroporation.

2.1.4. DNA extraction from ES cells

For genomic DNA extraction of ES cells grown in 96 well plates the cells were washed with 100 µl PBS/well and the cells were lysed at 55 ℃ overnight in a humidified chamber, with 50 µl/well of ES cell lysis buffer (10 mM Tris, pH 7.5, 10 mM EDTA, 10 mM NaOH, 0.5 % sarcosyl) and 1 mg/ml Proteinase K. The DNA was precipitated with 90 % ethanol and sodium chloride and left at room temperature for approximately 6-8 hours. The plates were then washed three times with 70 % ethanol, left to dry and subsequently stored at 4 ℃.

To extract genomic DNA from ES cells grown in 25 cm^2 flasks, cells were first washed with PBS and lysed at 55 ℃ overnight with 2 ml of lysis buffer (4M urea, 10 mM CDTA, 0.5 % sarcosyl, 0.1 M Tris pH8 and 0.2 M NaCl) with 1 mg/ml Proteinase K. The following day 2 ml of isopropanol was added to the lysate and the mixture rolled at 4 ℃ for 15 minutes. The precipitate of the genomic DNA was clearly visible at this point and was transferred to a fresh eppendorf and centrifuged at 13 000 rpm for 10 minutes. The pellet was washed twice with 70 % ethanol, dried and resuspended in 500 µl TE buffer and stored at 4 ℃.

2.1.5. Genomic DNA restriction digestions

For the digestion of genomic DNA from ES cells isolated in 96 well dishes a digestion reaction containing 1 x Buffer H, 1 unit/µl *Spe I* (Roche), 100 µg/ml RNase A, 1 mM Spermidine, 100 µg/ml Bovine Serum Albumin (BSA) was set up, 30 µl of the digestion mixture was added per well and the plate incubated overnight in a humidified chamber at 37 ℃. For the digestion of ES cell DNA isolated from culture flasks 20 µg DNA was digested and the volumes adjusted accordingly and the digests incubated overnight at 37 ℃.

2.1.6. Southern blots

Electrophoresis of the digested ES cell DNA samples was done on 0.7 % agarose gels with 1 x Tris-borate buffer (TBE) at 25 V overnight. The DNA was then transferred onto N+ Membrane Hybond (Amersham) overnight. The blot was probed using a 5' and 3' probe (Appendix Table 1 shows primers used to generate probe). A PCR reaction containing 100 ng template DNA, 1.5 mM $MgSO_4$, 1 x PCR buffer, 10 µM dNTPs, 10 µM each primer and 1 unit HIFI Taq DNA polymerase (Invitrogen) was set up. The PCR parameters used were 94 ℃ for 2 minutes followed by thirty cycles of 94 ℃ for 30 seconds, 55 ℃ for 1 minute, 72 ℃ for 45 seconds followed by a 72 ℃ incubation for 5 minutes and then a 4 ℃ hold. The PCR reaction was run on a 1 % agarose gel and the bands excised and purified using a Gel Extraction kit (Qiagen). 100 ng probe DNA was made up to 11 µl with distilled water, incubated at 100 ℃ for 5 minutes to denature the probe. 4 µl High Prime (Roche) was added to the probe followed by 5 µl of P^{32}-dCTP (PerkinElmer) and the probe incubated at 37 ℃ for 1 hour. The probe was filtered over a Sephadex G50 column and hybridised to the membrane in ExpressHyb hybridisation solution (BD Biosciences) overnight at 65 ˚C with rolling. The blots were washed twice with 2 x SSC/1 % SDS followed by two 15 minute washes with 0.2 x SSC/1 % SDS and then exposed to Kodak film for 3-7 days at – 80 ˚C. Autoradiographs were developed using a Konica SRX-101A developer.

2.1.7. RNA extractions from cells, tissues and zebrafish embryos and cDNA synthesis for RT-PCR

Total RNA was isolated using the RNeasy Mini kit (Qiagen) following the manufacturer's instructions. 1 µg of total RNA of each sample was reverse-transcribed using the High-Capacity cDNA Reverse Transcription kit (Applied Biosystems), which included 10 x RT buffer, 10 x RT random primers, 25 x dNTP mix (100 mM) and 50 U MultiScribe™ Reverse Transcriptase, and following the manufacturer's protocol. The parameters used were 25 °C for 10 minutes for primer annealing followed by 37 ℃ for 2 hours for reverse transcription and 85 ℃ for 5 minutes to inactivate the MultiScribe™ reverse transcriptase enzyme. A Hybaid PCR

Express machine was used to carry out cDNA synthesis and subsequent PCR reactions.

2.1.8. cDNA synthesis for qPCR

Total RNA was extracted as described above and treated with *DNAse I* to remove residual genomic DNA. cDNA was synthesised using the reverse transcription Superscript III kit (Invitrogen) which consisted of a 2x RT reaction mix and a 10x RT enzyme mix. These contained 2.5 µM oligo(dT), 2.5 ng/ µl ransom hexamers, 10 mM $MgCl_2$, 500 µM each dNTP, *Superscript III* RT enzyme and RNAseOUT. The reaction was set up with 600 ng of RNA and made up to 20 µl with nuclease-free water and incubated at 25 ℃ for 10 minutes for primer annealing, then 50 ℃ for 30 minutes for cDNA synthesis and then inactivated at 85 ℃ for 5 minutes. cDNA was stored at -20 ℃.

2.1.9. Quantitative real time reverse transcriptase PCR (q-RTPCR)

QPCR primers and probes were designed with the assistance of Dr Melany Jackson in the John Hughes Bennett Laboratory and obtained from MWG Eurofins. Table 3 in the Appendix lists the qPCR primers and probes used for gene expression analysis for zebrafish morpholino experiments described in section 2.4. Appendix Table 4 lists the primers used for gene expression analysis of bone differentiation experiments described in section 2.2.9. Appendix Table 5 shows the efficiencies of the primers. QPCR was performed on an ABI 7500 FAST qPCR machine (Applied Biosystems) using 10 ng cDNA per reaction. The house keeping gene *elongation factor 1 alpha* (*ef1α*) was used as the endogenous control for the zebrafish experiments and *hypoxanthine-guanine phosphoribosyltransferase* (*hprt*) for the bone experiments (mouse) to enable quantitation of gene expression according to the amount of cDNA loaded. For the qPCR of bone experiments SYBR green was used and a dissociation step added to the PCR. Reactions were set up in triplicate in 96 well plates. The PCR parameters were 55 ℃ for 2 minutes, 95 ℃ for 10 minutes,

followed by 40 cycles of 95 ℃ for 15 seconds to denature the cDNA and 60 ℃ for 1 minute to allow annealing and extension. Relative quantitation was calculated using the delta delta CT method using SDS v1.4 software from Applied Biosystems. Using this software the gene expression in each reaction was first normalised according to the endogenous control and the data was then shown as fold change in gene expression compared to an internal calibrator sample within each experiment.

2.1.10. Polymerase Chain Reaction (PCR) to assess gene expression

A PCR reaction contained 2 µl cDNA (served as the template DNA), 0.25 µM of each primer and 2 x PCR mastermix buffer (Promega) which contained 50 units/ml Taq DNA Polymerase in a reaction buffer (pH 8.5) with 400 µM each dNTP and 2 mM $MgCl_2$. The sequences for all primers used are given in Table 2 in the Appendix section. The PCR parameters used were a denaturation step of 94 ℃ for 2 minutes followed by thirty cycles of 94 ℃ for 30 seconds, an annealing step of 55 ℃ for 1 minute, an extension step of 72 ℃ for 45 seconds followed by a 72 ℃ incubation for 5 minutes and then a 4 ℃ hold. Individual 10 µl aliquots were analysed on a 1 % agarose gel.

2.2. Cell Culture and manipulation

2.2.1. Cell lines

Human keratinocytes (HaCaTs) (Boukamp *et al*., 1988) were obtained from Dr Nick Hole, University of Durham and the HUVEC/Hybridoma cells from Dr Robin Barclay, University of Edinburgh. COS 7 (monkey kidney cells) cells and E14 IV ES cells were from laboratory stocks.

2.2.2. Cell culture

All cell types were stored at -140 ˚C. Cells were thawed rapidly in a 37 ˚C water bath and added to 9 ml of pre-warmed media.

2.2.2.1. ES cell culture

ES cells were cultured in 1 x Glasgow Minimum Essential Medium (GMEM) (Gibco) supplemented with 10 % Fetal calf serum (FCS), 1 mM sodium pyruvate, 1 x non-essential amino acids (NEAA) and 0.1 mM β-mercaptoethanol. Leukaemia Inhibitory Factor (LIF) (1 in 1000 dilution) was added to the ES culture media. LIF was made by Helen Taylor and Julie Wilson by transfection of the pCAGGSLIF418 plasmid (Professor Austin Smith) in COS 7 cells and titration experiments performed to check the level of LIF required for optimal ES cell culture. New batches of FCS were tested for toxicity, and the ability to allow ES cell self-renewal and differentiation, by Helen Taylor and Julie Wilson. After thawing the cells were then centrifuged at 130 x g for 3 minutes. The supernatant was removed and the cells resuspended in 2 ml of media and added to 8 ml of media in a gelatinised 25 cm^2 flask. The flasks were incubated at 37 ˚C with 5 % CO_2 in a Galaxy incubator (Wolf Laboratories).

2.2.2.2. HaCaT and COS 7 cell culture

HaCaTs and COS 7 cells were cultured in 1 x GMEM (Gibco) supplemented with 10 % FCS, 1 mM sodium pyruvate, 1 x NEAA and 0.1 mM β-mercaptoethanol. After thawing, the cells were then centrifuged at 130 x g for 3 minutes. The supernatant was removed and the cells resuspended in 2 ml of media and added to 8 ml of media in a 25 cm^2 flask. The flasks were incubated at 37 ˚C with 5 % CO_2 in a Galaxy incubator (Wolf Laboratories).

2.2.2.3. HUVEC/Hybridoma cell culture

HUVEC/Hybridoma cells were cultured in 1x Iscove's modified Dulbecco media (IMDM) (Sigma) supplemented with 10 % Fetal calf serum (FCS), 1 mM sodium pyruvate, 1 x non-essential amino acids (NEAA) and 0.1 mM β-mercaptoethanol. After thawing the cells were then centrifuged at 130 x g for 3 minutes. The supernatant was removed and the cells resuspended in 2 ml of media and added to 8 ml of media in a 25 cm^2 flask. The flasks were incubated at 37 ˚C with 5 % CO_2 in a Galaxy incubator (Wolf Laboratories).

2.2.3. Passage of cells

Cells were passaged when they were 70-80 % confluent, generally every 2 days. The media was removed, the cells washed with pre-warmed PBS and incubated with sufficient trypsin solution (1 % trypsin, 1 % chick serum and EDTA in PBS) to cover the cells for 5 minutes at 37 ˚C to lift off the cells. In order to neutralise the trypsin the cells in trypsin solution were added to at least 5x the volume of media (FCS in the media inhibits trypsin) and centrifuged at 100 x g for 5 minutes. The cells were re-suspended with 10 ml fresh medium and a haemocytometer used to determine the cell number. 1 $x10^6$ ES cells were plated per 25 cm^2 gelatinised flask and the volume made up to 10 ml with ES cell medium including LIF. HACATs and COS 7 cells were split in a 1: 5 ratio whilst the HUVEC/HYBRIDOMA cells were split in 1: 10 ratio.

2.2.4. G418 concentration kill curve

To determine the optimal concentration of G418 to use 4 $x10^3$ wild type E14 IV ES cells were plated into each well of 6 well plates with 5 ml of media, including LIF, and incubated overnight. The following day the media was replaced with fresh media containing different concentrations (0, 100, 150, 200, 250, 300, 350, 400 μg/ml) of G418 (Geneticin, PAA) and LIF. The media was replaced daily and cells monitored to determine the optimum G418 concentration. This was defined as the minimum

amount of G418 that was required to kill all wild type E14 IV cells. 280 µg/ml G418 was used for the selection of clones.

2.2.5. ES cell electroporation

ES cells were washed with PBS, trypsinised for 5 minutes at 37 ˚C, added to media and centrifuged at 100 x g to pellet the cells. The cells were resuspended in PBS and counted. 20 µg of the *Mospd 1* targeting vector, linearised with *Pme I,* was electroporated into 3 x 10^7 cells in a 0.6 ml volume using a BIORAD gene pulser electroporator in a cuvette with a gap of 0.5 cm at 0.25 kV and 500 µF-capacitance. The electroporated ES cells were plated onto 10 gelatinised 100 mm x 20 mm plates in 10 ml ES medium plus LIF for each plate. The media was replaced the following day with ES medium plus LIF and 280 ng/ ml G418 in 9 plates. The remaining plate did not contain G418 drug selection. Media was replaced every day for approximately 10 days, until the drug resistant colonies were ready to be picked. Single ES clones were picked into 3 x 96 well gelatinised plates and grown in ES cell medium with LIF and G418 selection until most wells were confluent. The plates were then triplicate plated. Cells were washed with PBS, 30 µl trypsin solution added per well and the cells incubated at 37 ˚C for 5 minutes. 130 µl ES cell media was added per well and the cells pipetted to disaggregate clumps of cells. 50 µl of the cell mixture was added to the wells of 3 x pre-gelatinised 96 well dishes in the same order. 150 µl ES cell media, including LIF and G418, was added to the wells and the plates incubated at 37 ˚C until 70-80 % confluent. One of the triplicate plates was frozen with 10 % dimethyl sulfoxide (DMSO) in FCS and stored at – 80 ˚C. The remaining two plates were cultured until the wells were confluent to slightly overgrown and DNA was isolated from these plates.

2.2.6. Transient *Cre recombinase* expression in ES cells

5 x10^6 *Mospd 1* targeted ES cells (clone F6), were electroporated under the same conditions as above with 25 µg of the pCAGGS-Cre-IRESpuro plasmid (Ian Chambers) (Appendix Figure 4). Ten minutes after the electroporation the cells were

plated into a gelatinised 75 cm^2 flask and allowed to recover for 24 hours. The cells were then trypsinised and plated out at a range of densities from 100 to 5000 cells per gelatinised 10 cm diameter plate to ensure individual clones could be picked from plates. The cells were cultured in ES cell medium with LIF and individual clones were picked after approximately 5 days. The cells were then triplicate plated, one plate frozen and DNA was isolated from the remaining two plates.

2.2.7. ES cell self renewal

500 cells were plated per well in a gelatinised 6 well dish with ES cell medium with LIF and left overnight. The following day the media was removed, the cells thoroughly washed with PBS and fresh media added to the cells. In half of the wells the cells were cultured with LIF and the other half without LIF. After 5 days the medium was removed and the cells stained for alkaline phosphatase activity using the Alkaline Phosphatase kit (Sigma). The cells were washed with PBS, fixed with fixative (67 % acetone, 25 % citrate solution, 8 % formaldehyde) for 30 seconds and then rinsed with water. The colour substrate solution (0.02 mM sodium nitrite, 1 mg/ml Fast Red Violet alkaline solution and 0.8 mg/ ml naphthol AS-BI phosphate) was added to the wells and incubated for 15 minutes at room temperature in the dark. The cells were rinsed twice with water and the plates allowed to dry.

The alkaline phosphatase staining was analysed using an inverted Leitz Labovert microscope and the colonies scored as either stem (pink), mixed (pink and white) or differentiated (white). Pictures of colonies were taken using a digital camera (Nikon) attached to the microscope (Figure 2.1).

2.2.8. Formation of embryoid bodies (EBs) and cardiomyocyte assay

6 x10^5 ES cells were placed in a 20 ml universal tube and the volume made up to 20 ml with normal ES cell medium including LIF. 10 µl droplets (300 cells per droplet) were formed on the lid of square Petri dishes using a multichannel pipette and the lid replaced. 15 ml of sterile water was placed in the bottom of the Petri dishes to keep the hanging drops hydrated. The cells in the suspension congregate at the bottom of the droplet to form an EB. The hanging drops were cultured at 37 ˚C for 2 days and then harvested by collecting the hanging drops with a pipette and centrifuging them at 80 x g for 3 minutes. The EB pellet was resuspended with 20 ml media and transferred into bacteriological dishes (Figure 2.2). Penicillin/streptomycin were added to the medium on the day of harvesting the EBs to prevent any bacterial contamination. No LIF was added to the medium to allow the cells to differentiate. The media was changed every 2 days and the EBs collected for experiments, washed with PBS and stored at -80 ˚C. To set up cardiomyocyte assays individual day 5 EBs were plated in gelatinised 24 well dishes and observed every day for 10 days to check for regions of beating cardiomyocytes.

To prepare cells for immunocytochemistry, EBs were disaggregated by incubating them in 1 ml of PBS and 1 ml of *Dispase* including 20 µl *DNAse I* for 15 minutes with gentle shaking. The EBs were then passed through a needle (23 gauge) and media added to the cells to neutralise the *Dispase*. The cells were spun down at 100 x g for 5 minutes, plated on gelatinised dishes and incubated at 37 ˚C for 2 days prior to fixation and immunostaining.

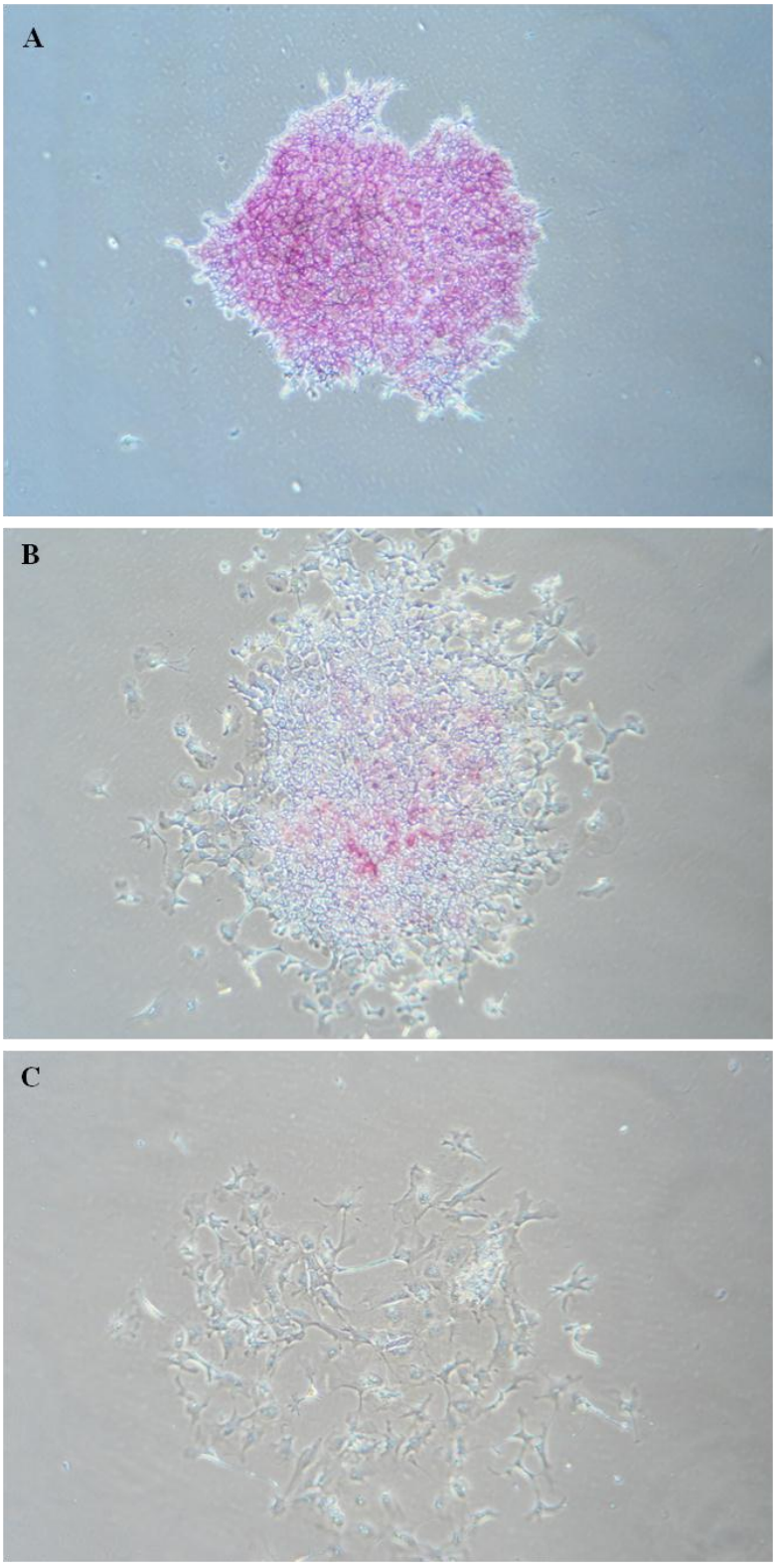

Figure 2.1: Colonies formed in ES cell self renewal assay. Cells were stained for alkaline phosphatase activity A: Undifferentiated colony (stem) was pink; B: Mixed colony with pink and white staining C: Differentiated colony containing no stained cells. All pictures were taken at x 10 magnification.

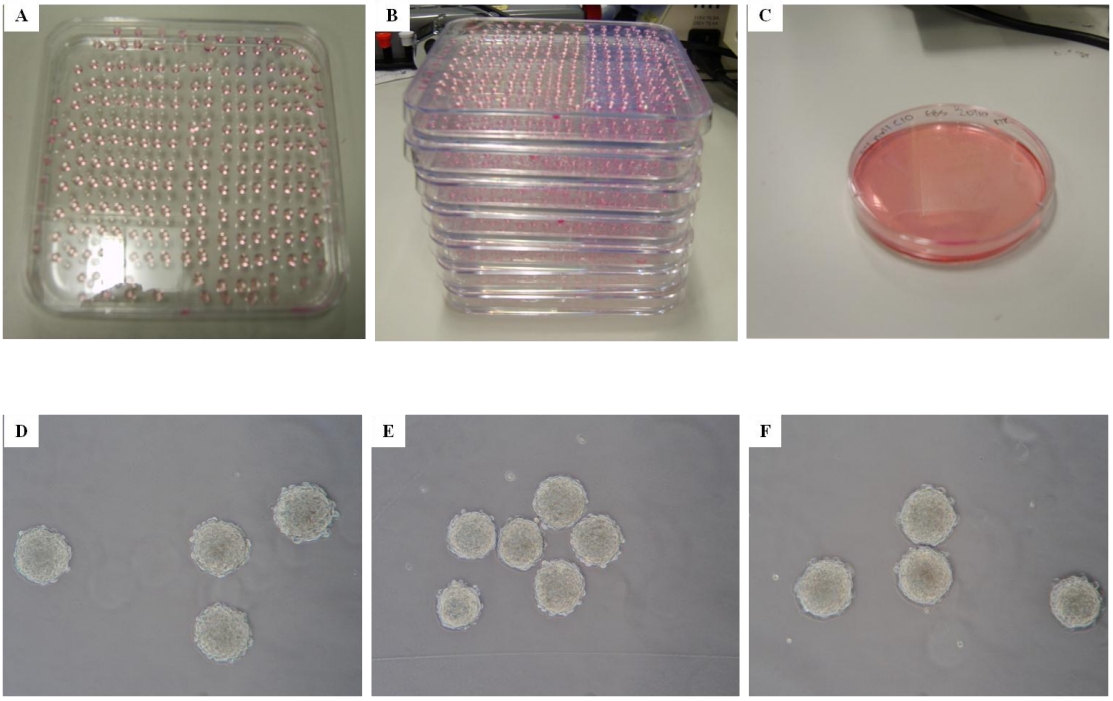

Figure 2.2: Differentiation of ES cells into embryoid bodies (EBs). 10 µl droplets, containing 300 cells, were formed on the lid of a square Petri dish (A) until all 20 ml of media containing ES cells were used to form droplets (B). After 2 days the EBs were harvested and cultured in a petri dish (C). D-F shows wild type, *Mospd 1* null C10 and C11 EBs, respectively (x10 magnification) on the day of harvesting (day 0).

2.2.9. Differentiation of ES cells into bone

Hanging drops were set up as described in section 2.2.8. for wild type E14 IV ES cells and *Mospd 1* null clones C10 and C11. On the day after the EBs were harvested the EBS were plated on gelatinised 75 cm^2 flasks and cultured in ES cell medium excluding LIF for 4 days. The cells were lifted by incubation with trypsin for 5 minutes at 37 ˚C and 5 x 10^4 cells were plated in each gelatinised well of a 6 well culture plate. 6 plates with 2 wells per cell line were set up for each experiment. Three biological triplicate experiments were performed. The cells were cultured in Alpha MEM (Invitrogen) including 15 % FCS, 0.05mM β-mercaptoethanol, and 2 mM glutamine. From Day 19 to the end of the experiment (Day 26) the cells were cultured with media supplemented with 50 mM β- glycerophosphate, 50 µg/ml ascorbic acid and 1 µM dexamethasone.

Cells were collected at Day 12, 19 and 26 for RNA extraction and subsequent qPCR analysis. At days 12, 19 and 26 one plate was stained to check for differentiation. Firstly, cell culture medium was aspirated, the cells washed twice with PBS and fixed with ice-cold 70 % ethanol at room temperature for 1 hour. The ethanol was removed and the cells washed twice with water and 500 µl/ well 10 mg/ml Alizarin Red (Sigma) was added and the plate incubated at room temperature in the dark for 1 hour. The cells were then washed with PBS for 30 minutes and left to dry overnight. All the stained colonies were counted in each of the wells. The 2 wells per cell line that had been stained were counted as a technical replicate and each of the three biological replicates were counted giving an n =3.

2.2.10. Karyotyping of ES clones

10 µl/ml KaryoMax (Colcemid, Invitrogen) was added per 25 cm^2 flask of ES cells, to arrest cells at metaphase of mitosis, and incubated at 37 ˚C for 3 hours. The cells were then trypsinised, pelletted and resuspended slowly in 8 mls pre-warmed hypotonic 0.075 M KCl solution. The cells were incubated at 37 ˚C for approximately 12 minutes and 2 ml of fresh fixative (3:1 v/v methanol/ acetic acid solution) subsequently added. The cells were re-pelletted, the KCl and fixative

treatment repeated a further two times and the cells were dropped onto glass slides. The slides were allowed to dry and stored at room temperature. The slides were stained with 1 µg/ml DAPI (Sigma) and viewed on a Zeiss Axioskop2 microscope using a 63x objective lens. Approximately 30 spreads were photographed using a ProgRes C14 camera from Jenoptik and the numbers of chromosomes per cell counted.

2.2.11. Transfection of DNA into cells

A pCMV6-AN-GFP vector containing the *Mospd 1* gene (Appendix Figure 5) was obtained from Origene (USA) and transformed, cultured and DNA obtained. *Mospd 3* had previously been cloned into the eGFP vector (Appendix Figure 6) by Dr Richard Axton in the lab. pEYFP-Nuc and pDSRed2-ER plasmids (Appendix Figure 7 and 8, respectively) were a kind gift from Dr Paul Skehel (University of Edinburgh).

To generate GFP- tagged proteins for use in western blots the MOSPD1-GFP and MOSPD3-eGFP plasmids were individually transfected into COS 7 cells using Lipofectamine 2000 (Invitrogen). On the day prior to transfection 2 $x10^5$ cells were plated per well of a 6 well dish so that cells were 90-95 % confluent at the time of transfection. 4 µg DNA was diluted in 50 µl of media lacking FCS (serum free) whilst 10 µl Lipofectamine 2000 was added to 40 µl of serum free medium and incubated at room temperature for 5 minutes. The DNA and Lipofectamine 2000 were mixed together and incubated for 20 minutes at room temperature. The DNA/Lipofectamine complexes were added to the cells in 2 ml COS 7 media containing 10 % FCS. The following day 3 ml of medium was added to each well and the cells incubated at 37 ˚C for a further 2 days. Untransfected COS7 cells and eGFP transfection served as controls.

As the human keratinocytes (HaCaTs) were unable to be successfully transfected using Lipofectamine 2000 a different transfection agent, Xfect^{TM} (Clonetech), was used. On the day prior to transfection 0.5 x10^5 cells per well of a 24 well dish were plated. 1 µg DNA was diluted in 25 µl of Xfect buffer and 0.3 µl of Xfect polymer diluted in buffer. The DNA and polymer solution were added to each other, mixed thoroughly and incubated at room temperature for 10 minutes. This mixture was added to 250 µl media in the wells and the cells incubated at 37 ˚C. After 4 hours the media was changed and the cells incubated for a further 2 days.

2.2.12. Preparation of cells for immunocytochemistry (cell synchronisation)

Human keratinocytes (HaCaTs) were grown to 70 % confluency and a double 2 mM thymidine block was performed to synchronise the cells at S phase. Thymidine was added, to a final concentration of 2 mM, to growing HaCaT cultures and incubated for 17 hours. The thymidine-containing media was removed, the cells thoroughly washed with PBS and fresh medium added for 10 hours. The media was replaced with media containing 2 mM thymidine and the cells incubated for a further 17 hours. The media was removed and the cells thoroughly washed with PBS and media lacking thymidine was added to the cells. Cells collected immediately after the second thymidine treatment (time 0), were at S phase. Cells collected at 8, 9 and 11 hours post thymidine block, were predicted to be at G2, M and G1 phases, respectively.

2.2.13. Culture of antibody-producing hybridoma cells

The hybridoma cells were cultured in RPMI-1640 media (Invitrogen) supplemented with 10 % heat inactivated fetal calf serum (FCS) and 2 mM L-glutamine. The cells were cultured with 100 Units penicillin-100 µg/ml streptomycin. A 75 cm^2 culture flask was set up with individual hybridoma clones and 40 ml of media added. The cells were then cultured for 2 weeks at 37 ˚C with 5 % CO_2 without changing the

media. After 2 weeks the media was collected by pelletting the cells and collecting the supernatant. This supernatant, containing either α-MOSPD1 or α-MOSPD3 antibodies was stored at -20 ˚C and working aliquots at 4 ˚C. Stocks of the individual hybridoma clones were increased by freezing 5 x 10^6 cells in 10 % DMSO in FCS. The cells were frozen at – 80 ˚C overnight and then transferred to -140 ˚C for long term storage.

2.3. Protein Analysis

2.3.1. Generation of mouse monoclonal antibodies

Monoclonal α–MOSPD1 and α–MOSPD3 specific antibodies were generated by Yorkshire Biosciences against chemically synthesised peptides. The MOSPD1 peptide (MHQQKRQPELVEGNLPVFVF) and MOSPD3 peptide (MRRGAPQDQELVGPGAPGRG) were synthesised by Thistle Research, Glasgow. Hybridoma clones were pre-screened to determine which clones would be optimal for detection of MOSPD1 or MOSPD3. Cell lysates of COS 7 cells, transfected with either the MOSPD1-GFP or MOSPD3-GFP plasmid (described in section 2.2.11), were used in western blots and blots were probed with the different hybridoma clones' supernatants. Hybridoma clones' supernatants were also used to probe western blots with adult mouse heart tissue lysates and the clones with the fewest bands and lowest level of background were chosen for expansion and subsequent use. A growing flask of each clone of hybridomas was received, one clone (C9) for α-MOSPD1 and 2 clones (E1 and E4) for α-MOSPD3.

2.3.2. Antibody isotype determination

A mouse monoclonal antibody isotyping test kit (AbD Serotec) was used to determine the isotype of each monoclonal antibody clone. Briefly, the supernatant was diluted to approximately 1 µg/ml in 1 % w/v BSA in PBS. 150 µl of this diluted supernatant was added to each development tube containing coloured microparticles, briefly vortexed and incubated for 30 seconds at room temperature. An isotyping

strip was placed into each development tube and after approximately 10 minutes blue bands appeared on the strip indicating the heavy and light chain composition.

2.3.3. Protein extraction from cells and animal tissues

The cells were washed with PBS and ice cold RIPA buffer (25 mM tris-HCl, pH 7.6, 150 mM NaCl, 1 % NP-40, 1 % sodium deoxycholate, 0.1 % SDS) (ThermoScientific, UK), containing protease inhibitors (Sigma), added to each well and the cells scraped using a cell scraper. The cell lysates were transferred into fresh eppendorfs and passed through a 19G needle to shear DNA and reduce the viscosity. Mouse tissues were dissected and to remove excess blood were washed in ice-cold PBS, containing protease inhibitors. The tissues were homogenised in RIPA buffer, containing protease inhibitors, using metal beads in a Retsch MM301 homogeniser and subsequently centrifuged to pellet cell debris. The lysate was transferred to a fresh tube and sonicated at a setting of 50 % with 4 x 5 second pulses using a Philip Harris Scientific sonicator. The samples were stored at – 20 ˚C.

2.3.4. Gel electrophoresis and western blotting

Protein samples were separated by 1D SDS/ polyacrylamide gel electrophoresis (PAGE) on a 12 % Tris-HCl gel (Bio-rad) and run alongside Kaleidoscope Prestained standards (Bio-Rad). 10 % (v/v) β-mercaptoethanol (Sigma) was added to the protein samples and the samples were heated at 100 ˚C for 5 minutes prior to loading. Gels were run at 80 V for approximately 2 hours with 1 x running buffer (25 mM Tris, 192 mM glycine and 0.1 % SDS) and then semidry electrotransfer onto nitrocellulose membranes was performed at 15 V for 1 hour with cold transfer buffer (25 mM Tris, 192 mM glycine and 20 % methanol. The blots were then blocked for 1 hour with 5 % dried milk powder (Marvel) in 1 x TBST (25 mM Tris-HCl, pH 8.0, 125 mM sodium chloride, 0.1 % Tween 20) before hybridisation with the primary antibodies in blocking solution overnight at 4 ℃. Table 2.1 lists the concentrations the primary antibodies were used at.

Primary Antibody	Concentration of primary antibody in blocking solution	Manufacturer	Secondary antibody (AlexaFluor 488 or 594)
α-MOSPD1	1: 100	-	α-mouse
α-MOSPD3	1: 100	-	α-mouse
α-GAPDH	1:2000	Abcam	α-mouse

Table 2.1: Antibodies used for western blots. Primary antibodies are listed with the concentration the antibody was used at, the manufacturer of the antibody and the secondary antibody used for detection. α-MOSPD1 and α-MOSPD3 antibodies were supernatants from the antibody producing hybridoma clones.

After 3x 15 minute washes in TBST the membranes were incubated with Horseradish -conjugated secondary antibody (α-mouse) (1:2000) for 1 hour at room temperature. Equal parts of ECL solution A (0.1M Tris pH 8.6, 25 mM luminal, 0.4 mM coumaric acid) and solution B (0.1 M Tris pH 8.6 and 0.02 % hydrogen peroxide) were mixed and added to the western blot which was exposed to light-sensitive film (Kodak) to visualise the antibody-antigen reactions.

2.3.5. Propidium iodide (PI) staining and flow cytometry to determine cell cycle stage

HaCaT cells were washed with PBS, trypsinised to lift the cells off the tissue culture flask and 1 x 10^6 cells collected, washed with PBS, resuspended in 70 % ethanol and stored at -20 ℃ until staining. The cells were pelletted at 400 x g for 5 minutes in a 4K15 centrifuge (Sigma Laboratory Centrifuges), the pellet was resuspended in 300 µl propidium iodide (PI) solution (50 µg/ml PI, 100 µg/ml *RNAse* in PBS) and the cells stained for 1 hour at room temperature in the dark. The samples were analysed using flow cytometry (BD Facs Calibur) which was carried out under the guidance of Shonna Johnston using the flow cytometry facilities at the Centre for Inflammation Research, Queen's Medical Research Institute, University of Edinburgh. Unsynchronised cells were used to set the cell cycle stages. The data was analysed using FlowJo Flow Cytometry Analysis Software (v7.6.1, Tree Star, Inc., USA).

2.3.6. Preparation of tissue sections for immunohistochemistry

Tissues were washed with ice-cold PBS several times to remove excess blood. Tissues were fixed with 4 % paraformaldehyde (PFA) overnight at 4 ℃ and transferred to 70 % ethanol and taken to be processed and sectioned by the Histology Core of the QMRI on a Leica TP 1050 processor. The tissues were dehydrated in an ethanol series, cleared using xylene and embedded in molten paraffin wax. 5 µm sections were cut on a paraffin microtome, floated onto a heated water bath and lifted

onto superfrost plus microscope slides. Slides were dried in a warm air oven at 50 ℃ overnight.

2.3.7. Immunocytochemistry (ICC)

Cells were grown on glass coverslips in 24 well plates, washed with PBS and fixed with 4 % PFA in PBS for 10 minutes at room temperature, followed by 3 x 5 minute PBS washes. Samples were incubated with PBS containing 0.1 % Triton X-100 for 5 minutes to permeabilise the cells. Samples were then washed with 0.001 % Tx-100/PBS (PBST) and blocked with 5 % donkey serum (Sigma)/PBST for 1 hour at room temperature. Isotype controls (IgG2b and IgG1) (Sigma and R&D Systems, respectively) served as negative controls. Primary antibodies (listed in Table 2.2) were diluted in blocking solution and incubated at 4 ℃ overnight in a humidified chamber. 3 x 5 minute PBST washes were applied to the samples followed by incubation with a 1: 200 dilution of secondary antibodies for 1 hour at room temperature in the dark. 1μg/ ml DAPI was included with the secondary antibody. After 3 x 5 minute PBST washes coverslips were mounted on glass microscope slides using a drop of Prolong Gold mounting medium (Invitrogen) and left overnight in the dark at room temperature to cure. The slides were subsequently stored at 4 ℃ in the dark.

2.3.8. Immunohistochemistry (IHC)

Sections were dewaxed by incubating the slides in xylene twice for 5 minutes and subsequently rehydrated through a series of ethanol (100 %, 95 %, 70 %) washes for 20 seconds each and the slides then rinsed in tap water. Antigen retrieval was carried out by pressure cooking the slides for 5 minutes in 0.01 M citrate buffer (Sigma). The slides were rinsed with tap water and the endogenous peroxidases were blocked by incubating the slides with 3 % hydrogen peroxide (Sigma) in methanol for 30 minutes at room temperature. The slides were rinsed with tap water, washed with 0.05 M Tris buffered saline (TBS). To reduce background caused by endogenous mouse IgG, samples were blocked with Rodent Block M (Biocare Medical) for 30 minutes at room temperature.

Primary Antibody	**Concentration of primary antibody in blocking solution**	**Manufacturer**	**Secondary antibody (AlexaFluor 488 or 594)**
α-MOSPD1	4:5	-	α-mouse
α-MOSPD3	4:5	-	α-mouse
α-Junction Plakoglobin (JUP)	1:5	Progen	α-mouse
α-Plakophilin-2 (Pkp2)	1:2	Progen	α-mouse

Table 2.2: Antibodies used for immunocytochemistry. Primary antibodies are listed with the concentration the antibody was used at, the manufacturer of the antibody and the secondary antibody used for detection. α-MOSPD1 and α-MOSPD3 antibodies were supernatants from the antibody producing hybridoma clones.

Sections were blocked with streptavidin (Vector) for 15 minutes at room temperature, washed with TBS and blocked with biotin (Vector) for 15 minutes at room temperature followed by two 5 minute TBS washes. Primary antibodies were diluted in Bond antibody diluent (Leica) and incubated on slides in a humidified chamber overnight at 4 ℃.

The slides were washed twice in TBS for 5 minutes each and mouse on mouse polymer HRP (Biocare Medical) added to the slides and incubated for 30 minutes at room temperature. The slides were washed twice in TBS for 5 minutes each and 3, 3'-Diaminobenzidine (DAB) added to the sections. The sections were monitored for colour changes and slides washed with tap water after colour developed (approximately 2 minutes). The slides were counterstained with haematoxylin, dehydrated through an ethanol series (70 %, 95 %, 100 %), treated with xylene and mounted in Pertex. The slides were dried and pictures taken on an Olympus AX70 microscope with an AxioCam HRc camera (Zeiss).

2.3.9. Fluorescence microscopy

Fluorescence microscopy was performed using an Eclipse Ti inverted fluorescence microscope (Nikon, Japan) and the software used to collect the images was Velocity (Improvision, UK). Confocal microscopy was performed in the Confocal and Advanced Light Microscopy (CALM) Facility in the Centre for Inflammation Research under the guidance of Shonna Johnston using a Leica TCS SP5 inverted confocal laser scanning microscope (Leica, UK). A 63x oil immersion objective was used. The 405 Blue Diode Laser was used to visualise DAPI staining, the argon laser, at a setting of 30 %, to visualise FITC and AlexaFluor 488 staining and the Helium Neon 2 laser for AlexaFluor 594 staining. The percentage of laser output for each laser was 70 % for the 405 blue diode, 15 % for the Argon laser and 50 % for the Helium Neon 2 laser. The Leica SP5 confocal microscope is equipped with 3 photo multiplier tubes (PMTs) allowing 3 different spectral channels to be recorded at the same time.

However, as this could result in cross talk the samples were scanned with a simultaneous scan of DAPI and AlexaFluor 594 samples and then a sequential scan of FITC or AlexFluor 488 samples. The slits of the spectroscopic detection unit can also be adjusted to reduce cross excitation of the lasers. Figure 2.3 shows the settings of the emission spectrum of DAPI and the secondary antibodies used and slits used in confocal experiments. The slits for collection of DAPI were 410-480 nm whilst the slits for AlexaFluor 488 were 495-575 nm and for AlexaFluor 594 were 600-765 nm. The smart offset was set at 1 % per turn and the final image acquired was an average from 2 scans. The image resolution was 1024 x 1024 pixels and the pin hole setting was 1 Airy unit. Images were converted to colour and merged using Image J (National Institute of Health, USA).

2.4. Zebrafish

2.4.1. Zebrafish husbandry

Wild type Golden zebrafish embryos were maintained in a Z-plex stand alone aquarium system (Aquatic habitats, Florida, USA) in the Queen's Medical Research Institute, University of Edinburgh Zebrafish Facility and raised and maintained according to Lawrence, 2007. The golden strain has a defect in melanocyte development and is, therefore, less pigmented and useful for observing early organ development *in vivo*. For the purposes of the project the golden strain was used as a wild type strain. Zebrafish were kept in a 14 hour light 10 hour dark cycle. The adult zebrafish were fed twice daily with commercial zebrafish diet (ZM-300, Advanced Fish Diets) and with live 24 hour old *artemia* (brine shrimp) by the Zebrafish Facility staff.

2.4.2. Collection of zebrafish embryos (marbling)

Zebrafish were marbled (according to Westerfield, 2007) and the embryos collected the following morning after the lights were switched on.

A

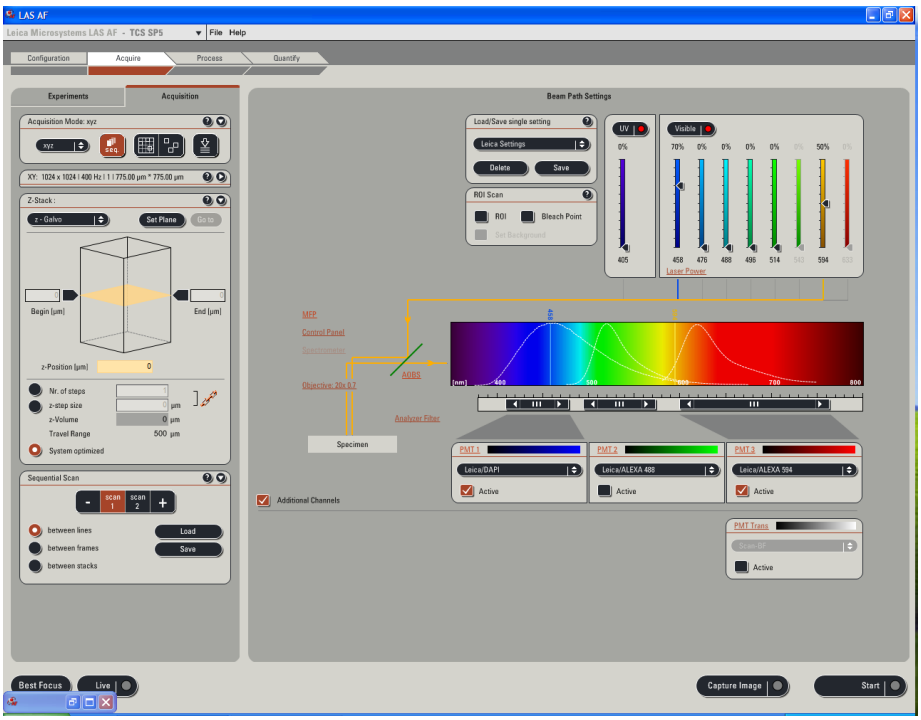

B

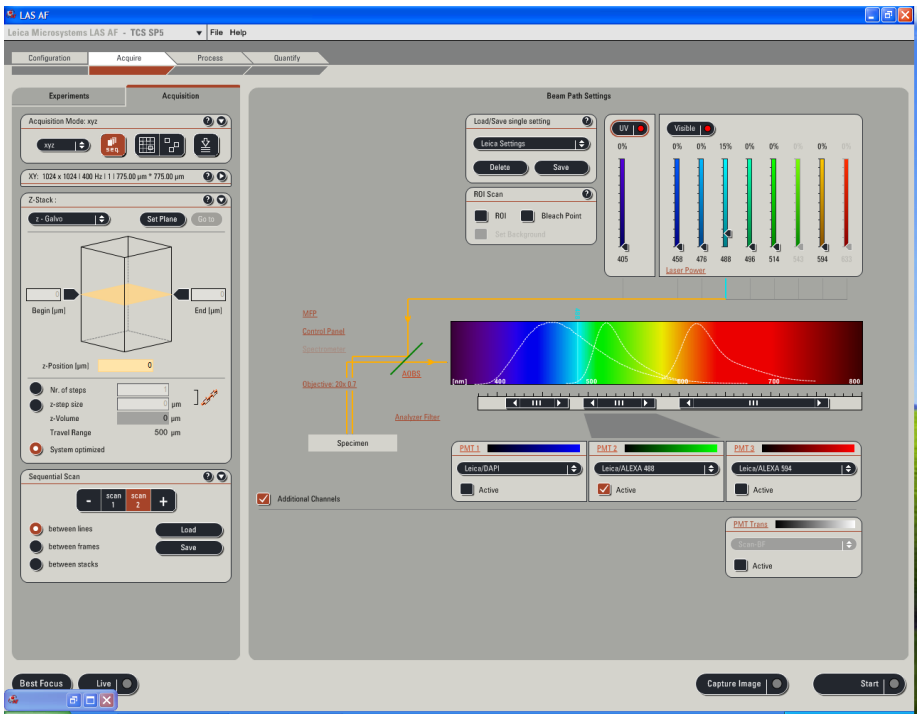

Figure 2.3: Confocal microscope settings. A: Settings for Scan 1, the simultaneous scan of DAPI and AlexaFluor 594 samples with the laser output for the 405 blue diode laser at 70 % and 50 % for the Helium Neon 2 laser. B: Scan 2, the sequential scan of FITC or AlexFluor 488 samples with the laser output for the Argon laser at 15 %. The slits for collection of DAPI were 410-480 nm, for FITC or AlexaFluor 488 were 495-575 nm and for AlexaFluor 594 were 600-765 nm to prevent cross excitation and emission.

The light induces the zebrafish to mate and the female fish lay their eggs in the marbles which are then fertilised by the male fish. The embryos fall through the mesh and are collected in the bottom container. The collected embryos were then placed in a petri dish containing water with dilute methylene blue, which prevents bacteria and fungal colonisation of the water. A maximum of 60 embryos were placed per petri dish and embryos were maintained at 28.5 ˚C in order to allow them to develop normally. Embryos can be incubated for 5 dpf for experimental use without the requirement of a Home Office Animal License.

2.4.3. Morpholino design

An anti-sense morpholino against the Start (ATG) site of the zebrafish *Mospd 1* gene (MO1) as well as a second morpholino targeted to the splice junction between exons 2 and 3 (MO2) were designed. 5 mispair controls for both the start morpholino and the splice-site morpholino were also designed to serve as negative controls. All morpholinos were synthesised by Gene tools (Oregon, USA). The morpholino sequences used are listed in Appendix Table 6). The morpholinos were 3' labelled with FITC to monitor for the oligonucleotide in injected embryos.

2.4.4. Morpholino injection procedure

The microinjection of newly fertilised eggs was performed at the 1-16 cell developmental stages using a Narishige IM300 Microinjector at an approximate injection pressure of 16 psi. Figure 2.4A shows the injection set up. A 1mm graticule with 0.01 mm divisions (Pyser-SGI Limited) was used to determine the bolus size of morpholino injected (Figure 2.4 B). The amount of morpholino injected was determined by using the radius of the injected bolus to calculate the volume of a sphere and then using the concentration of the injected morpholino.

Volume (V) of a sphere:

$$V = \frac{4}{3}\pi r^3$$

A

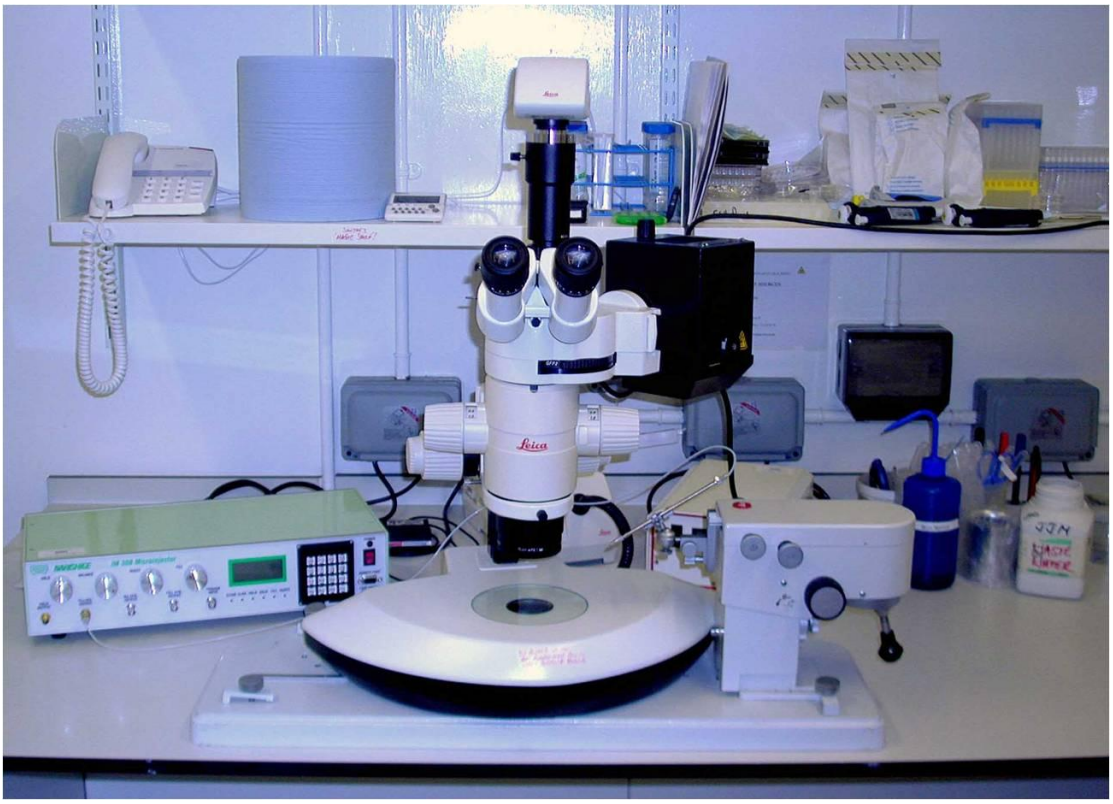

B

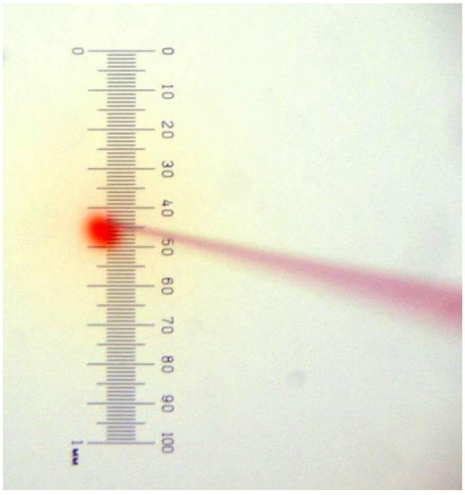

C

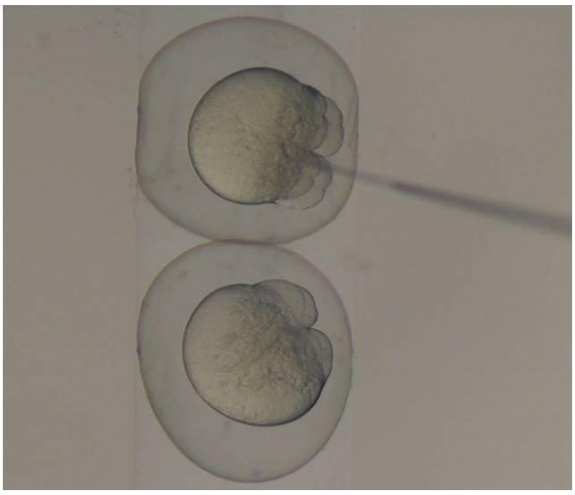

Figure 2.4: Injection of zebrafish embryos. A: the microscope and injection set up in the Zebrafish Facility. B indicates how the bolus size is determined by injecting the morpholino (phenol used in this picture to illustrate bolus size more clearly) into a drop of mineral oil placed on a graticule. C: the position of the needle in the zebrafish embryo when injecting the morpholino into the cytoplasmic streaming region (10x magnification). Pictures were taken with the assistance of Dr Carl Tucker.

Therefore, a bolus with a radius (r) of 0.05 mm resulted in a 0.5 nl volume of morpholino per injection. To increase the amount of morpholino injected to 1 nl two bursts of morpholino were injected. As both the concentration and the molecular weight of the morpholino were known the mass of morpholino injected could be accurately determined. Differing doses of morpholino (1 ng- 6ng per embryo) were injected into the cytoplasmic streaming region of embryos (Figure 2.4C). Embryos were screened with a Leica Fluo^{TM} fluorescence microscope (Leica Microsystems Ltd) to determine injection success and even distribution of the morpholino within the embryo. Embryos were checked at approximately 3-5 hours post injection to determine death or axis damage due to injection damage and these embryos removed.

2.4.5. Analysis of phenotype

Chordin knockdown experimental embryos were checked at 28 hours post fertilisation (hpf) for the published chordin phenotype (Nasevicius and Ekker, 2000). Zebrafish embryos were examined at 1, 2 and 3 days post fertilisation (dpf) for the *Mospd 1* morpholino experiments and some experiments were monitored until embryos were 5 dpf. The survival of the embryos was checked every day. The embryos were checked for body shape, presence of a heartbeat, circulation and any abnormalities, such as oedema, blood pooling and any morphological differences noted. The embryos were defined as normal if they resembled a wild type non-injected control, of mild phenotype if they had reduced circulation or body shape and severe if oedema, blood pooling, reduced heart beat and altered cardiac morphology and no circulation was present. Embryos were collected for RNA extraction and histology.

2.5. Data analysis

Quantifiable data was graphed and analysed using GraphPad Prism (version 5.00 for Windows, GraphPad Software, San Diego, California, USA). Analysis was performed on triplicate data sets unless otherwise stated.

CHAPTER 3: EXPRESSION AND LOCALISATION OF MOSPD1 AND MOSPD3 PROTEINS

3.1. Introduction

The only clue to the possible function of MOSPD1 came from a gene trap integration into the closely-related *Mospd 3* gene. There was 50 % neonatal lethality in homozygote nulls and *Mospd 3* was thought to play a role in the development of the right ventricle of the heart as neonate mice homozygous for the gene trap displayed a right ventricle defect characterized by a thinning of the right ventricle wall. This phenotype was lost upon backcrossing and it was hypothesized that there may be another genetic modifier (Pall *et al*., 2004). As *Mospd 1* is highly similar in structure and sequence to *Mospd 3* the loss of the cardiac phenotype could be due to genetic redundancy between *Mospd 1* and *Mospd 3*. The sub-cellular localization of the MOSPD proteins could give clues to their function and whether they could be genetically redundant as if MOSPD1 and MOSPD3 are not co-localised than they cannot be redundant.

Mospd 1 and *Mospd 3* have been shown to be expressed in a wide variety of tissues (Katrin Buerger, PhD thesis, 2009) by RT- PCR and *in situ* hybridisation. However, there is no information on their sub-cellular localisation. To determine whether these proteins were localized to cellular junctions, and therefore, possibly involved in desmosome structure and maintenance of tissue integrity, their sub-cellular localisation would need to be determined. There are no reported findings on the localisation of either MOSPD1 or MOSPD3 using antibodies against these proteins.

Studies using recombinant proteins can be useful to providing an idea of the localisation of the protein. A recent publication describes the localisation of MOSPD1-His transfected into MC3T3-E1 cells (Thaler *et al*., 2010). Full length MOSPD1-HIS localised to the cytoplasm, including the ER and perinuclear region, whilst a shorter version lacking the last exon of MOSPD1 localised to the nucleus. This could be due to a putative Nuclear Export Signal (NES) in the last exon of MOSPD1 due to the presence of the residues leucine, isoleucine, threonine and methionine (Thaler *et al*., 2010). We used recombinant a MOSPD1-GFP fusion

protein and MOSPD3 tagged with Enhanced-GFP (MOSPD3-GFP) to do preliminary studies on MOSPD1 and MOSPD3.

Specific antibodies are essential tools to investigate the sub-cellular localisation and tissue distribution of proteins. Peptides were designed to the 20 amino acids at the N terminal of either MOSPD1 or MOSPD3 and were designed to be specific to each. These peptides were synthesized by Thistle Research, and used to generate polyclonal antibodies against MOSPD1 and MOSPD3. These antibodies did not cross-react when tested on recombinant MOSPD1 and the MOSPD3-GFP fusion protein. However, when these polyclonal antibodies were used to test for endogenous MOSPD1 and MOSPD3 in mouse tissues there was a very high level of background making these antibodies unsuitable for use in determining the sub-cellular localisation and tissue distribution of MOSPD1 and MOSPD3 (Katrin Buerger, PhD thesis, 2009).

Antibodies that were more specific and would result in less background were required for use in immunochemistry. Monoclonal antibodies are more specific as they are generated from a single B-cell clone fused to a myeloma cell line to form a hybridoma cell line (Nelson *et al*., 2000). Supernatant from these hybridoma cell cultures can be used as a source of monoclonal antibodies. These monoclonal antibodies can then be used to assess protein distribution, localisation and to identify interacting proteins using various immunological techniques such as western blotting, immunocytochemistry and co-immunoprecipitation.

3.2. Aims

To test whether MOSPD1 and MOSPD3 could be genetically redundant:

- Assess the sub-cellular localisation of recombinant MOSPD1-GFP and MOSPD3-GFP
- Generate and test the tools required (monoclonal antibodies)
    - Generate specific monoclonal α-MOSPD1 and α-MOSPD3 antibodies.
    - Test the specificity of these monoclonal α-MOSPD1 and α-MOSPD3 antibodies using recombinant MOSPD1 and MOSPD3
    - Determine if the monoclonal antibodies could detect endogenous MOSPD1 and MOSPD3 by western blotting.
- Assess the sub-cellular localisation of MOSPD1 and MOSPD3 to determine whether they localised to the same cellular compartments
    - *in vitro* using immunocytochemistry (ICC) on human keratinocytes (HaCaTs).
    - *in vivo* using immunohistochemistry (IHC) on mouse tissue sections including ear, heart, kidney and skeletal muscle

3.3. Results

3.3.1. Localisation of recombinant MOSPD1-GFP and MOSPD3-GFP

To determine the localisation of recombinant MOSPD1 and MOSPD3 plasmids encoding MOSPD1-GFP and MOSPD3-GFP were transiently transfected into HaCaTS. A pCMV6-AC-GFP plasmid with the open reading frame of the *Mospd 1* gene cloned into it encoded MOSPD1-GFP (Origene) (Appendix Figure 5) whilst a pEGFP plasmid with the *Mospd 3* gene encoded MOSPD3-GFP (Dr Richard Axton, University of Edinburgh) (Appendix Figure 6). Not all cells expressed the transfected plasmids as transfection efficiency was only about 50 %. MOSPD1-GFP was localised throughout the cell, including the nucleus and cytoplasm whereas two distinct patterns of MOSPD3-GFP expression were observed, one where it was throughout the cell, like MOSPD1-GFP, and second some cells appeared to have more prominent MOSPD3-GFP expression in the cytoplasm compared to the nucleus as well as enhanced perinuclear localisation (Figure 3.1).

3.3.2. Strategy and testing of monoclonal α –MOSPD1 and α – MOSPD3 antibodies

3.3.2.1. Generation of mouse monoclonal antibodies

MOSPD1 and MOSPD3 share 38 % sequence homology and similar protein structure. They both have an MSP domain in the N terminal, two transmembrane domains in the C terminal and a putative Nuclear Export Signal (NES) (Figure 3.2 A and C). As these proteins are closely related any antibodies generated to test for their localisation would need to be designed so as not to cross-react. Peptides were designed by Thistle Research UK to correspond to the 20 amino acids at the N terminal of MOSPD1 and MOSPD3 (Figure 3.2 B and D) as this region has the least sequence similarity between the two closely-related proteins.

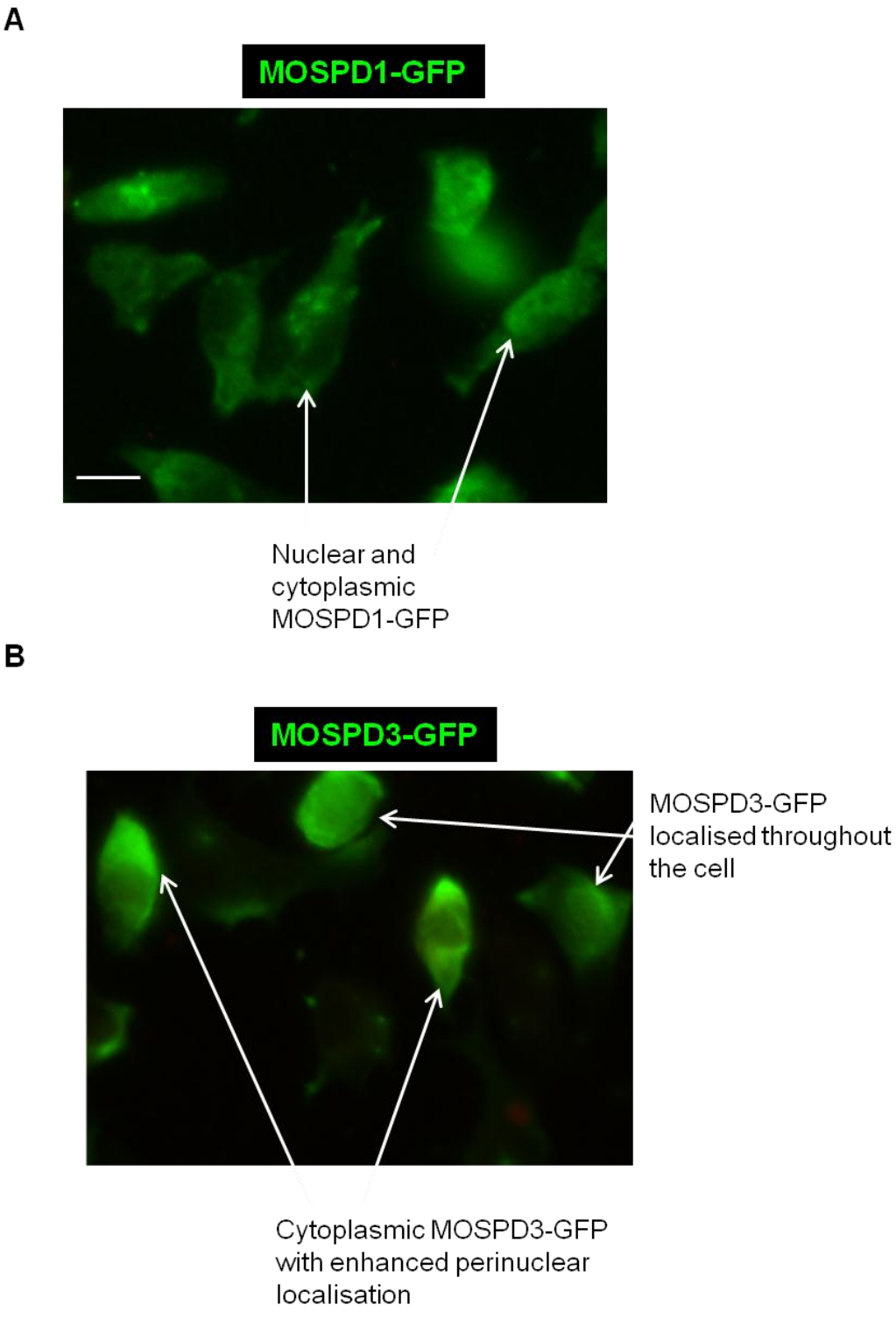

Figure 3.1: MOSPD1-GFP and MOSPD3-GFP localisation in HaCaTs. Cultured HaCaTs transfected with a MOSPD1-GFP plasmid and a MOSPD3-GFP plasmid transiently expressed MOSPD1-GFP (A) and MOSPD3-GFP (B). Scale bar =15 µm.

A

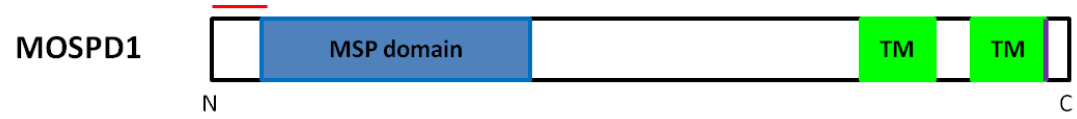

B

MOSPD1

MHQQKRQPELVEGNLPVFVFPTELIFYADDQSTHKQVLTLYNPYEFALKFK
VLCTTPNKYVVVDAAGAVKPQCCVDIVIRHRDVRSCHYGVIDKFRLQVSEQ
SQRKALGRKEVIATLLPSAKEQQKEEEEKRIKEHLTESVFFEQSCQPGKNR
AVSSGPSLLTVFLGVVCIAALMLPTLGDMESLVPLYLHLSVNQKLVAAYILGL
ITMAILRT

C

D

MOSPD3

MRRGAPQDQELVGPGAPGRGSRGSPPSSGPVVPVLVFPPDLVFRADQRS
GPRQLLTLYNPTGTALRFRVLCTAPAKYTVFDAEGYVKPQSCIDIVIRHVAP
VPSHYDVQDRFRIELSEEGTEGRVVGRKDITSVLRAPAYPLELQGHSEPTP
NPGPPVWTGLTPARHLQENAPQQLATSSFLLFLLAGVISVAFLLLPLQDELG
SQLPQVLHVSLGQKLVAAYVLGLLTMVLLRT

Figure: 3.2: Strategy to generate specific α-MOSPD1 and α-MOSPD3 monoclonal antibodies by specific peptides. A: Schematic representation of MOSPD1. B: Protein sequence of MOSPD1. C: Schematic representation of MOSPD3. D: Protein sequence of MOSPD3. Both proteins have an N terminal MSP domain (blue) and 2 C-terminus transmembrane domains (TM) (green). A putative Nuclear Export Signal (NES) (purple) is located in the last TM domain. The red lines in A and C show the relative position of the specific peptides used to generate the antibodies whilst the sequence is shown in the red box (C and D).

This should result in specific antibodies being generated against MOSPD1 and MOSPD3 which do not cross react. The peptide sequences were conjugated to the Keyhole Limpet Hemocyanin (KLH) carrier protein, by Thistle Research UK, which aids in eliciting an immunogenic response. These conjugated peptides were sent to Yorkshire Biosciences and used to generate monoclonal antibodies against MOSPD1 and MOSPD3. The conjugated peptides were inoculated into Balb/c mice. Tail bleeds and enzyme linked immunosorbent assay (ELISA) was used to select optimal mice showing an immunogenic response to the peptides. The B cells were removed from splenocytes or lymph node cells and fused to SP2/0 myeloma cells to form hybridomas. ELISA was then used to screen hybridoma clones to select highly positive clones which were then expanded, supernatant collected for further analysis of the monoclonal antibodies and cells frozen and stored.

3.3.2.2. Testing the specificity of α-MOSPD1 and α-MOSPD3 antibodies

As the α-MOSPD1 and α-MOSPD3 antibodies were going to be used to analyse the expression and sub-cellular localisation of MOSPD1 and MOSPD3 and these proteins share high sequence similarity western blot analysis was performed to assess whether the monoclonal α-MOSPD1 and α-MOSPD3 antibodies cross-react. The predicted size of MOSPD1 is 24 kDa and of MOSPD3 is 25 kDa whilst GFP is 27 kDa so the recombinant MOSPD1-GFP and MOSPD3-GFP fusion proteins, whose localisation was described in Section 3.3.1., are expected to be 51 kDa and 52 kDa, respectively. Western blots probed with the monoclonal α-MOSPD1 antibody showed a protein band (~50 kDa) in the MOSPD1-GFP fusion over expressed COS7 lysate but not in the un-transfected or MOSPD3-GFP sample (Figure 3.3). α-MOSPD3 detected the over expressed MOSPD3-GFP fusion protein (~50 kDa) but not the MOSPD1-GFP fusion protein. The α-GFP antibody detected the MOSPD3-GFP band and eGFP band (~25 kDa) from over expression of the eGFP vector but not the MOSPD1-GFP fusion protein as this is turbo-GFP, which is from the Copepod *Pontellina plumata*, and is not sufficiently similar to eGFP, from the jellyfish *Aequorea Victoria*, to be detected by the α-eGFP antibody.

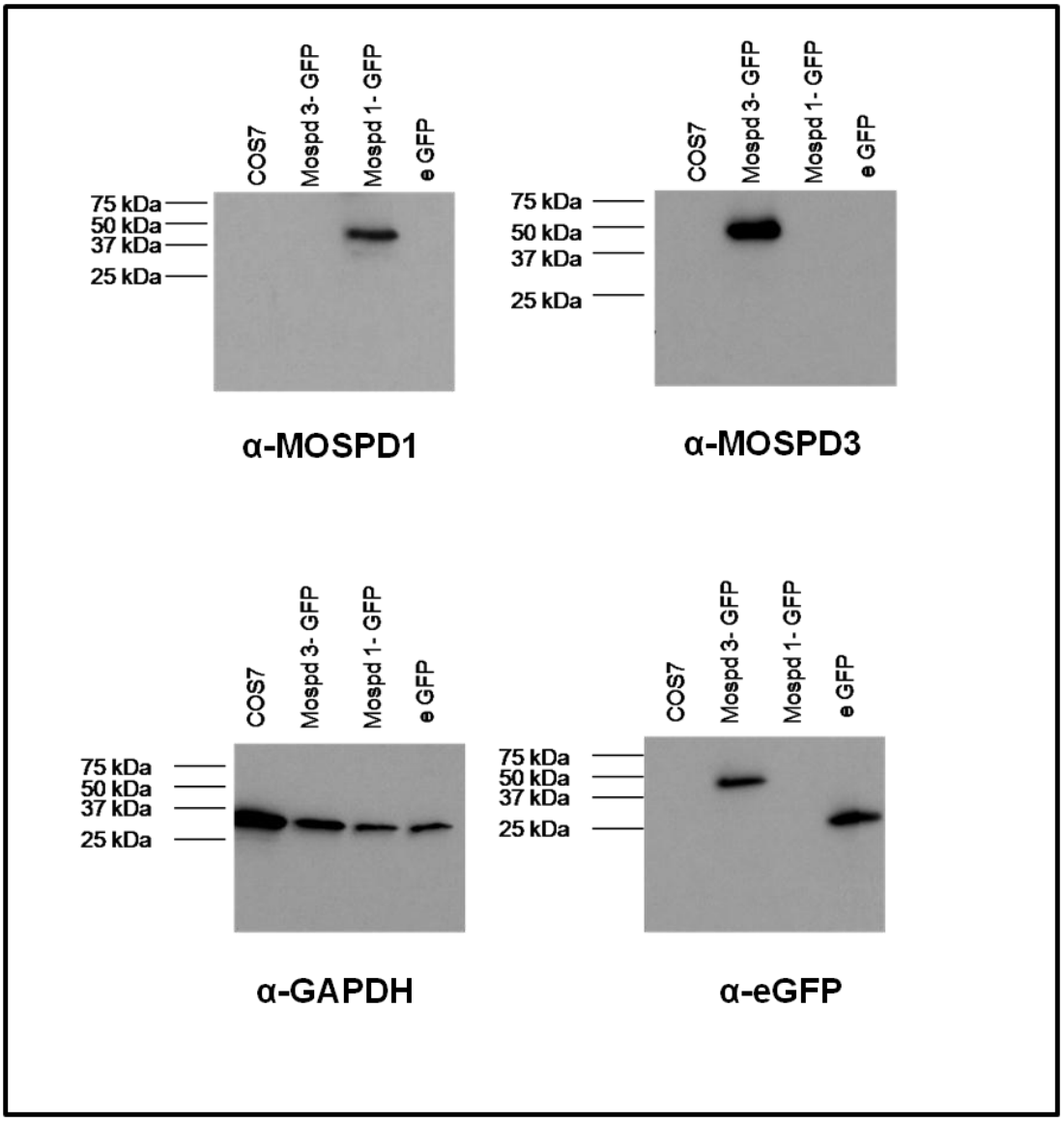

Figure 3.3: Western blot analysis to assess cross-reactivity between monoclonal α-MOSPD1 and α-MOSPD3 antibodies. The antibodies were tested on lysates from un-transfected COS7 cells and lysates from COS7 cells transfected with plasmids expressing MOSPD3-GFP (52 kDa), MOSPD1-GFP (51 kDa) or GFP (27 kDa). The western blots were probed with α-MOSPD1, α-MOSPD3, α-GFP and α-GAPDH as a loading control.

The western blots were probed with α-GAPDH to serve as a loading control. These experiments, therefore, confirmed that the monoclonal α-MOSPD1 and α-MOSPD3 antibodies are specific and do not cross-react.

3.3.2.3. Testing whether endogenous MOSPD1 and MOSPD3 could be detected using the mouse monoclonal antibodies

Previously generated polyclonal antibodies showed high levels of non-specific background staining on western blots (Katrin Buerger, PhD thesis, 2009). As a result the polyclonal antibodies were unsuitable for investigating the expression and localisation of MOSPD1 and MOSPD3 in cells and tissues. It was therefore, important we tested whether the mouse monoclonal α-MOSPD1 and α-MOSPD3 antibodies could detect specific endogenous MOSPD1 and MOSPD3, respectively.

To do this adult mouse heart tissue lysate was tested by western blot using the monoclonal antibodies as the primary antibodies (Figure 3.4). A band was observed that was the predicted size of MOSPD1 (24 kDa) in the heart sample incubated with the α-MOSPD1 antibody and a band the predicted size of MOSPD3 (25 kDa) was observed in the heart sample incubated with α-MOSPD3. Bands of 50 kDa and 75 kDa were also observed in the heart cell lysates. However, as the western blot membrane probed only with secondary α-mouse antibody also detected a 75 kDa band this band is likely due to non-specific background. The 50 kDa band was not detected by secondary antibody alone and was possibly a dimer due to it being double the size of MOSPD1 or MOSPD3. However, as only one band, of 51 kDa, was observed in western blots of MOSPD1-GFP and MOSPD3-GFP (Figure 3.3), it indicates that these MOSPD proteins may not dimerise. If they did, you would expect to observe an additional 102 kDa band from the dimerised GFP-tagged proteins on the western blot. Wild type E14 IV ES cell lysate was used as a negative control and no bands were observed in the ES cell lysates in either the α-MOSPD1 or α-MOSPD3 blots. α-GAPDH was used as a loading control and detected bands of 36 kDa corresponding to endogenous GAPDH.

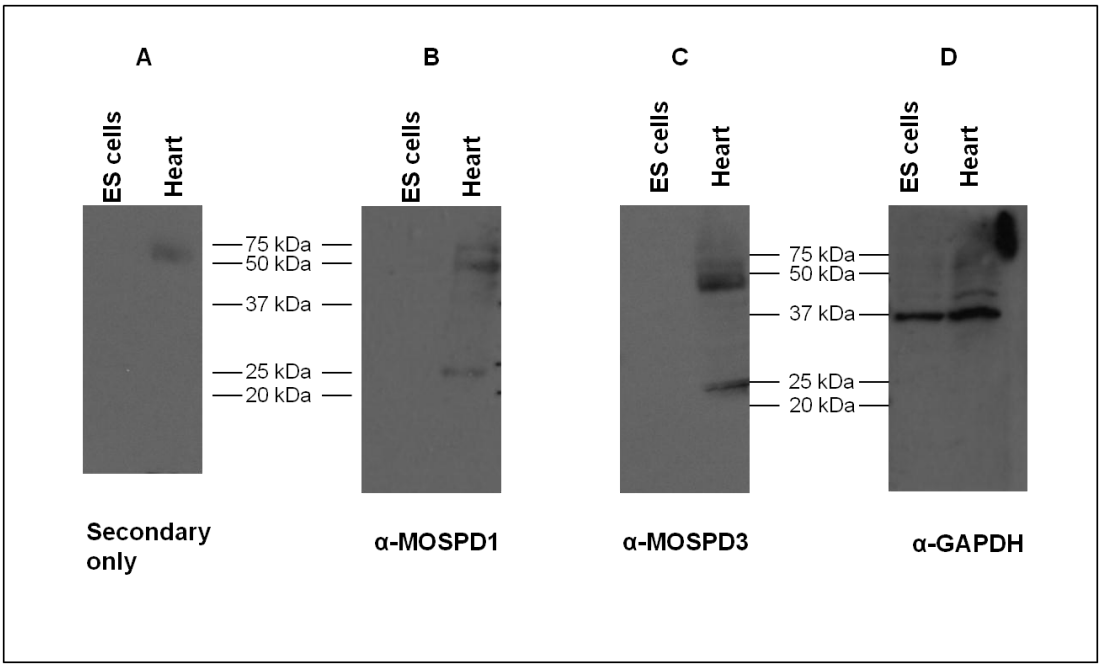

Figure 3.4: Detection of endogenous MOSPD1 and MOSPD3 by western blotting using monoclonal α-MOSPD1 and α-MOSPD3. Lysates of undifferentiated ES cells and adult mouse heart were probed with secondary antibody only (A), monoclonal α-MOSPD1 (B), to detect MOSPD1 (24 kDa), α-MOSPD3 (C), to detect MOSPD3 (25 kDa), and α-GAPDH (D) was used as a loading control.

As the western blots showed little background staining it was hoped the monoclonal antibodies could be used for immunohistochemistry to determine the sub-cellular localisation of MOSPD1 and MOSPD3. However, if the 50 kDa band observed is not due to a MOSPD dimer then it would be due to the monoclonal antibodies detecting a non-specific protein. This would call into question any results from immunocytochemistry and immunohistochemistry experiments.

3.3.3. Sub-cellular localisation of MOSPD1 and MOSPD3

3.3.3.1. Determination of whether monoclonal α-MOSPD1 and α-MOSPD3 antibodies were suitable for localisation studies

Testing for MOSPD1 and MOSPD3 expression in ES cells by western blots of ES cell lysates using the monoclonal α-MOSPD1 and α-MOSPD3 antibodies indicated that ES cells did not express MOSPD1 and MOSPD3 (Figure 3.4). *Mospd 1* null ES cells (described in Chapter 5) were chosen as the negative control for immunofluorescence detection of MOSPD1. α-MOSPD1 did not detect any MOSPD1 expression and α-MOSPD3 did not detect any MOSPD3 expression in these ES cells (Figure 3.5). These results indicated that both α-MOSPD1 and α-MOSPD3 antibodies did not detect any background staining and would be suitable for detection of endogenous MOSPD1 and MOSPD3 expression in cells expressing these proteins, such as the human keratinocytes (HaCaTs).

3.3.3.2. *In vitro* determination of the sub-cellular localisation of MOSPD1

Given that we hypothesised that the MOSPD proteins might be localised to desmosomes, we tested the localisation of a known desmosome component, PKP2, which was localised to cell junctions (Figure 3.6) of HaCaTs. Under the same growth conditions and immunocytochemistry (ICC) protocol MOSPD1 was localised to the nuclei of cells (Figure 3.7). MOSPD1 is not localised to the cell junctions and does not have the same sub-cellular localisation of PKP2. In the majority of HaCaT cells MOSPD1 was predominantly localised to the nucleus and appears to be absent from the nucleoli. The IgG2b isotype control was used as a negative control for the ICC experiments investigating MOSPD1 localisation. However, we noted different sub-cellular localisation in cells that appeared to be dividing so further investigated MOSPD1 localisation in these cells (see Section 3.3.3.4.).

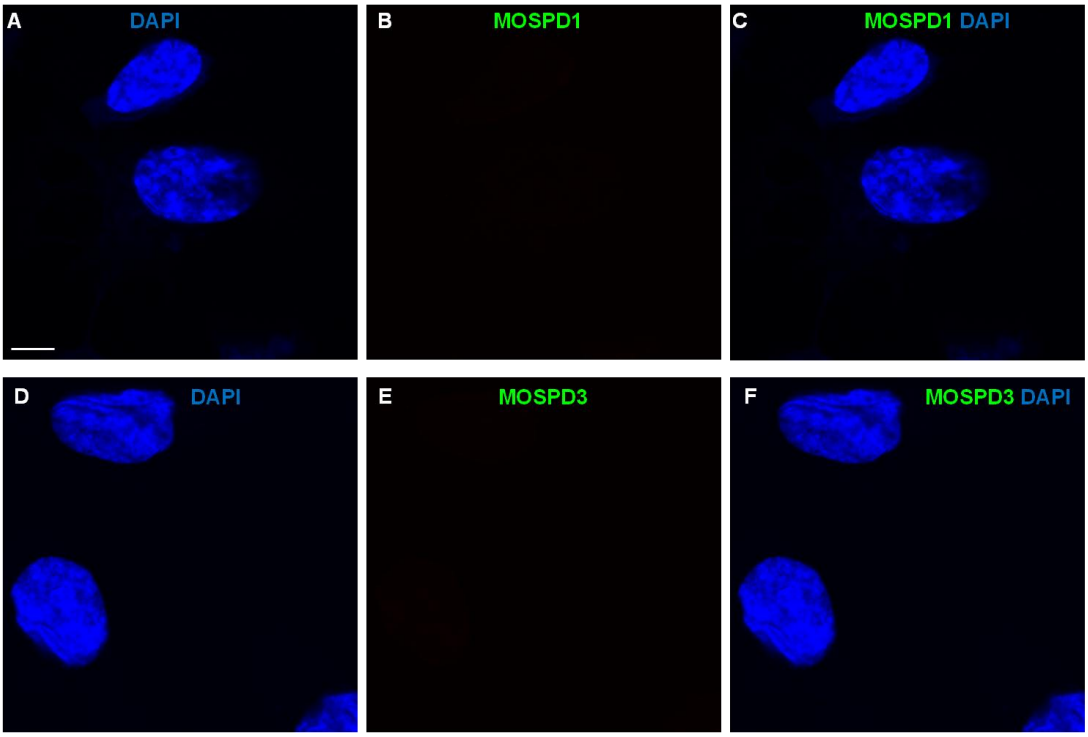

Figure 3.5: Negative control for immunofluorescence with monoclonal α-MOSPD1 and α-MOSPD3 antibodies. Immunofluorescence was carried out on *Mospd 1* null ES cells to check for MOSPD1 (B) and MOSPD3 (E) expression. DAPI was used to stain the nuclei (A and D). Merged images of MOSPD1 and DAPI (C) and MOSPD3 and DAPI (F) are shown. Scale bar = 3 µm.

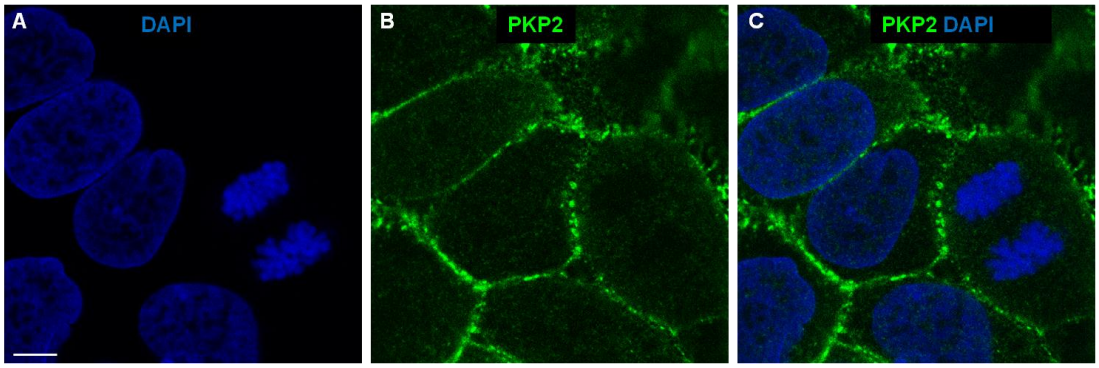

Figure 3.6: Plakophilin 2 (PKP2) localisation in desmosomes. Cultured HaCaTs were immunolabelled with an antibody against PKP2 (B) and DAPI was used to stain the nuclei (A). A merged image of PKP2 and DAPI (C) is shown. Scale bar = 4 µm.

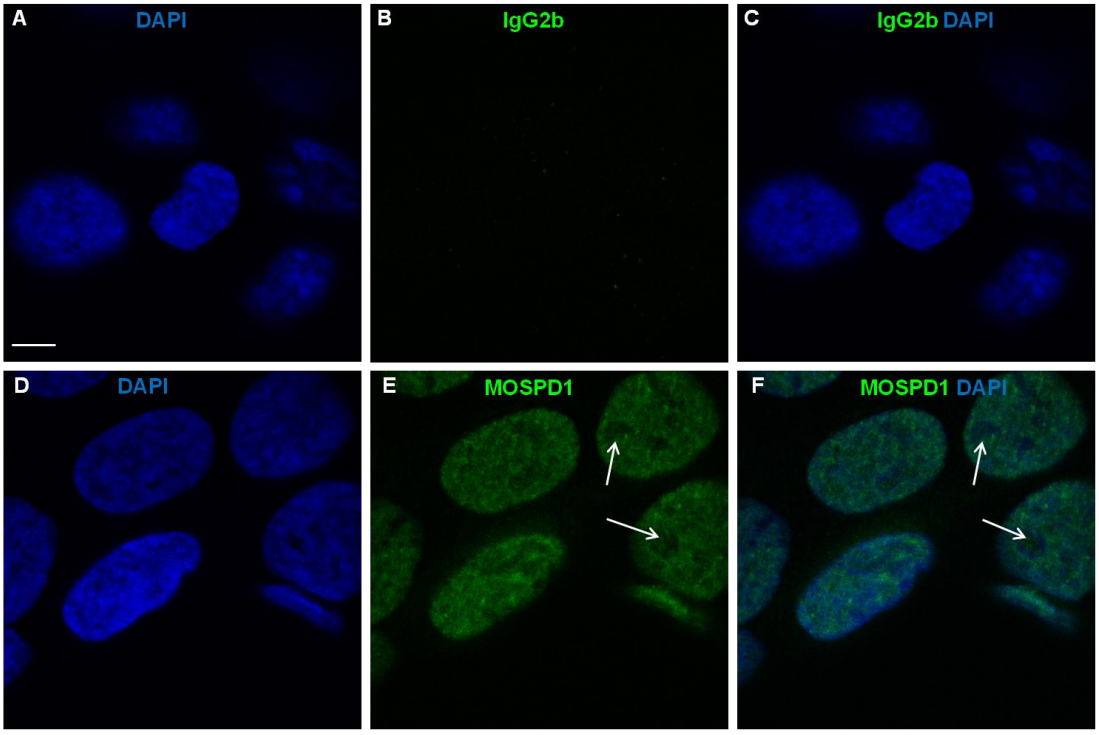

Figure 3.7: Nuclear localisation of MOSPD1. Cultured HaCaTs were immunolabelled with either the IgG2b isotype control (B) or the monoclonal α-MOSPD1antibody (E). DAPI was used to stain the nuclei (A and D). Merged images of IgG2b and DAPI (C) and MOSPD1 and DAPI (F) are shown. The arrows indicate nucleoli. Scale bar = 4 µm.

3.3.3.3. *In vitro* determination of the sub-cellular localisation of MOSPD3

Like MOSPD1, MOSPD3 was localised to the nuclei of cells. However, MOSPD3 was also localised to the cytoplasm of cells (Figure 3.8). There was no evidence of MOSPD3 being localised to desmosomes or cell junctions as the sub-cellular localisation differed to that of PKP2. Again the sub-cellular localisation appeared to be different in cells undergoing cell division.

3.3.3.4. MOSPD1 and MOSPD3 localisation changes depending on the cell cycle stage

As there was a hint of cell division altering the sub-cellular localisation of MOSPD1 and MOSPD3 and there were few cells undergoing cell division (mitosis) in unsynchronised cells an increase in the number of cells undergoing mitosis was required to try and investigate whether MOSPD1 and MOSPD3 localisation changed depending on the cell cycle stage. Cells were synchronised by blocking the cells at S phase of the cell cycle by two blocks of 2 mM thymidine for 17 hours each. Cells collected when the thymidine was removed (time 0) corresponded to S phase as shown by PI staining. Cells were also collected at 8 hours, 9 hours and 11 hours post thymidine removal and these time points should increase the number of cells at G2 phase, M phase and G1 phase, respectively. PI staining showed that synchronicity was lost at later time points (Figure 3.9 A).

Four views of the cells were randomly selected on the microscope at a magnification of x40 and the protein localisation was determined in at least 100 cells. MOSPD1 localisation changed in the hours post thymidine removal (Figure 3.9 B and Figure 3.10). At 0 hours post thymidine removal 47 % of cells showed MOSPD1 staining in the nuclei (Figure 3.7), 26 % in a perinuclear region and 27 % nuclear and perinuclear staining (Figure 3.10 B and C).

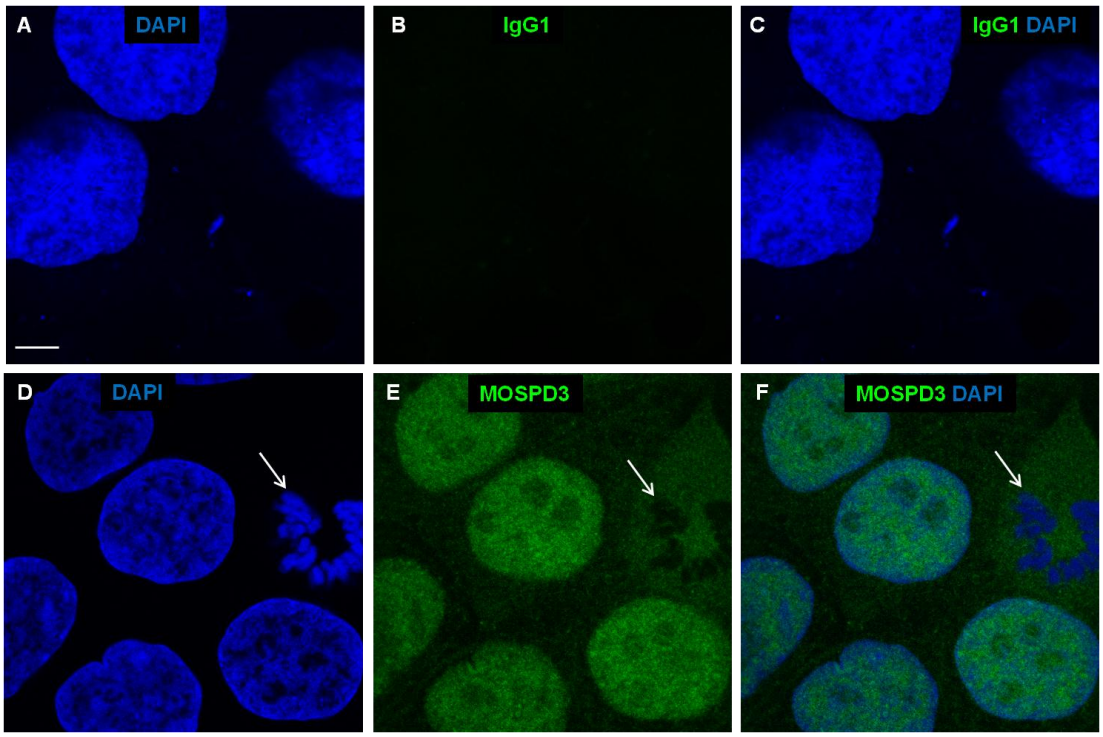

Figure 3.8: Nuclear and cytoplasmic localisation of MOSPD3. Cultured HaCaTs were immunolabelled with either the IgG1 isotype control (B) or the monoclonal α-MOSPD3 antibody (E). DAPI was used to stain the nuclei (A and D). Merged images of IgG1 and DAPI (C) and MOSPD3 and DAPI (F) are shown. The arrow indicates a dividing cell. Scale bar = 4 μm.

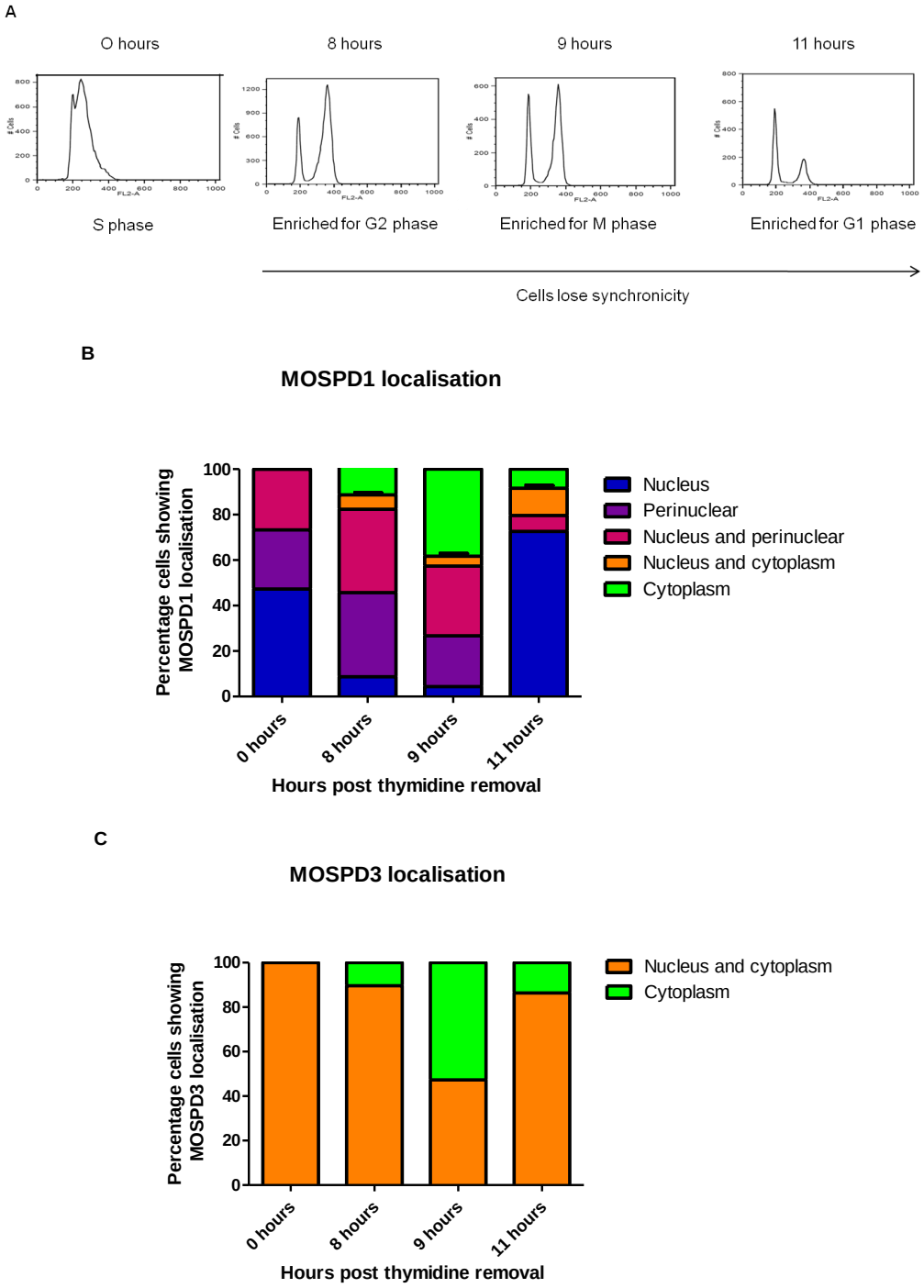

Figure 3.9: Localisation of MOSPD1 and MOSPD3 during the cell cycle. A: PI staining to determine cell cycle stage. The percentage of cells showing MOSPD1 (B) and MOSPD3 (C) localisation at 0, 8, 9 and 11 hours post thymidine removal.

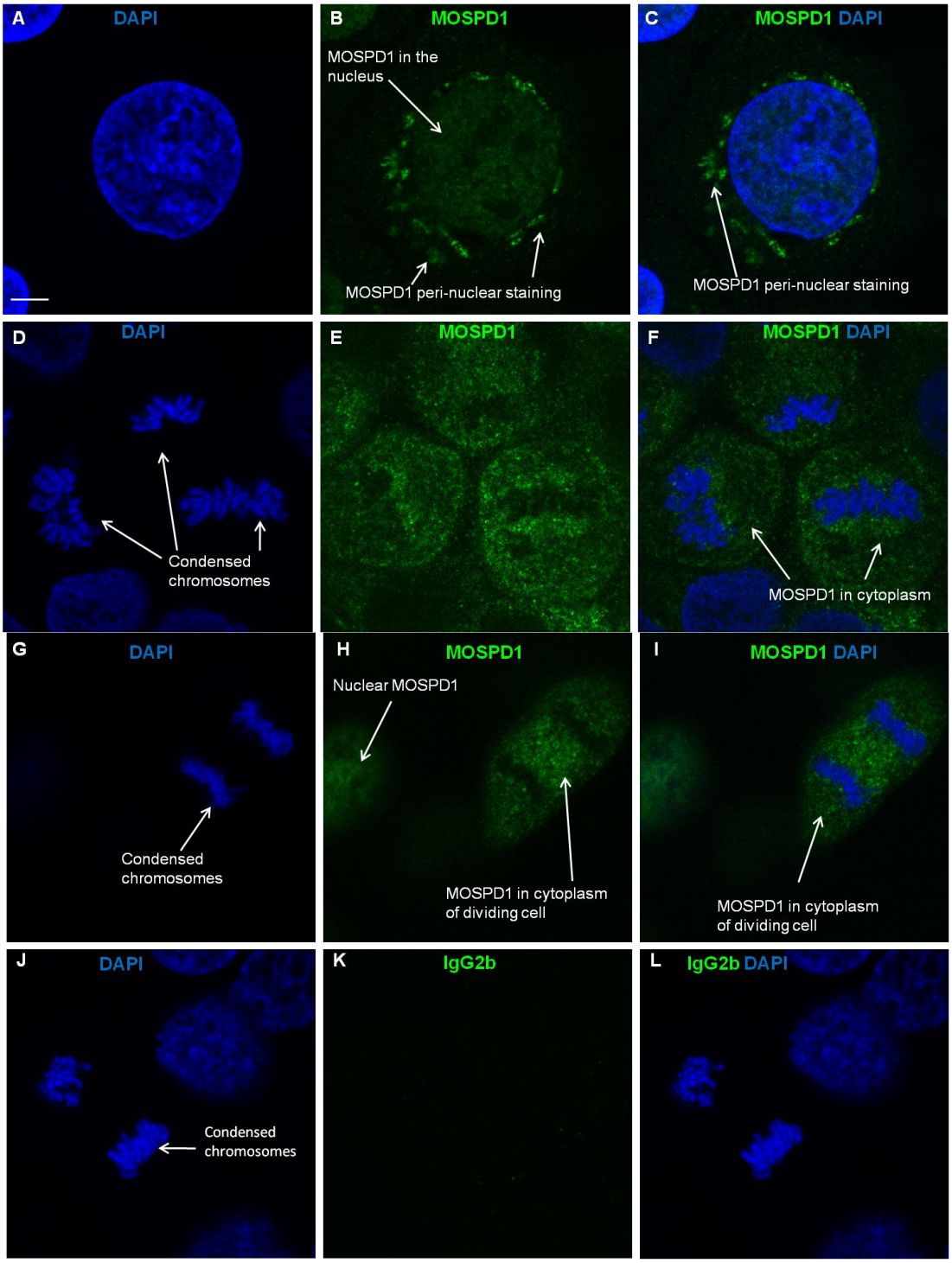

Figure 3.10: Localisation of MOSPD1 changes depending on the cell cycle. Cultured HaCaTs were immunolabelled with the monoclonal α-MOSPD1antibody (B, E and H) or the Ig2b isotype control (K). DAPI was used to stain the nuclei (A, D, G and J). Merged images of MOSPD1 and DAPI (C, F and I) and IgG2b and DAPI (L) are shown. The arrows indicate cells undergoing mitosis (D-F: metaphase and G-L: anaphase). Scale bar = 4 µm.

By 8 hours post thymidine removal the percentage of cells with MOSPD1 in the nucleus had been reduced to 9 % with 37 % showing perinuclear staining and 37 % nuclear and perinuclear localisation. At this time there were also 6 % of cells with MOSPD1 in the nucleus and cytoplasm and 11 % with cytoplasmic staining only (Figure 3.9 B and 3.10 E, F, H and I), corresponding to dividing cells. At 9 hours post thymidine removal 5 % cells showed nuclear MOSPD1, 22 % perinuclear, 31 % nuclear and perinuclear, 4 % nuclear and cytoplasmic and 38 % cytoplasmic (dividing cells). By 11 hours post thymidine removal 73 % of cells showed MOSPD1 localised to the nucleus, 7 % to the nucleus and perinuclear region. 12 % of cells showed MOSPD1 localised to the nucleus and cytoplasm and 8 % to the cytoplasm only.

MOSPD3 localisation differed between non-dividing and dividing cells. Non-dividing cells showed MOSPD3 localised to the nucleus and cytoplasm whilst dividing cells showed MOSPD3 localised to the cytoplasm and not with the condensed chromatin (Figure 3.8). In cells synchronised with 2 mM thymidine 100 % of cells at time O (S phase) showed MOSPD3 localised to the nucleus and cytoplasm. By 8 hours post thymidine removal 90 % of cells showed nuclear and cytoplasmic MOSPD3 whilst 10 % showed cytoplasmic staining. At 9 hours post thymidine removal 47 % of cells had MOSPD3 localised to the nucleus and 53 % to the cytoplasm. At 11 hours post thymidine removal 86 % of cells showed MOSPD3 in the nucleus and cytoplasm and 14 % in the cytoplasm (Figure 3.9 C). Cells showing MOSPD3 localised to the cytoplasm were all observed to be undergoing cell division and the majority of these were observed at 9 hours post thymidine removal which showed the most cells undergoing mitosis (M phase).

3.3.4. MOSPD1 and MOSPD3 expression *in vivo*

3.3.4.1. In the keratinocytes of the adult mouse ear

The mouse ear was chosen as a source of keratinocytes to explore if MOSPD1 and MOSPD3 had the same sub-cellular localisation *in vivo* as they had *in vitro* in the HaCaTs. MOSPD1 was localised to the nuclei of the keratinocytes of the mouse ear and other nuclei in the ear (Figure 3.11B). There was also expression of MOSPD1 in the nuclei and cytoplasm of the sebaceous gland. In comparison MOSPD3 was expressed in the cytoplasm and nuclei of the keratinocytes in the mouse ear as well as the sebaceous gland (Figure 3.11 D). There were some nuclei in the cells of the mouse ear that were negative for MOSPD3 expression. It can, therefore, be concluded that MOSPD1 and MOSPD3 have the same localisation *in vivo* in keratinocytes as *in vitro*. The IgG2b and IgG1 isotype controls (Figure 3.11 A and C) were used as negative controls for MOSPD1 and MOSPD3 expression, respectively, and these showed no specific staining.

3.3.4.2. MOSPD1 and MOSPD3 in the adult mouse heart

MOSPD1 and MOSPD3 showed similar localisation in the adult mouse heart. Both MOSPD1 and MOSPD3 were expressed in cardiomyocytes as well as the endothelial cells of blood vessels (Figure 3.12 B and 3.12 D). Both proteins were predominantly expressed in the nuclei of cardiomyocytes but both showed a low level in the cytoplasm. MOSPD1 and MOSPD3 were also expressed in the cytoplasm of endothelial cells. Both the IgG2b and IgG1 isotype controls were negative for any specific staining (Figure 3.12 A and C). Confirmation of MOSPD1 and MOSPD3 expression in endothelial cells was done using RT-PCR and immunocytochemistry on Human Umbilical Vein Endothelial Cells (HUVECs) (data not shown).

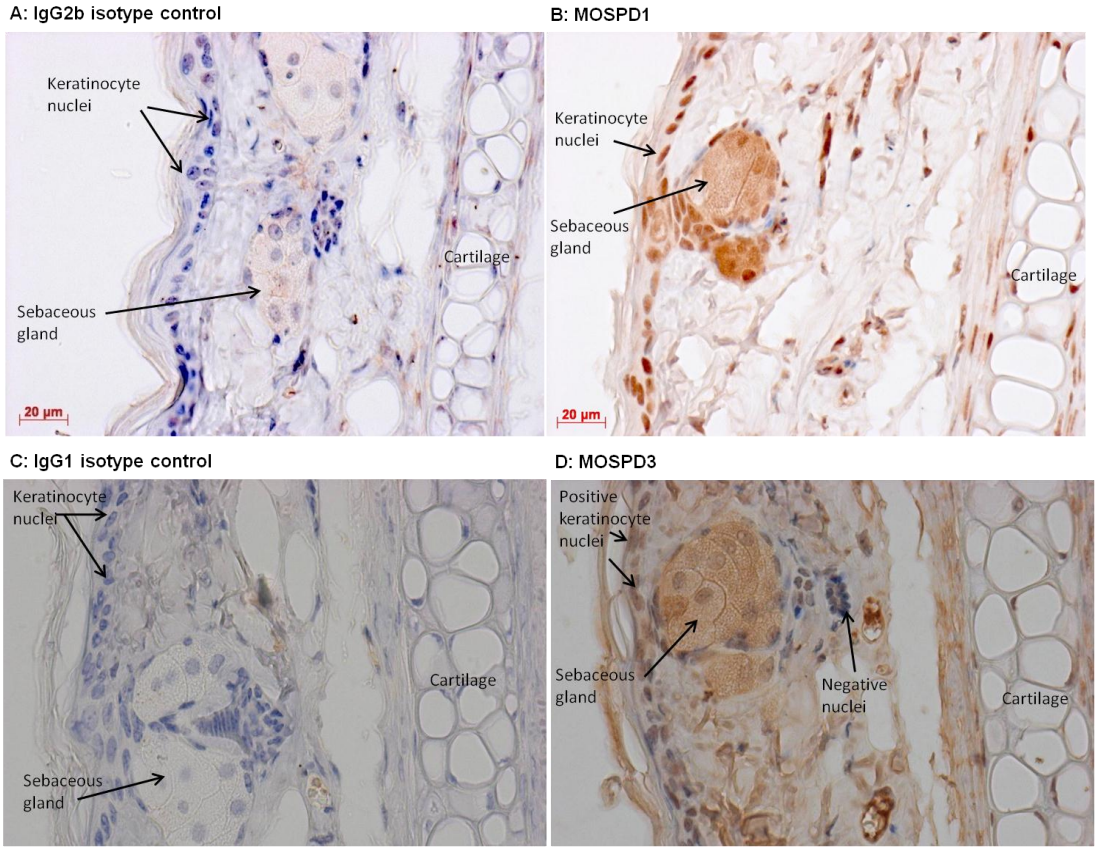

Figure 3.11: MOSPD1 and MOSPD3 localisation in the cells of the adult mouse ear. Sections of adult mouse ear were immunolabelled with the monoclonal α-MOSPD1 (B) or α-MOSPD3 (D) antibody. The IgG2b (A) and IgG1 (C) isotype controls served as negative controls. The sebaceous gland and nuclei of the keratinocytes are indicated with arrows. Scale bar = 20 µm.

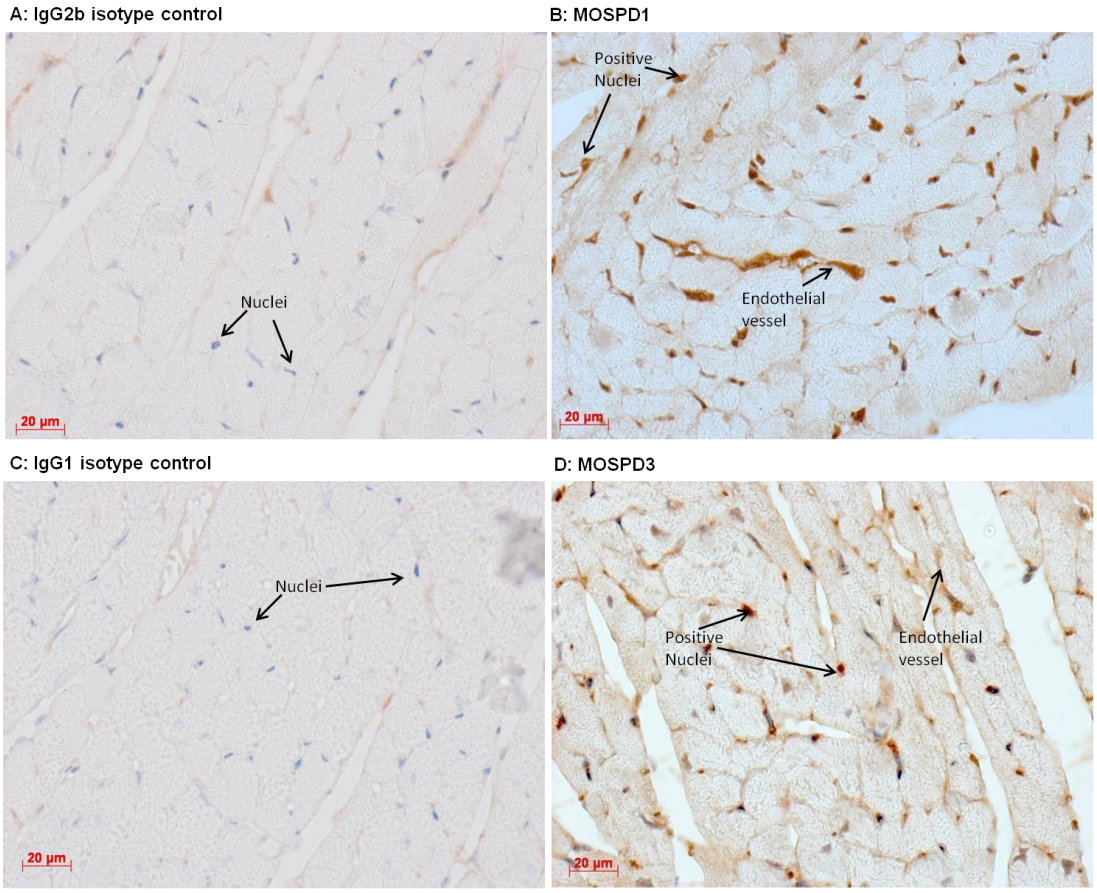

Figure 3.12: MOSPD1 and MOSPD3 localisation in the cells of the adult mouse heart. Sections of adult mouse heart were immunolabelled with the monoclonal α-MOSPD1 (B) or α-MOSPD3 (D) antibody. The IgG2b (A) and IgG1 (C) isotype controls served as negative controls. Cardiomyocyte nuclei and endothelial vessels are indicated with arrows. Scale bar = 20 µm.

3.3.4.3. MOSPD1 and MOSPD3 in the adult mouse kidney

MOSPD1 was localised to the nucleus and cytoplasm of the cortex and medulla of the adult mouse kidney. The tubular epithelium (Figure 3.13 B and Figure 3.14 A) shows MOSPD1 in the nuclei and cytoplasm. MOSPD1 is localised to some but not all the nuclei in the Bowman's Capsule. The IgG2b isotype control did not show any specific staining (Figure 3.13 A).

The localisation of MOSPD3 in the kidney was different to that of MOSPD1. MOSPD3 was localised to the apical brush border of the proximal convoluted tubule epithelium and the apical border of the parietal epithelium of the Bowman's Capsule. The apical cytoplasm of the distal convoluted tubule epithelium and the nuclei of the proximal tubular epithelium also showed MOSPD3 staining. The nuclei outside of the tubules were negative for MOSPD3 expression (Figure 3.13 D and Figure 3.14 B). The IgG1 isotype control served as a negative control (Figure 3.13 C). Figure 3.14 shows the localisation of MOSPD1 (A) and MOSPD3 (B) at higher magnification.

3.3.4.4. MOSPD1 and MOSPD3 in skeletal muscle

MOSPD1 was localised to most of the nuclei in the skeletal muscle. However, there were a few nuclei negative for MOSPD1 staining. There was also cytoplasmic staining of the muscle cells with strong expression observed in the muscle striations (Figure 3.15 B). Blood vessels were also positive for MOSPD1 expression (data not shown). There was some non-specific background staining in the IgG2b isotype control but no staining in the nuclei (Figure 3.15 A). MOSPD3 was localised to the cytoplasm of the muscle with strong staining of the muscle striations observed. The nuclei were absent for MOSPD3. A blood vessel shown in the figure was also positive for MOSPD3 expression (Figure 3.15 D). The IgG1 isotype control showed no specific background staining (Figure 3.15 C).

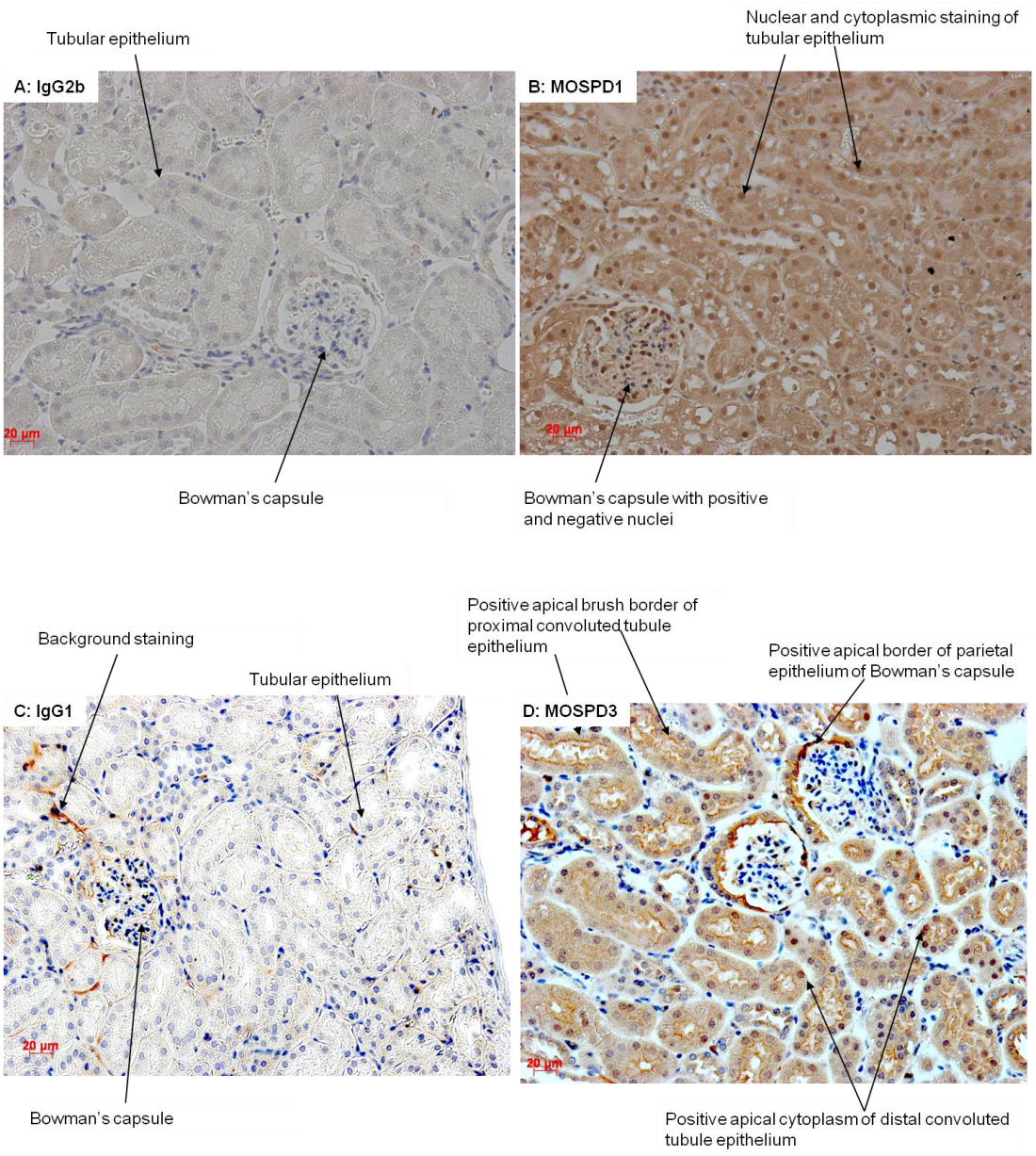

Figure 3.13: MOSPD1 and MOSPD3 localisation in the cells of the adult mouse kidney. Sections of adult mouse kidney were immunolabelled with the monoclonal α-MOSPD1 (B) or α-MOSPD3 (D) antibody. The IgG2b (A) and IgG1 (C) isotype controls served as negative controls. The tubular epithelium, apical border of the proximal convoluted tubule epithelium and the Bowman's Capsule are indicated with arrows. Scale bar = 20 µm. Pictures were labelled with the assistance of Dr David Brownstein (University of Edinburgh).

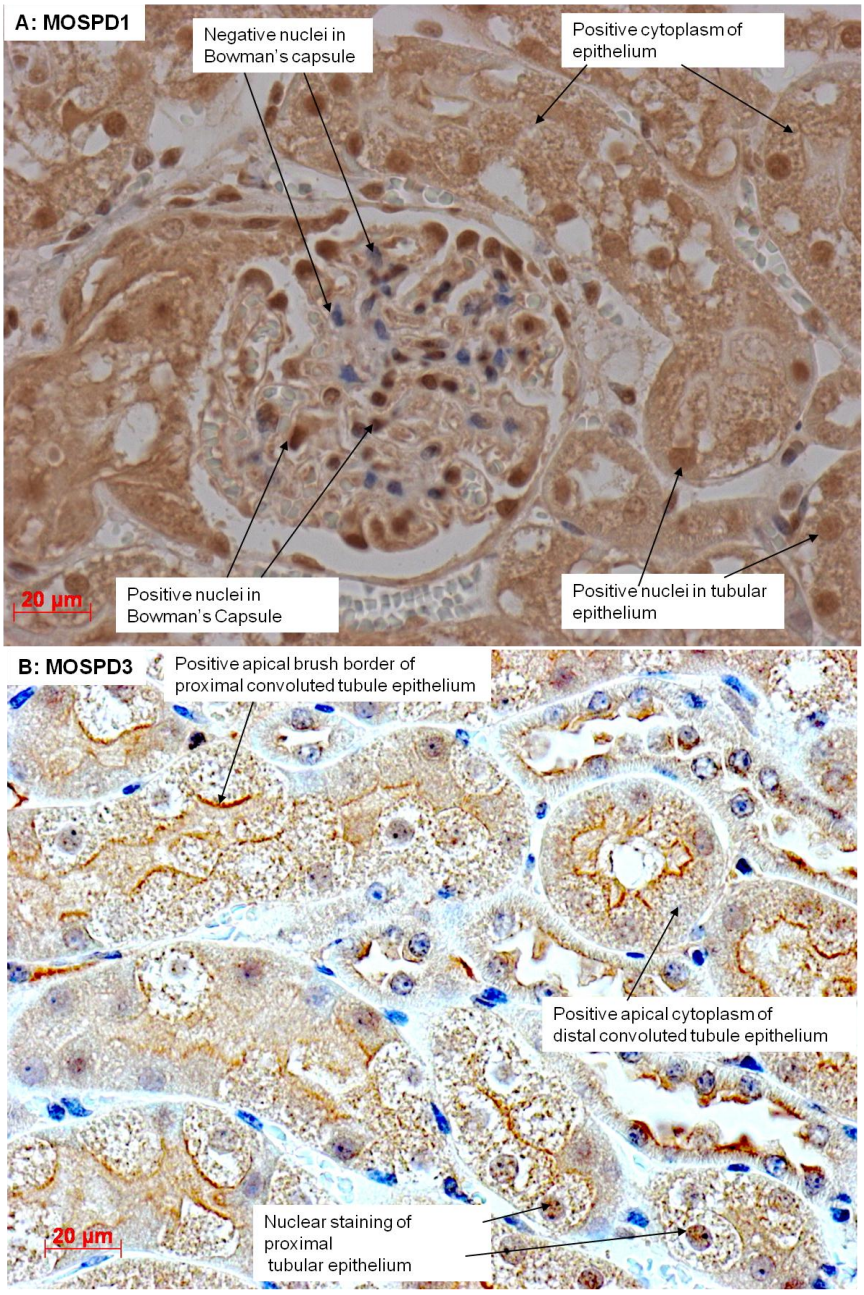

Figure 3.14: MOSPD1 and MOSPD3 localisation in the adult mouse kidney (higher magnification). Higher magnification of immunolabelled sections of adult mouse kidney showing the localisation of MOSPD1 (A) and MOSPD3 (B). The tubular epithelium, apical border of the proximal convoluted tubule epithelium and the Bowman's Capsule are indicated with arrows. Scale bar = 20 µm. Pictures were labelled with the assistance of Dr David Brownstein (University of Edinburgh).

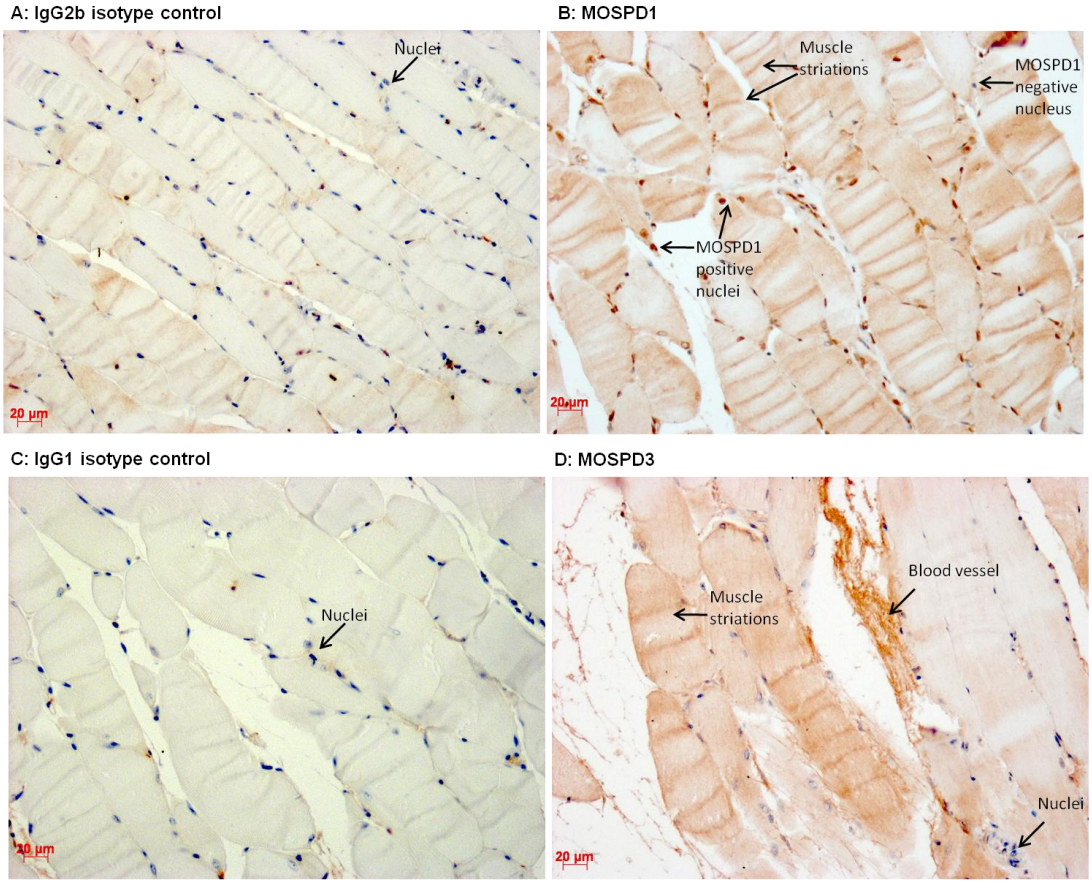

Figure 3.15: MOSPD1 and MOSPD3 localisation in skeletal muscle. Sections of adult mouse skeletal muscle were immunolabelled with the monoclonal α-MOSPD1 (B) or α-MOSPD3 (D) antibody. The IgG2b (A) and IgG1 (C) isotype controls served as negative controls. The muscle striations, a blood vessel and nuclei are labelled and indicated with arrows. Scale bars = 20 µm.

3.3.5. MOSPD1 and MOSPD3 localisation in sub-cellular compartments

3.3.5.1 MOSPD1 and MOSPD3 localisation in the nucleus

A pEYFP-Nuc plasmid (nuc-YFP) (Clontech) (Appendix Figure 7), with three nuclear localisation signals (NLS) of the simian virus 40 large T antigen fused to the C terminus of YFP, was transiently transfected into HaCaTs to label the nuclei. The localisation of MOSPD1 and MOSPD3 was determined using the monoclonal antibodies against each in the cultures transfected with nuc-YFP. This served to confirm the co-localisation of MOSPD1 and MOSPD3 with DAPI observed in HaCaTs (Figures 3.7 and 3.8). MOSPD1 co-localised with nuc-YFP in cells (yellow) that expressed the plasmid (Figure 3.16 A-C). Due to the transfection efficiency being less than 100 % not all the cells expressed nuc-YFP. Cells that did not express the plasmid only showed MOSPD1 expression (red) showing there was no cross-excitation of fluorescence. MOSPD3 also co-localised with nuc-YFP expression in the nucleus (yellow) but only MOSPD3 expression (red) was observed in the cytoplasm of cells with nuc-YFP, as expected, as well as in the nucleus and cytoplasm of cells not expressing nuc-YFP (Figure 3.16 D-F). This again showed that there was no cross-excitation of fluorescence signal.

3.3.5.2 MOSPD1 localisation in the ER

MOSPD1 observed to be localised to the perinuclear region in some cells (Figure 3.10 B) could be due to localisation to the ER. To determine whether this was the case a pDSRed2-ER plasmid (Clontech) (Appendix Figure 8), with the ER targeting sequence from calreticulin fused to the 5' end of DSRed2, was transiently transfected into unsynchronised HaCaTs and the monoclonal α-MOSPD1 antibody used to detect the localisation of MOSPD1. Nuclear MOSPD1 (green) was not co-localised with the DSRed-ER expression (Figure 3.17 A-C) but perinuclear MOSPD1 was co-localised with the DSRed-ER expression (Figure 3.17 D-F).

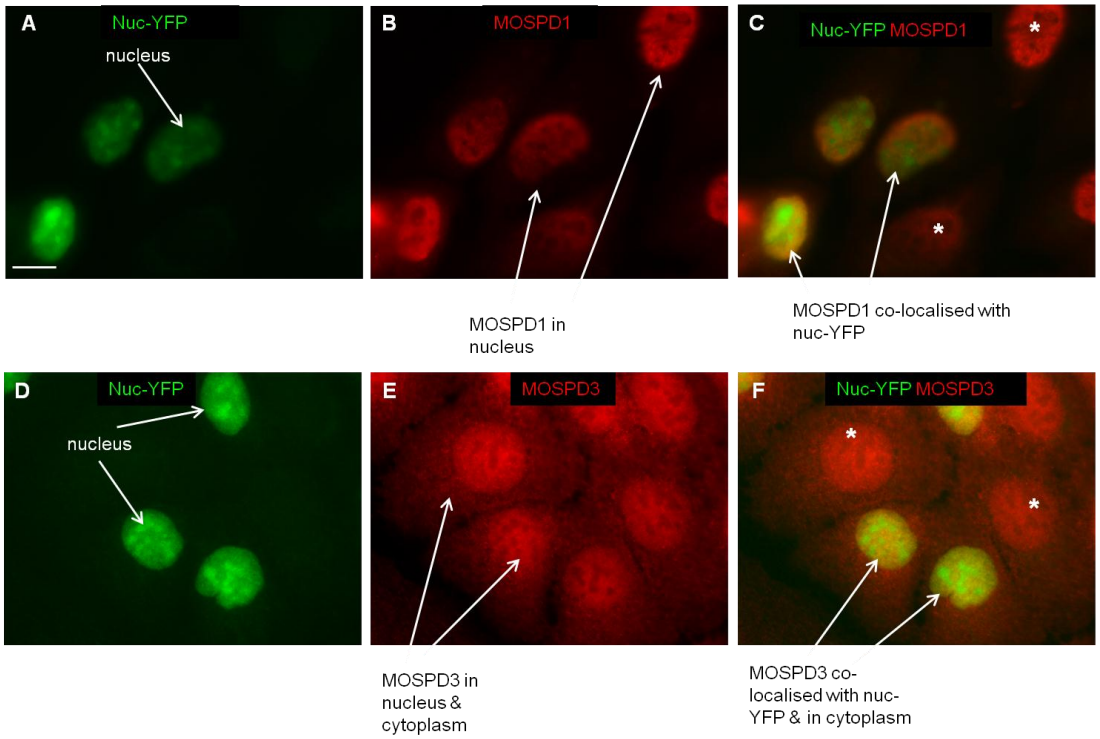

Figure 3.16: MOSPD1 and MOSPD3 co-localisation with nuc-YFP. Cultured HaCaTs transfected with a nuc-YFP plasmid transiently expressed nuc-YFP (A and D). The localisation of MOSPD1 (B) and MOSPD3 (E) was assessed using the monoclonal α-MOSPD1 and α-MOSPD3 antibodies and AlexaFluor594 secondary antibody (red). Merged images of nuc-YFP and MOSPD1 (C) and nuc-YFP and MOSPD3 (F) are shown. The cells labelled with a * indicate cells that do not express nuc-YFP as transfection efficiency is not 100 %. Scale bar = 9 µm.

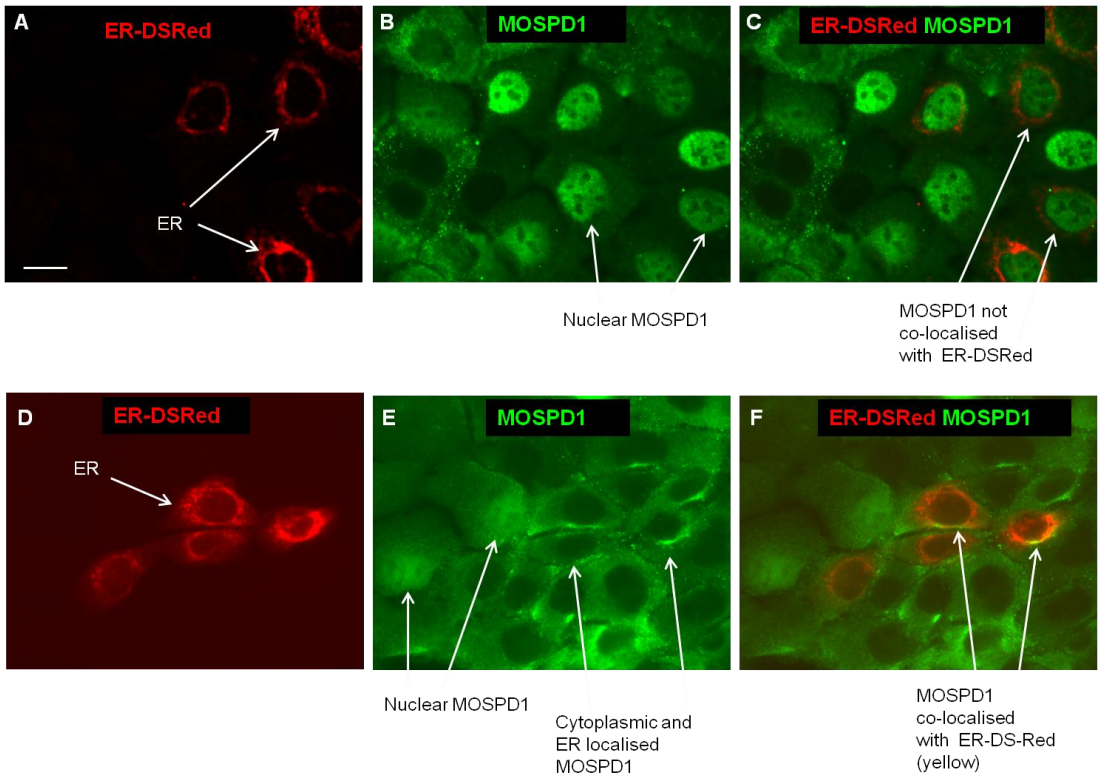

Figure 3.17: MOSPD1 localisation with pDSRed2-ER. A pDSRed2-ER plasmid transfected into unsynchronised HaCaTs transiently expressed ER-DSRed (A and D) in some cells (red). As transfection efficiency was less than 100 % not all cells expressed DSRed-ER. The localisation of MOSPD1 (B and E) was assessed using the monoclonal α-MOSPD1 antibody and AlexFluor488 secondary antibody (green). DSRed-ER and MOSPD1 merged images are shown (C and F). Scale bar = 9 µm.

3.4. Discussion

The localisation of recombinant MOSPD1-GFP reported in this Chapter differed to that reported by Thaler *et al*. (2010) who reported that full length recombinant MOSPD1 tagged with HIS was localised to the ER and removal of the last exon of MOSPD1 resulted in MOSPD1 localisation in the nucleus. They postulated that this could be due to a putative nuclear export signal (NES) located in the last exon. I found that full length MOSPD1-GFP was localised in the cytoplasm and nuclei of transfected cells.

The differences between Thaler *et al*. (2010) and my findings may be due to differences in the plasmids encoding the *Mospd 1* gene that were transfected and, therefore, differences in the recombinant MOSPD1 proteins. Whilst both recombinant proteins have C terminal tags, GFP in the recombinant MOSPD1 reported in this chapter and HIS in Thaler *et al*. (2010), the two tags differ in their size as GFP is 27 kDa and a HIS tag does not add more than 1 kDa to the size of the protein. Another possible explanation for the difference in recombinant MOSPD1 localisation is that the localisation of MOSPD1-GFP in transfected keratinocytes is reported in this chapter whereas Thaler *et al*. (2010) reported recombinant MOSPD1-HIS localisation in transfected MC3T3-E1 cells. Keratinocytes are epithelial cells whilst MC3T3-E1 cells are an osteoblastic cell line and, therefore, mesenchymal and so the differences in localisation may be due to the differences in the cell types. In the experiments reported here the localisation of MOSPD1-GFP was directly assessed using microscopy to assess GFP fluorescence whereas Thaler *et al*. (2010) detected MOSPD1-HIS expression by immunocytochemistry using an α-HIS primary antibody and a FITC-labelled secondary antibody so the difference in methods used to assess the localisation could also be responsible for the differences observed. As there are no reports in the literature for the localisation of MOSPD3 there is nothing to compare the localisation reported in this chapter.

Whilst recombinant proteins are useful in initial assessment of a protein's localisation the localisation of endogenous protein is much more informative. To this end antibodies are a useful tool to investigate expression and localisation of endogenous proteins. I was able to generate monoclonal antibodies that were specific and did not cross-react with each other even though the two proteins, MOSPD1 and MOSPD3 are closely related. These monoclonal antibodies did not show the background that the polyclonal antibodies (Katrin Buerger, PhD thesis, 2009) did when detecting endogenous MOSPD1 and MOSPD3 in mouse tissues and were, therefore, used for determination of the tissue distribution and sub-cellular localisation of these proteins. The samples were treated with β-mercaptoethanol and boiled prior to loading on gels for western blots which should result in disruption of protein complexes and, therefore, the 50 kDa band may not be due to a dimer. Therefore, due to the presence of this extra 50 kDa band in western blots of heart lysates, which could be due to non-specific binding of the monoclonal antibodies, the sub-cellular localisation results from immunocytochemistry and immunohistochemistry may not be accurate. To address this western blots could be carried out on lysates from *Mospd 1* null day 5 embryoid bodies (described in section 5.3.4.1.) as well as immunocytochemistry of these cells using the α-MOSPD1 antibody. If there is no background staining it would indicate the antibody was specific for MOSPD1. The α-MOSPD1 and α-MOSPD3 antibodies could also be tested on cells in which siRNA had been used to knockdown MOSPD1 and MOSPD3. The monoclonal α-MOSPD1 antibody and α-MOSPD3 antibody have one isotype each indicating the antibodies are formed from only one B-cell clone and, therefore, are specific to one epitope each.

The recombinant MOSPD1-GFP and MOSPD3-GFP localisation is slightly different to that of the endogenous proteins detected using the monoclonal antibodies. Endogenous MOSPD1 was found to be nuclear and MOSPD3 to be nuclear and cytoplasmic. There are a number of possible explanations for this. Firstly, recombinant proteins differ from their endogenous counterparts as the cDNA has been synthesised *in vitro* and this may influence the ability of the ER to synthesise

these proteins correctly. Secondly recombinant proteins often have the reporter tag on the N-terminal or C-terminal and this is not the best position for them as these sites are often important for correct protein folding. Incorrect folding of a protein can result in its accumulation in the ER (Viallet and Vo-Dinh, 2003) and it not being transported to the site the correctly folded protein would be. Thirdly, transfection of recombinant proteins results in over expression of the protein and this may have effects on the transfected cells and the protein's localisation. Thaler *et al*. (2010) only observed MOSPD1-HIS in the nucleus when the last exon of *Mospd 1* was removed. However, using the monoclonal α-MOSPD1, the endogenous protein was localised in the nucleus. One possible explanation is that there could be alternative isoforms of MOSPD1 which could include an endogenous form that does not have the last exon and as the peptide used to generate the antibody was at the N terminal of MOSPD1, the monoclonal α-MOSPD1 antibody would detect this shortened isoform. However, no shorter forms of MOSPD1 were detected on the western blots probed with the monoclonal α-MOSPD1 antibody.

Due to the similarities between the phenotype of the homozygous MOSPD3 gene trap mice (Pall *et al*., 2004) and of mice with mutations in desmosome components such as *Plakophilin 2* (Grossmann *et al*., 2004) which show neonatal lethality with a thinning of the right ventricle wall it was hypothesised that MOSPD3 could be part of the desmosome structure and, therefore, localised to the cell membrane. The presence of two transmembrane domains in MOSPD3, and the closely related MOSPD1, indicated that these proteins could be localised to membranes. The human keratinocyte cell line, HaCaTs, was chosen for the localisation studies as they are rich in desmosomes and have been used to study the localisation of desmosome components such as PKP2 (Mertens *et al*., 1996). MOSPD1 was localised to the nucleus and MOSPD3 to the nucleus and cytoplasm of HaCaTS *in vitro*. MOSPD1 and MOSPD3 were not localised to the cell membrane and did not show the same desmosomal localisation of PKP2 and as MOSPD1 and MOSPD3 are not localised to cell junctions they do not form part of the desmosome structure and are not crucial components of the cell membrane. The phenotype of the *Mospd 3* gene trap mouse,

although similar to that of desmosome mutants, is not due to a MOSPD3 desmosomal defect based on the differences in localisation of MOSPD3 and desmosome components.

Investigations to check whether MOSPD1 and MOSPD3 localisation is the same *in vivo* as it is *in vitro* were done by immunohistochemistry of adult mouse tissue sections. The mouse ear was chosen as a source of keratinocytes *in vivo* and MOSPD1 and MOSPD3 localisation was the same in these keratinocytes as in the HaCaTs grown *in vitro*. The proliferation of keratinocytes in the mouse ear are approximately 3 cells/ mm of tissue (Hill *et al*., 1981) and could possibly account for the nuclei that are absent for MOSPD proteins. To confirm this Bromodeoxyuridine (BrdU) could be used to detect proliferating cells *in vivo* as it is a thymidine analogue incorporated into DNA during S phase of the cell cycle. α-BrdU antibody could be used to detect the incorporated BrdU. The fact that MOSPD1 and MOSPD3 have similar localisation in HaCaTs and keratinocytes *in vivo* indicates that MOSPD proteins are involved in the same processes in keratinocytes *in vitro* as they are *in vivo*. Also it provides evidence that the immunostaining results are accurate as DAB staining was used to detect immunolabelled MOSPD1 and MOSPD3 in mouse tissue sections whilst fluorescence was used for HaCaTs.

As the localisation of MOSPD1 and MOSPD3 was different in the few dividing cells observed in unsynchronised cultures it was decided to synchronise the cells to increase the number of dividing cells seen. Incubation of HaCaTs with 2 mM thymidine results in the synchronisation of the cells at S phase and an increase in cells at G2 phase at 8 hours post thymidine removal, at M phase (9 hours) and G1 phase (11 hours) (He *et al*., 2005). The percentage of cells showing different MOSPD1 localisation differed at these times indicating that MOSPD1 localisation changed during the cell cycle from mainly nuclear (during G1 and S phases) and perinuclear (S phase) to cytoplasmic in all dividing cells (M phase). In all non-dividing cells MOSPD3 was localised to the nucleus and cytoplasm and, therefore,

differed to MOSPD1 localisation. However, MOSPD3 was localised to the cytoplasm of all dividing cells in the same way as MOSPD1. This could be due to a similar role they are involved with during cell division. It is unknown whether MOSPD1 and MOSPD3 are actively removed from the nucleus in dividing cells or whether their cytoplasmic localisation is passive and only due to nuclear envelope breakdown that occurs during cell division. HaCaTs treated in this way lost synchronicity but did show increased numbers of dividing cells at 9 hours post thymidine which was the objective of the synchronisation. To synchronise cells at M phase an alternative drug such as colcemid could be used which blocks cells at mitosis (Lam *et al*., 1997).

There are other proteins that show similar changes in localisation, to those observed in MOSPD1 and MOSPD3, depending on the cell cycle, such as BRCA1 (Breast Cancer Susceptibility gene 1) (Glover-Collins and Thompson, 2008) and PTHrP (Parathyroid hormone-related protein) (Lam *et al*., 1997). BRCA1 is a tumour suppressor and its localisation changes depending on the cell cycle. It has both NLS and NES and is localised to the nuclei of cells. During S phase BRCA1 is localised to the perinuclear region. This exclusion from the nucleus can be blocked by the antifungal agent, Leptomycin B, which is an inhibitor of the CRM1 (exportin1) protein (Nishi *et al*., 1994) involved in nuclear export. Therefore, BRCA1 export from the nucleus is dependent on CRM1 (Glover-Collins and Thompson, 2008). PTHrP localisation also changes depending on the cell cycle with dividing cells showing both an increased expression of PTHrP as well as a change of localisation from nuclear (during G1 phase) and nuclear and perinuclear (G1/S phase) to cytoplasmic (M phase) (Lam *et al*., 1997).

A putative NES in MOSPD1 has been reported (Thaler *et al*., 2010) and the presence of the same 4 residues, leucine, isoleucine, threonine and methionine, in MOSPD3 could mean MOSPD3 also has this NES. The presence of this NES could explain how MOSPD1 and MOSPD3 are translocated from the nucleus into the cytoplasm

and could be due to CRM1 mediated export. Assessment of the localisation of MOSPD1 and MOSPD3 in cells where CRM1 has been inhibited by Leptomycin B treatment could address whether MOSPD protein nuclear export is dependent on CRM1. As MOSPD protein localisation changes during the cell cycle it would be interesting to assess whether these changes in localisation are accompanied by a change in the level of expression of these proteins.

The perinuclear localisation of MOSPD1, which appears to be MOSPD1 localised to the ER based on co-localisation of MOSPD1 and DS-Red2-ER, indicates a similarity to another protein family characterised by an N terminal MSP domain and a transmembrane domain. These are the VAMP-associated proteins (VAPs) (Weir *et al*., 1998; Nishimura *et al*., 1999). VAPB is localised to the ER and has a secreted form which binds to Ephrin (Eph) receptors (Tsuda *et al*., 2008). VAPA has been shown to be localised to the ER (Skehel *et al*., 2000) and Golgi apparatus (Soussan *et al*., 1999). The function of the VAP family is not fully understood. However, a mutated form of the VAPB protein has been implicated in Amyotrophic Lateral Schlerosis (ALS) (Nishimura *et al*., 2004). This similarity in localisation may indicate these proteins may share certain characteristics and possible functions. The transmembrane domains in MOSPD proteins could be involved in the localisation of these proteins in the ER, possibly on the membranes.

Within the kidney localisation of MOSPD1 and MOSPD3 differed indicating they could serve different roles in this organ. The localisation of MOSPD3 to the membranes of the tubular epithelium could be due to the transmembrane domains in the MOSPD3 protein. The nuclei that are negative for MOSPD1 expression in the Bowman's Capsule could be dividing cells that do not have MOSPD1 associated with the DNA and it is known that there are dividing cells within the Bowman's Capsule (Jennette and Heptinstall, 2007). There were similarities between the localisation of MOSPD1 and MOSPD3 in some tissues such as the heart where both

proteins were localised to nuclei and cytoplasm of endothelial cells of blood vessels and skeletal muscle where they were both localised to muscle striations.

This chapter investigated the expression pattern of MOSPD1 and MOSPD3 (summarised in Table 3.1) and whether they could be genetically redundant due to having the same sub-cellular localisation. The localisation of these proteins differed to each other with MOSPD1 being predominantly nuclear in cells tested whilst MOPSD3 was nuclear and cytoplasmic. However, both proteins show the same cytoplasmic localisation in dividing cells. Within certain tissues they exhibited similar localisation. Based on the evidence *Mospd 1* and *Mospd 3* could be genetically redundant as they may be able to compensate for each other in some tissues where they have the same localisation, such as the heart, or cells undergoing cell division if this is a process MOSPD proteins are involved in.

A

Protein	Recombinant protein	Endogenous protein localisation in non-dividing cells	Endogenous protein localisation during mitosis
MOSPD1	MOSPD1-GFP localised to the nucleus and cytoplasm	Nucleus and perinuclear region	Cytoplasm
MOSPD3	MOSPD3-GFP localised to throughout the cell and in some cells was in the cytoplasm+ perinuclear	Nucleus and cytoplasm	Cytoplasm

B

Protein	Cells of ear	Heart	Kidney	Skeletal muscle
MOSPD1	Keratinocyte nuclei; sebaceous gland	Cardiomyocyte nuclei and cytoplasm of endothelial cells of blood vessels	Cytoplasm and nuclei of epithelium; some nuclei within the Bowman's Capsule	Cell nuclei and muscle striations
MOSPD3	Keratinocyte nuclei and cytoplasm; sebaceous gland; cytoplasm of all cells	Cardiomyocyte nuclei and cytoplasm of endothelial cells of blood vessels	Apical brush borders of the proximal convoluted tubule epithelium and epithelium of Bowman's Capsule; cytoplasm and nuclei of distal convoluted tubule epithelium	Cytoplasm and muscle striations

Table 3.1: Localisation of MOSPD1 and MOSPD3 in HaCaTs *in vitro* and *in vivo*. Localisation of recombinant and endogenous MOSPD1 and MOSPD3 *in vitro* (A) and of MOSPD1 and MOSPD3 in different adult mouse tissues (B).

CHAPTER 4:
FUNCTIONAL ROLE OF MOSPD1 IN DEVELOPING ZEBRAFISH EMBRYOS

4.1. Introduction

Zebrafish are an excellent model organism for vertebrate development as they possess many advantages. They are easy and inexpensive to maintain and large numbers of embryos can be obtained from a single mating. These embryos can be assessed from the earliest developmental stages as eggs are externally fertilised and the embryos are transparent allowing the observation of organ development *in vivo* using simple light microscopy. Zebrafish embryos do not require normal blood circulation during early development as they acquire sufficient oxygen through diffusion (Burggren and Pinder, 1991). This allows embryos with cardiovascular defects to survive and develop and facilitates the phenotypic assessment of these embryos. This is a distinct advantage of using zebrafish as a model organism compared to mice as it allows mutations that act at early stages of development to be assessed which would be difficult to study in mice as they are dependent on normal blood circulation for survival.

As *Mospd 1* is a gene expressed in vertebrates it was expected that the zebrafish genome would have a *Mospd 1* gene. Bioinformatics studies on the zebrafish genome have shown that a *Mospd 1* gene (NCBI accession NM_007878.1) is present which has not undergone duplication and, therefore, there is only one copy of the *Mospd 1* gene. A *Mospd 3* gene is not present in the zebrafish genome which is as expected as *Mospd 3* is thought to be mammalian specific. Another *Mospd* gene family member, *Mospd 2* is present in the zebrafish genome (NCBI accession NM_001007293.1). There is limited information in the literature about the expression of *Mospd 1* in zebrafish. Whole mount *in situ* hybridisation (WISH) carried out on developing zebrafish embryos has shown that *Mospd 1* is expressed throughout the embryo (Thisse *et al*., 2004). WISH shows the presence of *Mospd 1* RNA transcripts but there is no MOSPD1 protein expression data in the literature. Zebrafish MOSPD1 (NCBI accession NP_998534.1) and mouse MOSPD1 (NCBI accession NP_081685.1) share 77 % sequence identity showing the protein is highly conserved. Assessment of the sub-cellular localisation of MOSPD1 in embryos is important as it

would add information about the MOSPD1 protein expression as well as enhance functional studies.

Another advantage of using zebrafish is that the expression of any gene of interest can be knocked down by injecting morpholinos targeted to that gene. Morpholinos are short oligonucleotides that are comprised of the standard nucleic bases. However, morpholino rings replace ribose or deoxyribose rings and phosphorodiamidate linkages are present instead of the phosphodiester linkages found in DNA and RNA (Summerton and Weller, 1997). This results in morpholinos being resistant to nuclease activity (Hudziak *et al*., 1996). Microinjection of a morpholino anti-sense onligonucleotide targeted to a splice junction or an exon- intron boundary can result in the inhibition of gene expression by inhibiting spliceosome components and thereby inhibiting pre-mRNA processing. This inhibition of correct splicing can result in a number of possible outcomes such as the deletion of the targeted exon, the inclusion of the targeted intron or the introduction of a frame shift or a premature stop codon (Morcos, 2007). These events result in gene knockdown and the level of this knockdown can be assessed using quantitative real-time PCR to measure the level of expression of the transcript of interest and comparing that to non-injected and negative-morpholino injected controls.

Morpholinos that bind to the start codon or 5'UTR can inhibit translation of a protein by inhibiting the ribosomal initiation complex (Summerton, 1999). Morpholinos are fluorescent and, therefore, the uptake and distribution of the morpholino can be assessed easily. Negative controls are injected at the same dose as the morpholino and are necessary to aid in distinguishing off target effects of morpholinos. 5 base pair mismatch (5MP) morpholinos serve as negative controls as they are highly similar in sequence to gene specific morpholinos but should not cause knockdown of the gene of interest. These controls are used to determine the effect of morpholino toxicity and to distinguish between specific phenotypes and those observed due to off target effects of the morpholino.

As a positive control microinjection of the *chordin* morpholino into zebrafish embryos was performed and the embryos assessed for the published *chordin* knockdown phenotype (Nasevicius and Ekker, 2000). Both the mild and severe *chordin* phenotypes published in the literature were observed at 2 ng and 4 ng doses of the *chordin* morpholino, respectively (Appendix Figures 10 and 11). The ability to replicate a published phenotype was followed by the use of morpholinos to knockdown *Mospd 1*, a relatively uncharacterised gene. In order to establish the role of *Mospd 1* in early development both a morpholino targeted to the start site (MO1) of *Mospd 1* and a splice-site morpholino (MO2) were generated. The splice-site morpholino was targeted to the splice junction between exons 2 and 3 at the boundary between exon 2 and intron 2. 1-16 cell embryos were injected with either morpholino or their 5 mispair morpholino controls. Different doses of morpholinos were injected into the embryos and the survival and phenotypes of these embryos were assessed throughout the experimental procedure.

4.2. Aims

- Assess the expression of *Mospd 1* throughout early zebrafish development

- Determine the sub-cellular localisation of MOSPD1 in the developing zebrafish embryo using the mouse monoclonal α-MOSPD1 antibody described in Chapter 3.

- Determine the function of *Mospd 1* in zebrafish embryo development using morpholino knockdown technology
    - Using a morpholino targeted to the start codon of *Mospd 1* (MO1) to assess the phenotype of these embryos
    - Measuring knockdown of *Mospd 1* expression using qPCR
    - Confirming any observed *Mospd 1* phenotype using a splice-site targeted morpholino (MO2)

4.3. Results

4.3.1. Expression of *Mospd 1*

4.3.1.1. Expression of *Mospd 1* in developing embryos

A pool of zebrafish embryos was collected at different time points from pre-mid blastula transition (MBT) (1 hpf) through to 5 dpf (Figure 4.1 A) and RNA extracted from these embryos. The cDNA synthesised from the RNA was used as a template for semi-quantitative RT-PCR in order to determine when *Mospd 1* was expressed in the developing embryo. *Mospd 1* is expressed from the pre-MBT stage, which indicates the presence of maternal *Mospd 1* transcripts, right through to 5 dpf (Figure 4.1B). The expression of *Mospd 1* increases as development continues as there are higher levels of *Mospd 1* from 2 dpf to 5 dpf. The house keeping gene *β-actin* was used as an internal control. The samples where reverse transcriptase was not added showed larger PCR products on the gel due to the intron-spanning primers, used for the RT-PCR, detecting some genomic contamination. The water control, where water was in place of cDNA, was negative for PCR product.

4.3.1.2. Expression of MOSPD1 protein in zebrafish embryos

Whole mount *in situ* hybridisation (WISH) has shown that *Mospd 1* transcript is expressed throughout the zebrafish embryo (Thisse *et al*., 2004). There is no information in the literature about the MOSPD1 protein expression pattern. As there is 50 % sequence identity between the peptide used to generate the mouse monoclonal α-MOSPD1 antibody, described in Chapter 3, and the corresponding zebrafish peptide the antibody was used to try and identify the sub-cellular localisation of MOSPD1 in zebrafish embryos. Immunohistochemistry was performed on sagittal sections of 3 dpf embryos. The mouse monoclonal α-MOSPD1 antibody was able to detect zebrafish MOSPD1.

A

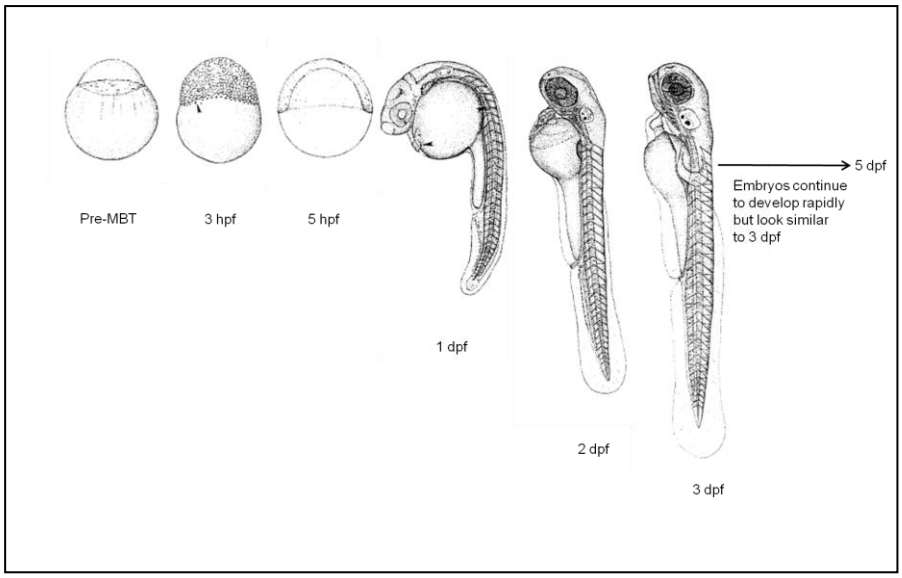

B

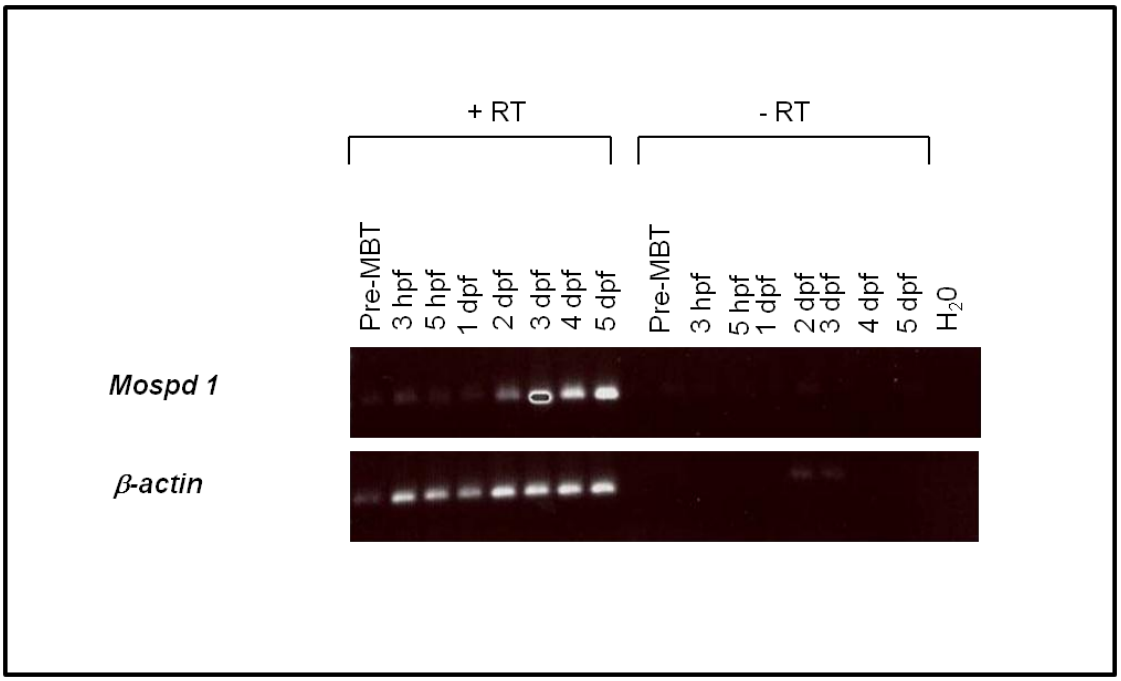

Figure 4.1: *Mospd 1* expression in developing zebrafish embryos. A: Sketches of zebrafish embryos corresponding to the time collected for RNA extraction (pictures from Kimmel *et al.*, 1995). B: RT-PCR on cDNA from pre-MBT (1 hpf) embryos through to 5 dpf embryos using *Mospd 1* and *β-actin* primers (endogenous control). *Mospd 1* expression is low during early development (pre-MBT to 2 dpf) and increases as the embryos get older with a high expression observed at 3 ,4 and 5 dpf. H_2O served as a negative control. +RT= reverse transcriptase added to cDNA reaction; -RT= reverse transcriptase omitted from cDNA reaction. PCR products were of the expected size (approximately 500 bp).

MOSPD 1 protein was expressed throughout the zebrafish embryo confirming the WISH data showing expression of *Mospd 1* transcripts throughout the embryo (Thisse *et al*., 2004). MOSPD1 was found to be localised to the nuclei and cytoplasm of the developing embryo (Figures 4.2). There were some unstained cells within the embryo particularly within the heart (Figure 4.3) which could correspond to blood cells which are nucleated in zebrafish embryos. MOSPD1 was localised to the cytoplasm at the anterior of somites and nuclei in the posterior (Figure 4.4). An isotype control was used as a negative control and this did not show any non-specific staining (Figure 4.2 A). Immunohistochemistry on zebrafish embryos was also performed using the mouse monoclonal α-MOSPD3 antibody which did not show any specific staining and, therefore, confirmed the absence of MOSPD3 in zebrafish embryos as expected due to its absence from the zebrafish genome.

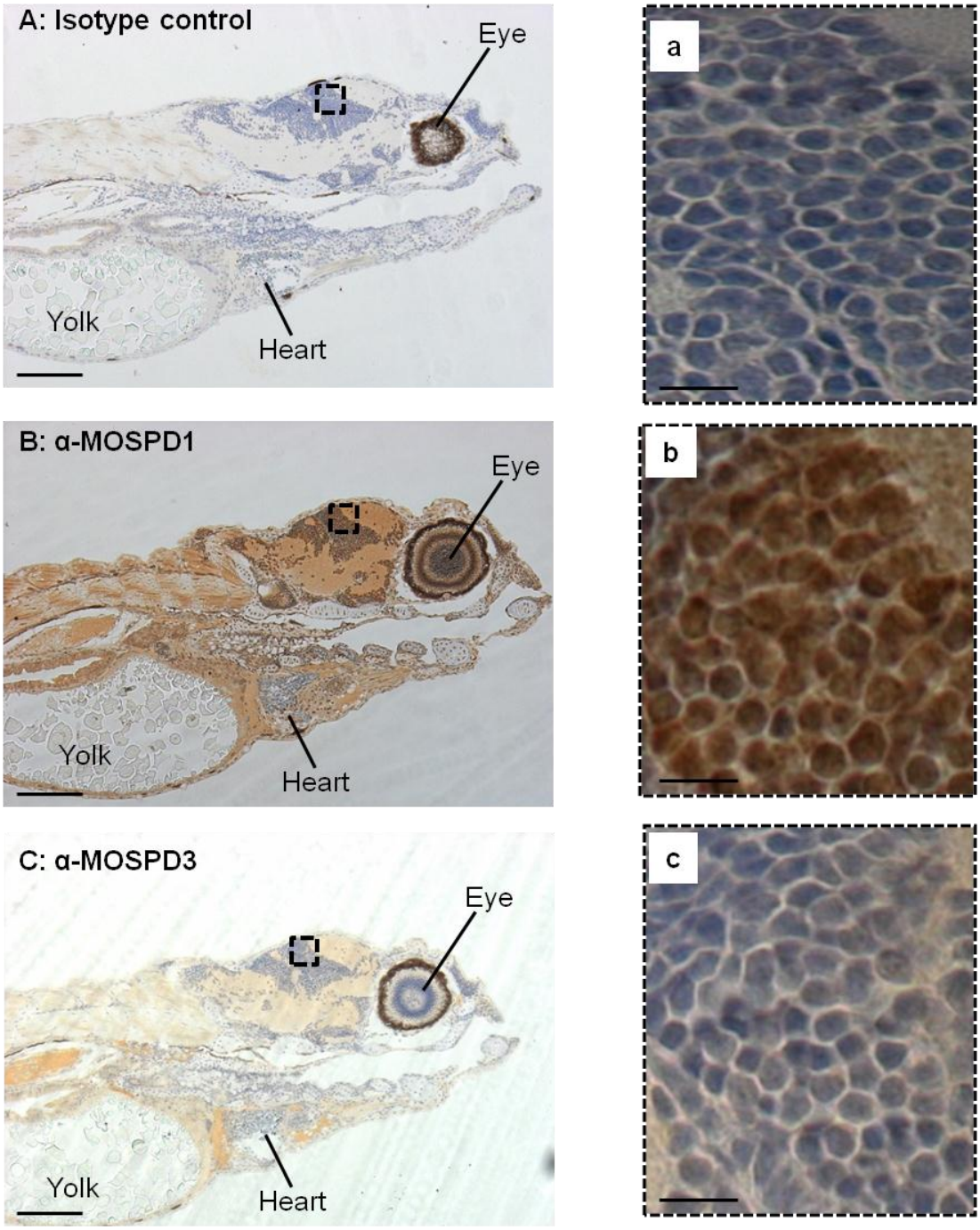

Figure 4.2: MOSPD1 localisation in 3 dpf zebrafish embryos.
Immunohistochemistry on sagittal sections of 3 dpf embryos using the IgG2b isotype control (A), the mouse monoclonal α-MOSPD1 antibody (B) and the mouse monoclonal α-MOSPD3 antibody (C) are shown. Higher magnification of the boxed section (A-C) showing the nuclei for the embryo stained for the isotype control (a), MOSPD1 (b) and MOSPD3 (c). Scale bars = 100 µm (A-C) and 12 µm (a-c).

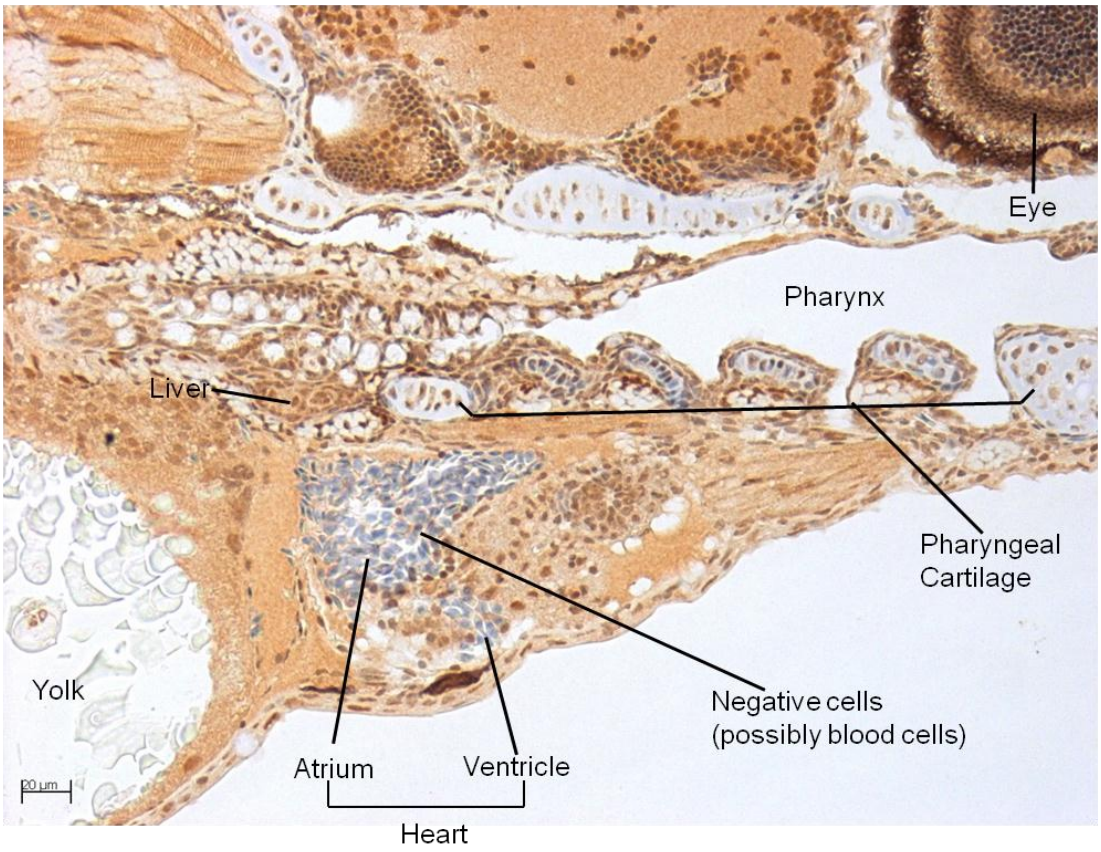

Figure 4.3: MOSPD1 localisation in the heart and surrounding tissue of a 3 dpf zebrafish embryo. A sagittal section of a 3 dpf embryo stained with the mouse monoclonal α-MOSPD1 antibody showing the localisation of MOSPD1 in the heart and surrounding tissue is shown. Scale bar = 20 µm.

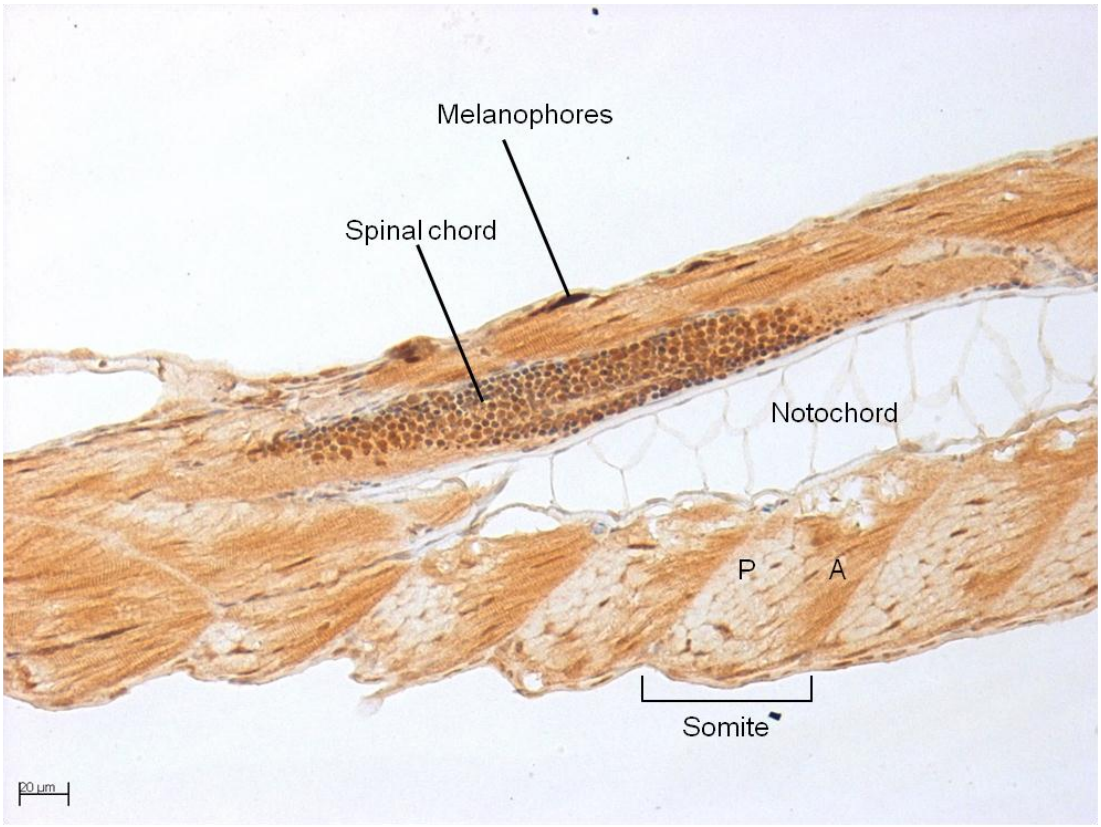

Figure 4.4: MOSPD1 localisation in the tail of a 3 dpf zebrafish embryo. A sagittal section of a 3 dpf embryo stained with the mouse monoclonal α-MOSPD1 antibody showing the localisation of MOSPD1 in the tail is shown. A somite is indicated with the anterior (A) and posterior (P) marked. Scale bar = 20 µm.

4.3.2. Functional analysis of *Mospd 1*

4.3.2.1. Analysis of embryos injected with a start morpholino against *Mospd 1*

4.3.2.1.1 Survival of start morpholino-injected embryos

To assess the general toxicity of the start morpholino the survival of embryos injected with different doses was monitored daily for 3 dpf for 3 individual experiments. This survival was then compared to the survival of negative control 5 mis-pair morpholino-injected embryos and non-injected embryos. At an injected dose of 1 ng 88 % of the start morpholino-injected embryos (n=171) survived to 3 dpf compared to 90 % of the 5MP control-injected embryos (n= 181) and 92 % of the non-injected embryos (n=149) (Figure 4.5A). The survival curve of the morpholino-injected embryos was not significantly different to that of the 5 mis-pair morpholino-injected or the non-injected controls (p= 0.58) (Log-rank (Mantel-Cox) test) and a log rank test for trend showed no significant difference (p=0.31).

When the dose of morpholino injected was doubled to 2 ng per embryo 72 % of the start morpholino-injected embryos (n=203) survived to 3 dpf compared to 68 % of the 5 mis-pair morpholino–injected embryos (n=190) and 84 % non-injected (n=172) control embryos. The survival curves (Figure 4.5B) for the start morpholino-injected and 5 mis-pair morpholino-injected embryos were significantly different to that of the non-injected control embryos ($p<0.01$) (Log-rank Mantel-Cox test). However, the difference in survival between the start morpholino-injected embryos and the 5 mis-pair morpholino-injected embryos was not significantly different (p=0.56).

A

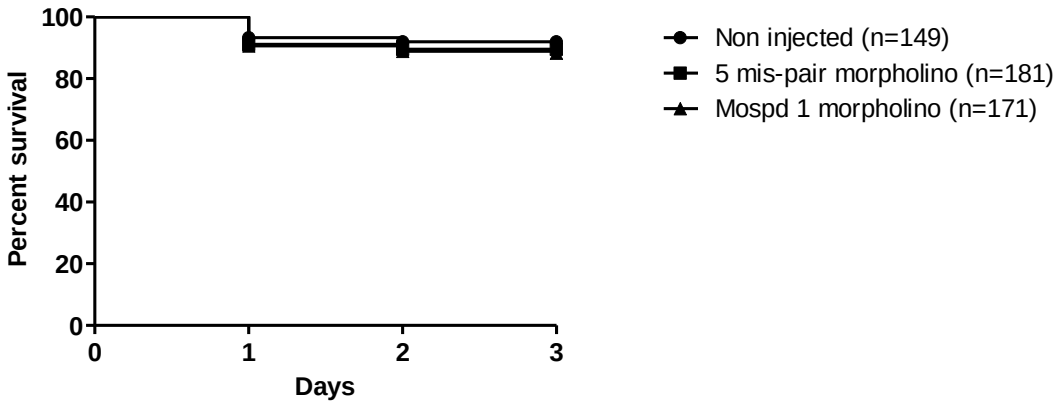

B

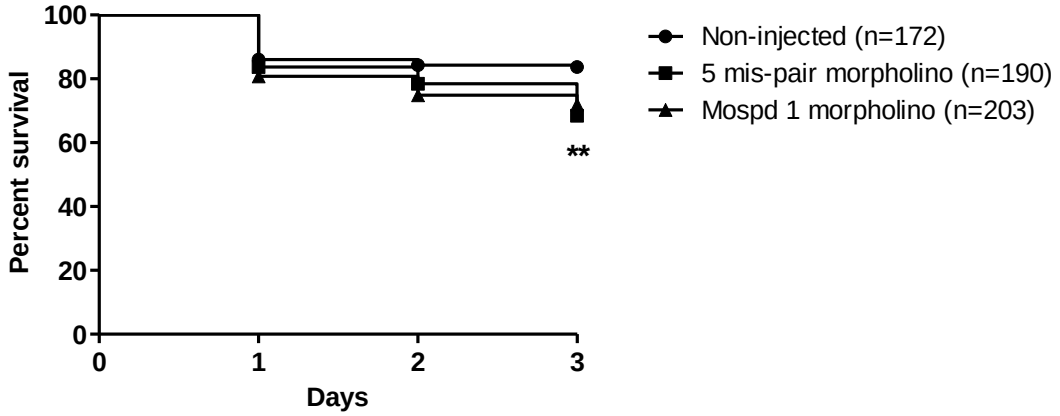

Figure 4.5: Survival to 3 dpf of start morpholino-injected embryos. A: 1ng and B: 2 ng start morpholino- injected embryo survival. Survival curves of Mospd 1 morpholino and 5 mis-pair morpholino-injected embryos were not significantly different (p=0.58) (Log-rank (Mantel-Cox) Test compared to non-injected embryo survival (A). The survival curves for the 2 ng Mospd 1 morpholino-injected and 5 mis-pair morpholino-injected embryos were significantly different to that of non-injected controls (** p=0.008) but were not significantly different (p<0.01) from each other. Data pooled from 3 experiments for each dose.

4.3.2.1.2. Phenotypic analysis of start morpholino-injected embryos

The start morpholino was injected into zebrafish embryos, the fluorescent embryos monitored, as they showed good distribution of the morpholino, and the phenotypes of these embryos assessed daily. The embryos were categorised as either normal, mild or severe. Normal embryos displayed good development, a normal cardiovascular system with a functioning heart and blood circulation throughout the body (Figure 4.6). Embryos that were classified as mild were mostly normal but had a slower heart beat and circulation or mild body deformities whilst severe embryos had blood pooling, oedema or severe axis deformities (Figure 4.7).

91 % of embryos injected with 1 ng of the start morpholino (n=171) were phenotypically normal at 1 dpf with 3 % showing a mild phenotype and 6 % showing a severe phenotype (Figure 4.8 A). This compared to 90 % of the 5 mis-pair morpholino-injected embryos (n=181) being normal, 5 % mild and 5 % severe and 95 % normal non-injected embryos (n=149), 2 % mild and 3 % severe. At 2 dpf 91 % of start morpholino embryos (n=155) were normal, 2 % mild and 7 % severe compared to 92 % normal, 4 % mild and 4 % severe 5 mis-pair morpholino-injected embryos (n=165) and 96 % normal, 1 % mild and 3 % severe non-injected embryos (n=139) (Figure 4.8 B).

By 3dpf 90 % of the start morpholino embryos (n=152) were phenotypically normal, 3 % mild and 7 % severe whilst 91 % of the 5 mis-pair morpholino-injected embryos (n=162) were normal, 3 % mild and 6 % severe and 95 % of the non-injected embryos (n=137) were normal, 2 % mild and 3 % severe (Figure 4.8 C). Two way ANOVA and Bonferroni post hoc tests were used to analyse the data and the phenotypes of the start morpholino-injected embryos were not significantly different to that of the 5 mis-pair morpholino-injected embryos or the non-injected embryos at 1, 2 or 3 dpf ($p>0.05$).

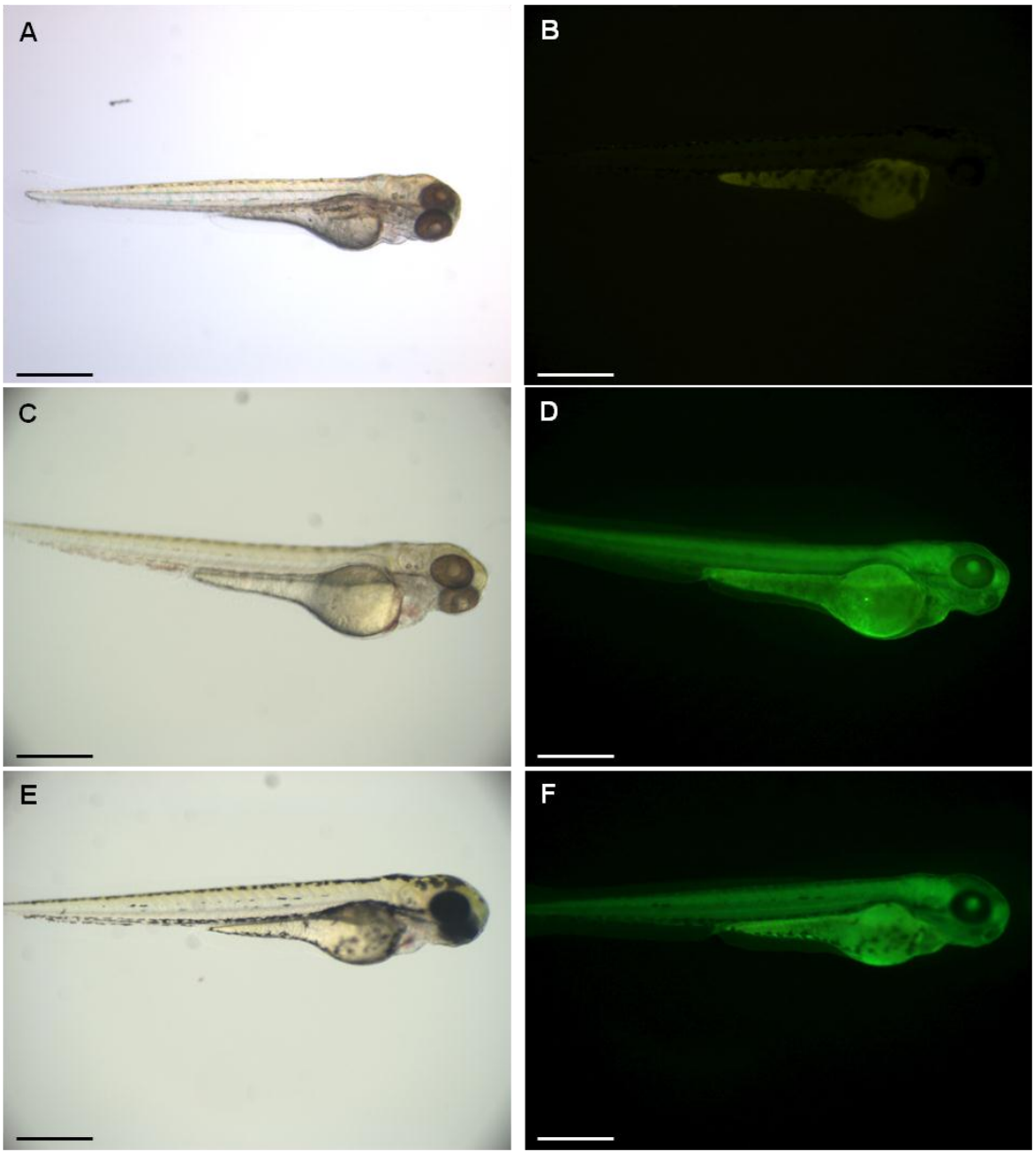

Figure 4.6: 3 dpf phenotypically normal zebrafish embryos. Embryos had developed normally, had a well developed cardiovascular system including looped, beating heart with chambers and blood circulation throughout the body. A and B: non-injected; C and D: 5 mis-pair morpholino-injected; E and F: splice-site injected morpholino (MO2). A, C and E are taken with white light. B, D and F are fluorescence images showing good uptake of the morpholino. Scale bars = 500 µm.

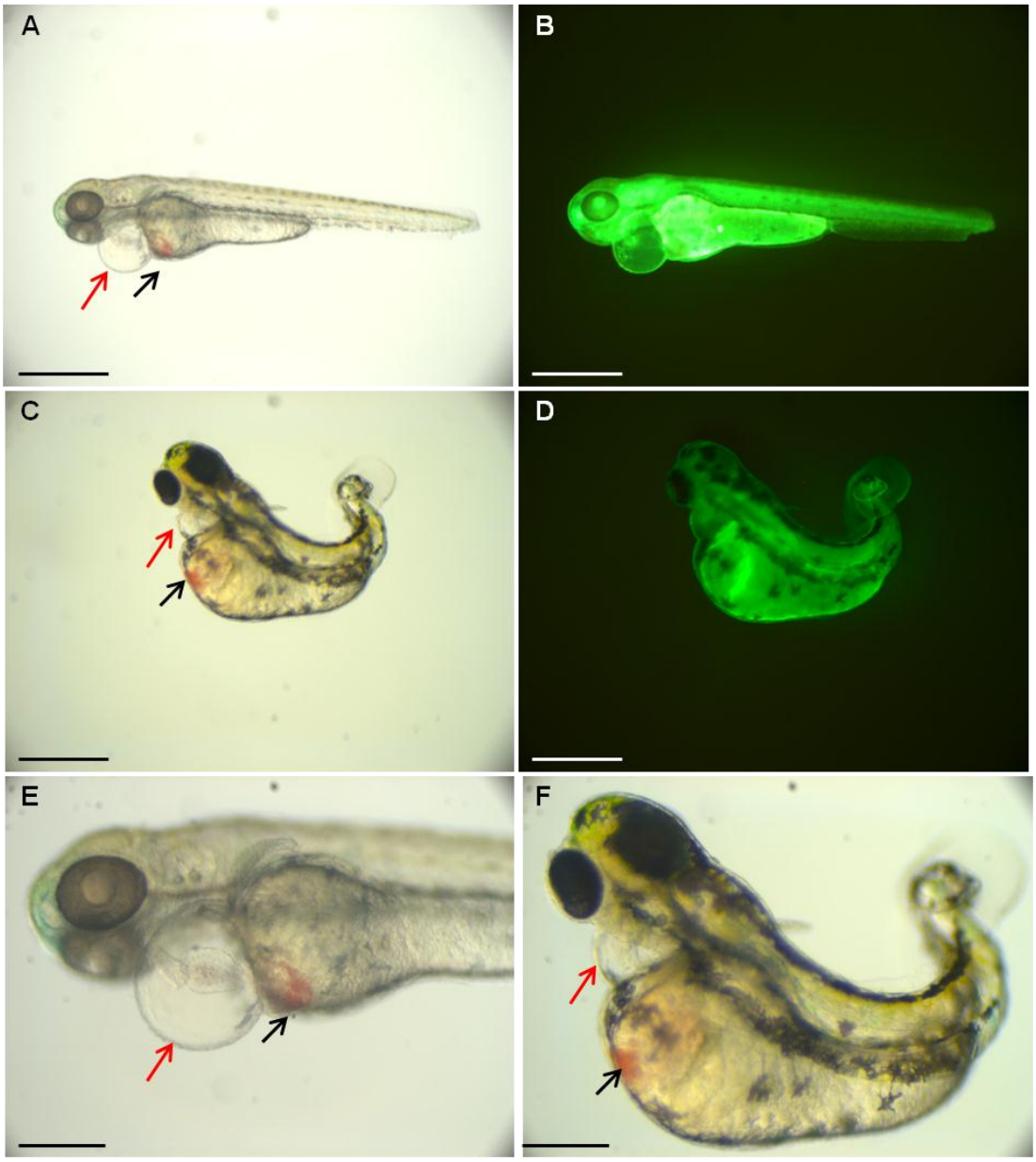

Figure 4.7: 3 dpf phenotypically severe zebrafish embryos. Embryos displayed blood pooling (black arrows), oedema (red arrows) with altered heart morphology and altered body shape. A, C , E and F are taken with white light and B and D are fluorescence images showing uptake of the morpholino. A-D were taken at x5 magnification (Scale bars = 500 µm). E and F were taken at 10x magnification (Scale bars =250 µm).

A

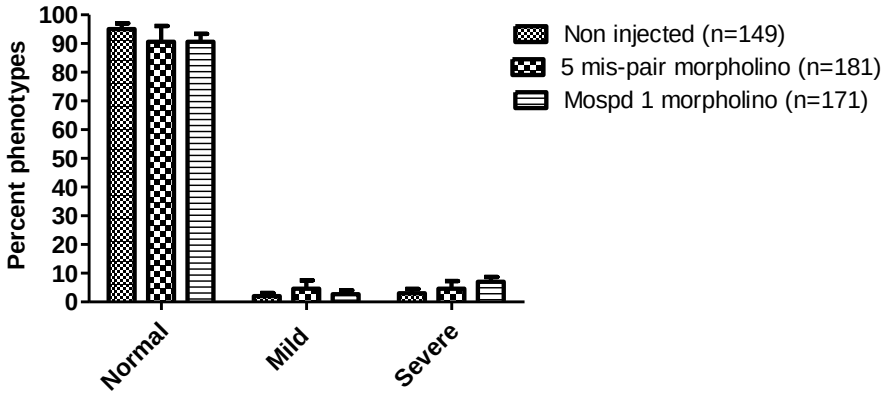

B

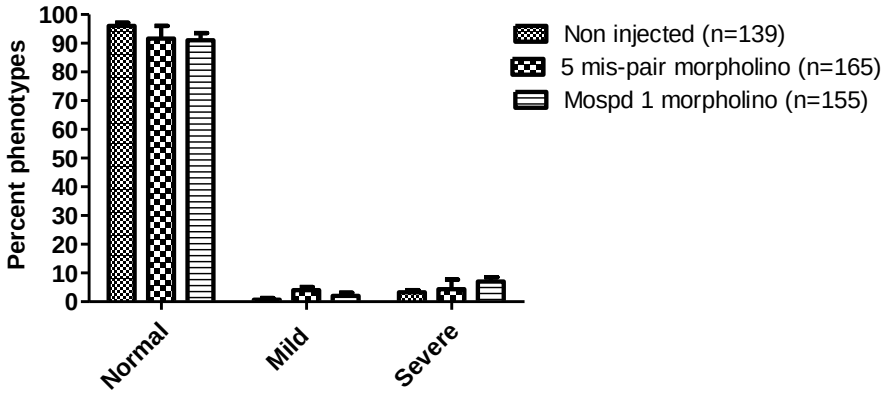

C

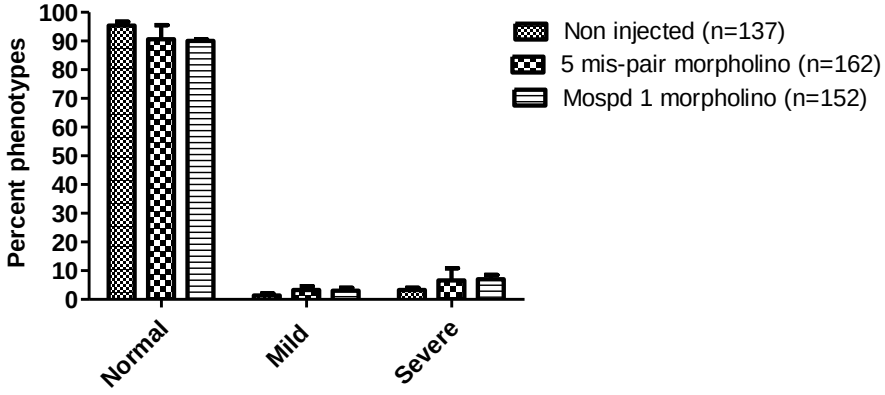

Figure 4.8: Percentage of embryos that displayed a normal, mild or severe phenotype after being injected with 1 ng start morpholino. A: 1 dpf, B: 2 dpf and C: 3 dpf. 2 way ANOVA and Bonferroni post hoc tests indicate that there were no significant differences in phenotypes at 1, 2 or 3 dpf between Mospd 1 start morpholino-injected embryos and the 5 mis-pair morpholino and non-injected controls ($p>0.05$). Data is from 3 individual experiments.

The dose of the start morpholino was increased to 2 ng to check whether an increase would result in a *Mospd 1* phenotype and the embryos monitored daily until 3 dpf. At 1 dpf 65 % of the Mospd 1 morpholino-injected embryos (n=203) were normal, 17 % showed a mild phenotype and 18 % were severe (Figure 4.9A). This compared to 63 % normal, 16 % mild and 21 % severe phenotypes in the 5 mis-pair morpholino-injected embryos (n=190) and 92 % normal, 3 % mild and 5 % severe embryos in the non-injected controls (n=172).

At 2 dpf 93 % of the non-injected controls embryos (n=143) were normal, 1 % showed a mild phenotype and 6 % had a severe phenotype. Embryos injected with either the Mospd 1 morpholino (n=164) or the 5 mis-pair morpholino (n=159) had reduced numbers of normal embryos and increased numbers of mild and severe embryos (MO: 54 % normal, 17 % mild and 29 % severe; 5MP: 50 % normal, 19 % mild and 32 % severe embryos) (Figure 4.9B). By 3 dpf the Mospd 1 morpholino-injected group (n=152) had 44 % normal, 19 % mild and 37 % severe embryos whilst the 5 mis-pair morpholino group (n=149) had 43 % normal, 16 % mild and 7 % severe embryos. The majority of the non-injected embryos (n=140), 92 %, were phenotypically normal with 1 % showing a mild phenotype and 7 % severe (Figure 4.9C).

The differences in the numbers of embryos showing normal, mild and severe phenotypes were significantly different for both the Mospd 1 morpholino-injected and the 5 mis-pair morpholino-injected embryos when compared to the non-injected controls. Two way ANOVA and Bonferroni post hoc tests indicated $p<0.001$ for 2 dpf and 3 dpf for all phenotypes. For 1 dpf $p<0.001$ for normal and $p<0.05$ for mild and severe. However, there were no significant differences in the numbers of normal, mild and severe embryos between the Mospd 1 morpholino and the 5 mis-pair morpholino-injected embryos.

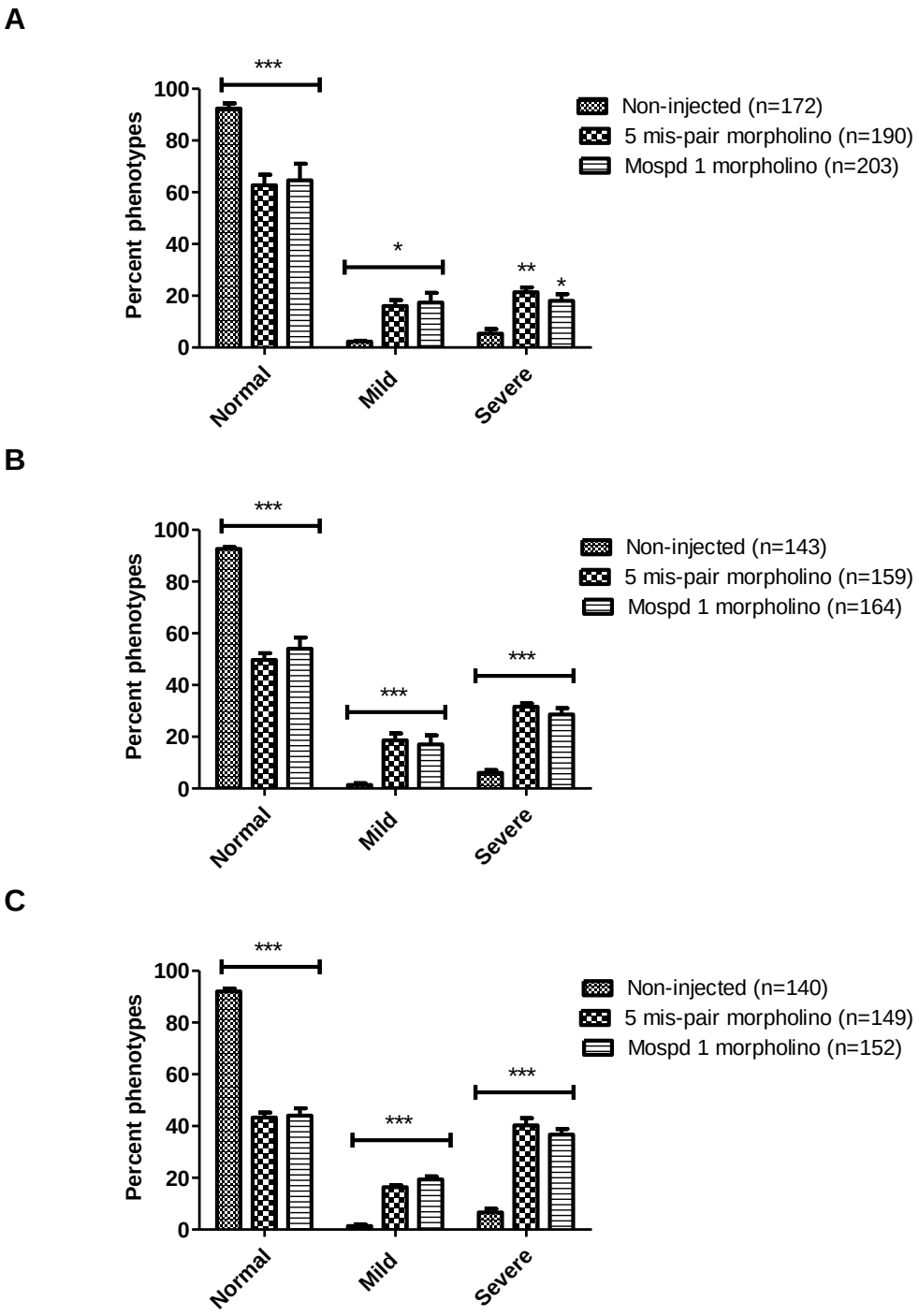

Figure 4.9: Percentage of embryos that displayed a normal, mild or severe phenotype after being injected with 2 ng start morpholino. A: 1 dpf, B: 2 dpf and C: 3 dpf. 2 way ANOVA and Bonferroni post hoc tests indicate that there were significant differences in phenotypes at 1, 2 or 3 dpf between Mospd 1 start morpholino-injected embryos and the 5 mis-pair morpholino when compared to non-injected controls (*: $p<0.05$, **: $p<0.01$, ***: $p<0.001$). There were no significant differences between Mospd 1 morpholino and 5 mis-pair morpholino-injected embryo phenotypes. Data is from 3 individual experiments.

As injection of the 5 mis-pair control morpholino was resulting in a similar phenotype to that observed in the Mospd 1 start morpholino injected embryos it could not be concluded from this data whether the observed phenotype was specific and due to the knock down of MOSPD1 or due to toxicity of the morpholino. It was, therefore, decided to use another morpholino to knockdown *Mospd 1* expression to check whether the same phenotype seen with the start morpholino was observed. The injection of a splice-site morpholino would allow the level of *Mospd 1* expression to be measured. Figure 4.10 shows a schematic representation of *Mospd 1* showing the positions of the start morpholino and the splice-site morpholino. The splice-site morpholino was targeted to the splice junction between exons 2 and 3 and primers designed to measure the knockdown of *Mospd 1* expression by qPCR.

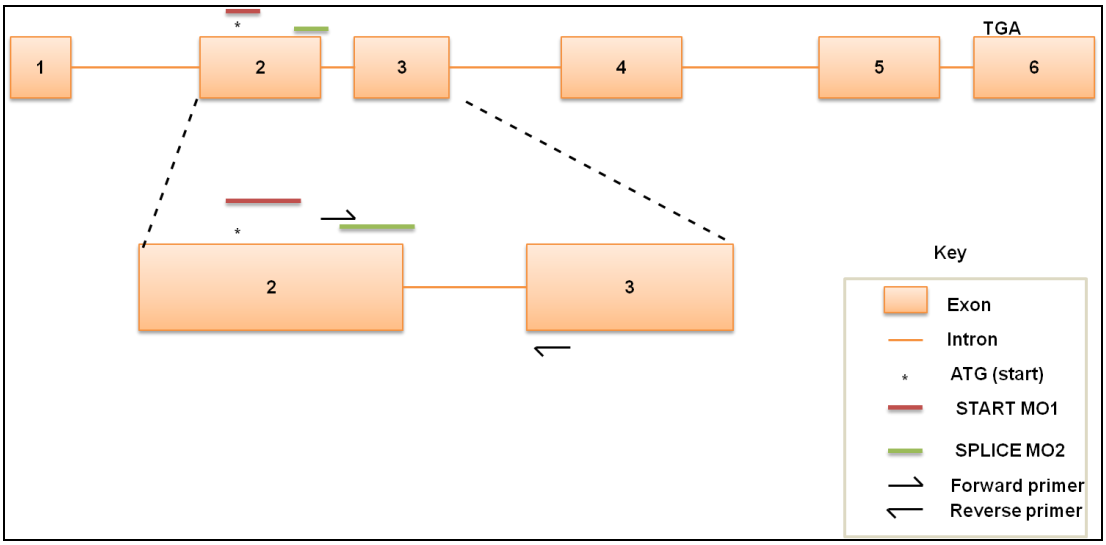

Figure 4.10: Schematic representation of *Mospd 1* and positions of morpholinos. The positions of the Start morpholino (red line) and the splice-site morpholino (green) targeted to the splice junction between exons 2 and 3 are indicated. The positions of the primers used for qPCR to measure knockdown of *Mospd 1* expression is indicated on the enlarged exons 2 and 3.

4.3.2.2. Quantification of *Mospd 1* knockdown

Quantitative real-time PCR was used to measure the expression level of *Mospd 1* in injected embryos to assess if injection of the splice-site morpholino resulted in knockdown of *Mospd 1* expression. The embryos injected with different doses of either Mospd 1 morpholino or its 5 mis-pair morpholino were collected, RNA extracted and qPCR performed on the synthesised cDNA (n=3 per dose). *Mospd 1* expression levels were normalised against the endogenous control, *Elongation factor 1 alpha* (*Ef1α*). The qPCR primers and probes for both *Mospd 1* and *ef1α* were validated using a pool of zebrafish cDNA. All data was statistically analysed using One-way ANOVA with a Bonfferoni's Multiple Comparison post test. There was no significant difference in *Mospd 1* expression levels between non-injected and 5 mis-pair morpholino- injected embryos. In embryos injected with 2 ng of the splice-site Mospd 1 morpholino there was a 53 % level of *Mospd 1* expression compared to non-injected control levels (Figure 4.11A). The 5 mis-pair morpholino- injected embryos had a level of 92 % *Mospd 1*. The level of *Mospd 1* in Mospd 1 morpholino-injected embryos was significantly reduced to 47 % ($p<0.001$) compared to both non-injected and 5 mis-pair morpholino- injected embryo *Mospd 1* levels (Figure 4.11B).

When the dose of Mospd 1 morpholino injected was increased to 4 ng the *Mospd 1* expression level was 41 % of that of non-injected controls. Embryos injected with 4 ng of the 5 mis-pair morpholino had 96 % *Mospd 1* expression compared to non-injected embryos (Figure 4.12A). This 59 % knockdown of *Mospd 1* expression was significantly ($p<0.001$) lower than *Mospd 1* expression levels in the control embryos (Figure 4.12B). A further increase in the dose of Mospd 1 morpholino to 6 ng resulted in a 36 % *Mospd 1* expression level compared to non-injected embryos and 96 % *Mospd 1* expression in 5 mis-pair morpholino-injected embryos (Figure 4.13A). This 64 % reduction in *Mospd 1* levels in the morpholino-injected embryos was significant ($p<0.001$) when compared to control embryos (Figure 4.13B).

A

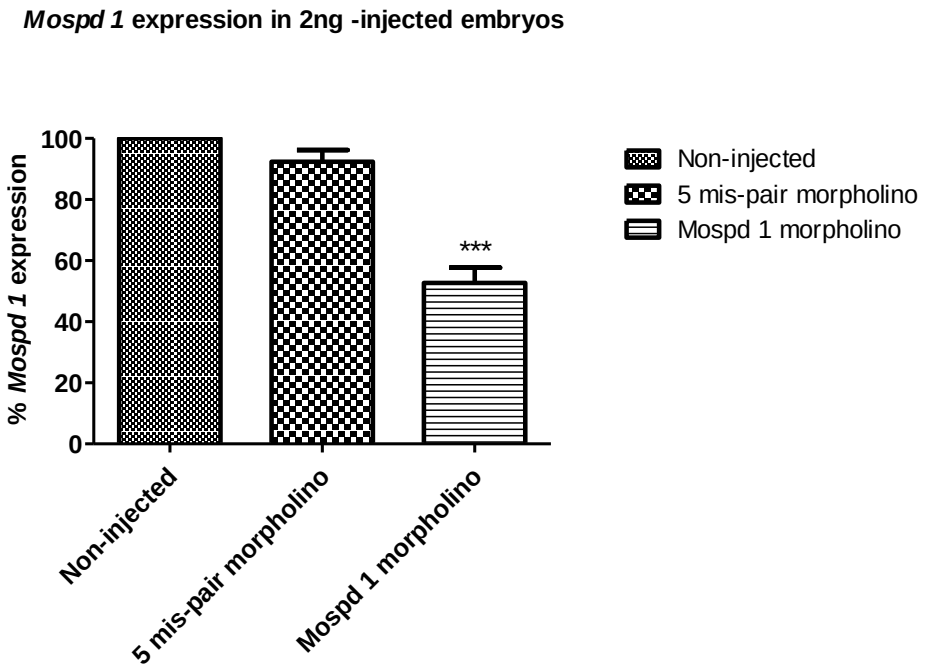

B

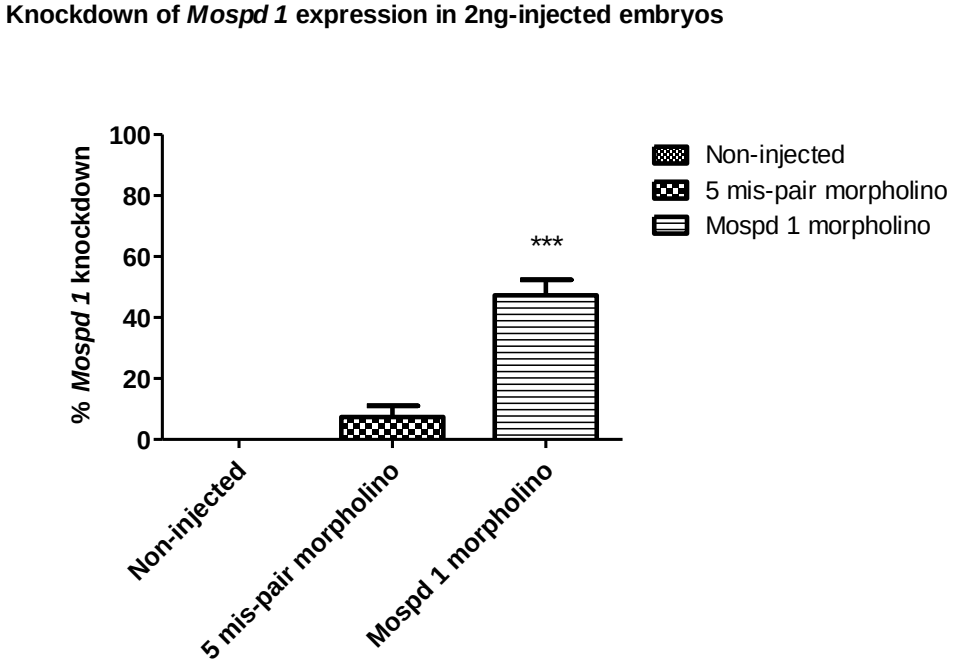

Figure 4.11: Level of *Mospd 1* expression and knockdown in 2 ng splice-site morpholino-injected embryos. The level of *Mospd 1* expression (A) is significantly lower (53 %) in embryos injected with 2 ng morpholino compared to non-injected and negative-control injected embryos with a knockdown of *Mospd 1* expression of 47 % (B). (*** p<0.001) (One-way ANOVA with Bonferroni post hoc test). n=3.

A

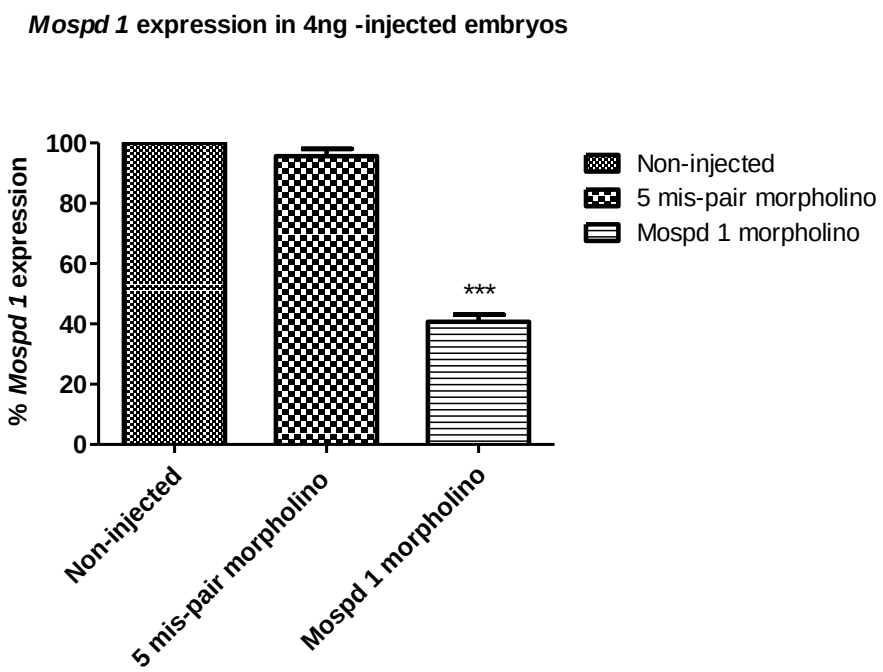

B

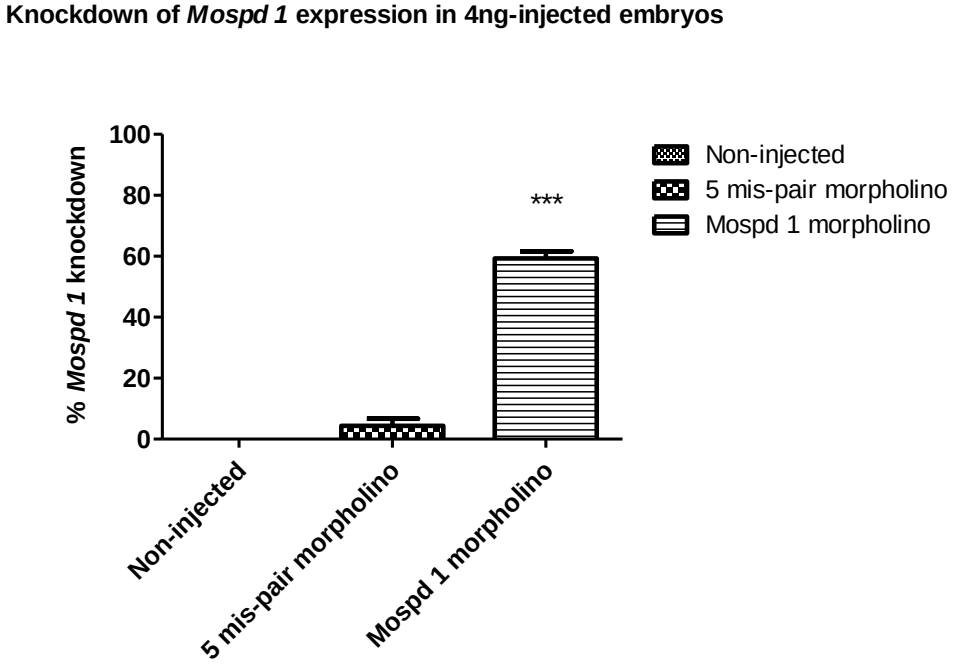

Figure 4.12: Level of *Mospd 1* expression and knockdown in 4 ng splice-site morpholino-injected embryos. The level of *Mospd 1* expression (A) is significantly lower (41 %) in embryos injected with 4 ng morpholino compared to non-injected and negative-control injected embryos with a knockdown of *Mospd 1* expression of 59 % (B). (*** p<0.001) (One-way ANOVA with Bonferroni post hoc test). n=3.

A

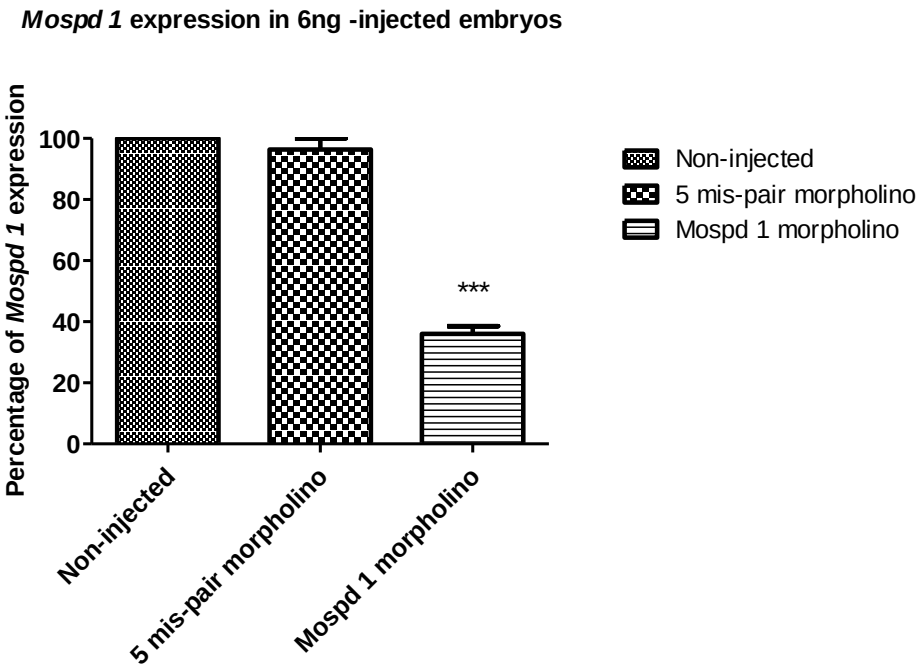

B

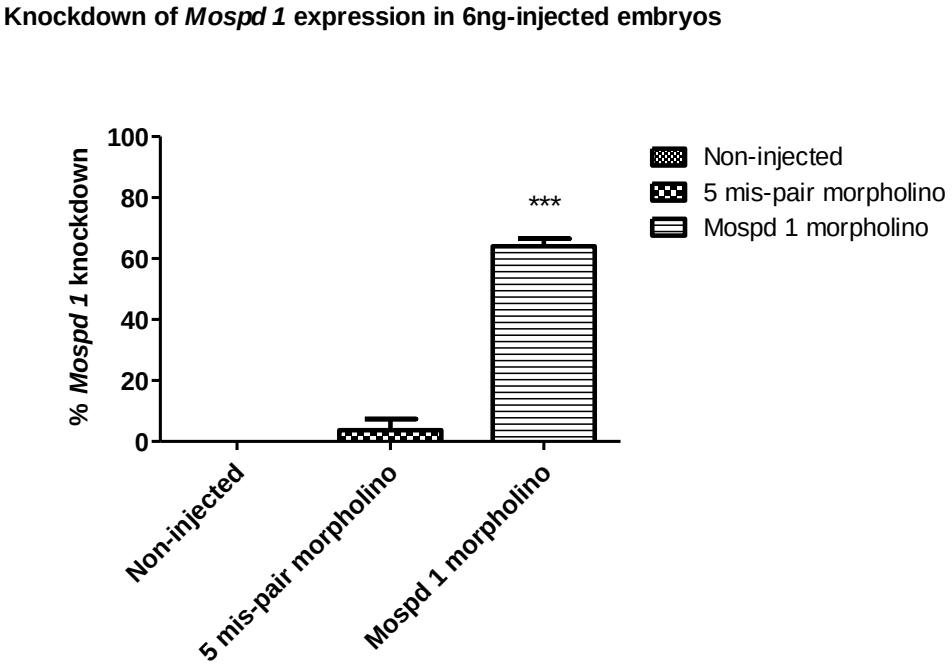

Figure 4.13: Level of *Mospd 1* expression and knockdown in 6 ng splice-site morpholino-injected embryos. The level of *Mospd 1* expression (A) is significantly lower (36 %) in embryos injected with 6 ng morpholino compared to non-injected and negative control-injected embryos with a knockdown of *Mospd 1* expression of 64 % (B). (*** p<0.001) (One-way ANOVA with Bonferroni post hoc test). n=3.

A dose-response analysis was carried out to determine whether the knockdown of *Mospd 1* expression observed in the 2 ng, 4ng and 6 ng doses resulted in a significant reduction in *Mospd 1* expression levels when compared to each other. The level of knockdown was not significantly increased when 2ng embryo levels were compared to 4 ng embryo levels or when 4 ng embryo levels were compared to 6 ng embryo levels. However, the level of knockdown in 6 ng embryos was significantly reduced when compared to 2 ng embryo levels of *Mospd 1* expression ($p<0.05$) (Figure 4.14).

***Mospd 1* knockdown in response to increasing morpholino dose**

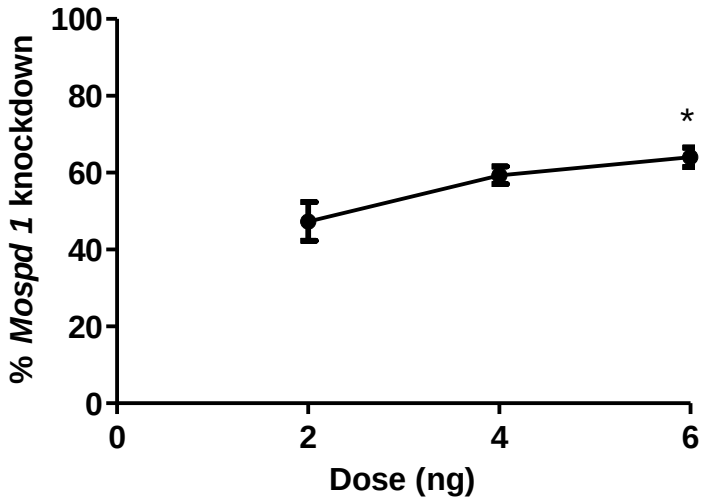

Figure 4.14: Knockdown of *Mospd 1* in response to increasing morpholino dose. As the dose of morpholino injected into embryos is increased from 2 ng to 6ng the percentage of *Mospd 1* knockdown increases. The increased knockdown of *Mospd 1* gene expression is not significant between 2ng and 4 ng or between 4 ng and 6 ng but is significant between 2 ng and 6 ng (* $p<0.05$) analysed by one-way ANOVA).

4.3.2.3. Assessment of *Mospd 1* knockdown phenotype using a splice-site morpholino (MO2)

4.3.2.3.1. Survival of embryos injected with a splice-site morpholino against *Mospd 1*

To assess the general toxicity of the splice-site morpholino (MO2) the survival of embryos injected with different doses was monitored daily for 3 dpf for 3 individual experiments. This survival was then compared to the survival of 5 mis-pair morpholino-injected embryos and non-injected embryos. 90 % of 2ng Mospd 1 morpholino-injected embryos survived to 3 dpf (n=207) compared to 87 % of 5 mis-pair morpholino-injected embryos (n= 165) and 95 % of non-injected embryos (n=149) (Figure 4.15A). The survival curves of the three groups were not significantly different (p=0.10) when compared using a Log-rank (Mantel-Cox) Test and a log rank test for trend showed that the curves showed no significant difference in survival trends (p=0.23).

When the dose of splice-site morpholino was increased to 4 ng 91 % of the Mospd 1 morpholino-injected embryos (n=268) survived to 3 dpf compared to 89 % of the 5 mis-pair morpholino-injected embryos (n=221) and 95 % non-injected embryos (n=189) (Figure 4.15B). The survival curves were not significantly different (p=0.10) and the curves did not show a significant difference in trend (p=0.29) (Log-rank test for trend).

An increase in the dose, to 6 ng, of morpholino injected resulted in a significant difference in the survival of morpholino-injected embryos (n=184) and the survival of non-injected controls (n=180) with 77 % Mospd 1 morpholino-injected embryos surviving to 3 dpf compared to 97 % of the non-injected embryos ($p<0.001$). 78 % of the 5 mis-pair morpholino-injected embryos (n=170) survived to 3 dpf, significantly less than non-injected controls ($p<0.001$) (Figure 4.15C).

A

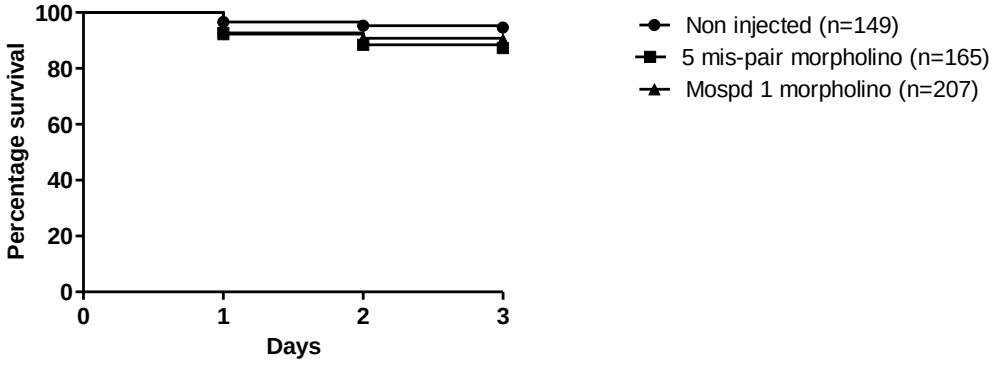

B

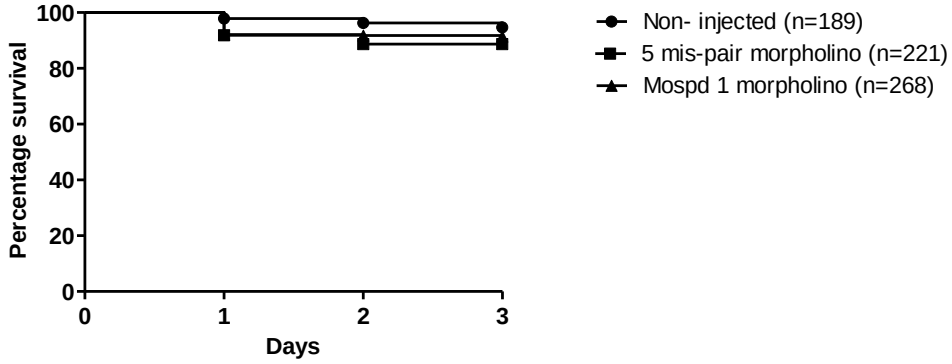

C

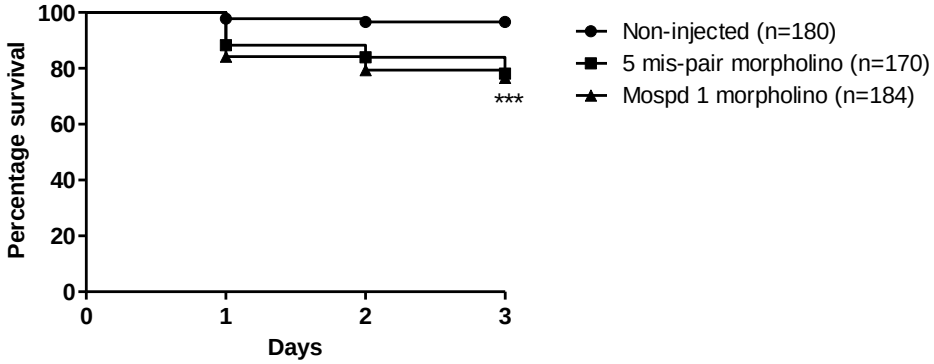

Figure 4.15: Survival to 3 dpf of splice site morpholino-injected embryos. A: 2 ng, B: 4 ng and C: 6 ng morpholino-injected embryo survival. Survival curves of 2 ng and 4 ng Mospd 1 morpholino and 5 mis-pair morpholino-injected embryos were not significantly different (p=0.10) (Log-rank (Mantel-Cox) Test compared to non-injected embryo survival (A and B). The survival curves for the 6 ng Mospd 1 morpholino-injected and 5 mis-pair morpholino-injected embryos were significantly different to that of non-injected controls (*** p<0.001) but were not significantly different (p=0.71) to each other. Data pooled from 3 experiments for each dose.

However, the survival of Mospd 1 morpholino-injected and 5 mis-pair morpholino-injected embryos was not significantly different to each other (p=0.71) (Log-rank (Mantel-Cox) Test). This suggests that at a dose of 6 ng the morpholino was toxic to the embryos and that 2 ng and 4 ng doses would be more suitable to assessment of a Mospd 1 phenotype.

4.3.2.3.2. Phenotypic analysis of splice-site morpholino (MO2)-injected embryos

A morpholino targeted to the splice junction between exons 2 and 3 of the *Mospd 1* gene was injected into zebrafish embryos in order to knockdown the gene expression of *Mospd 1*. A 5 mispair morpholino was also injected into embryos at the same dose as the splice-site morpholino (MO2) and non-injected embryos served as another negative control. The embryos were categorised into normal, mild or severe groups in the same way as the embryos injected with the start morpholino and its 5 mis-pair control.

At a dose of 2 ng the majority of MO2-injected embryos (n=207) were phenotypically normal at 1 dpf with 96 % normal, 2 % mild and 2 % severe embryos compared to 5 mis-pair morpholino-injected embryos (n=165) that had 94 % normal, 3 % mild and 3 % severe embryos. 96 % of the non-injected embryos (n=149) were normal whilst there were 2 % mild and 2 % severe embryos. At 2 dpf 91 % of the MO2-injected embryos (n=191) were normal with 4 % mild and 5 % severe embryos compared to 88 % normal, 6 % mild and 6 % severe embryos injected with the 5 mis-pair morpholino (n=153). In the non-injected embryos (n=144) 92 % were normal, 3 % mild and 5 % severe. At 3 dpf the MO2-injected embryos (n=188) had the same percentage of normal, mild and severe phenotypes as at 2 dpf whilst the 5 mis-pair morpholino-injected embryos (n=146) had 89 % normal, 6 % mild and 5 % severe embryos and 94 % of the non-injected controls (n=142) were normal with 1 % mild and 5 % severe embryos (Figure 4.16).

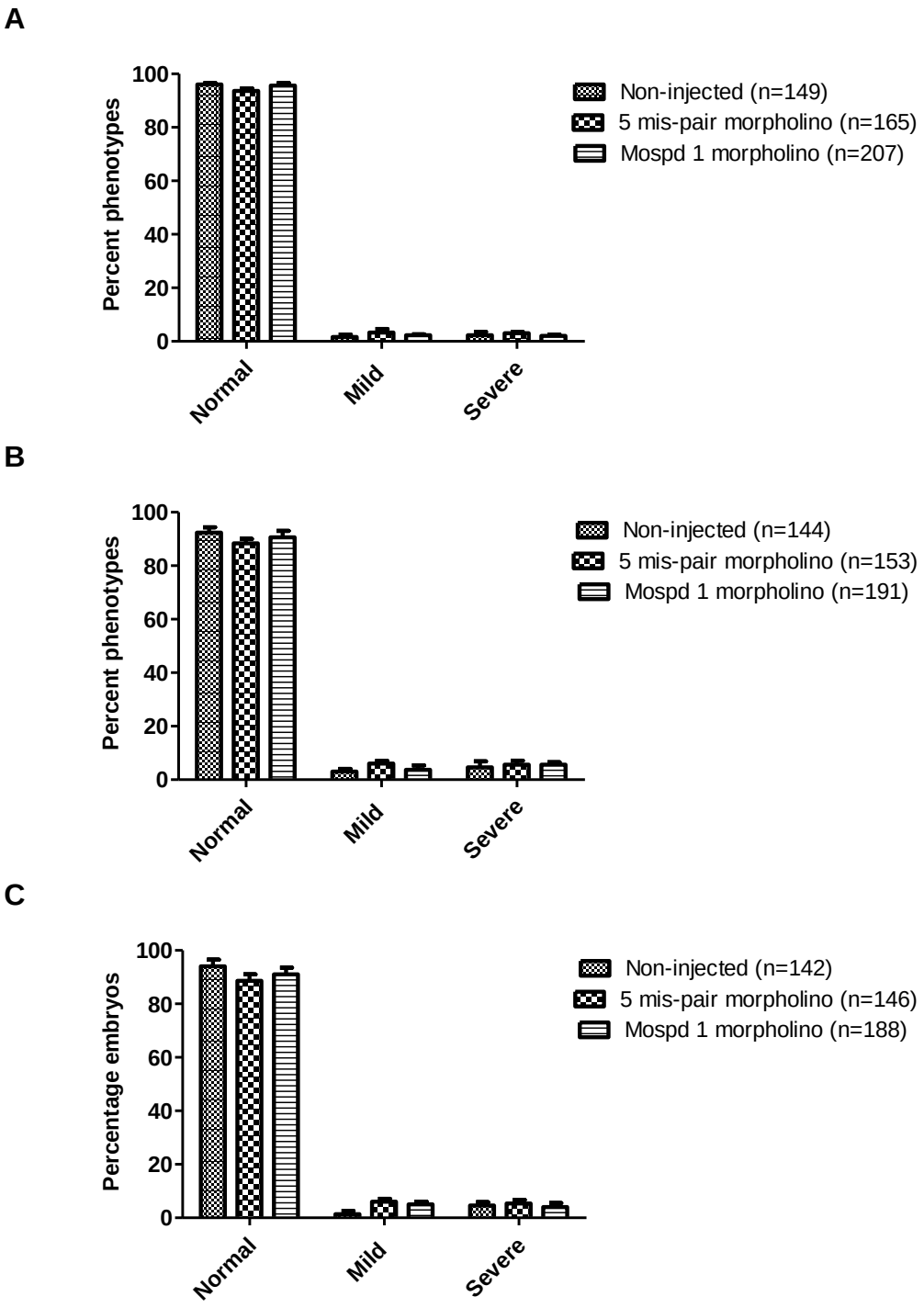

Figure 4.16: Percentage of embryos that displayed a normal, mild or severe phenotype after being injected with 2 ng splice-site morpholino. A: 1 dpf, B: 2 dpf and C: 3 dpf. 2 way ANOVA and Bonferroni post hoc tests indicate that there were no significant differences in phenotypes at 1, 2 or 3 dpf between Mospd 1 morpholino-injected embryos and the mis-pair morpholino and non-injected controls ($p>0.05$). Data is from 3 individual experiments.

2-way ANOVA with Bonferroni's post tests showed that the percentage of normal, mild and severe phenotypes of 2ng MO2-injected embryos was not significantly different in comparison to both 5 mis-pair morpholino -injected embryos and non-injected controls ($p>0.05$).

The dose of the splice-site morpholino was increased to 4 ng to check whether an increase would result in a *Mospd 1* knockdown phenotype. However, when the percentages of phenotypes were compared to both non-injected controls and 5 mis-pair morpholino-injected controls there was no significant difference in the phenotypes observed at 1, 2 or 3 dpf. At 1 dpf 88 % of the MO2-injected embryos (n=268) were normal, 4 % mild and 8 % severe compared to 85 % normal, 6 % mild and 9 % severe embryos in the 5 mis-pair morpholino-injected group (n=221). 93 % of the non-injected controls (n=189) were normal, 2 % mild and 5 % severe at 1 dpf whilst at 2 dpf there were 89 % normal, 2 % mild and 9 % severe in this control group (n=185). Both the MO2-injected (n=247) and 5 mis-pair morpholino-injected (n=203) groups had 81 % normal embryos. There were 6 % mild and 13 % severe 5 mis-pair morpholino-injected embryos compared to 4 % mild and 16 % severe in the MO2 group. At 3 dpf there were 82 % normal, 2 % mild and 16 % severe MO2-injected embryos (n=246) whilst there were 80 % normal, 6 % mild and 14 % severe 5 mis-pair morpholino- injected embryos (n=196). 90 % of the non-injected controls (n=182) were normal and 2 % mild and 16 % severe (Figure 4.17).

To ensure that a phenotype that arose at a later stage of development was not missed 4 ng morpholino-injected embryos were assessed until 5 dpf. 80 % of the MO2-injected embryos (n=243) were normal, 4 % mild and 16 % severe compared to 78 % normal, 7 % mild and 15 % severe embryos in the 5 mis-pair morpholino-injected group (n=195). The non-injected control group (n=180) had 87 % normal, 4 % mild and 9 % severe embryos (Figure 4.18). There were no significant differences in the phenotypes observed in all three groups ($p>0.05$) (Two way ANOVA and Bonferroni's post hoc test).

A

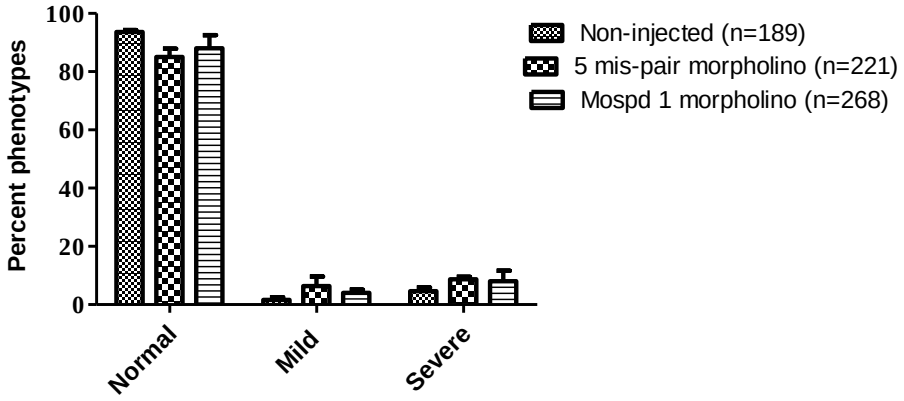

B

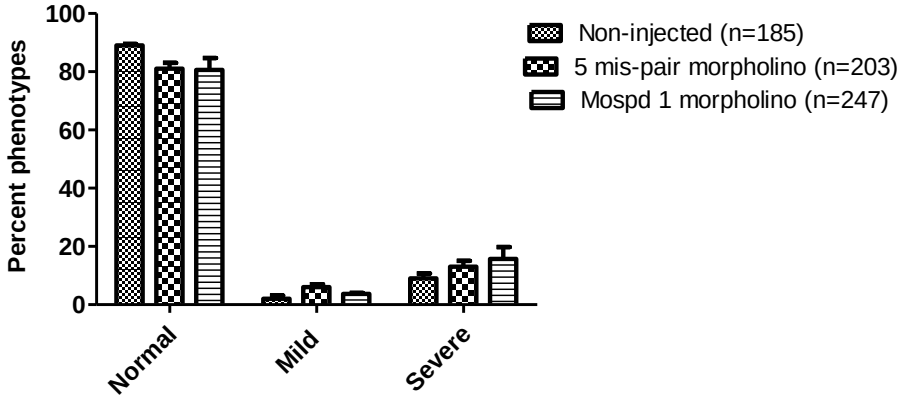

C

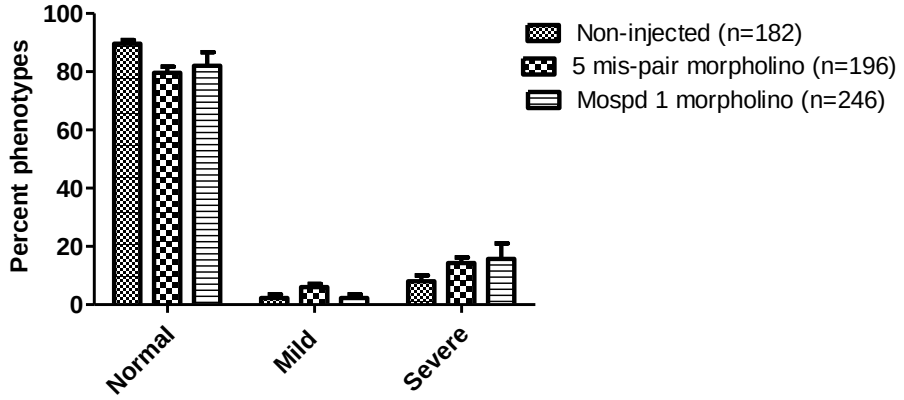

Figure 4.17: Percentage of embryos that displayed a normal, mild or severe phenotype after being injected with 4 ng splice-site morpholino. A: 1 dpf, B: 2 dpf and C: 3 dpf. 2 way ANOVA and Bonferroni post hoc tests indicate that there were no significant differences in phenotypes at 1, 2 or 3 dpf between Mospd 1 morpholino-injected embryos and the 5 mis-pair morpholino and non-injected controls ($p>0.05$). Data is from 3 individual experiments.

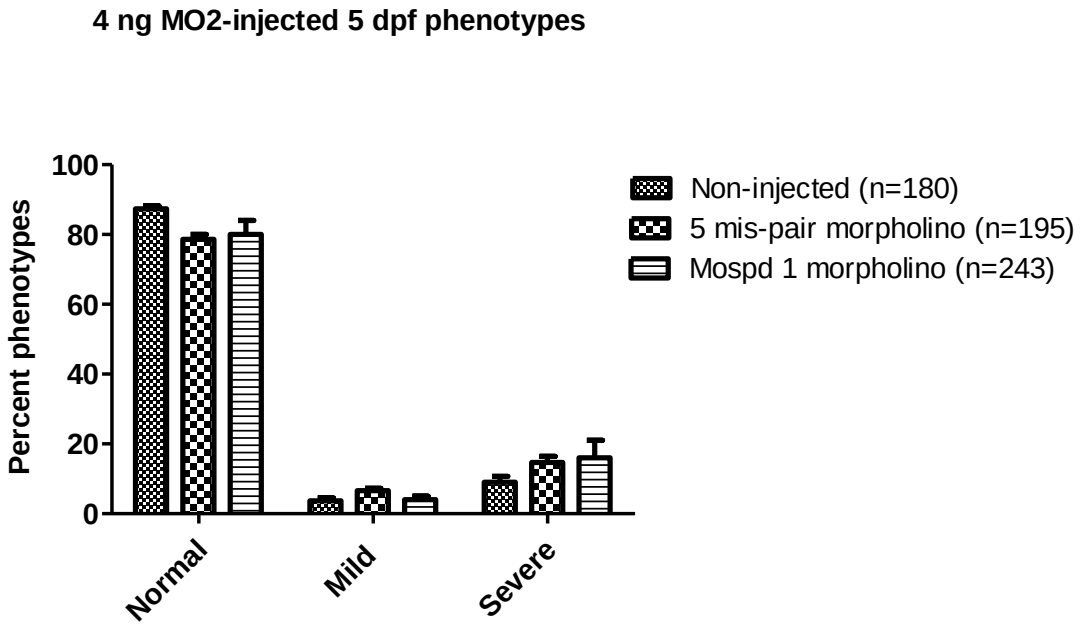

Figure 4.18: Percentage of embryos that displayed a normal, mild or severe phenotype after being injected with 4 ng splice-site morpholino at 5 dpf. 2 way ANOVA and Bonferroni post hoc tests indicate that there were no significant differences in the percentage of embryos with normal, mild or severe phenotypes at 5 dpf between Mospd 1 morpholino-injected embryos and the 5 mis-pair morpholino and non-injected controls ($p>0.05$). Data is from 3 individual experiments.

The injected splice-site morpholino dose was increased to 6 ng and the observed phenotypes of the embryos compared to 6 ng 5 mis-pair morpholino-injected embryos and non-injected controls. At 1 dpf 46 % of the MO2-injected embryos (n=184) were normal, 11 % mild and 43 % had a severe phenotype. This was compared to 53 % normal, 11 % mild and 36 % severe embryos in the 5 mis-pair morpholino-injected group (n=137) and 95 % normal, 2 % mild and 3 % severe in the non-injected control group (n=180). There were significantly more normal embryos in the non-injected group compared to both Mospd 1 morpholino and 5 mis-pair morpholino-injected embryos which had significantly more severe embryos ($p<0.001$). However, there was no significant difference between 5 mis-pair morpholino-injected embryos and MO2-injected embryos ($p>0.05$) (Figure 4.19 A).

At 2 dpf there was no significant differences in the proportion of phenotypes observed between the MO2- (n=155) and 5 mis-pair morpholino-injected (n=121) groups with 44 % of the MO2-injected embryos being normal, 8 % mild and 48 % severe compared to 41 % normal, 18 % mild, 41 % severe embryos in the 5 mis-pair morpholino-injected group ($p>0.05$). The proportion of normal and severe phenotypes observed in the non-injected control group (n=176) was significantly different to the 2 injected groups ($p<0.001$) (Figure 4.19 B).

By 3 dpf there were 42 % normal, 8 % mild and 50 % severe embryos in the MO2-injected group (n=146) compared to 38 % normal, 17 % mild and 45 % severe in the 5 mis-pair morpholino-injected group (n=115). The proportion of these phenotypes was not significantly different between the two groups ($p>0.05$). However, the proportion of normal and severe phenotypes was significantly different to that of the non-injected control group (n=174) that had 92 % normal, 1 % mild and 7 % severe embryos ($p<0.001$) (Figure 4.19 C). Data was analysed using 2 way ANOVA and Bonferroni's post hoc tests.

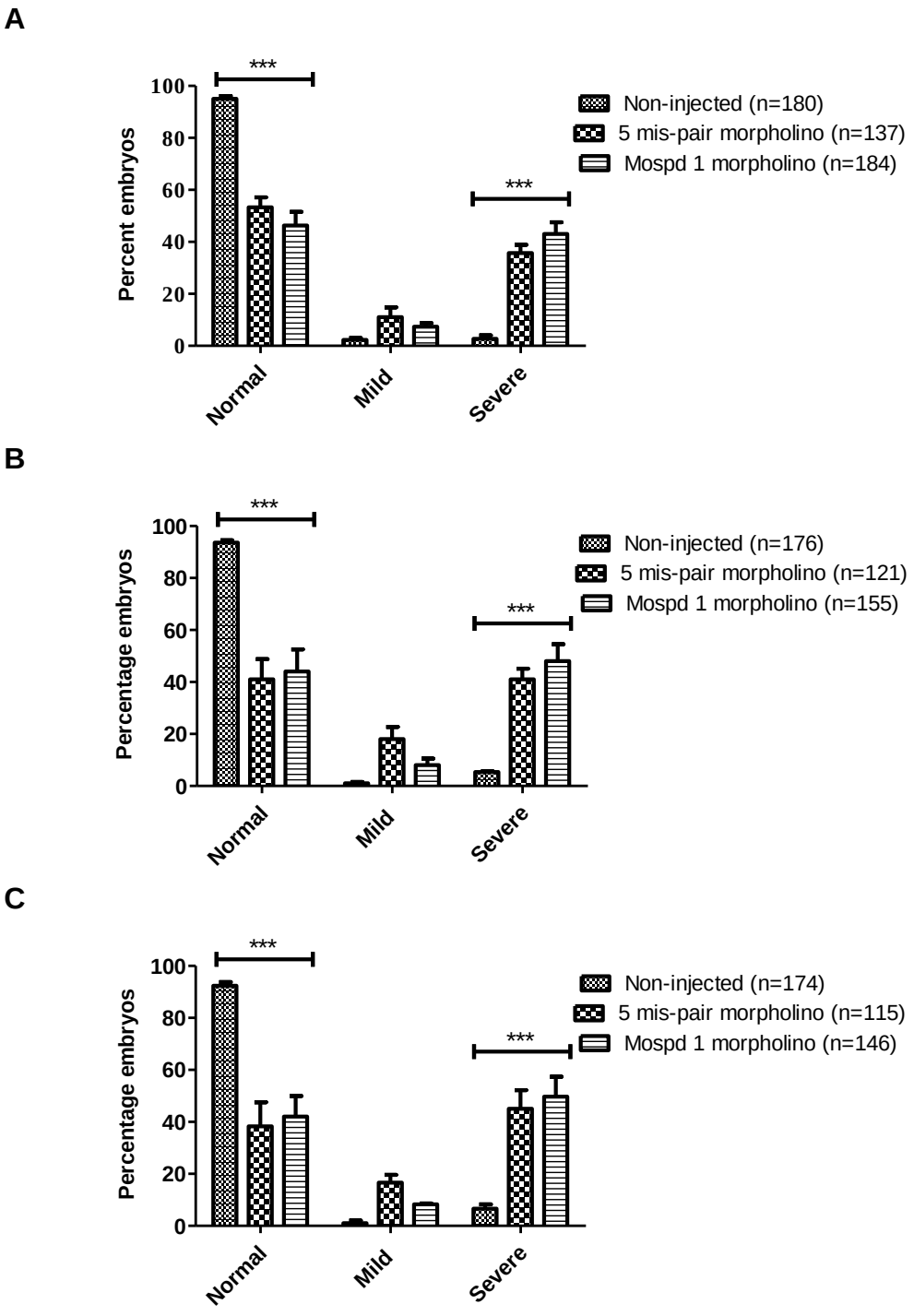

Figure 4.19: Percentage of embryos that displayed a normal, mild or severe phenotype after being injected with 6 ng splice-site morpholino. A: 1 dpf, B: 2 dpf and C: 3 dpf. The proportion of normal and severe embryos in Mospd 1 morpholino and 5 mis-pair morpholino-injected groups were significantly different ($p<0.001$) compared to non-injected controls but not to each other ($p>0.05$) (2 way ANOVA and Bonferroni post hoc tests). Data is from 3 individual experiments.

4.4. Discussion

The *Mospd 1* gene is present in the zebrafish genome as expected as it is a vertebrate gene and *Mospd 1* transcripts have been found to be expressed throughout the developing zebrafish embryo by WISH (Thisse *et al*., 2004). However, the presence of *Mospd 1* transcripts does not necessarily mean that the MOSPD1 protein is present. Mouse MOSPD1 and zebrafish MOSPD1 share 77 % sequence identity and as the peptide used to generate the mouse monoclonal α-MOSPD1 (described in Chapter 3) shares 50 % sequence identity with the corresponding zebrafish sequence it was thought it could be used to detect MOSPD1 expression in the developing embryo.

Immunohistochemistry showed that the mouse monoclonal α-MOSPD1antibody was able to detect MOSPD1 in zebrafish embryos and that MOSPD1 was localised throughout the developing embryo confirming the *Mospd 1* transcript expression from the WISH. MOSPD1 was localised to the nucleus which is similar to its localisation *in vitro* in HaCaTs and *in vivo* in mouse adult tissues (Chapter 3). This could indicate that *Mospd 1* has a conserved role in vertebrates. The cytoplasmic localisation of MOSPD1 in zebrafish embryos could be due to the presence of rapidly dividing cells in zebrafish embryos as they develop quickly and, therefore, have high cell proliferation rates. The localisation of MOSPD1 in somites was cytoplasmic in the anterior and nuclear in the posterior. This difference in MOSPD1 localisation in somites could indicate that MOSPD1 is involved in different roles within different parts of the somites. The α-MOSPD3 antibody did not detect MOSPD3 protein expression in zebrafish embryos as expected due to the absence of a *Mospd 3* gene in the zebrafish genome.

When *Mospd 1* gene expression is significantly reduced in zebrafish embryos using morpholinos the ability of these embryos to survive is not affected. The majority of these morpholino-injected embryos have a normal gross phenotype. Given the cardiac phenotype of the *Mospd 3* gene trap mice (Pall *et al*., 2004) and the fact that

Mospd 1 is closely related to *Mospd 3* the morpholino-injected embryos were assessed for any cardiac phenotype. The gross structure of the heart, heart rate and heart function appeared to be normal in Mospd 1 morpholino-injected embryos. This could possibly be due to *Mospd 1* not being essential for early zebrafish embryo development or survival. However, the main limitation of the current study is the level of knockdown of *Mospd 1* expression achieved which may not be sufficient to result in a phenotype. Embryos with approximately 50 % of *Mospd 1* expression have the level of gene expression of a heterozygous embryo and many heterozygous animals do not display the phenotype of their homozygous null counterparts during early development which is when these zebrafish embryos are being assessed. The level of *Mospd 1* knockdown may need to be increased further. Increasing the dose of the morpholino did not result in a very large increase in knockdown in *Mospd 1* expression and only resulted in an increase in non-specific phenotypes being observed, indicated by the fact that the 5 mis-pair control-injected embryos showed the same levels of phenotype but not significant knockdown of *Mospd 1* expression. Therefore, these phenotypes were most likely due to off target effects such as knockdown of a gene other than the target *Mospd 1* gene. (Morcos, 2007) reported that injection of an individual morpholino targeted to a splice-site could reduce knockdown of gene expression to 50 % whereas a combination of 3 non-overlapping morpholinos targeted to the same gene being co-injected into embryos could result in approximately 90 % knockdown. Therefore, in order to increase the amount of knockdown of *Mospd 1* gene expression a second morpholino targeted to a different splice-site could be co-injected into the embryos with the original splice-site morpholino.

Off target effects are common in morpholino experiments as the dose of morpholino injected is increased (Robu *et al*., 2007). The injection of the 5 mis-pair morpholino is used to monitor whether an observed phenotype is specific as the 5 mis-pair morpholino should not result in the specific phenotype at a dose seen in the morpholino. Injection damage can also result in abnormal development. However, this should have been minimised in the experiments since 3 hours after the

morpholino was injected, embryos were sorted and injection damaged embryos removed. Morpholino toxicity can also result in abnormal phenotypes being observed and this makes the use of controls essential to confirming whether a phenotype is due to the knockdown of the gene of interest or an off target effect. The most common off target effect of morpholino use is the activation of the p53 pathway (Robu *et al*., 2007) resulting in apoptosis and neural death, in about 15-20 % of morpholino experiments (Ekker and Larson, 2001). The co-injection of a p53 morpholino is often used to reduce this non-specific neural death phenotype. However, as this phenotype was not observed in the Mospd 1 morpholino experiments it does not seem to be necessary to co-inject the p53 morpholino.

The morpholinos used to knockdown *Mospd 1* expression in zebrafish embryos showed effects due to toxicity as demonstrated by the 5 mis-pair control morpholino-injected embryos showing the same adverse developmental defects such as axis damage, oedema and blood pooling as those injected with the Mospd 1 morpholinos. At a dose of 2 ng the start morpholino was toxic and at a dose of 6 ng the splice-site morpholino was toxic. The severe phenotypes observed in morpholino-injected embryos were due to the toxicity of the morpholino at the doses used and not due to the knockdown of *Mospd 1* expression.

As only the gross phenotype of the embryos was assessed in these experiments the fact that they appeared normal does not necessarily mean that they were phenotypically normal. It is possible that intracellular changes have occurred in these embryos that cannot be measured by simple microscopic examination. As the immunohistochemistry of zebrafish embryos has shown that MOSPD1 is expressed in the nucleus of these embryos knockdown of *Mospd 1* could result in a phenotype that cannot be detected by microscopy but requires more complex studies.

A recent study trying to identify genes important in angiogenesis investigated 50 genes found to be highly expressed in the microvasculature, including *Mospd 1* (Kalen *et al*., 2009). *Mospd 1* expression was knocked down using two non-overlapping translational blocking morpholinos and the embryos examined at 24 hpf (1 dpf) and 56 hpf. The embryos were checked for any changes in morphology as wells as whether blood flow was defective and whether there was a reduction in intersegmental vessel sprouting. Microangiography was performed on the embryos and heart beat measured. In the *Mospd 1* knockdown embryos no gross phenotype was reported and there were no changes in the microvasculature of these embryos. It was determined that *Mospd 1* was not required for angiogenesis (Kalen *et al*., 2009). These findings have the limitation that the level of MOSPD1 knockdown was not reported and due to the lack of availability of a commercial α-MOSPD1 antibody it was likely not measured in this study. Therefore, the lack of phenotype may be due to insufficient knockdown.

In conclusion, it appears that knockdown of *Mospd 1* expression by about 60 % does not result in an observable phenotype. However, further knockdown of *Mospd 1* may result in a phenotype and, therefore, due to the limitations discussed above the current study cannot establish whether *Mospd 1* is essential to early zebrafish development and survival. In order to establish the function of *Mospd 1* in zebrafish it would be useful to further knockdown expression. It would also be worth trying to identify any proteins that MOSPD1 may associate with and co-inject morpholinos against those genes with the *Mospd 1* morpholino. This may result an observable phenotype and establish the function of *Mospd 1*.

CHAPTER 5:

GENERATION AND PHENOTYPIC ASSESSMENT OF *MOSPD 1* NULL ES CELLS

5.1 Introduction

Mospd 1 is a gene that belongs to the, relatively uncharacterised, *Mospd* gene family and its function is yet to be determined. In parallel with the knockdown of *Mospd 1* in zebrafish, described in Chapter 4, a conditional knockout of *Mospd 1* in ES cells was generated. A targeting vector was generated by Katrin Buerger (PhD thesis, 2009) that has exons 2-4 of the *Mospd 1* gene flanked by lox P sites (Figure 5.1 A). As the transcriptional start site of the *Mospd 1* gene is in exon 2 the *Cre recombinase* (*Cre*) mediated deletion of these exons would result in functional loss of the MOSPD1 protein. A neomycin cassette was incorporated into the targeting vector allowing for the selection of targeted clones. As *Mospd 1* is an X-linked gene and the E14 IV ES cell line was generated from male mice the introduction of *Cre recombinase* would result in a null cell line.

Generation of *Mospd 1* null ES cells will provide a valuable tool to investigate the function of *Mospd 1*. These cells can be used for *in vitro* functional tests as well as assessment of the role of *Mospd 1 in vivo* if used to generate a *Mospd 1* null mouse. The *Mospd 1* null ES cells can be differentiated *in vitro* and compared to wild type ES cells to investigate whether *Mospd 1* is required for differentiation. The use of *Cre* -mediated excision to generate null ES cells for functional studies has been used to study the function of genes *in vitro*. For example the function of *Jsap 1*, a gene encoding a scaffold protein involved in JNK signalling, in cardiomyocyte differentiation (Sato *et al*., 2005) and that of the *LIM-domain binding protein 1* (*Ldb1*) in neuronal differentiation (Hwang *et al*., 2008) have been determined using ES cells null for these genes.

Conditional *Mospd 1* and *Mospd 3* alleles in the CGR8 ES cell line had been generated previously but were found to be karyotypically abnormal with trisomy of one of the chromosomes. It was found that the parental CGR8 cell line was also karyotypically abnormal (Katrin Buerger, PhD thesis, 2009). It is well established that in long term culture of ES cells the cells can become karyotypically unstable

resulting in trisomy of chromosomes (Liu *et al*., 1997; Rebuzzini *et al*., 2008). This abnormal chromosome number likely explains the low number of chimeric mice generated from the CGR8 conditional ES cells (Katrin Buerger, PhD thesis, 2009). Therefore, E14 IV ES cells were chosen as the wild type ES cells that the targeting vectors were electroporated into in this study because they were found to be the most karyotypically stable parental cell line in our hands.

Epithelial- Mesenchymal Transition (EMT) (Greenburg and Hay, 1982) and its reverse process Mesenchymal- Epithelial Transition (MET) are essential processes during embryogenesis. As epithelial cells are held together by tight junctions, adherens junctions and desmosomes they are immobile and cannot migrate to other areas of the embryo. During EMT changes in gene expression result in the loss of these cell junctions and the ability for these cells to migrate. Epithelial cells express *Chd1* (*E-cadherin*) which is important for cell adhesion (Takeichi, 1988). The genes *Snail* and *Snai2* (*Slug*) repress *Cdh1* expression which causes a disruption to cell adhesion in epithelial cells which then undergo EMT (Cano *et al*., 2000; Bolos *et al*., 2003). *Mospd 1* expression has been found to be up regulated in myoblastic and osteoblastic cell lines during differentiation. Knockdown of *Mospd 1* expression in MC3T3-E1 cells using siRNA resulted in changes in gene expression with up regulation of epithelial genes such as *Cdh1* and down regulation of mesenchymal genes *Cdh11*, and the *Cdh1* repressor genes *Snai1* and *Snai2*. The finding that the knockdown of *Mospd 1* results in increased *Cdh1* and decreased *Snail* and *Snai2* indicates *Mospd 1* may play a role in MET (Thaler *et al*. 2010). However, this has only been shown during osteoblast differentiation.

ES cells are pluripotent and can, therefore, differentiate into any cell type. Depending on culture conditions ES cells can be differentiated into cardiomyocytes (Doetschman *et al*., 1985; Maltsev *et al*., 1994) or osteoblasts (bone) (Buttery *et al*., 2001). Using the *Mospd 1* null ES cells the role of *Mospd 1* in cardiomyocyte and osteoblast differentiation was assessed. Thaler *et al*. (2010) reported that knockdown

of *Mospd 1* expression in the osteoblastic cell line MC3T3-E1 cells by siRNA resulted in down regulation of several genes including *Cdh11*, *Snai1* and *Snai2* (*Slug*). We assessed the expression of these down-regulated genes and they show the same expression pattern as *Mospd 1* during ES cell differentiation according to the FunGenES database (Schulz *et al.*, 2009) (www.fungenes.org). Any changes in the expression levels of these genes in *Mospd 1* null cells compared to wild type cells is reported in this chapter.

This chapter describes the generation of *Mospd 1* null ES cell lines and the phenotypic assessment of these null cell lines in comparison to wild type ES cells to assess the function of *Mospd 1*.

5.2. Aims

Given that *Mospd 1* is widely expressed in cells and tissues and its sub-cellular localisation changes during the cell cycle (Chapter 3) *Mospd 1* may be critical for cell function and proliferation. To test this it was necessary to:

- Generate a *Mospd 1* conditional allele by targeting *Mospd 1* in ES cells

- Generate a *Mospd 1* null ES cell line by expressing *Cre recombinase* in targeted *Mospd 1* null ES cells

- Assess the functional of *Mospd 1 in vitro*

    - Phenotypically characterise the *Mospd 1* null clones to assess whether:
        - *Mospd 1* plays a role in ES cell proliferation and/or self renewal

        - *Mospd 1* is required for differentiation (early differentiation, cardiomyocyte and osteoblast differentiation).

        - Measure gene expression changes in differentiated *Mospd 1* null cells to assess whether any genes change expression level in response to *Mospd 1* being knocked out during osteoblast differentiation.

5.3. Results

5.3.1. Generation of *Mospd 1* conditional allele in ES cells

5.3.1.1. Southern blot screening of *Mospd 1* targeted ES clones

To generate a conditional *Mospd 1* allele the *Mospd 1* targeting vector (Figure 5.1 A) was electroporated into wild type E14 IV ES cells and the cells grown under G418 drug selection. 288 colonies were picked and *Spe I* digests of the ES clone DNA were analysed by Southern blot to determine whether any of the picked ES clones were correctly targeted (Figure 5.1 B). As *Mospd 1* is an X-linked gene and the E14 IV cell line used in the targeting experiments was generated from male mice there would only be one allele present. We designed a Southern blot strategy in which either a restriction fragment of 14.8 kb corresponding to the wild type allele or a restriction fragment of 7 kb (with the 5' probe) or 4.7 kb (with the 3' probe) corresponding to the targeted allele would be observed (Figure 5.1C). Of the 179 clones that were successfully screened 4 clones appeared to have been correctly targeted. This corresponds to a targeting frequency of 2.2 % for *Mospd 1* in the E14 IV cell line. Previous studies using the CGR8 cell line had a targeting frequency of 1.7 % (Katrin Buerger, PhD thesis, 2009).

5.3.1.2. Karyotype of targeted *Mospd 1* clones

To check whether the targeted clones had a normal chromosome number and had not become unstable due to the electroporation and selection process the clones were karyotyped. The chromosome number was determined for at least 30 cells per clone by counting the chromosome spreads after DAPI staining. A clone was accepted as being of normal chromosome number, as shown in Figure 5.2, if more than 80 % of its cells possessed 39-40 chromosomes. Table 5.1 shows the percentage of cells for each clone with a normal chromosome number.

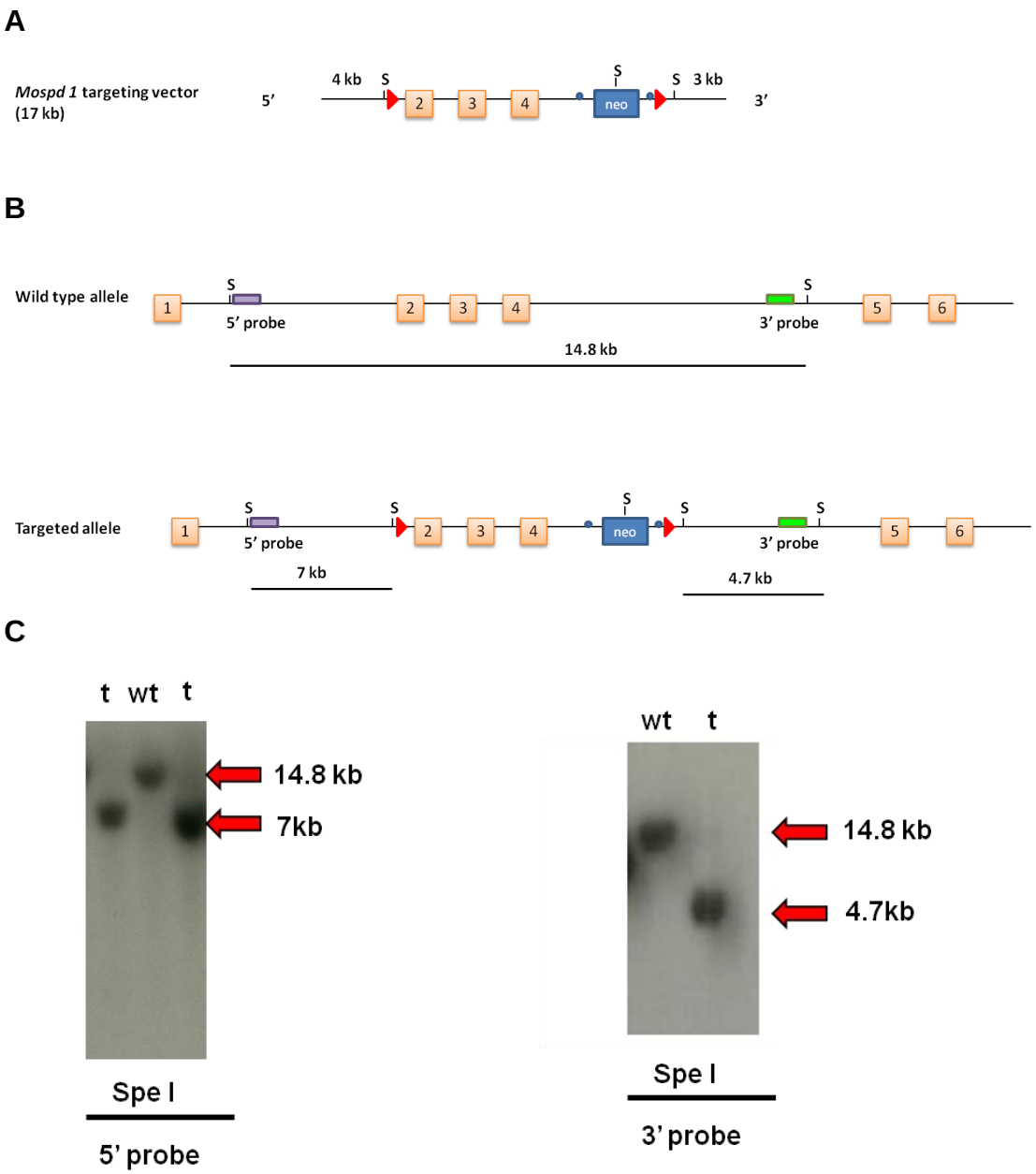

Figure 5.1: Southern blot screening of *Mospd 1* targeted ES clones. ES cells were screened for the correct vector integration at the *Mospd 1* locus using *Spe I* digestion. A: Schematic representation of the *Mospd 1* targeting vector. B: Schematic representation of the wild type *Mospd 1* allele and the targeted *Mospd 1* allele (S= *Spe I*; neo= neomycin cassette; red triangle represents lox P sites; blue circles represent the frt loci; purple box represents the 5' probe; green box represents the 3' probe). B: Southern blot showing wild type and targeted *Mospd 1* clones. The 14.8 kb labelled fragment corresponds to wild type *Mospd 1*, 7 kb fragment (5' probe) and the 4.7 kb (3' probe) correspond to the correctly targeted *Mospd 1* locus (wt= wild type and t= correctly targeted clone).

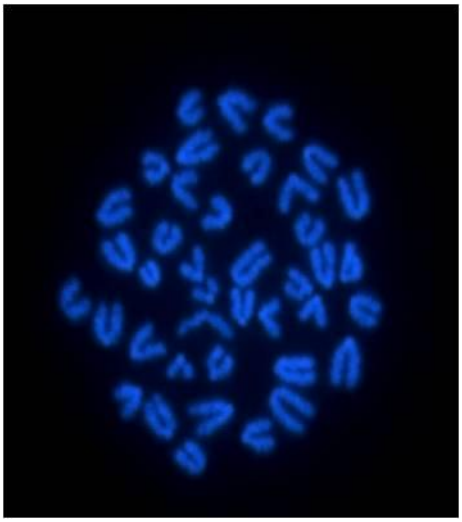

Figure 5.2: A typical chromosome spread from a *Mospd 1* targeted clone. An example of a chromosome spread (one cell) stained with DAPI showing the correct karyotype of 40 chromosomes (100x magnification).

Clone	Percentage clones with normal chromosome number (40)
E14 IV (Passage 23)	93
Mospd 1 B3	82
Mospd 1 B10	85
Mospd 1 C4	80
Mospd 1 F6	100

Table 5.1: Karyotype of targeted *Mospd 1* ES clones. All the clones were in the acceptable range of chromosome numbers i.e. more than 80 % of the cells had 39-40 chromosomes. No cells in any of the clones appeared to have more than 40 chromosomes. E14 IV cells of passage 23 were also of the correct chromosome number.

During long term ES cell culture the cells can accumulate chromosomal abnormalities (Liu *et al*., 1997) and, therefore, the chromosome number of E14 IV cells at passage 23 was determined. These cells and all the targeted clones that were karyotyped were of the correct chromosome number and none possessed extra chromosomes. All the cells of the *Mospd 1* F6 (M1 F6) clone had a 100 % normal karyotype.

5.3.2. Generation of *Mospd 1* null ES clones

5.3.2.1. Southern blot screening of *Cre recombinase* electroporated *Mospd 1* targeted ES clones

To generate a *Mospd 1* null allele the pCAGGS-*Cre*-IRESpuro plasmid (Appendix Figure 4) was electroporated into *Mospd 1* clone F6 targeted cells, which had normal karyotype, and 48 clones picked. To determine whether any of the picked ES clones were *Mospd 1* nulls DNA was screened by Southern blot. As *Mospd 1* is an X-linked gene and the E14 IV cell line used in the targeting experiments was generated from male mice either a restriction fragment corresponding to the targeted allele or to a null allele would be generated. *Hind III* digests of the ES clone DNA were analysed by Southern blot. For *Mospd 1* the restriction fragment that corresponds to the targeted allele is predicted to be 6.7 kb in size and the restriction fragment that corresponds to the null allele is predicted to be 8.3 kb (Figure 5.3). 48 ES clones were screened of which only 10 clones showed a restriction fragment. 7 of these were identified as being *Mospd 1* null clones.

A

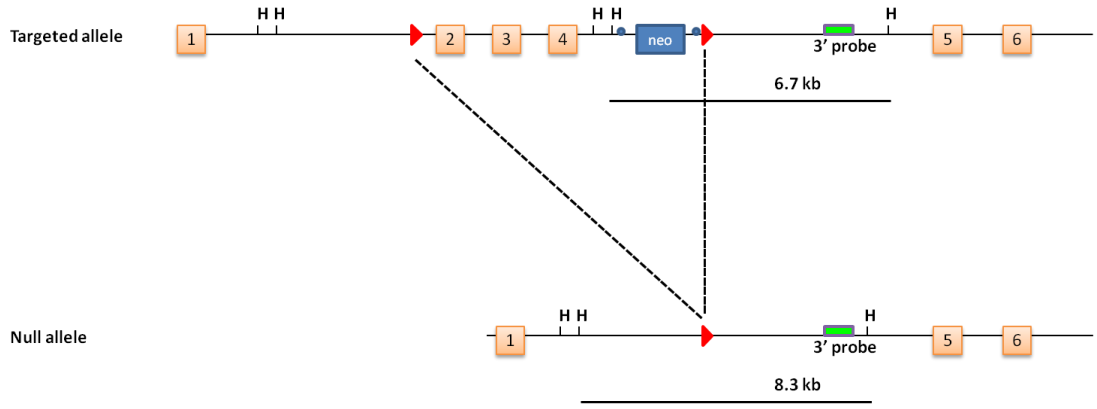

B

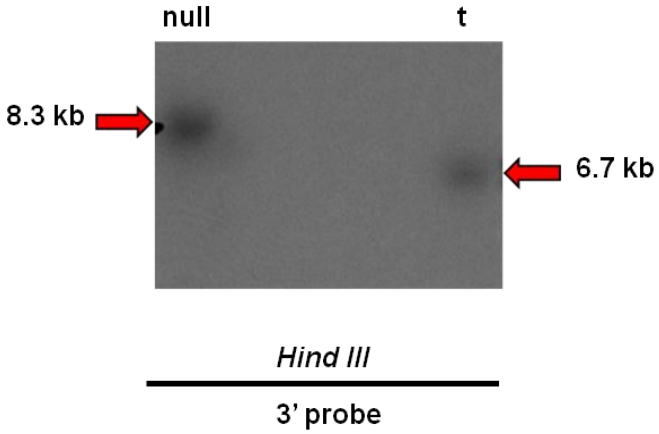

Figure 5.3: Generation of *Mospd 1* null allele. A: Schematic representation of the targeted *Mospd 1* allele and null allele. B: Southern blot of *Hind III* digestion using the 3' probe. The 6.7 kb fragment corresponds to the targeted allele and the 8.3 kb fragment to the *Mospd 1* null allele. (H= *Hind III*; neo= neomycin cassette; red triangle represents lox P sites; blue circles represent the frt loci; purple box represents the probe; t= targeted).

5.3.2.2. Karyotype of *Mospd 1* null clones

To check whether the *Mospd 1* null clones had a normal chromosome number and had not become unstable due to the electroporation of the *Cre recombinase* plasmid the clones were karyotyped. The chromosome number of wild type, E14 IV, cells at passage 23 was determined. Both *Mospd 1* null clones, C10 and C11, which were checked, possessed the correct chromosome number, 86 % and 100 % respectively and none possessed extra chromosomes (Table 5.2).

5.3.3. *Mospd 1* and *Mospd 3* expression in differentiating ES cells

To determine when *Mospd 1* and *Mospd 3* were expressed during ES cell differentiation wild type E14 IV ES cells were differentiated using the hanging drop method and the embryonic bodies (EBs) collected every day for 5 days. Individual EBs were plated on gelatinised 24 well dishes and cultured for a further 10 days. Cells were monitored for the formation of beating regions. The plated cells were then trypsinised, pooled and the cells pelletted. RNA was extracted from wild type ES cells, EBs from each day and the differentiated cells with and without beating populations and cDNA was reverse transcribed. Semi-quantitative RT-PCR, using intron-spanning primers, was performed in order to examine whether *Mospd 1* and *Mospd 3* were expressed in differentiating cells. *Mospd 1* expression appeared to be very low to absent in undifferentiated ES cells and its expression increased in older EBs (Figure 5.4). EBs collected from day 3 onwards expressed *Mospd 1* as did differentiated cells. *Mospd 3* expression varied to that of *Mospd 1* in that *Mospd 3* was expressed from undifferentiated ES cells through the different stages of EBs and in differentiated cells. *β-tubulin* was used as an internal control (Figure 5.4).

Clone	Percentage clones with normal chromosome number (40)
E14 IV (Passage 23)	90
Mospd 1 null C10	86
Mospd 1 null C11	100

Table 5.2: Karyotype of *Mospd 1* null ES clones. All the clones were in the acceptable range of chromosome numbers i.e. more than 80 % of the cells had 39-40 chromosomes. No cells in any clones appeared to have more than 40 chromosomes. E14 IV cells of passage 23 were also of the correct chromosome number.

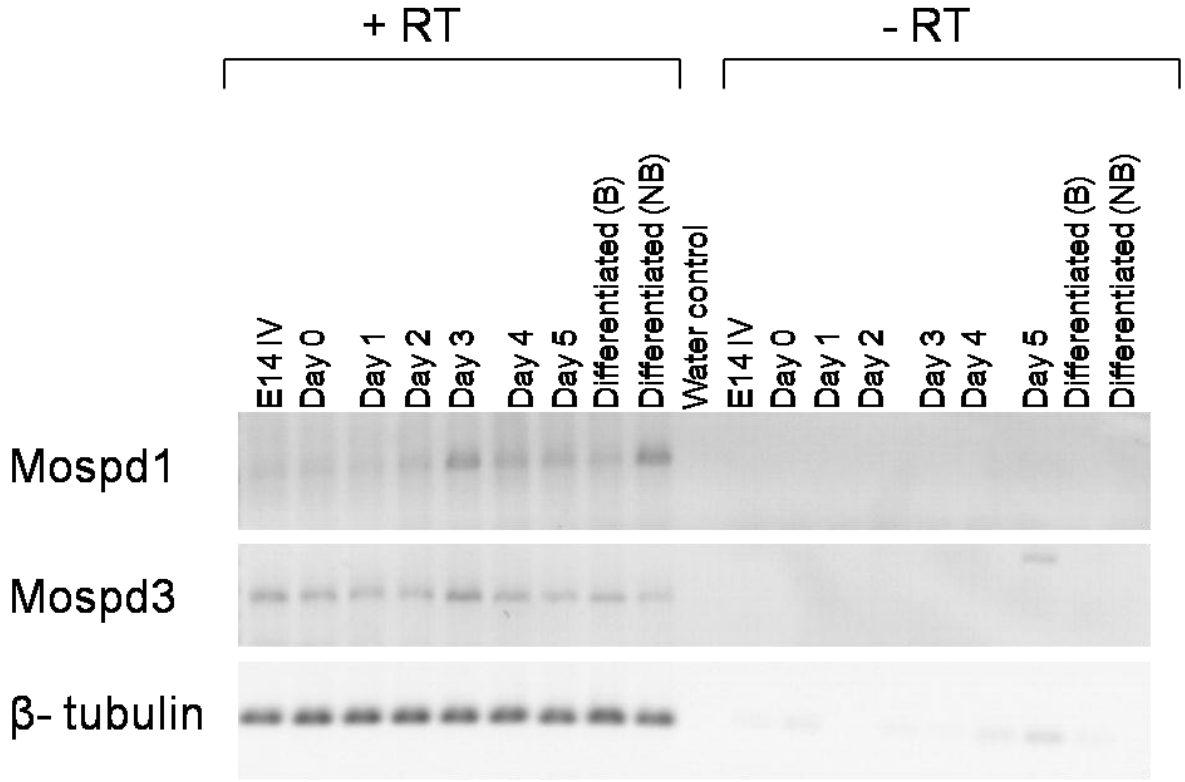

Figure 5.4: RT-PCR of *Mospd 1* and *Mospd 3* expression from undifferentiated ES cells, day 0 through to day 5 embryoid bodies and differentiated cells. *β-tubulin* was used as a housekeeping gene. E14 IV = undifferentiated ES cells; B = cultures containing beating regions; NB= cultures absent for beating regions; + RT= *reverse transcriptase* added during cDNA synthesis; -RT = no *reverse transcriptase* added to the cDNA synthesis. Bands were of the expected size (~ 500 bp).

5.3.4. Phenotypic assessment of *Mospd 1* null ES cells to assess function of *Mospd 1 in vitro*

5.3.4.1. Lack of *Mospd 1* expression in *Mospd 1* null day 5 EBs compared to wild type

The *Mospd 1* null clones, C10 and C11, which had been screened by Southern blot, were used to confirm that the *Mospd 1* null ES cells did not express *Mospd 1* by qPCR. Briefly, the cells were differentiated using the hanging drop method and after 2 days the resulting embryoid bodies (EBs) were harvested and cultured for a further 5 days and then collected for RNA extraction. As *Mospd 1* is not expressed in ES cells and its expression increases during differentiation (Figure 5.4) the expression of *Mospd 1* in day 5 EBs was checked in *Mospd 1* null cells and compared to wild type E14 IV cells. Wild type E14 IV day 5 EBs expressed *Mospd 1* and were used as the internal calibrator (gene expression in the *Mospd 1* null cells was measured in relation to this) and was set as 1. The *Mospd 1* null cells did not express *Mospd 1* in the differentiated cells (Figure 5.5). This served as confirmation that the *Cre recombinase* electroporation was a success and *Mospd 1* null cells had been successfully generated. The difference in expression of *Mospd 1* between wild type and *Mospd 1* null C10 and C11 clones was significantly different ($p<0.001$) and there was no difference between the *Mospd 1* null clones (One-way ANOVA and Bonferroni post test).

5.3.3.2. *Mospd 3* expression in *Mospd 1* null cells compared to wild type

To determine whether *Mospd 3* could be compensating for the loss of *Mospd 1* in *Mospd 1* null cells the level of *Mospd 3* in day 5 EBs was measured by qPCR. *Mospd 1* null clones C10 and C11 had a 0.84 and 0.76 level of *Mospd 3* expression, respectively, compared to wild type E14 IV expression which was set at 1 (Figure 5.6). There was no significant difference ($p=0.20$) in *Mospd 3* expression between wild type and *Mospd 1* null cells (One way ANOVA and Bonferroni post test).

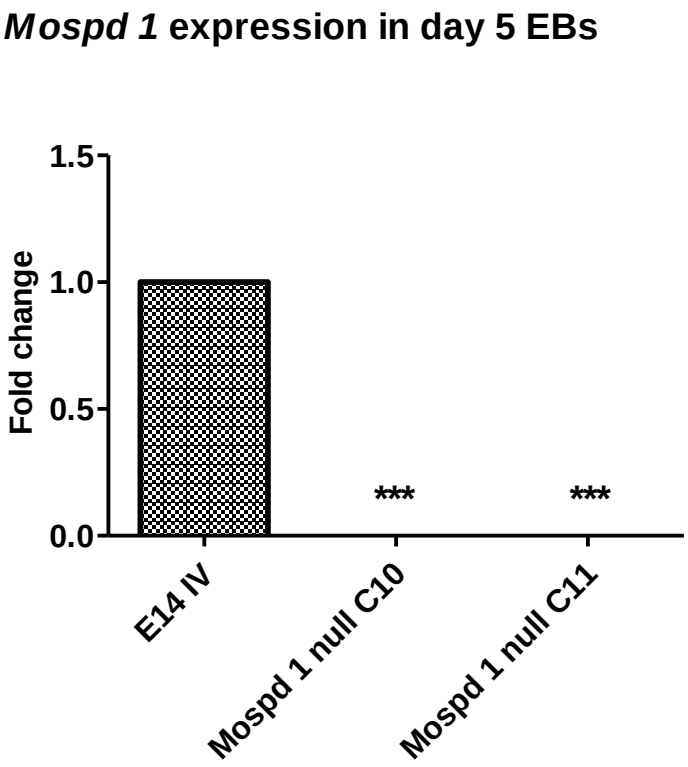

Figure 5.5: *Mospd 1* null cells lack *Mospd 1* expression. qPCR was used to confirm that the *Mospd 1* null cells did not express *Mospd 1* in differentiated cells. *Mospd 1* was expressed in wild type E14 IV day 5 EBs whilst *Mospd 1* null cells did not express *Mospd 1*. One-way ANOVA and Bonferroni post hoc test indicated that the difference in expression of *Mospd 1* between wild type and *Mospd 1* null C10 and C11 clones was significantly different ($p<0.001$).

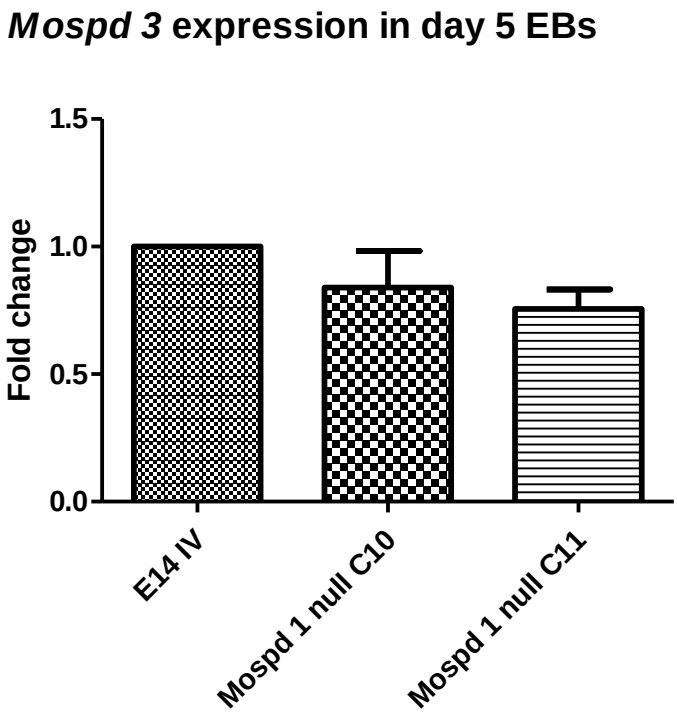

Figure 5.6: The level of *Mospd 3* expression is not significantly changed in cells lacking *Mospd 1*. qPCR was used to measure the expression of *Mospd 3* in *Mospd 1* null day 5 EBs compared to wild type E14 IV *Mospd 3* expression. *Mospd 3* expression was not significantly altered (p=0.20) in *Mospd 1* null cells compared to E14 IV wild type day 5 EBs (One-way ANOVA and Bonferroni post test).

5.3.4.3. *Mospd 1* null ES cells express stem cell markers

To check that the *Mospd 1* null cells were still behaving as ES cells and to determine whether lack of *Mospd 1* expression resulted in the loss of ES cell characteristics a number of phenotypic tests were carried out on the *Mospd 1* null clones, C10 and C11. ES cells express the genes *Oct 4* (Niwa *et al*., 2000) and *Nanog* (Chambers *et al*., 2003) which are responsible for maintaining the self renewing abilities of ES cells. In generating the *Mospd 1* null ES cells the cells have been electroporated twice, once with the *Mospd 1* targeting vector and once with the *Cre recombinase* vector as well as selected with G418 to select targeted clones. RT-PCR was used to check whether the *Mospd 1* null clones C10 and C11 expressed the ES cell markers *Oct 4* and *Nanog*. Figure 5.7 shows that like wild type ES cells, both *Mospd 1* null clones, C10 and C11, expressed *Oct 4* and *Nanog* indicating that these *Mospd 1* null ES cells still express ES cell markers and are, therefore, still ES cells. *β-tubulin* was used as an endogenous control.

5.3.4.4. Self-renewal capacity of *Mospd 1* null ES cells

The *Mospd 1* null ES cells express ES cell markers but do they still function as ES cells that can self renew? To assess whether the loss of *Mospd 1* from ES cells affected their ability to self-renew or begin early differentiation depending on growth conditions a self-renewal assay was undertaken. The self-renewal capability of 2 *Mospd 1* null clones, C10 and C11, was compared to wild type E14 IV cells. 2 different *Mospd 1* null clones were assessed to show that there were no clonal differences. Briefly, undifferentiated cells were plated in 2 wells of a gelatinised 6 well tissue culture dish and grown in the presence of LIF. The following day the cells were washed with PBS and one set of cells grown in the presence of LIF, to maintain the ES cells in a self-renewing, undifferentiated state, and the other in the absence of LIF, to differentiate the ES cells. The cells were grown in these conditions for 5 days, after which they were fixed and stained for alkaline phosphatase, a known stem cell marker.

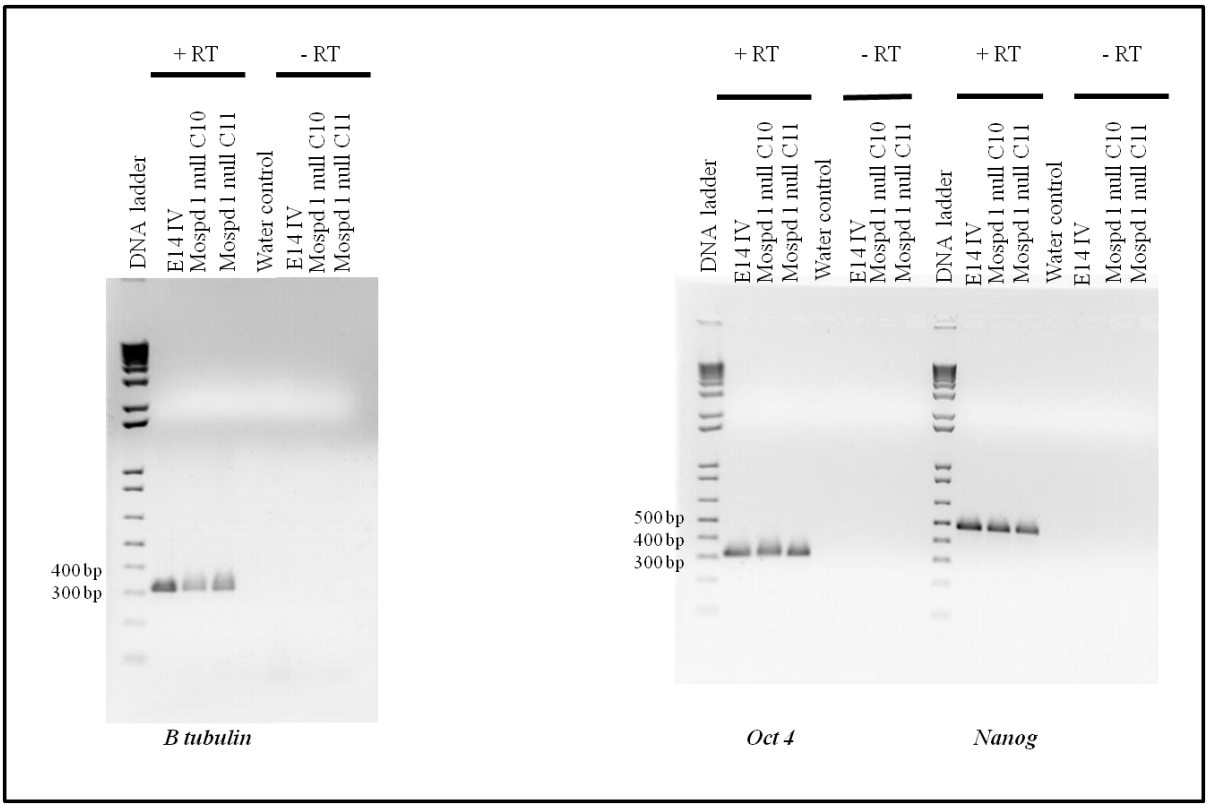

Figure 5.7: *Mospd 1* null cells express the ES cell markers *Oct 4* and *Nanog*. RT-PCR shows that *Mospd 1* null clones C10 and C11 expressed the ES cell markers *Oct 4* and *Nanog* at a similar level to wild type E14 IV ES cells. *β- tubulin* was used as an endogenous control. (RT = *reverse transcriptase*; bp = base pairs). There was no contamination in either the water controls or controls lacking *reverse transcriptase*.

Colonies were scored according to their colour; stem cell colonies were pink, mixed were a mixture of pink and white cells and differentiated cells were white. The number of colonies was analysed by a one way ANOVA followed by a Dunnett's Multiple Comparison Test. No significant differences in the self renewal capability was found between wild type E14 IV cells and *Mospd 1* null (C10 and C11) ES cells with p values of 0.12, 0.85 and 0.64 for stem, mixed and differentiated colonies, respectively, in the cells grown in the presence of LIF (Figure 5.8 A). In the absence of LIF (Figure 5.8 B) there was no significant difference in the *Mospd 1* null ES cells' ability to differentiate compared to wild type ES cells (p=0.18, p=0.34 and p=0.16 for stem, mixed and differentiated colonies, respectively.)

5.3.4.5. Ability of *Mospd 1* null ES cells to differentiate into cardiomyocytes

The ability of *Mospd 1* null clones to differentiate into beating cardiomyocytes was assessed by differentiating the cells using the hanging drop method described previously. Individual day 5 EBs were plated in gelatinised 24 well culture dishes and monitored for the presence of beating cells for 10 days. The ability to differentiate and form beating cells of 2 different *Mospd 1* null clones, C10 and C11, was assessed and compared to wild type E14 IV cells (Figure 5.9). 85 % of EBs formed from wild type E14 IV cells were able to form beating cells, whilst 89 % of *Mospd 1* null C10 EBs and 86 % of *Mospd 1* null C11 EBs formed beating cells. The data was analysed using a One way ANOVA followed by a Bonferroni's Multiple Comparison Test. There was no significant difference in the ability of *Mospd 1* null ES cells to differentiate into cardiomyocytes compared to wild type (p=0.81).

A

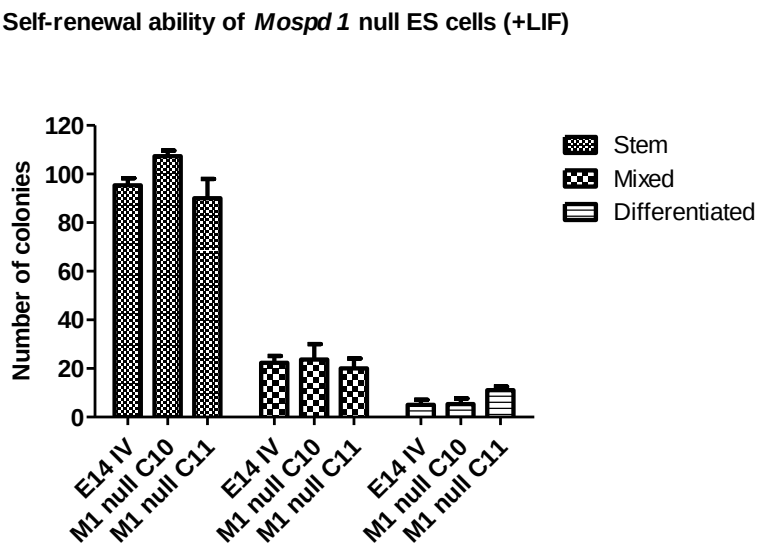

B

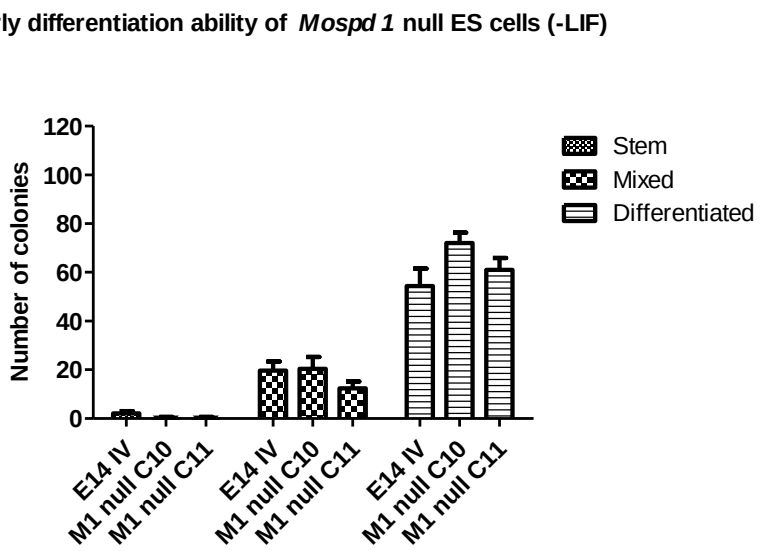

Figure 5.8: Self-renewal of *Mospd 1* null ES cells compared to wild type E14 IV cells. The graphs show the number of stem (undifferentiated), mixed or differentiated colonies formed by wild type E14 IV cells, *Mospd 1* null clones C10 and C11 cells grown in the presence (A) or absence (B) of LIF. A one way ANOVA followed by Dunnett's Multiple Comparison Test indicated that there is no statistically significant difference between the stem, mixed and differentiated colonies of wild type E14 IV cells and both clones of *Mospd 1* null ES cells grown in the presence (stem p=0.12, mixed p=0.85 and differentiated p=0.64) or absence (stem p=0.18, mixed p=0.34 and differentiated p=0.16) of LIF.

***Mospd 1* null embryoid bodies can differentiate into beating cardiomyocytes**

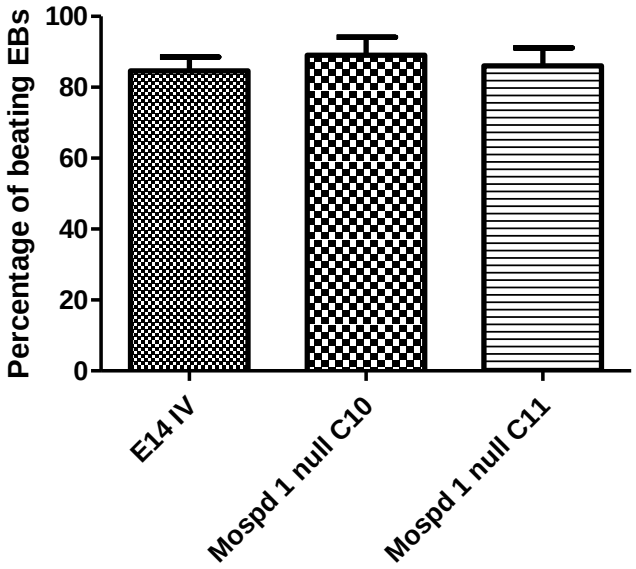

Figure 5.9: *Mospd 1* null ES cell can differentiate and form beating cardiomyocytes. 85 % of embryoid bodies (EBs) differentiated from wild type E14 IV cells showed the presence of beating cardiomyocytes compared to 89 % of *Mospd 1* null C10 EBs and 86 % *Mospd 1* null C11 EBs. There was no significant difference in the percentage of beating EBs between *Mospd 1* nulls when compared to wild type EBs (p=0.81). (Analysed by a One way ANOVA and Bonferroni's Multiple Comparison test).

5.3.4.6. Ability of *Mospd 1* null ES cells to differentiate into bone (osteoblasts)

As *Mospd 1* expression had been reported to be higher in osteoblastic cells (Thaler *et al*., 2010) the *Mospd 1* null ES cells, C10 and C11, were differentiated into osteoblasts. EBs were formed, as previously described, 1 day EBs plated in gelatinised tissue culture flasks and allowed to differentiate until day 5 (Figure 2.10 A). These cells were then trypsinised to form a single cell suspension and 5 x 10^4 cells were plated in each gelatinised well of a 6 well culture plate. A 6 well plate was stained with Alizarin Red to check for mineralisation at days 12, 19 and 26 (Figure 5.10 B-D). The colonies were counted and analysed using a One way ANOVA and Bonferroni Multiple Comparison Test).

At day 12 there was a significant reduction ($p<0.01$) in the number of colonies formed by *Mospd 1* null cells for both clones C10 and C11 (Figure 5.11 A). Wild type ES cells formed an average of 106 colonies compared to 32 colonies formed by *Mospd 1* null clone C10 and 25 colonies formed by *Mospd 1* null clone C11 (n=3).

By day 19 there was an average of 82 E14 IV colonies, 28 *Mospd 1* null C10 colonies and 21 *Mospd 1* null C11 colonies formed (Figure 5.11 B). This reduction in the number of colonies formed was significantly different ($p<0.001$). From Day 19 to the end of the experiment (Day 26) the cells were cultured with media supplemented with 50 mM β- glycerophosphate, 50 μg/ml ascorbic acid and 1 μM dexamethasone. At day 26 when the colonies were stained there was an average of 83 E14 IV colonies compared to 31 and 22 colonies formed by *Mospd 1* null C10 and C11, respectively (Figure 5.11 C). By this time the wild type clones covered the majority of the surface of the culture dish whilst there were large spaces in the *Mospd 1* null cultures (Figure 5.10 D). This reduction in the number of colonies was significant ($p<0.001$). There was no significant difference in the number of colonies formed between the *Mospd 1* null clones at any time point when compared to each other.

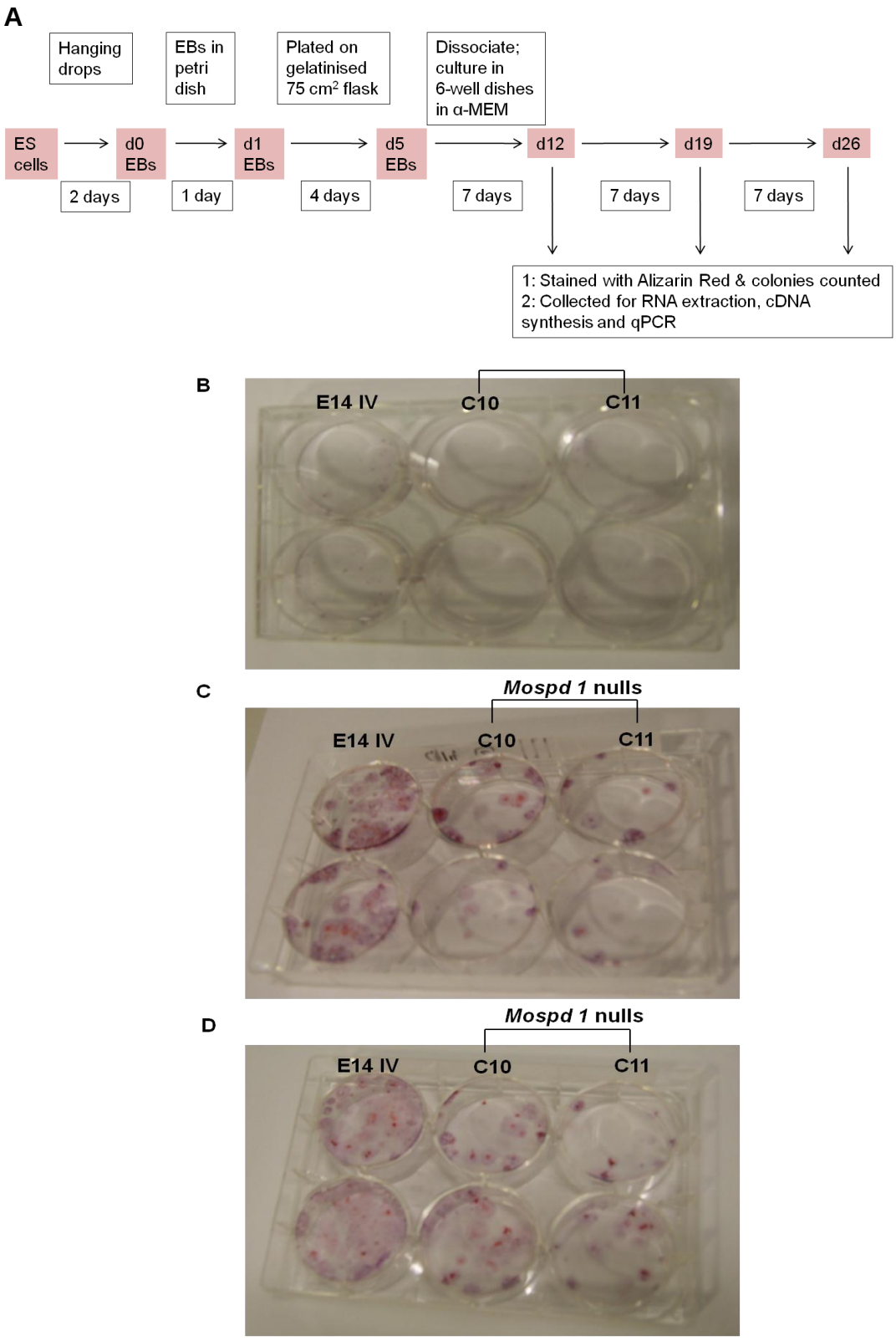

Figure 5.10: Differentiation of ES cells into bone. Protocol used to differentiate ES cells into bone (A) and Photos of the clones formed at Day 12(B), Day 19 (C) and Day 26(D) by E14 IV and *Mospd 1* null cells, clones C10 and C11, are shown.

A

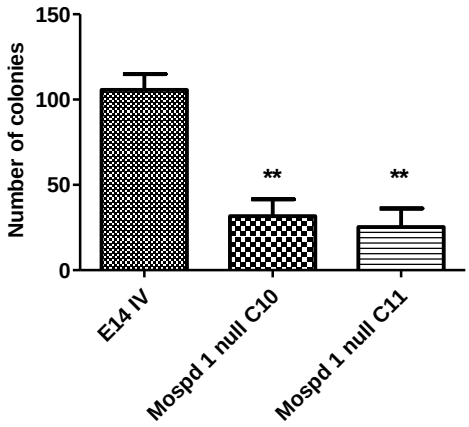

B

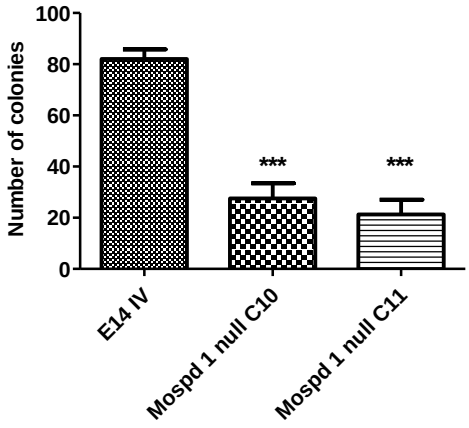

C

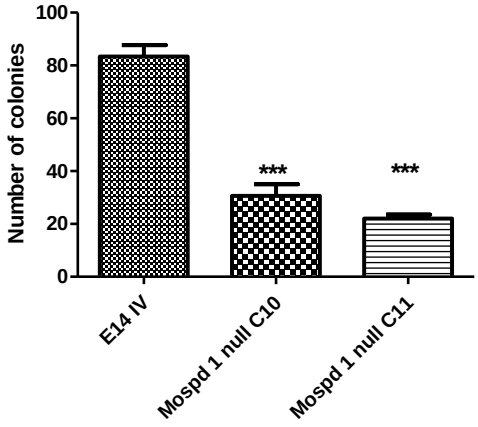

Figure 5.11: The ability of *Mospd 1* null cells to differentiate into bone. The number of colonies formed by *Mospd 1* null clones, C10 and C11, is significantly different when compared to wild type E14 IV cells at Day 12 (A), Day 19 (B) and Day 26 (C) of differentiation (** $p<0.01$;***$p<0.001$) (One way ANOVA and Bonferroni post test). (n=3).

5.3.4.7. Gene expression changes in differentiation of *Mospd 1* null ES cells into bone

Thaler *et al*. (2010) reported that knockdown of *Mospd 1* expression in MC3T3-E1 cells by siRNA resulted in down regulation of several genes including *Cdh11*, *Snai1* and *Snai2* (*Slug*) which showed a similar expression pattern to *Mospd 1* (Figure 5.12 A) according to FunGenES database (Schulz *et al*., 2009) (www.fungenes.org). Therefore, the expression level of *Cdh11*, *Snai1* and *Snai2* was assessed in the day 5 EBs used for the bone differentiation protocol to check whether the level of these genes was altered in *Mospd 1* null cells compared to wild type E14 IV cells (n=3). The expression level of *Cdh11* was 0.81 and 0.76 in day 5 *Mospd 1* null EBs (C10 and C11, respectively) compared to E14 IV expression level (1) ($p = 0.16$) (Figure 5.12 B). *Snai1* expression was not significantly different ($p=0.17$) between E14 IV (1) and *Mospd 1* null EBs (0.78 and 0.97) (Figure 5.12 C) nor was the expression of *Snai2*. *Mospd 1* null clones C10 and C11 had 0.81 and 1.04 *Snai2* expression (Figure 5.12 D) compared to E14 IV cells (1) and this difference was not significant ($p=0.31$) (One way ANOVA and Bonferroni post test).

Cells were collected at Day 12, 19 and 26 for RNA extraction and subsequent qPCR analysis. *Mospd 1* null cells were confirmed to be absent for *Mospd 1* expression compared to wild type cells that expressed *Mospd 1* at all time points (Figure 5.13.) ($p<0.001$) (One way ANOVA and Bonferroni post test). Day 12 *Mospd 1* null differentiated cells showed an up-regulation of *Mospd 3*, *Cdh11*, *Snai1* and *Snai2* (Figure 5.14). *Mospd 1* null clones C10 and C11 had a 2.84 and 2.48 fold increase, respectively, in *Mospd 3* expression when compared to wild type cells (Figure 5.14 A). There were 1.47 and 1.45 fold increases in *Cdh11* expression in *Mospd 1* null clones C10 and C11, respectively (Figure 5.14 B). *Snai1* expression was increased 1.73 and 1.89 fold (Figure 5.14 C) and *Snai2* expression was increased 1.46 and 1.75 fold (Figure 5.14 D) in *Mospd 1* null clones C10 and C11, respectively. These increases in gene expression in Day 12 differentiated cells were statistically significant for *Mospd 3* ($p<0.001$), *Cdh11* ($p<0.01$), *Snai1* ($p<0.05$), *Snai2* ($p<0.01$) (One way ANOVA and Bonferroni post test).

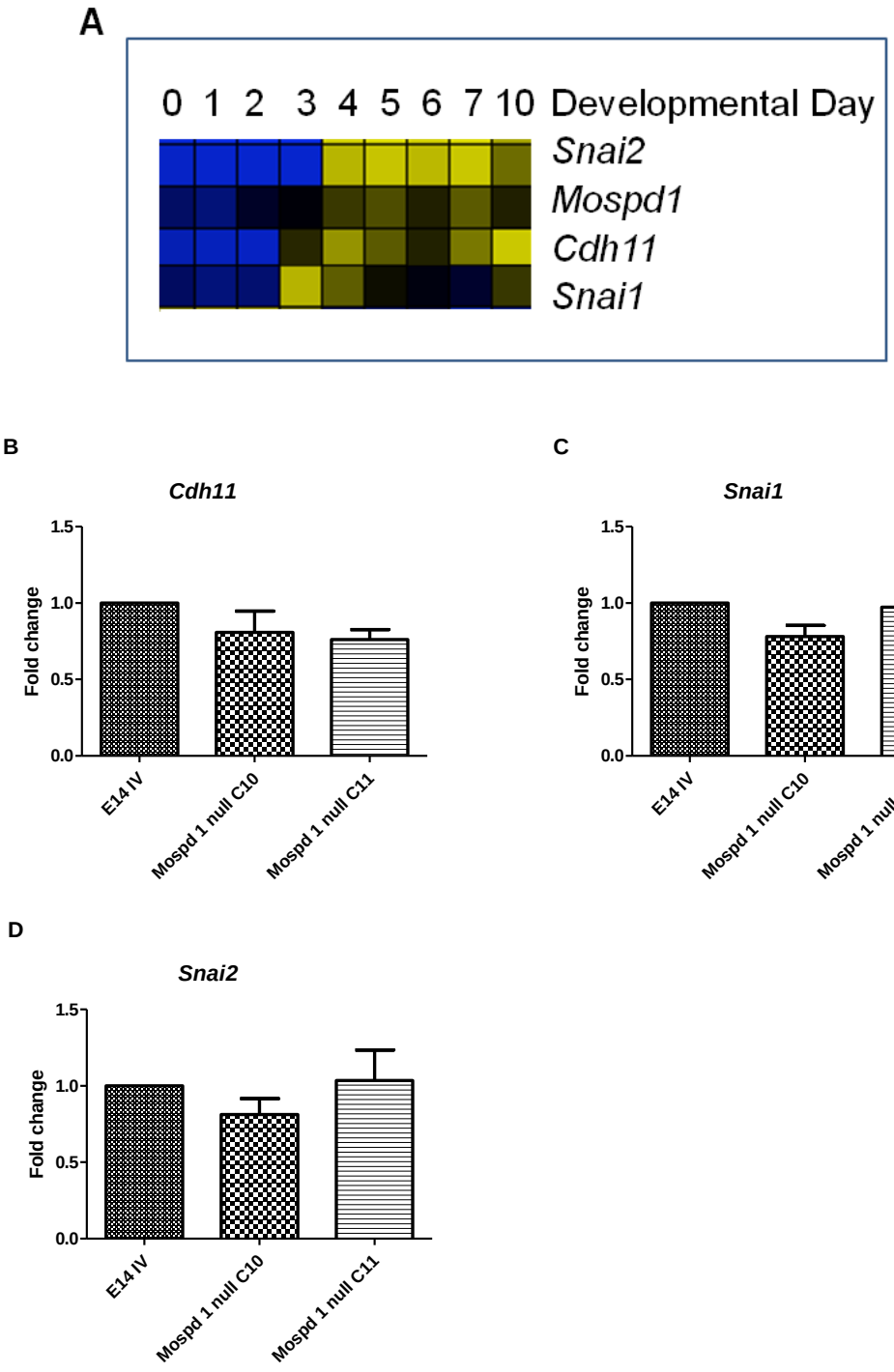

Figure 5.12: Expression changes of *Cdh11*, *Snai1* and *Snai2*. FunGenES heat map for expression of *Snai2*, *Mospd 1*, *Cdh11* and *Snai1* (A) (Day 0= undifferentiated ES cells; blue=no expression, black= very low expression, yellow=high expression). The expression levels of *Cdh11* (B), *Snai1* (C) and *Snai2* (D) were not significantly different between wild type E14 IV cells and *Mospd 1* null cells (p=0.16, p=0.17, p=0.31, respectively) in day 5 EBs. Data analysed by One way ANOVA and Bonferroni post test. (n=3).

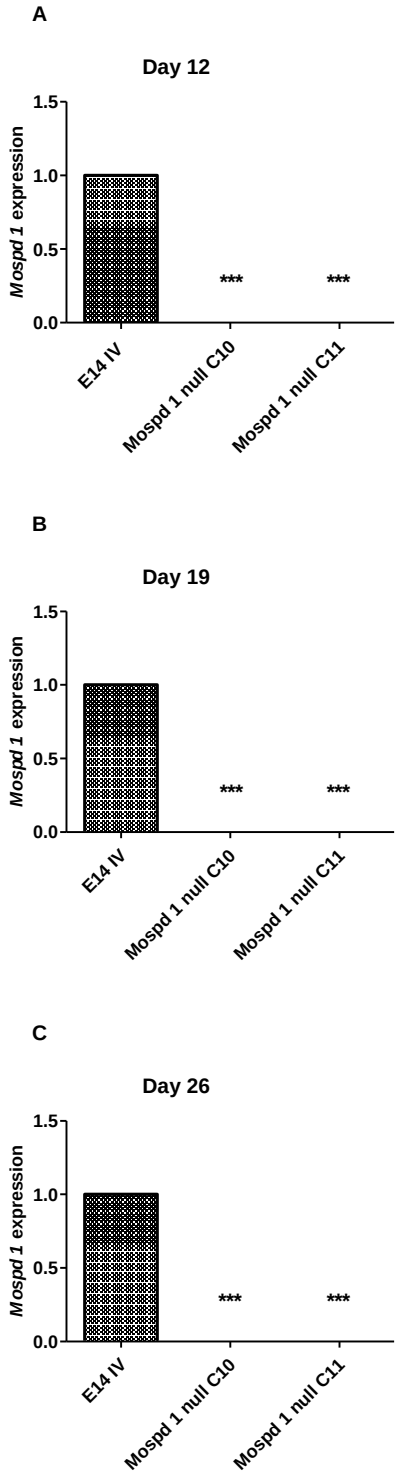

Figure 5.13: *Mospd 1* expression is absent in differentiating osteoblasts from *Mospd 1* null ES cells. Wild type E14 IV cells expressed *Mospd 1* at Days 12, 19 and 26. As expected neither *Mospd 1* clone C10 nor C11 had any *Mospd 1* expression at any time point which was significantly different to wild type *Mospd 1* expression (*** $p<0.001$) (One way ANOVA and Bonferroni post test).

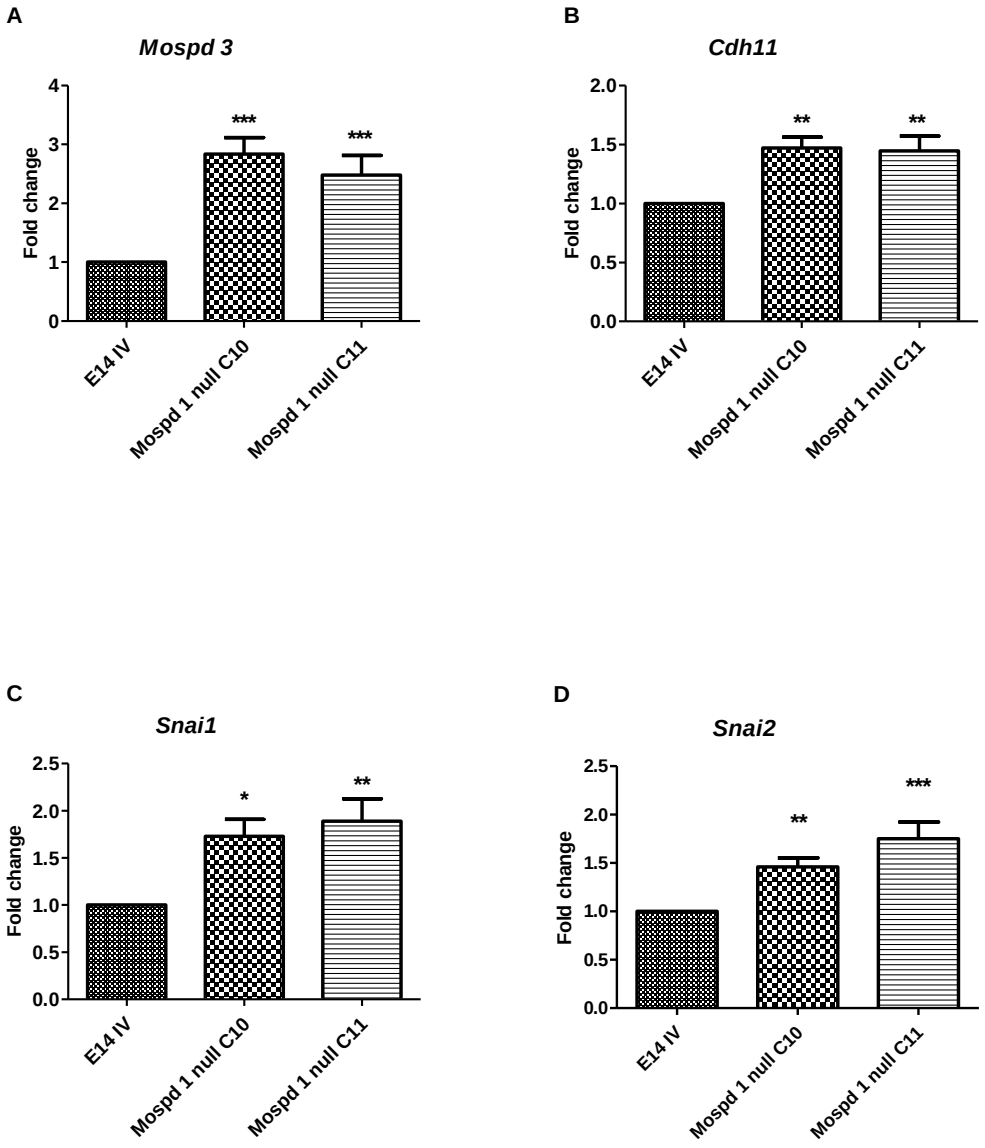

Figure 5.14: Gene expression in cells differentiating into bone at Day 12. The level of *Mospd 3* (A), *Cdh11* (B), *Snai1* (C) and *Snai2* (D) were significantly up regulated between wild type E14 IV cells and *Mospd 1* null cells (* $p<0.05$; ** $p<0.01$; *** $p<0.001$). Data analysed by One way ANOVA and Bonferroni post test. (n=3).

At Day 19 of bone differentiation there were no significant changes in gene expression for *Mospd 3* ($p=0.25$), *Cdh11* ($p=0.13$), *Snai1* ($p=0.83$) and *Snai2* ($p=0.31$) (One-way ANOVA and Bonferroni post test) (n=3) (Figure 5.15). Fold changes were measured against wild type E14 IV gene expression levels (set as 1). *Mospd 1* null clones C10 and C11 had a 1.09 and 1.37 level of *Mospd 3* expression, respectively, and 0.95 and 1.38 for *Cdh11* expression, respectively. *Snai1* and *Snai2* expression in *Mospd 1* null C10 was 0.90 and 0.82, respectively, and in *Mospd 1* null C11 was 1.07 and 1.05, respectively. The differences in gene expression between clones C10 and C11 were not significantly different for any of the genes tested.

From Day 19 to Day 26 cells were cultured with media containing ascorbic acid, dexamethasone and β-glycerophosphate to enhance osteoblast cell formation. At Day 26 there was no significant difference in the level of *Mospd 3* in *Mospd 1* null cells ($p=0.09$) as clone C10 had a 1.21 level and C11 a 1.07 level of *Mospd 3* expression (Figure 5.16 A). *Cdh11* expression was also not significantly altered in *Mospd 1* null cells ($p=0.06$) at day 26 as *Mospd 1* null clone C10 and C11 had a 1.12 and 0.91 *Cdh11* expression, respectively (Figure 5.16 B). At Day 26 both *Snai1* and *Snai2* expression was significantly reduced in *Mospd 1* null cells compared to wild type ($p<0.001$) (One way ANOVA and Bonferroni post test) (Figure 5.16 C and D). *Mospd 1* null C10 and C11 had 0.75 and 0.61 level of *Snai1* expression compared to an E14 IV expression of 1. The reduction of *Snai1* expression in clone C10 was less significant ($p<0.05$) than that of clone C11 ($p<0.001$). *Snai2* expression was reduced to 0.65 and 0.60 in *Mospd 1* null clones C10 and C11, respectively, which was significantly different in both clones ($p<0.001$) (One way ANOVA and Bonferroni post test). There were no significant differences in gene expression between the two *Mospd 1* null clones.

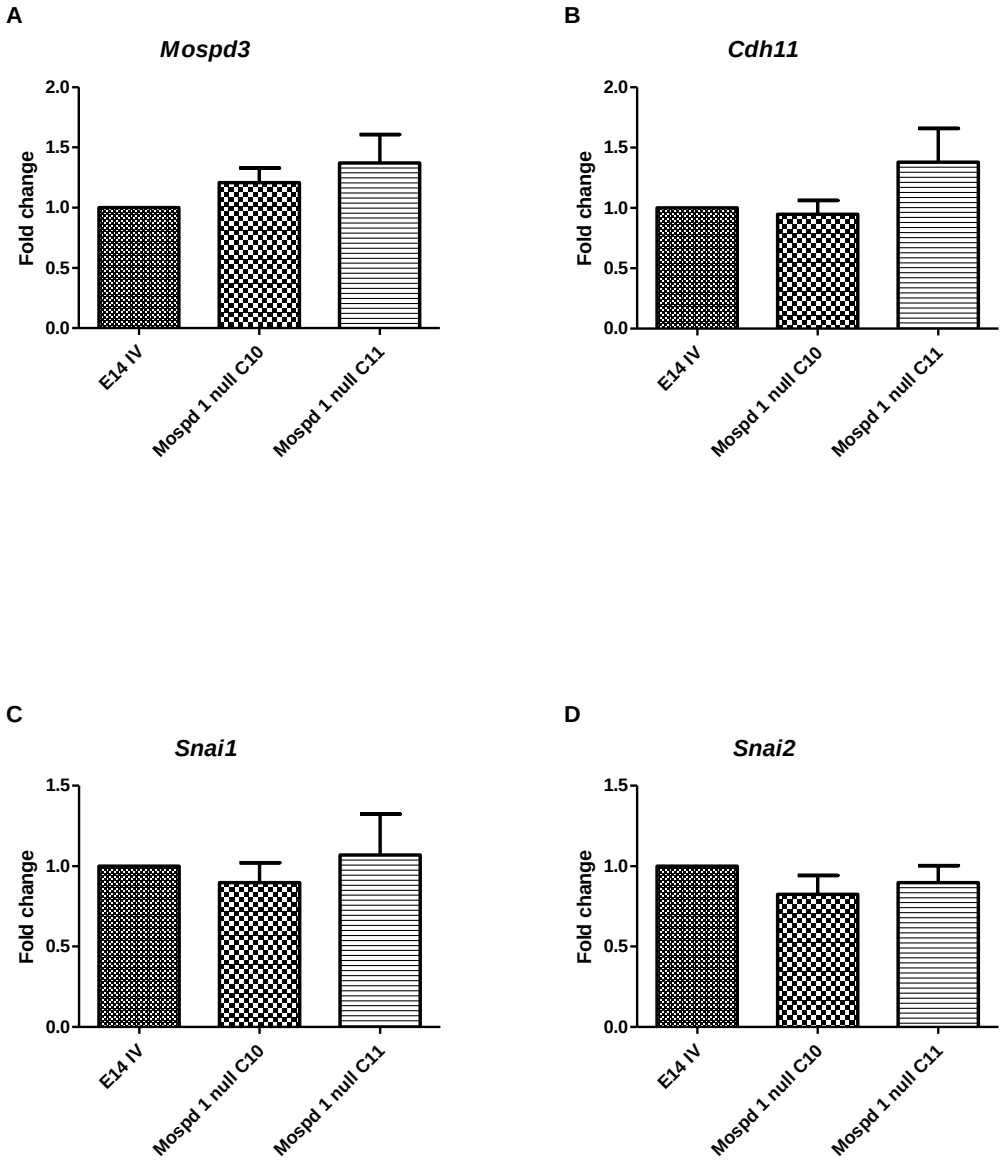

Figure 5.15: Gene expression in cells differentiating into bone at Day 19. The level of *Mospd 3* (A), *Cdh11* (B), *Snai1* (C) and *Snai2* (D) were not significantly different between wild type E14 IV cells and *Mospd 1* null cells (p=0.25, p=0.13, p=0.83 and p=0.31, respectively. Data analysed by One way ANOVA and Bonferroni post test. (n=3).

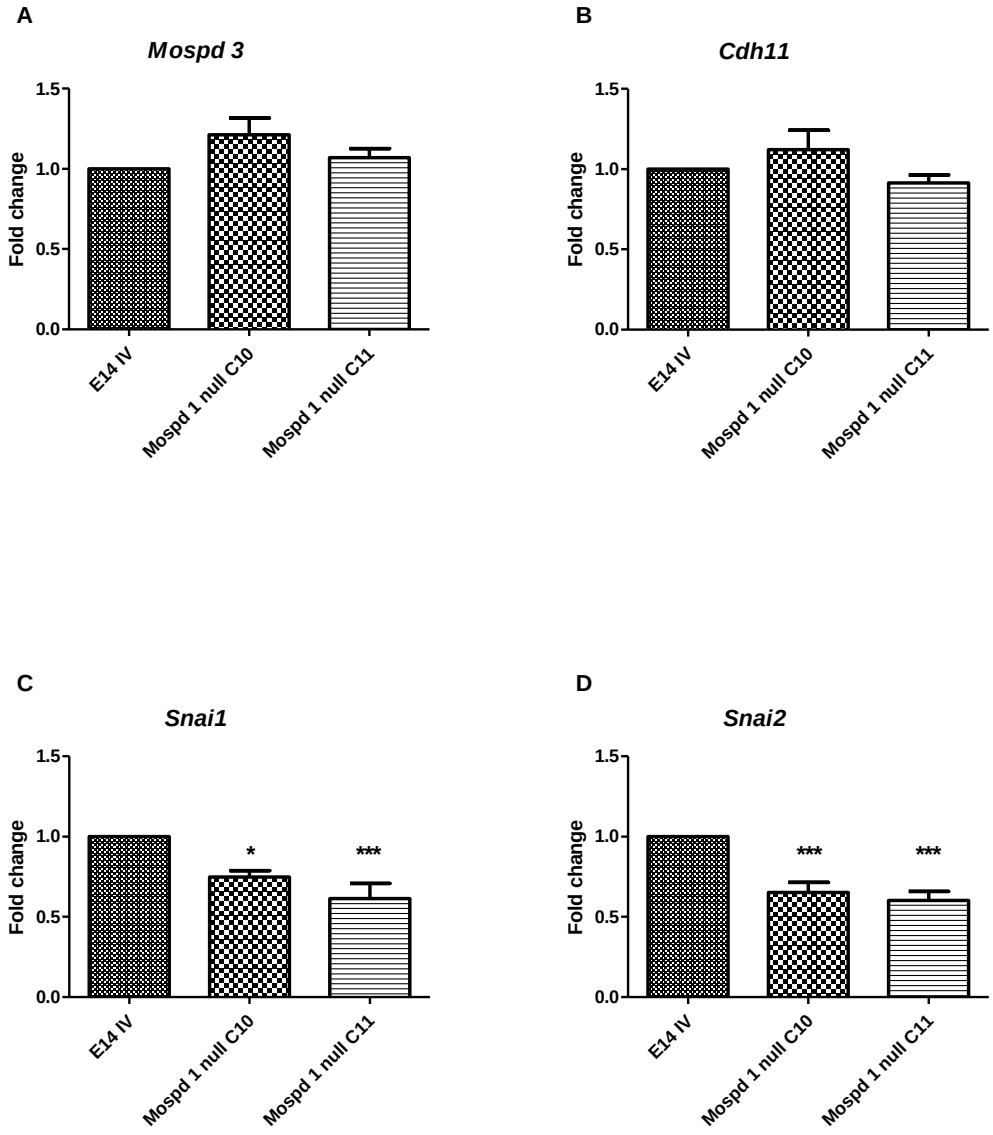

Figure 5.16: Gene expression in cells differentiating into bone at Day 26. The level of *Mospd 3* (A) and *Cdh11* (B) were not significantly different, between wild type E14 IV cells and *Mospd 1* null cells (p=0.09 and p=0.06, respectively). *Snai1* (C) and *Snai2* (D) were significantly down regulated in *Mospd 1* null cells (* p<0.05; **p<0.01; ***p<0.001). Data analysed by One way ANOVA and Bonferroni post test. (n=3).

5.5. Discussion

Mospd 1 is a gene that belongs to the *Mospd* gene family and there is little information in the literature about its function. To address this *Mospd 1* targeted ES cells were successfully generated and *Cre recombinase* mediated deletion of the lox P flanked exons resulted in the generation of *Mospd 1* null ES cells. These ES cells allowed functional analysis of *Mospd 1 in vitro* as they could be used to test whether *Mospd 1* was essential for ES cell self renewal or differentiation.

Mospd 1 is not essential for ES cell survival or self-renewal as there were no differences in the ability of the *Mospd 1* null ES cells to self renew in the presence of LIF when compared to wild type cells. This can be explained by the fact that *Mospd 1* expression is very low in undifferentiated ES cells and, therefore, not likely to be essential for ES cells characteristics. This is further confirmed by the fact that the *Mospd 1* nulls show similar levels of expression for ES cell markers, *Oct 4* and *Nanog*.

Investigating whether *Mospd 1* is essential for differentiation was done by looking at whether *Mospd 1* null cells could begin early differentiation by the removal of LIF and by trying to differentiate these cells into cardiomyocytes and osteoblasts. Osteoblast differentiation was chosen due to evidence that *Mospd 1* expression was up regulated in differentiating osteoblastic cells (Thaler *et al*., 2010). *Mospd 1* is not essential for early differentiation nor was it involved in cardiomyocyte differentiation. However, in a differentiation protocol to form osteoblasts the reduction in colonies formed by *Mospd 1* null cells in comparison to wild type cells indicates that *Mospd 1* could be involved in osteoblastic differentiation. The reduction in the number of bone colonies from the first time point (day 12) checked indicates *Mospd 1* plays a role early in osteoblast differentiation. The population of cells at day 12 is less differentiated than at later time points (Days 19 and 26) and may be a population of mesenchymal stem cells (MSCs)/ progenitors. MSCs can give rise to osteoblasts, adipogenic and myogenic cells (Muraglia *et al*., 2000; Sung *et al*., 2008)). The

reduction in colonies may be due to a loss of these progenitor cells. This population of MSCs could be measured using flow cytometry to detect cell surface markers such as CD29, CD44, CD105 and SCA-1 (Sung *et al*., 2008). The later time points (Days 19 and 26) had reduced numbers of colonies because those colonies had not formed at Day 12.

To check whether the loss of *Mospd 1* is responsible for the reduction in the number of colonies by Day 12 a rescue experiment could be performed. A vector containing *Mospd 1* could be electroporated into the *Mospd 1* null ES cells and clones that expressed *Mospd 1* could be differentiated in the same way as control *Mospd 1* null ES cells. If the number of colonies differentiated from the rescued *Mospd 1* ES cells do not show the reduction in colony numbers than that proves *Mospd 1* is responsible for the reduction in the *Mospd 1* null cells.

The hypothesis that *Mospd 1* and *Mospd 3* are genetically redundant may be supported by the increase in *Mospd 3* expression in Day 12 *Mospd 1* null differentiating cells as this could indicate that the cells are trying to compensate for the loss of *Mospd 1* by up regulating *Mospd 3* initially. This difference is lost as differentiation continues and could mean these genes have different roles as development continues or that *Mospd 1* is not required at later time points so compensation is not required.

From the genes that showed a change in expression reported in Thaler *et al*. (2010) *Snai1*, *Snai2* (*Slug*) and *Cdh11* showed a similar expression pattern to *Mospd 1* in differentiating ES cells (FunGenES database) (Schulz *et al*., 2009) and were, therefore, chosen as genes to check during the differentiation of *Mospd 1* null ES cells. *Snail* and *Snai2* are expressed during organogenesis in mesenchymal tissues in the developing embryo (Smith *et al*., 1992; Oram *et al*., 2003). The initial increase in *Cdh11*, *Snai1* and *Snai2* expression compared to wild type observed at Day 12

could indicate the loss of *Mospd 1* leads to an Epithelial-Mesenchymal Transition (EMT) during this stage of differentiation. This is because *Snai1* and *Snai2* are essential for mesenchyme formation and for EMT (Alberga *et al*., 1991; Nieto *et al*., 1994). As *Snai1* and *Snai2* repress *Cdh1* (*E-cadherin*) (Cano *et al*., 2000; Bolos *et al*., 2003) the *cadherin* present in epithelial cells (Takeichi, 1988) the increase of these repressors should decrease the expression of *Cdh1*. *Cdh11* is a mesenchymal *cadherin* expressed in the osteoblastic lineage (Kii *et al*., 2004) and, therefore, the increase in *Cdh11* expression compared to wild type at Day 12 indicates more mesenchyme is present in *Mospd 1* null cells and these cells are differentiating into osteoblastic cells. However, due to the presence of non-specific amplification in the qPCR reaction using the Cdh11 primers (Appendix Figure 3) this increase in expression may not be accurate and, therefore, this should be repeated with another set of primers for Cdh11 which do not amplify non-specific products.

The addition of ascorbic acid, β-glycerophosphate and dexamethasone to the culture medium between days 19 and 26 of differentiation enhances osteoblast differentiation (Buttery *et al*., 2001). It has been reported that dexamethasone acts on mesenchymal stem cells to make bone (Beresford *et al*., 1993). Therefore, at Day 26 of differentiation the cells present are osteoblasts. The decrease in *Snai1* and *Snai2* expression in Day 26 osteoblast cells indicates that there is a reduction in mesenchyme formation. It would be useful to measure the level of *Cdh1* in *Mospd 1* null cells, at this time, to check whether it is increased due to the down regulation of its repressors. This together would mean that *Mospd 1* was essential for mesenchyme formation and loss of *Mospd 1* resulted in a Mesenchymal- Epithelial Transition (MET) during osteogenesis. The down regulation of *Snai1* and *Snai2* in *Mospd 1* null cells confirms the findings of Thaler *et al*. (2010) who reported that *Snai1* and *Snai2* expression was reduced in osteoblastic cells where *Mospd 1* expression had been knocked down using siRNA.

The *Mospd 1* null cells described in this chapter are better tools than the siRNA knockdown described by Thaler *et al*. (2010) as these cells lack any *Mospd 1* expression and all cells differentiated from them will lack *Mospd 1* expression whereas siRNA knocks down expression for shorter time periods. Using these *Mospd 1* null ES cells the role of *Mospd 1* during ES cell differentiation can be found. Thaler *et al*. (2010) only examined gene expression changes in osteoblast differentiation whereas I have examined the role of *Mospd 1* from earlier differentiation time points and found a phenotype occurs much earlier in the differentiation process.

The use of ES cells to study EMT has previously been reported using wild type MESC20 ES cells (Spencer *et al*., 2007). During differentiation a decrease in CDH1 (E-CADHERIN) protein expression occurred and an increase in *Cdh1* repressor genes, *Snail* and *Snai2*. Interestingly *Cdh1* transcript levels remained the same during -differentiation when measured by semi-quantitative RT-PCR (Spencer *et al*., 2007). Similar findings have been reported using human ES cells (Eastham *et al*., 2007). During human ES cell differentiation *Snail* and *Snai2* transcript levels as well as mesenchymal markers, such as *Vimentin*, increase whilst *Cdh1* expression falls (Eastham *et al*., 2007). *Snail* and *Snai2* transcript levels increased in *Cdh1* null ES cells and *N-cadherin* null ES cells upon spontaneous differentiation by removal of LIF indicating these two *Cadherin* genes are not required for the up-regulation of *Snail* and *Snai2* (Spencer *et al*., 2007). The *Mospd 1* null ES cell line reported here could be another useful tool to study EMT *in vitro*. Expression changes of other genes involved in EMT, such as *Cdh1* (*E-cadherin*), *N-cadherin* and mesenchymal markers would need to be measured in *Mospd 1* null cells to determine whether *Mospd 1* was involved in their regulation.

Figure 5.17 shows a summary of the differentiation process of the *Mospd 1* null ES cells and proposes the possibility that the loss of *Mospd 1* may result in EMT during ES cell differentiation (at Day 12) but may result in MET during osteogenesis (Day

26). This could be a possibility as during embryogenesis EMT and MET occur depending on the tissues being formed. Cells can switch from epithelial to mesenchymal and back to epithelial.

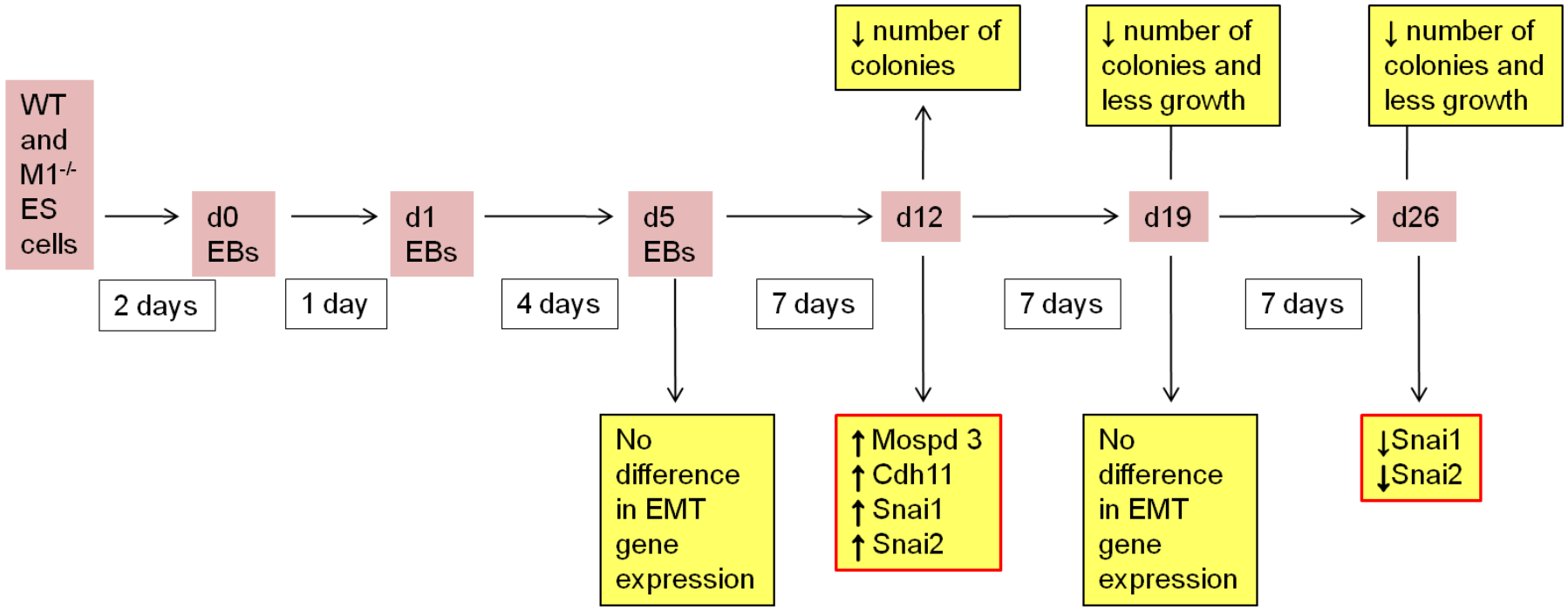

Figure 5.17: Summary of findings of *Mospd 1* null cells during osteoblast differentiation. The protocol for differentiation of wild type (WT) and *Mospd 1* null (Mospd $1^{-/-)}$ ES cells from undifferentiated ES cells to differentiated osteoblasts is shown. The changes in the numbers of colonies and gene expression (yellow) measured at each time point (pink) of bone differentiation. The boxes outlined in red show gene expression changes in genes involved in EMT.

CHAPTER 6:

SUMMARY AND PROSPECTIVES

6.1. Summary

6.1.1. MOSPD1 localisation

I successfully generated specific monoclonal α-MOSPD1 and α-MOSPD3 antibodies as described in Chapter 3. The monoclonal α-MOSPD1 antibody was used to study the sub-cellular localisation of MOSPD1 *in vitro* in HaCaTs and *in vivo* in mouse tissue sections and zebrafish embryo sections. MOSPD1 was found to be localised to the nucleus in HaCaTs and showed the same localisation in keratinocytes of the mouse ear. This indicates that MOSPD1 may play the same role *in vitro* as *in vivo*. MOSPD1 was localised throughout 3 dpf zebrafish embryos in the nucleus and cytoplasm.

MOSPD1 localisation changed depending on the cell cycle in HaCaTs *in vitro* with dividing cells showing MOSPD1 localised to the cytoplasm and not associated with the DNA. At certain cell cycle stages MOSPD1 also showed perinuclear localisation which is due to localisation of MOSPD1 to the ER. The finding that MOSPD1 was co-localised with a DSRed-ER marker in some cells is similar to the localisation of another MSP domain-containing family, the VAPs. This common localisation of MOSPD1 and VAP may indicate a common role.

The sub-cellular localisation of MOSPD1 and MOSPD3 was different in HaCaTs *in vitro* as MOSPD1 was predominantly nuclear and MOSPD3 was nuclear and cytoplasmic. However, both MOSPD1 and MOSPD3 were cytoplasmic in dividing cells indicating that they may have a similar role in cell division. Within certain tissues such as the heart the two proteins have similar localisation in the nuclei of cardiomyocytes and cytoplasm of endothelial cells of blood vessels but within other tissues such as the kidney their localisation was different. This data could indicate that these proteins could compensate for each other in certain tissues but to answer the question of genetic redundancy a double knockout of *Mospd 1* and *Mospd 3* would be required.

6.1.2. Functional analysis of *Mospd 1*

To assess the function of *Mospd 1 in vivo* morpholinos against *Mospd 1* were injected into zebrafish embryos. Injection of the morpholino targeted to the start site of *Mospd 1* (MO1) resulted in a severe phenotype being observed in both MO1-injected embryos and 5-mispair control morpholino-injected embryos indicating the phenotype could be non-specific. Injection of a morpholino targeted to a splice-site of *Mospd 1* (MO2) resulted in approximately 60 % knockdown of *Mospd 1* expression but no phenotype was observed in these embryos.

In parallel to the functional analysis of *Mospd 1* in zebrafish embryos the function of *Mospd 1 in vitro* was assessed by generating a *Mospd 1* null ES cell line. *Mospd 1* null ES cells were capable of self renewal and expressed the ES cell markers *Oct4* and *Nanog* indicating that the loss of *Mospd 1* did not alter their stem cell characteristics. The *Mospd 1* null cells did not show any early differentiation defects as they formed differentiated colonies upon the removal of LIF. The cells were also able to form EBs and did not show any difference in their ability to form beating cardiomyocytes compared to wild type E14 IV control cells.

We did, however, observe a phenotype when cells were differentiated along the osteoblastic lineage. At Day 12 of differentiation there was a significant reduction in the number of colonies formed by *Mospd 1* null cells compared to wild type. In addition to the reduced number of colonies a difference in gene expression was measured using qPCR in the *Mospd 1* null cells compared to wild type. The genes assessed had been reported to have been down regulated in MC3T3-E1 cells in which *Mospd 1* had been knocked down using siRNA (Thaler *et al*., 2010). An increased expression of *Snail* and *Snai2* was measured at Day 12 indicating that the cells could be undergoing EMT at Day 12 of differentiation. At this time an increase in the osteoblastic cadherin, *Cdh11* (Kii *et al*., 2004), was also observed in the *Mospd 1* null cells indicating an increased mesenchymal cell population formed by the *Mospd 1* null cells. There was a significant increase in *Mospd 3* expression in Day 12 *Mospd*

1 null cells compared to wild type and this increase could indicate that the cells may be trying to compensate for the loss of *Mospd 1* by up regulating *Mospd 3* expression and, therefore, there may be some genetic redundancy between *Mospd 1* and *Mospd 3*. By Day 19 of differentiation there were no changes in the levels of *Snail*, *Snai2* and *Cdh11* in *Mospd 1* null cells compared to wild type cells. At Day 26 the level of *Snail* and *Snai2* expression was decreased in *Mospd 1* null cells compared to wild type indicating that MET may be occurring. This reduction of *Snail* and *Snai2* at Day 26 is similar to the down regulation of these genes in MC3T3-E1 cells when *Mospd 1* was knocked down using siRNA (Thaler *et al*., 2010) as MC3T3-E1 cells are osteoblastic and by Day 26 of differentiation of the *Mospd 1* null cells reported here were osteoblasts.

In conclusion, the tools to study *Mospd 1* have been generated and reported in this thesis. Specific monoclonal antibodies have been generated to assess the sub-cellular localisation of MOSPD1 and its close relative MOSPD3. Tools to study the function of *Mospd 1* have been generated, morpholinos to knockdown *Mospd 1* expression in zebrafish *in vivo*, and a *Mospd 1* null ES cell line which can be used for *in vitro* functional analysis or used for the generation of a *Mospd 1* null mouse for functional assessment of *Mospd 1 in vivo*.

6.2. Prospectives

6.2.1.1. Investigation of MOSPD1 during the cell cycle

The change in localisation of MOSPD1 during the cell cycle, in which MOSPD1 was predominantly nuclear in non-dividing cells and cytoplasmic in dividing cells, could indicate that MOSPD1 is involved in the cell cycle. The levels of MOSPD1 should be assessed at the different cell cycle stages by western blot to investigate whether there is a change in MOSPD1 expression during the cell cycle. This could provide further evidence that MOSPD1 may be involved in the cell cycle. As synchronicity was lost at later stages in cells treated with thymidine alternative synchronisation methods could be used to collect cells at the different cell cycle stages. To further increase the numbers of dividing cells in culture an alternative drug to thymidine such as Colcemid which blocks cells at mitosis (Lam *et al*., 1997) could be used.

The localisation of MOSPD1 in the cytoplasm in dividing cells may be a passive occurrence due to the loss of the nuclear envelop during mitosis or an active process involving nuclear export. CRM1 (EXPORTIN1) is a receptor that binds to the NES of proteins and exports them from the nucleus (Fukuda *et al*., 1997). It has been shown that CRM1 can be blocked by addition of the antifungal agent Leptomycin B (Nishi *et al*., 1994; Fukuda *et al*., 1997). Proteins that show a similar change in sub-cellular localisation during the cell cycle, such as BRCA1, have been shown to be exported from the nucleus via its NES binding to CRM1 and that treatment with Leptomycin B blocks their export from the nucleus (Glover-Collins and Thompson, 2008). The discovery of a putative NES in the last exon of MOSPD1 (Thaler *et al*., 2010) could indicate that MOSPD1 could bind to CRM1 and be actively removed from the nucleus. To investigate this, the HaCaT cells could be treated with Leptomycin B and the sub-cellular localisation of MOSPD1 assessed. If treatment with Leptomycin B blocks nuclear export this would indicate that MOSPD1 was exported from the nucleus by CRM1.

6.2.1.2. Identification of MOSPD1 protein partners

MOSPD1 is localised the nucleus and loss of MOSPD1 results in the expression of EMT genes being altered. MOSPD1 does not have a DNA binding domain so it cannot act as a transcription factor and directly alter gene expression. However, the IgG-like fold of the MSP domain is thought to be involved in protein-protein interactions (Bork *et al*., 1994). It is possible that MOSPD1 may interact with other proteins, perhaps in a complex, and in this way alter gene expression. To determine if MOSPD1 forms protein complexes the monoclonal α-MOSPD1 antibody could be used for co-immunoprecipitation experiments. Cell lysates can be incubated with the monoclonal α-MOSPD1 antibody which will bind to MOSPD1. Addition of Protein G sepharose beads will bind the antibody allowing the antibody- protein complex to be obtained which can then be further analysed. The proteins bound to MOSPD1 could be identified using mass spectrometry. However, co-immunoprecipitation can result in non-specific binding to the antibody due to the fact that proteins are more likely to precipitate during cell lysis. Also during cell lysis the disruption of organelles results in proteins that may not interact physiologically, mixing and binding to the target complex. Another problem with co-immunoprecipitation is that low affinity bound proteins can be lost during the lysis and wash steps.

An alternative to determine protein-protein interactions is the yeast two hybrid system which makes use of bait and prey plasmids introduced into yeast. The bait plasmid carries the DNA binding domain of the reporter protein linked to the protein of interest, in this case MOSPD1, whilst the prey is a library of proteins linked to the activation domain of the reporter. When the bait protein binds to a prey protein the DNA binding domain and the activation domain are brought into close proximity resulting in transcription of the reporter gene. Using this system a protein that interacts with MOSPD1 could be detected.

6.2.2. Functional analysis of *Mospd 1*

6.2.2.1. Functional analysis of *Mospd 1* in zebrafish

As there was no phenotype observed in zebrafish embryos when the level of knockdown of *Mospd 1* expression was approximately 60 % the level of *Mospd 1* knockdown should be increased. To increase the level of knockdown another morpholino (MO3) targeted to a different splice junction should be designed and co-injected with the splice-site morpholino (MO2) reported in this thesis. It has been reported that knockdown of gene expression can be increased from 50 % to 90 % by the injection of three morpholinos targeted to the same gene (Morcos, 2007). The optimal doses of the morpholinos injected would have to be determined to prevent toxicity. The correct controls, such as co-injection of the 5-mispair morpholinos, would also be essential to ensure any phenotype observed was not due to non-specific effects.

As there was expression changes for genes involved in EMT in the *Mospd 1* null ES cells reported in Chapter 5, and in cells where *Mospd 1* expression had been knocked down by siRNA (Thaler *et al*., 2010) the level of these genes should be measured in the morpholino-injected zebrafish embryos. If the expression levels of *Snail*, *Snai2*, *Cdh11* and *Cdh1* are altered in embryos where *Mospd 1* has been knocked down this gives further evidence that *Mospd 1* may be involved in EMT. As this would be in zebrafish embryos this would show *Mospd 1* may be involved in EMT *in vivo* which has yet to be shown.

In zebrafish embryos that have had *Mospd 1* expression further knocked down the embryos should be observed for any changes during gastrulation as this is the stage of embryo development that is affected when *E-cadherin* (*Cdh1*) expression (Babb and Marrs, 2004) and *Snail* expression (Blanco *et al*., 2007) is knocked down in zebrafish embryos. This stage is affected as this is when cell movement starts to

occur in the embryo to form the three germ layers and EMT is important and, therefore, altering the genes involved in EMT can affect gastrulation.

If a phenotype is observed when the level of *Mospd 1* is further knocked down a rescue experiment would be required to prove that the phenotype observed is due to the reduction of *Mospd 1*. To rescue a phenotype the full length *Mospd 1* mRNA would need to be co-injected with the morpholinos and the embryos observed. If the phenotype is not observed in these 'rescued' embryos then the phenotype was due to the loss or reduction of *Mospd 1*. To determine the optimal dose of mRNA to inject to rescue a phenotype a dose- response experiment would need to be done. As the mRNA does not have the splice-site that the morpholinos recognise these morpholinos cannot knockdown the injected 'rescue' mRNA level. This is only true for the splice-site morpholinos as a start morpholino would still be able to knockdown mRNA expression as the recognition site would be the same.

6.2.2.2. Analysis of MOSPD1 in EMT *in vitro*

As there were fewer colonies at Day 12 in the differentiating *Mospd 1* null ES cells compared to wild type it was hypothesised this could be due to a reduction in the differentiation of mesenchymal stem cells (MSC). Using flow cytometry the presence of MSC markers could be assessed. There are MSC markers such as CD29, CD44, Cd105 and SCA-1 (Sung *et al*., 2008) and antibody panels are available to assess the presence of these markers.

To prove that the loss of *Mospd 1* is responsible for the reduction in colonies a rescue experiment would need to be carried out. This would involve electroporating a vector containing *Mospd 1* into the *Mospd 1* null ES cells and differentiating them in the same way. If there is no reduction in the colony numbers in the 'rescued' cells this proves that the loss of *Mospd 1* was responsible for the reduction.

Further to finding that genes involved in EMT have altered expression levels in *Mospd 1* null cells it would be interesting to observe whether knockdown of *Mospd 1* in an epithelial cell type can induce EMT. To do this siRNA could be introduced into HaCaTs to knockdown *Mospd 1* expression and the cells observed to check for the characteristic morphology changes that occur during EMT such as the loss of cell-cell contacts and the cells looking more spindle shaped. The expression of genes involved in EMT, mesenchymal markers and epithelial markers should be measured by qPCR in these siRNA knockdown cells and their controls. This would determine if knockdown of *Mospd 1* in epithelial cells made them more mesenchymal. Alternatively, *Mospd 1* could be knocked down in mesenchymal cells to determine the role of *Mospd 1* in MET as *Mospd 1* may be involved in EMT and MET depending on the differentiation or developmental stage.

6.2.2.3. Functional analysis of *Mospd 1* in mice

The ultimate functional assessment of a gene is creating a mouse knockout. Loss of function mouse models are very useful tools in identifying the function of a gene. The generation of conditional *Mospd 1* cell lines will allow conditional knockout mouse models to be generated. Using *Cre*-mediated deletion, whether in a tissue-specific or at a specific time of development depending on the promoter controlling *Cre* expression, will allow the function of *Mospd 1* to be determined. The *Mospd 1* null ES cells can also be used to generate *Mospd 1* null mice in a shorter time frame to the conditional ES cells. However, if *Mospd 1* was essential to development and loss of *Mospd 1* resulted in neonatal lethality there would be no mice to assess. Therefore, the conditional *Mospd 1* mice offer more control as to when the *Mospd 1* gene is knocked out.

To address the issue of whether *Mospd 1* and *Mospd 3* are genetically redundant the *Mospd 1* null mice generated using the ES cells described in this chapter could be crossed with *Mospd 3* null mice resulting in a double knockout. Conditional *Mospd 3* ES cells have been generated (Katrin Buerger, PhD thesis, 2009). In this way if the

loss of one *Mospd* gene compensates for the loss of the other than knocking out both genes could result in a phenotype or a more severe phenotype being observed. This would provide evidence for whether *Mospd 1* and *Mospd 3* are genetically redundant.

REFERENCES

Alberga, A., Boulay, J. L., Kempe, E., Dennefeld, C. and Haenlin, M. (1991). The snail gene required for mesoderm formation in Drosophila is expressed dynamically in derivatives of all three germ layers. *Development* **111**, 983-92.

Andrews, B. J., Proteau, G. A., Beatty, L. G. and Sadowski, P. D. (1985). The FLP recombinase of the 2 micron circle DNA of yeast: interaction with its target sequences. *Cell* **40**, 795-803.

Awad, M. M., Dalal, D., Cho, E., Amat-Alarcon, N., James, C., Tichnell, C., Tucker, A., Russell, S. D., Bluemke, D. A., Dietz, H. C. et al. (2006). DSG2 mutations contribute to arrhythmogenic right ventricular dysplasia/cardiomyopathy. *Am J Hum Genet* **79**, 136-42.

Babb, S. G. and Marrs, J. A. (2004). E-cadherin regulates cell movements and tissue formation in early zebrafish embryos. *Dev Dyn* **230**, 263-77.

Bahary, N., Goishi, K., Stuckenholz, C., Weber, G., Leblanc, J., Schafer, C. A., Berman, S. S., Klagsbrun, M. and Zon, L. I. (2007). Duplicate VegfA genes and orthologues of the KDR receptor tyrosine kinase family mediate vascular development in the zebrafish. *Blood* **110**, 3627-36.

Bateman, A., Coin, L., Durbin, R., Finn, R. D., Hollich, V., Griffiths-Jones, S., Khanna, A., Marshall, M., Moxon, S., Sonnhammer, E. L. et al. (2004). The Pfam protein families database. *Nucleic Acids Res* **32**, D138-41.

Batlle, E., Sancho, E., Franci, C., Dominguez, D., Monfar, M., Baulida, J. and Garcia de Herreros, A. (2000). The transcription factor snail is a repressor of E-cadherin gene expression in epithelial tumour cells. *Nat Cell Biol* **2**, 84-89.

Behrens, J., Lowrick, O., Klein-Hitpass, L. and Birchmeier, W. (1991). The E-cadherin promoter: functional analysis of a G.C-rich region and an epithelial cell-specific palindromic regulatory element. *Proc Natl Acad Sci U S A* **88**, 11495-9.

Beresford, J. N., Graves, S. E. and Smoothy, C. A. (1993). Formation of mineralized nodules by bone derived cells in vitro: a model of bone formation? *Am J Med Genet* **45**, 163-78.

Bhuiyan, Z. A., Jongbloed, J. D., van der Smagt, J., Lombardi, P. M., Wiesfeld, A. C., Nelen, M., Schouten, M., Jongbloed, R., Cox, M. G., van Wolferen, M. et al. (2009). Desmoglein-2 and desmocollin-2 mutations in dutch arrhythmogenic right ventricular dysplasia/cardiomypathy patients: results from a multicenter study. *Circ Cardiovasc Genet* **2**, 418-27.

Bierkamp, C., McLaughlin, K. J., Schwarz, H., Huber, O. and Kemler, R. (1996). Embryonic heart and skin defects in mice lacking plakoglobin. *Dev Biol* **180**, 780-5.

Blanco, M. J., Tada, M., Allende, M. L., Mayor, R. andNieto, M. A. (2007). Snail1a and Snail1b co-operate in the anterior migration of the axial mesendoderm in the zebrafish embryo. *Development* **134**, 4073-81.

Bode, V. C. (1984). Ethylnitrosourea mutagenesis and the isolation of mutant alleles for specific genes located in the T region of mouse chromosome 17. *Genetics* **108**, 457-70.

Bolos, V., Peinado, H., Perez-Moreno, M. A., Fraga, M. F., Esteller, M. and Cano, A. (2003). The transcription factor Slug represses E-cadherin expression and induces epithelial to mesenchymal transitions: a comparison with Snail and E47 repressors. *J Cell Sci* **116**, 499-511.

Bork, P., Holm, L. and Sander, C. (1994). The immunoglobulin fold. Structural classification, sequence patterns and common core. *J Mol Biol* **242**, 309-20.

Boukamp, P., Petrussevska, R. T., Breitkreutz, D., Hornung, J., Markham, A. and Fusenig, N. E. (1988). Normal keratinization in a spontaneously immortalised aneuploid human keratinocyte cell line. *J Cell Biol* **106**, 761-71.

Bouvrette, D. J., Sittaramane, V., Heidel, J. R., Chandrasekhar, A. and Bryda, E. C. (2010). Knockdown of bicaudal C in zebrafish (Danio rerio) causes cystic kidneys: a nonmammalian model of polycystic kidney disease. *Comp Med* **60**, 96-106.

Bullock, T. L., Roberts, T. M. and Stewart, M. (1996). 2.5 A resolution crystal structure of the motile major sperm protein (MSP) of Ascaris suum. *J Mol Biol* **263**, 284-96.

Burggren, W. W. and Pinder, A. W. (1991). Ontogeny of cardiovascular and respiratory physiology in lower vertebrates. *Annu Rev Physiol* **53**, 107-35.

Buttery, L. D., Bourne, S., Xynos, J. D., Wood, H., Hughes, F. J., Hughes, S. P., Episkopou, V. and Polak, J. M. (2001). Differentiation of osteoblasts and in vitro bone formation from murine embryonic stem cells. *Tissue Eng* **7**, 89-99.

Cano, A., Perez-Moreno, M. A., Rodrigo, I., Locascio, A., Blanco, M. J., del Barrio, M. G., Portillo, F. and Nieto, M. A. (2000). The transcription factor snail controls epithelial-mesenchymal transitions by repressing E-cadherin expression. *Nat Cell Biol* **2**, 76-83.

Carver, E. A., Jiang, R., Lan, Y., Oram, K. F. and Gridley, T. (2001). The mouse snail gene encodes a key regulator of the epithelial-mesenchymal transition. *Mol Cell Biol* **21**, 8184-8.

Cermenati, S., Moleri, S., Cimbro, S., Corti, P., Del Giacco, L., Amodeo, R., Dejana, E., Koopman, P., Cotelli, F. and Beltrame, M. (2008). Sox18 and Sox7 play redundant roles in vascular development. *Blood* **111**, 2657-66.

Chen, J. N., Haffter, P., Odenthal, J., Vogelsang, E., Brand, M., van Eeden, F. J., Furutani-Seiki, M., Granato, M., Hammerschmidt, M., Heisenberg, C. P. et al. (1996). Mutations affecting the cardiovascular system and other internal organs in zebrafish. *Development* **123**, 293-302.

Cvetkovic, B. and Sigmund, C. D. (2000). Understanding hypertension through genetic manipulation in mice. *Kidney Int* **57**, 863-74.

Dale, J. K., Malapert, P., Chal, J., Vilhais-Neto, G., Maroto, M., Johnson, T., Jayasinghe, S., Trainor, P., Herrmann, B. and Pourquie, O. (2006). Oscillations of the snail genes in the presomitic mesoderm coordinate segmental patterning and morphogenesis in vertebrate somitogenesis. *Dev Cell* **10**, 355-66.

Dani, C., Smith, A. G., Dessolin, S., Leroy, P., Staccini, L., Villageois, P., Darimont, C. and Ailhaud, G. (1997). Differentiation of embryonic stem cells into adipocytes in vitro. *J Cell Sci* **110 (Pt 11)**, 1279-85.

Delva, E., Tucker, D. K. and Kowalczyk, A. P. (2009). The desmosome. *Cold Spring Harb Perspect Biol* **1**, a002543.

den Haan, A. D., Tan, B. Y., Zikusoka, M. N., Llado, L. I., Jain, R., Daly, A., Tichnell, C., James, C., Amat-Alarcon, N., Abraham, T. et al. (2009). Comprehensive desmosome mutation analysis in north americans with arrhythmogenic right ventricular dysplasia/cardiomyopathy. *Circ Cardiovasc Genet* **2**, 428-35.

Denvir, M. A., Tucker, C. S. and Mullins, J. J. (2008). Systolic and diastolic ventricular function in zebrafish embryos: influence of norepenephrine, MS-222 and temperature. *BMC Biotechnol* **8**, 21.

Diehl, F., Brown, M. A., van Amerongen, M. J., Novoyatleva, T., Wietelmann, A., Harriss, J., Ferrazzi, F., Bottger, T., Harvey, R. P., Tucker, P. W. et al. (2010). Cardiac deletion of Smyd2 is dispensable for mouse heart development. *PLoS One* **5**, e9748.

Doetschman, T. C., Eistetter, H., Katz, M., Schmidt, W. and Kemler, R. (1985). The in vitro development of blastocyst-derived embryonic stem cell lines: formation of visceral yolk sac, blood islands and myocardium. *J Embryol Exp Morphol* **87**, 27-45.

Dooley, K. A., Fraenkel, P. G., Langer, N. B., Schmid, B., Davidson, A. J., Weber, G., Chiang, K., Foott, H., Dwyer, C., Wingert, R. A. et al. (2008). montalcino, A zebrafish model for variegate porphyria. *Exp Hematol* **36**, 1132-42.

Driever, W., Solnica-Krezel, L., Schier, A. F., Neuhauss, S. C., Malicki, J., Stemple, D. L., Stainier, D. Y., Zwartkruis, F., Abdelilah, S., Rangini, Z. et al. (1996). A genetic screen for mutations affecting embryogenesis in zebrafish. *Development* **123**, 37-46.

Dutton, K., Dutton, J. R., Pauliny, A. and Kelsh, R. N. (2001). A morpholino phenocopy of the colourless mutant. *Genesis* **30**, 188-9.

Eastham, A. M., Spencer, H., Soncin, F., Ritson, S., Merry, C. L., Stern, P. L. and Ward, C. M. (2007). Epithelial-mesenchymal transition events during human embryonic stem cell differentiation. *Cancer Res* **67**, 11254-62.

Ekker, S. C. and Larson, J. D. (2001). Morphant technology in model developmental systems. *Genesis* **30**, 89-93.

Eshkind, L., Tian, Q., Schmidt, A., Franke, W. W., Windoffer, R. and Leube, R. E. (2002). Loss of desmoglein 2 suggests essential functions for early embryonic development and proliferation of embryonal stem cells. *Eur J Cell Biol* **81**, 592-8.

Evans, M. J. and Kaufman, M. H. (1981). Establishment in culture of pluripotential cells from mouse embryos. *Nature* **292**, 154-6.

Fontaine, G., Fontaliran, F., Hebert, J. L., Chemla, D., Zenati, O., Lecarpentier, Y. and Frank, R. (1999). Arrhythmogenic right ventricular dysplasia. *Annu Rev Med* **50**, 17-35.

Forrester, L. M., Nagy, A., Sam, M., Watt, A., Stevenson, L., Bernstein, A., Joyner, A. L. and Wurst, W. (1996). An induction gene trap screen in embryonic stem cells: Identification of genes that respond to retinoic acid in vitro. *Proc Natl Acad Sci U S A* **93**, 1677-82.

Fraichard, A., Chassande, O., Bilbaut, G., Dehay, C., Savatier, P. and Samarut, J. (1995). In vitro differentiation of embryonic stem cells into glial cells and functional neurons. *J Cell Sci* **108 (Pt 10)**, 3181-8.

Fukuda, M., Asano, S., Nakamura, T., Adachi, M., Yoshida, M., Yanagida, M. and Nishida, E. (1997). CRM1 is responsible for intracellular transport mediated by the nuclear export signal. *Nature* **390**, 308-11.

Gallicano, G. I., Kouklis, P., Bauer, C., Yin, M., Vasioukhin, V., Degenstein, L. and Fuchs, E. (1998). Desmoplakin is required early in development for assembly of desmosomes and cytoskeletal linkage. *J Cell Biol* **143**, 2009-22.

Gansner, J. M., Madsen, E. C., Mecham, R. P. and Gitlin, J. D. (2008). Essential role for fibrillin-2 in zebrafish notochord and vascular morphogenesis. *Dev Dyn* **237**, 2844-61.

Garcia-Gras, E., Lombardi, R., Giocondo, M. J., Willerson, J. T., Schneider, M. D., Khoury, D. S. and Marian, A. J. (2006). Suppression of canonical Wnt/beta-catenin signaling by nuclear plakoglobin recapitulates phenotype of arrhythmogenic right ventricular cardiomyopathy. *J Clin Invest* **116**, 2012-21.

Garrod, D. and Chidgey, M. (2008). Desmosome structure, composition and function. *Biochim Biophys Acta* **1778**, 572-87.

Gerull, B., Heuser, A., Wichter, T., Paul, M., Basson, C. T., McDermott, D. A., Lerman, B. B., Markowitz, S. M., Ellinor, P. T., MacRae, C. A. et al. (2004). Mutations in the desmosomal protein plakophilin-2 are common in arrhythmogenic right ventricular cardiomyopathy. *Nat Genet* **36**, 1162-4.

Glover-Collins, K. and Thompson, M. E. (2008). Nuclear export of BRCA1 occurs during early S phase and is calcium-dependent. *Cell Signal* **20**, 958-68.

Gossler, A., Doetschman, T., Korn, R., Serfling, E. and Kemler, R. (1986). Transgenesis by means of blastocyst-derived embryonic stem cell lines. *Proc Natl Acad Sci U S A* **83**, 9065-9.

Greenburg, G. and Hay, E. D. (1982). Epithelia suspended in collagen gels can lose polarity and express characteristics of migrating mesenchymal cells. *J Cell Biol* **95**, 333-9.

Grossmann, K. S., Grund, C., Huelsken, J., Behrend, M., Erdmann, B., Franke, W. W. and Birchmeier, W. (2004). Requirement of plakophilin 2 for heart morphogenesis and cardiac junction formation. *J Cell Biol* **167**, 149-60.

Gu, H., Marth, J. D., Orban, P. C., Mossmann, H. and Rajewsky, K. (1994). Deletion of a DNA polymerase beta gene segment in T cells using cell type-specific gene targeting. *Science* **265**, 103-6.

Gumbiner, B. (1988). Cadherins: a family of Ca2+-dependent adhesion molecules. *Trends Biochem Sci* **13**, 75-6.

Haaf, A., Butler, P. J., Kent, H. M., Fearnley, I. M., Roberts, T. M., Neuhaus, D. and Stewart, M. (1996). The motile major sperm protein (MSP) from Ascaris suum is a symmetric dimer in solution. *J Mol Biol* **260**, 251-60.

Haffter, P., Granato, M., Brand, M., Mullins, M. C., Hammerschmidt, M., Kane, D. A., Odenthal, J., van Eeden, F. J., Jiang, Y. J., Heisenberg, C. P. et al. (1996). The identification of genes with unique and essential functions in the development of the zebrafish, Danio rerio. *Development* **123**, 1-36.

Hammerschmidt, M., Pelegri, F., Mullins, M. C., Kane, D. A., van Eeden, F. J., Granato, M., Brand, M., Furutani-Seiki, M., Haffter, P., Heisenberg, C. P. et al. (1996). dino and mercedes, two genes regulating dorsal development in the zebrafish embryo. *Development* **123**, 95-102.

Hansen, J., Floss, T., Van Sloun, P., Fuchtbauer, E. M., Vauti, F., Arnold, H. H., Schnutgen, F., Wurst, W., von Melchner, H. and Ruiz, P. (2003). A large-scale, gene-driven mutagenesis approach for the functional analysis of the mouse genome. *Proc Natl Acad Sci U S A* **100**, 9918-22.
Hardy, S., Legagneux, V., Audic, Y. and Paillard, L. (2010). Reverse genetics in eukaryotes. *Biol Cell* **102**, 561-80.

He, Y., Brown, M. A., Rothnagel, J. A., Saunders, N. A. and Smith, R. (2005). Roles of heterogeneous nuclear ribonucleoproteins A and B in cell proliferation. *J Cell Sci* **118**, 3173-83.

Hescheler, J., Fleischmann, B. K., Lentini, S., Maltsev, V. A., Rohwedel, J., Wobus, A. M. and Addicks, K. (1997). Embryonic stem cells: a model to study structural and functional properties in cardiomyogenesis. *Cardiovasc Res* **36**, 149-62.

Heuser, A., Plovie, E. R., Ellinor, P. T., Grossmann, K. S., Shin, J. T., Wichter, T., Basson, C. T., Lerman, B. B., Sasse-Klaassen, S., Thierfelder, L. et al. (2006). Mutant desmocollin-2 causes arrhythmogenic right ventricular cardiomyopathy. *Am J Hum Genet* **79**, 1081-8.

Hill, M. W., Berg, J. H. and Mackenzie, I. C. (1981). Quantitative evaluation of regional differences between epithelia in the adult mouse. *Arch Oral Biol* **26**, 1063-7.

Hong, S. K., Levin, C. S., Brown, J. L., Wan, H., Sherman, B. T., Hunag da, W., Lempicki, R. A. and Feldman, B. (2010). Pre-gastrula expression of zebrafish extraembryonic genes. *BMC Dev Biol*. 10:42.

Huang, C. J., Tu, C. T., Hsiao, C. D., Hsieh, F. J. and Tsai, H. J. (2003). Germ-line transmission of a myocardium-specific GFP transgene reveals critical regulatory elements in the cardiac myosin light chain 2 promoter of zebrafish. *Dev Dyn* **228**, 30-40.

Hudziak, R. M., Barofsky, E., Barofsky, D. F., Weller, D. L., Huang, S. B. and Weller, D. D. (1996). Resistance of morpholino phosphorodiamidate oligomers to enzymatic degradation. *Antisense Nucleic Acid Drug Dev* **6**, 267-72.

Hwang, M., Gorivodsky, M., Kim, M., Westphal, H. and Geum, D. (2008). The neuronal differentiation potential of Ldb1-null mutant embryonic stem cells is dependent on extrinsic influences. *Stem Cells* **26**, 1490-5.

Italiano, J. E., Jr., Stewart, M. and Roberts, T. M. (1999). Localized depolymerization of the major sperm protein cytoskeleton correlates with the forward movement of the cell body in the amoeboid movement of nematode sperm. *J Cell Biol* **146**, 1087-96.

Jennette, J. C. and Heptinstall, R. H. (2007). Heptinstall's pathology of the kidney: Lippincott Williams & Wilkins.

Kagiwada, S., Hosaka, K., Murata, M., Nikawa, J. and Takatsuki, A. (1998). The Saccharomyces cerevisiae SCS2 gene product, a homolog of a synaptobrevin-associated protein, is an integral membrane protein of the endoplasmic reticulum and is required for inositol metabolism. *J Bacteriol* **180**, 1700-8.

Kalen, M., Wallgard, E., Asker, N., Nasevicius, A., Athley, E., Billgren, E., Larson, J. D., Wadman, S. A., Norseng, E., Clark, K. J. et al. (2009). Combination of reverse and chemical genetic screens reveals angiogenesis inhibitors and targets. *Chem Biol* **16**, 432-41.

Kane, D. A. and Kimmel, C. B. (1993). The zebrafish midblastula transition. *Development* **119**, 447-56.

Kanekura, K., Nishimoto, I., Aiso, S. and Matsuoka, M. (2006). Characterization of amyotrophic lateral sclerosis-linked P56S mutation of vesicle-associated membrane protein-associated protein B (VAPB/ALS8). *J Biol Chem* **281**, 30223-33.

Kawahara, G., Guyon, J. R., Nakamura, Y. and Kunkel, L. M. (2010). Zebrafish models for human FKRP muscular dystrophies. *Hum Mol Genet* **19**, 623-33.

Kii, I., Amizuka, N., Shimomura, J., Saga, Y. and Kudo, A. (2004). Cell-cell interaction mediated by cadherin-11 directly regulates the differentiation of mesenchymal cells into the cells of the osteo-lineage and the chondro-lineage. *J Bone Miner Res* **19**, 1840-9.

Kimmel, C. B., Ballard, W. W., Kimmel, S. R., Ullmann, B. and Schilling, T. F. (1995). Stages of embryonic development of the zebrafish. *Dev Dyn* **203**, 253-310.

King, K. L., Stewart, M. and Roberts, T. M. (1994). Supramolecular assemblies of the Ascaris suum major sperm protein (MSP) associated with amoeboid cell motility. *J Cell Sci* **107 (Pt 10)**, 2941-9.

Kirchhof, P., Fabritz, L., Zwiener, M., Witt, H., Schafers, M., Zellerhoff, S., Paul, M., Athai, T., Hiller, K. H., Baba, H. A. et al. (2006). Age- and training-dependent development of arrhythmogenic right ventricular cardiomyopathy in heterozygous plakoglobin-deficient mice. *Circulation* **114**, 1799-806.

Klass, M. R. and Hirsh, D. (1981). Sperm isolation and biochemical analysis of the major sperm protein from Caenorhabditis elegans. *Dev Biol* **84**, 299-312.

Klug, M. G., Soonpaa, M. H., Koh, G. Y. and Field, L. J. (1996). Genetically selected cardiomyocytes from differentiating embronic stem cells form stable intracardiac grafts. *J Clin Invest* **98**, 216-24.

Klymkowsky, M. W. (1999). Plakophilin, armadillo repeats, and nuclear localization. *Microsc Res Tech* **45**, 43-54.

Kolossov, E., Fleischmann, B. K., Liu, Q., Bloch, W., Viatchenko-Karpinski, S., Manzke, O., Ji, G. J., Bohlen, H., Addicks, K. and Hescheler, J. (1998). Functional characteristics of ES cell-derived cardiac precursor cells identified by tissue-specific expression of the green fluorescent protein. *J Cell Biol* **143**, 2045-56.

Koster, M. I., Kim, S., Mills, A. A., DeMayo, F. J. and Roop, D. R. (2004). p63 is the molecular switch for initiation of an epithelial stratification program. *Genes Dev* 18(2):126-31.

Kramer, J., Hegert, C., Guan, K., Wobus, A. M., Muller, P. K. and Rohwedel, J. (2000). Embryonic stem cell-derived chondrogenic differentiation in vitro: activation by BMP-2 and BMP-4. *Mech Dev* **92**, 193-205.

Lam, M. H., Olsen, S. L., Rankin, W. A., Ho, P. W., Martin, T. J., Gillespie, M. T. and Moseley, J. M. (1997). PTHrP and cell division: expression and localization of PTHrP in a keratinocyte cell line (HaCaT) during the cell cycle. *J Cell Physiol* **173**, 433-46.

Larue, L., Ohsugi, M., Hirchenhain, J. and Kemler, R. (1994). E-cadherin null mutant embryos fail to form a trophectoderm epithelium. *Proc Natl Acad Sci U S A* **91**, 8263-7.

Laurent, F., Labesse, G. and de Wit, P. (2000). Molecular cloning and partial characterization of a plant VAP33 homologue with a major sperm protein domain. *Biochem Biophys Res Commun* **270**, 286-92.

Lawrence, C. (2007). The husbandry of zebrafish (Danio rerio): A review. *Aquaculture* **269**, 1-20.

Lawson, N. D. and Weinstein, B. M. (2002). In vivo imaging of embryonic vascular development using transgenic zebrafish. *Dev Biol* **248**, 307-18.

Le, Y. Z., Bai, Y., Zhu, M. and Zheng, L. (2010). Temporal requirement of RPE-derived VEGF in the development of choroidal vasculature. *J Neurochem* **112**, 1584-92.

Le, Y. Z., Zheng, W., Rao, P. C., Zheng, L., Anderson, R. E., Esumi, N., Zack, D. J. and Zhu, M. (2008). Inducible expression of cre recombinase in the retinal pigmented epithelium. *Invest Ophthalmol Vis Sci* **49**, 1248-53.

Lele, Z., Nowak, M. and Hammerschmidt, M. (2001). Zebrafish admp is required to restrict the size of the organizer and to promote posterior and ventral development. *Dev Dyn* **222**, 681-7.

Liu, X., Wu, H., Loring, J., Hormuzdi, S., Disteche, C. M., Bornstein, P. and Jaenisch, R. (1997). Trisomy eight in ES cells is a common potential problem in gene targeting and interferes with germ line transmission. *Dev Dyn* **209**, 85-91.

Long, Q., Meng, A., Wang, H., Jessen, J. R., Farrell, M. J. and Lin, S. (1997). GATA-1 expression pattern can be recapitulated in living transgenic zebrafish using GFP reporter gene. *Development* **124**, 4105-11.

Maltsev, V. A., Rohwedel, J., Hescheler, J. and Wobus, A. M. (1993). Embryonic stem cells differentiate in vitro into cardiomyocytes representing sinusnodal, atrial and ventricular cell types. *Mech Dev* **44**, 41-50.

Maltsev, V. A., Wobus, A. M., Rohwedel, J., Bader, M. and Hescheler, J. (1994). Cardiomyocytes differentiated in vitro from embryonic stem cells developmentally express cardiac-specific genes and ionic currents. *Circ Res* **75**, 233-44.

Manzanares, M., Locascio, A. and Nieto, M. A. (2001). The increasing complexity of the Snail gene superfamily in metazoan evolution. *Trends Genet* **17**, 178-81.

Martin, G. R. (1981). Isolation of a pluripotent cell line from early mouse embryos cultured in medium conditioned by teratocarcinoma stem cells. *Proc Natl Acad Sci U S A* **78**, 7634-8.

McClive, P., Pall, G., Newton, K., Lee, M., Mullins, J. and Forrester, L. (1998). Gene trap integrations expressed in the developing heart: insertion site affects splicing of the PT1-ATG vector. *Dev Dyn* **212**, 267-76.

McKoy, G., Protonotarios, N., Crosby, A., Tsatsopoulou, A., Anastasakis, A., Coonar, A., Norman, M., Baboonian, C., Jeffery, S. and McKenna, W. J. (2000). Identification of a deletion in plakoglobin in arrhythmogenic right ventricular cardiomyopathy with palmoplantar keratoderma and woolly hair (Naxos disease). *Lancet* **355**, 2119-24.

Mertens, C., Kuhn, C. and Franke, W. W. (1996). Plakophilins 2a and 2b: constitutive proteins of dual location in the karyoplasm and the desmosomal plaque. *J Cell Biol* **135**, 1009-25.

Miller, M. A., Nguyen, V. Q., Lee, M. H., Kosinski, M., Schedl, T., Caprioli, R. M. and Greenstein, D. (2001). A sperm cytoskeletal protein that signals oocyte meiotic maturation and ovulation. *Science* **291**, 2144-7.

Miller, M. A., Ruest, P. J., Kosinski, M., Hanks, S. K. and Greenstein, D. (2003). An Eph receptor sperm-sensing control mechanism for oocyte meiotic maturation in Caenorhabditis elegans. *Genes Dev* **17**, 187-200.

Mills, A. A., Zheng, B., Wang, X. J., Vogel, H., Roop, D. R. and Bradley, A. (1999). p63 is a p53 homolog required for limb and epidermal morphogenesis. *Nature* 398 (6729), 708-13.

Morcos, P. A. (2007). Achieving targeted and quantifiable alteration of mRNA splicing with Morpholino oligos. *Biochem Biophys Res Commun* **358**, 521-7.

Muller, M., Fleischmann, B. K., Selbert, S., Ji, G. J., Endl, E., Middeler, G., Muller, O. J., Schlenke, P., Frese, S., Wobus, A. M. et al. (2000). Selection of ventricular-like cardiomyocytes from ES cells in vitro. *Faseb J* **14**, 2540-8.

Muraglia, A., Cancedda, R. and Quarto, R. (2000). Clonal mesenchymal progenitors from human bone marrow differentiate in vitro according to a hierarchical model. *J Cell Sci* **113 (Pt 7)**, 1161-6.

Nakano, T., Kodama, H. and Honjo, T. (1994). Generation of lymphohematopoietic cells from embryonic stem cells in culture. *Science* **265**, 1098-101.

Nasevicius, A. and Ekker, S. C. (2000). Effective targeted gene 'knockdown' in zebrafish. *Nat Genet* **26**, 216-20.

Nava, A., Scognamiglio, R., Thiene, G., Canciani, B., Daliento, L., Buja, G., Stritoni, P., Fasoli, G. and Dalla Volta, S. (1987). A polymorphic form of familial arrhythmogenic right ventricular dysplasia. *Am J Cardiol* **59**, 1405-9.

Nava, A., Thiene, G., Canciani, B., Scognamiglio, R., Daliento, L., Buja, G., Martini, B., Stritoni, P. and Fasoli, G. (1988). Familial occurrence of right ventricular dysplasia: a study involving nine families. *J Am Coll Cardiol* **12**, 1222-8.

Nelson, G. A. and Ward, S. (1981). Amoeboid motility and actin in Ascaris lumbricoides sperm. *Exp Cell Res* **131**, 149-60.

Nelson, P. N., Reynolds, G. M., Waldron, E. E., Ward, E., Giannopoulos, K. and Murray, P. G. (2000). Monoclonal antibodies. *Mol Pathol* **53**, 111-7.

Nieto, M. A., Sargent, M. G., Wilkinson, D. G. and Cooke, J. (1994). Control of cell behavior during vertebrate development by Slug, a zinc finger gene. *Science* **264**, 835-9.

Nishi, K., Yoshida, M., Fujiwara, D., Nishikawa, M., Horinouchi, S. and Beppu, T. (1994). Leptomycin B targets a regulatory cascade of crm1, a fission yeast nuclear protein, involved in control of higher order chromosome structure and gene expression. *J Biol Chem* **269**, 6320-4.

Nishimura, A. L., Mitne-Neto, M., Silva, H. C., Richieri-Costa, A., Middleton, S., Cascio, D., Kok, F., Oliveira, J. R., Gillingwater, T., Webb, J. et al. (2004). A mutation in the vesicle-trafficking protein VAPB causes late-onset spinal muscular atrophy and amyotrophic lateral sclerosis. *Am J Hum Genet* **75**, 822-31.

Nishimura, Y., Hayashi, M., Inada, H. and Tanaka, T. (1999). Molecular cloning and characterization of mammalian homologues of vesicle-associated membrane protein-associated (VAMP-associated) proteins. *Biochem Biophys Res Commun* **254**, 21-6.

Norgett, E. E., Hatsell, S. J., Carvajal-Huerta, L., Cabezas, J. C., Common, J., Purkis, P. E., Whittock, N., Leigh, I. M., Stevens, H. P. and Kelsell, D. P. (2000). Recessive mutation in desmoplakin disrupts desmoplakin-intermediate filament interactions and causes dilated cardiomyopathy, woolly hair and keratoderma. *Hum Mol Genet* **9**, 2761-6.

O'Gorman, S., Fox, D. T. and Wahl, G. M. (1991). Recombinase-mediated gene activation and site-specific integration in mammalian cells. *Science* **251**, 1351-5.

Oram, K. F., Carver, E. A. and Gridley, T. (2003). Slug expression during organogenesis in mice. *Anat Rec A Discov Mol Cell Evol Biol* **271**, 189-91.

Pall, G. S., Wallis, J., Axton, R., Brownstein, D. G., Gautier, P., Buerger, K., Mulford, C., Mullins, J. J. and Forrester, L. M. (2004). A novel transmembrane MSP-containing protein that plays a role in right ventricle development. *Genomics* **84**, 1051-9.

Pennetta, G., Hiesinger, P. R., Fabian-Fine, R., Meinertzhagen, I. A. and Bellen, H. J. (2002). Drosophila VAP-33A directs bouton formation at neuromuscular junctions in a dosage-dependent manner. *Neuron* **35**, 291-306.

Perl, A. K., Wilgenbus, P., Dahl, U., Semb, H. and Christofori, G. (1998). A causal role for E-cadherin in the transition from adenoma to carcinoma. *Nature* **392** (6672) 190-3.

Peterson, R. T., Mably, J. D., Chen, J. N. and Fishman, M. C. (2001). Convergence of distinct pathways to heart patterning revealed by the small molecule concentramide and the mutation heart-and-soul. *Curr Biol* **11**, 1481-91.

Pilichou, K., Nava, A., Basso, C., Beffagna, G., Bauce, B., Lorenzon, A., Frigo, G., Vettori, A., Valente, M., Towbin, J. et al. (2006). Mutations in desmoglein-2 gene are associated with arrhythmogenic right ventricular cardiomyopathy. *Circulation* **113**, 1171-9.

Protonotarios, N., Tsatsopoulou, A., Anastasakis, A., Sevdalis, E., McKoy, G., Stratos, K., Gatzoulis, K., Tentolouris, K., Spiliopoulou, C., Panagiotakos, D. et al. (2001). Genotype-phenotype assessment in autosomal recessive arrhythmogenic right ventricular cardiomyopathy (Naxos disease) caused by a deletion in plakoglobin. *J Am Coll Cardiol* **38**, 1477-84.

Protonotarios, N., Tsatsopoulou, A., Patsourakos, P., Alexopoulos, D., Gezerlis, P., Simitsis, S. and Scampardonis, G. (1986). Cardiac abnormalities in familial palmoplantar keratosis. *Br Heart J* **56**, 321-6.

Rao, B. H., Reddy, I. S. and Chandra, K. S. (1996). Familial occurrence of a rare combination of dilated cardiomyopathy with palmoplantar keratoderma and curly hair. *Indian Heart J* **48**, 161-2.

Rebuzzini, P., Neri, T., Zuccotti, M., Redi, C. A. and Garagna, S. (2008). Chromosome number variation in three mouse embryonic stem cell lines during culture. *Cytotechnology* **58**, 17-23.

Riethmacher, D., Brinkmann, V. and Birchmeier, C. (1995). A targeted mutation in the mouse E-cadherin gene results in defective preimplantation development. *Proc Natl Acad Sci U S A* **92**, 855-9.

Robbins, J., Gulick, J., Sanchez, A., Howles, P. and Doetschman, T. (1990). Mouse embryonic stem cells express the cardiac myosin heavy chain genes during development in vitro. *J Biol Chem* **265**, 11905-9.

Robertson, E., Bradley, A., Kuehn, M. and Evans, M. (1986). Germ-line transmission of genes introduced into cultured pluripotential cells by retroviral vector. *Nature* **323**, 445-8.

Robu, M. E., Larson, J. D., Nasevicius, A., Beiraghi, S., Brenner, C., Farber, S. A. and Ekker, S. C. (2007). p53 activation by knockdown technologies. *PLoS Genet* **3**, e78.

Ruiz, P., Brinkmann, V., Ledermann, B., Behrend, M., Grund, C., Thalhammer, C., Vogel, F., Birchmeier, C., Gunthert, U., Franke, W. W. et al. (1996). Targeted mutation of plakoglobin in mice reveals essential functions of desmosomes in the embryonic heart. *J Cell Biol* **135**, 215-25.

Sato, T., Hidaka, K., Iwanaga, A., Ito, M., Asano, M., Nakabeppu, Y., Morisaki, T. and Yoshioka, K. (2005). Impairment of cardiomyogenesis in embryonic stem cells lacking scaffold protein JSAP1. *Biochem Biophys Res Commun* **338**, 1152-7.

Sauer, B. and Henderson, N. (1989). Cre-stimulated recombination at loxP-containing DNA sequences placed into the mammalian genome. *Nucleic Acids Res* **17**, 147-61.

Savagner, P., Yamada, K. M. and Thiery, J. P. (1997). The zinc-finger protein slug causes desmosome dissociation, an initial and necessary step for growth factor-induced epithelial-mesenchymal transition. *J Cell Biol* **137**, 1403-19.

Schafer, S., Koch, P. J. and Franke, W. W. (1994). Identification of the ubiquitous human desmoglein, Dsg2, and the expression catalogue of the desmoglein subfamily of desmosomal cadherins. *Exp Cell Res* **211**, 391-9.

Schulz, H., Kolde, R., Adler, P., Aksoy, I., Anastassiadis, K., Bader, M., Billon, N., Boeuf, H., Bourillot, P. Y., Buchholz, F. et al. (2009). The FunGenES database: a genomics resource for mouse embryonic stem cell differentiation. *PLoS One* **4**, e6804.

Shi, J., Lua, S., Tong, J. S. and Song, J. (2010). Elimination of the native structure and solubility of the hVAPB MSP domain by the Pro56Ser mutation that causes amyotrophic lateral sclerosis. *Biochemistry* **49**, 3887-97.

Skarnes, W. C., von Melchner, H., Wurst, W., Hicks, G., Nord, A. S., Cox, T., Young, S. G., Ruiz, P., Soriano, P., Tessier-Lavigne, M. et al. (2004). A public gene trap resource for mouse functional genomics. *Nat Genet* **36**, 543-4.

Skehel, P. A., Fabian-Fine, R. and Kandel, E. R. (2000). Mouse VAP33 is associated with the endoplasmic reticulum and microtubules. *Proc Natl Acad Sci U S A* **97**, 1101-6.

Skehel, P. A., Martin, K. C., Kandel, E. R. and Bartsch, D. (1995). A VAMP-binding protein from Aplysia required for neurotransmitter release. *Science* **269**, 1580-3.

Smith, A. G., Heath, J. K., Donaldson, D. D., Wong, G. G., Moreau, J., Stahl, M. and Rogers, D. (1988). Inhibition of pluripotential embryonic stem cell differentiation by purified polypeptides. *Nature* **336**, 688-90.

Smith, D. E., Franco del Amo, F. and Gridley, T. (1992). Isolation of Sna, a mouse gene homologous to the Drosophila genes snail and escargot: its expression pattern suggests multiple roles during postimplantation development. *Development* **116**, 1033-9.

Smithies, O., Gregg, R. G., Boggs, S. S., Koralewski, M. A. and Kucherlapati, R. S. (1985). Insertion of DNA sequences into the human chromosomal beta-globin locus by homologous recombination. *Nature* **317**, 230-4.

Soussan, L., Burakov, D., Daniels, M. P., Toister-Achituv, M., Porat, A., Yarden, Y. and Elazar, Z. (1999). ERG30, a VAP-33-related protein, functions in protein transport mediated by COPI vesicles. *J Cell Biol* **146**, 301-11.

Spencer, H. L., Eastham, A. M., Merry, C. L., Southgate, T. D., Perez-Campo, F., Soncin, F., Ritson, S., Kemler, R., Stern, P. L. and Ward, C. M. (2007). E-cadherin inhibits cell surface localization of the pro-migratory 5T4 oncofetal antigen in mouse embryonic stem cells. *Mol Biol Cell* **18**, 2838-51.

St-Onge, L., Furth, P. A. and Gruss, P. (1996). Temporal control of the Cre recombinase in transgenic mice by a tetracycline responsive promoter. *Nucleic Acids Res* **24**, 3875-7.

Stainier, D. Y., Fouquet, B., Chen, J. N., Warren, K. S., Weinstein, B. M., Meiler, S. E., Mohideen, M. A., Neuhauss, S. C., Solnica-Krezel, L., Schier, A. F. et al. (1996). Mutations affecting the formation and function of the cardiovascular system in the zebrafish embryo. *Development* **123**, 285-92.

Stainier, D. Y., Lee, R. K. and Fishman, M. C. (1993). Cardiovascular development in the zebrafish. I. Myocardial fate map and heart tube formation. *Development* **119**, 31-40.

Sumanas, S. and Larson, J. D. (2002). Morpholino phosphorodiamidate oligonucleotides in zebrafish: a recipe for functional genomics? *Brief Funct Genomic Proteomic* **1**, 239-56.

Summerton, J. (1999). Morpholino antisense oligomers: the case for an RNase H-independent structural type. *Biochim Biophys Acta* **1489**, 141-58.

Summerton, J. and Weller, D. (1997). Morpholino antisense oligomers: design, preparation, and properties. *Antisense Nucleic Acid Drug Dev* **7**, 187-95.

Sung, J. H., Yang, H. M., Park, J. B., Choi, G. S., Joh, J. W., Kwon, C. H., Chun, J. M., Lee, S. K. and Kim, S. J. (2008). Isolation and characterization of mouse mesenchymal stem cells. *Transplant Proc* **40**, 2649-54.

Syrris, P., Ward, D., Evans, A., Asimaki, A., Gandjbakhch, E., Sen-Chowdhry, S. and McKenna, W. J. (2006). Arrhythmogenic right ventricular dysplasia/cardiomyopathy associated with mutations in the desmosomal gene desmocollin-2. *Am J Hum Genet* **79**, 978-84.

Takeichi, M. (1988). The cadherins: cell-cell adhesion molecules controlling animal morphogenesis. *Development* **102**, 639-55.

Tarr, D. E. and Scott, A. L. (2004). MSP domain proteins show enhanced expression in male germ line cells. *Mol Biochem Parasitol* **137**, 87-98.

Tarr, D. E. and Scott, A. L. (2005a). MSP domain protein-1 from Ascaris suum and its possible role in the regulation of major sperm protein-based crawling motility. *Mol Biochem Parasitol* **143**, 165-72.

Tarr, D. E. and Scott, A. L. (2005b). MSP domain proteins. *Trends Parasitol* **21**, 224-31.

Thaler, R., Rumpler, M., Spitzer, S., Klaushofer, K. and Varga, F. (2010). Mospd1, a new player in mesenchymal versus epidermal cell differentiation. *J Cell Physiol*.

Thiene, G., Nava, A., Corrado, D., Rossi, L. and Pennelli, N. (1988). Right ventricular cardiomyopathy and sudden death in young people. *N Engl J Med* **318**, 129-33.

Thiery, J. P. and Sleeman, J. P. (2006). Complex networks orchestrate epithelial-mesenchymal transitions. *Nat Rev Mol Cell Biol* **7**, 131-42.

Thisse, B., Heyer, V., Lux, A., Alunni, V., Degrave, A., Seiliez, I., Kirchner, J., Parkhill, J. P. and Thisse, C. (2004). Spatial and temporal expression of the zebrafish genome by large-scale in situ hybridization screening. *Methods Cell Biol* **77**, 505-19.

Tsuda, H., Han, S. M., Yang, Y., Tong, C., Lin, Y. Q., Mohan, K., Haueter, C., Zoghbi, A., Harati, Y., Kwan, J. et al. (2008). The amyotrophic lateral sclerosis 8 protein VAPB is cleaved, secreted, and acts as a ligand for Eph receptors. *Cell* **133**, 963-77.

Van Epps, H. A., Hayashi, M., Lucast, L., Stearns, G. W., Hurley, J. B., De Camilli, P. and Brockerhoff, S. E. (2004). The zebrafish nrc mutant reveals a role for the polyphosphoinositide phosphatase synaptojanin 1 in cone photoreceptor ribbon anchoring. *J Neurosci* **24**, 8641-50.

Viallet, P. M. and Vo-Dinh, T. (2003). Monitoring intracellular proteins using fluorescence techniques: from protein synthesis and localization to activity. *Curr Protein Pept Sci* **4**, 375-88.

Weir, M. L., Klip, A. and Trimble, W. S. (1998). Identification of a human homologue of the vesicle-associated membrane protein (VAMP)-associated protein of 33 kDa (VAP-33): a broadly expressed protein that binds to VAMP. *Biochem J* **333 (Pt 2)**, 247-51.

Westerfield, M. (2007). The Zebrafish Book. A Guide for the Laboratory Use of Zebrafish (*Danio rerio*). 5th Edition, University of Oregon Press, Eugene.

Wolff, S., Talos, F., Palacios, G., Beyer, U., Dobbelstein, M. and Moll, U. M. (2009). The alpha/beta carboxy-terminal domains of p63 are required for skin and limb development. New insights from the Brdm2 mouse which is not a complete p63 knockout but expresses p63 gamma-like proteins. *Cell Death Differ* **16**, 1108-17.

Yang, L., Morriello, G., Pan, Y., Nargund, R. P., Barakat, K., Prendergast, K., Cheng, K., Chan, W. W., Smith, R. G. and Patchett, A. A. (1998). Tripeptide growth hormone secretagogues. *Bioorg Med Chem Lett* **8**, 759-64.

APPENDIX

Primer name	Forward primer	Reverse primer
Mospd 1_up1	CAGAAGGCAGGAGCAGG AAGAC	CACAGGGCATTAGGGACAG AAA
Mospd1_do wn3	GTGCCAAGGATGCGACTC AG	CCAGAAGGCACAGGCTCAA AT
Mospd3_up 1	GGCCCCAAACAACCCTGA C	GATCGCTTCCCCTTTTATTT TTGA
Mospd3_do wn2	TCTGGCTCGGGTGAATGT CTGCT	TTTGTTTTGGGGGAAGGGA GTTGG

Appendix Table 1: Primer sequences used for Southern blot probe synthesis.

Primer name	**Forward primer**	**Reverse Primer**
Mouse		
Mospd 1	GACAACCAGAGTTAGTGGAAGGG	GACAGTTAGCAAACTAGGTCCTG
Mospd 3	TCAAGGAAAGGGCACAGGGAC	GCACAGAACTCGGAAGCGAAG
β-tubulin	GGAACATAGCCGTAAACTGC	TCACTGTGCCTGAACTTACC
Nanog	CAGATAGGCTGATTTGGTTGGTGT	CATCTTCTGCTTCCTGGCAA
Oct4	GGCGTTCTCTTTGGAAAGGTGTTC	CTCGAACCACATCCTTCTCT
Zebrafish		
Mospd 1	CTTGTGTTCTACGCAGATGAGC	GCACTGTGGATTCCTGCTCTC
Mospd 1 ORF	ATGCAGCAGCAGCAGAGCC	TCAAGTGCGCAGAATAACCATTG
β-actin	CTGGGTATGGAATCTTGCGGTATC	CGAGAGTTTAGGTTGGTCGTTCG
Gapdh	GTCTGGTGACCCGTGCTGCT	GTTTGCCGCCTTCTGCCTTAAC

Appendix Table 2: Primer sequences used for RT-PCR.

*Mospd 1*_forward	CACGCTCTACAACCCCTATGAGT
*Mospd 1*_reverse	CGTCCACCACGGCATACTT
Mospd 1 probe	TGCACAGCGCCAAA
Elongation factor 1 α (*elf1 α*)_forward	TGCGGTGGAATCGACAAGA
Elongation factor 1 α (*elf1 α*)_reverse	CCATCTCAGCGGCTTCCTT
Elongation factor 1 α (*elf1 α*) probe	AACCATCGAGAAGTTCGA

Appendix Table 3: Primers and probes used for zebrafish qPCR.
Elongation factor 1 α (*elf1 α*) was used as an endogenous control and *Mospd 1* was the target. The probe had 3' Black Hole Quencher 1 and 5' FAM modifications (MWG, Eurofins).

Gene	Forward primer	Reverse primer
Hprt	GCTCGAGATGTCATGAAGGAGA	AAAGAACTTATAGCCCCCCTTGA
Mospd 1	GCTGCCGGTGCAGTGAA	AGGATCGAACATCTCTATGACGAAT
Mospd 3	CGATGCAGAGGGATATGTGAAG	GGCCACGTGCCGTATCA
Cdh11	GACAACCCACCAAAGTTTCCA	CGGGACAGCTGCTTCTGATAC
Snai1	GCCGGAAGCCCAACTATAGC	AGGGCTGCTGGAAGGTGAA
Snai2	CCCTGGCTGCTTCAAGGA	TGAGGGCAAGAGAAAGGCTTT

Appendix Table 4: Primers used for qPCR for bone experiments.

Primer efficiency and melting curve analysis for QPCR

Serial dilutions of template cDNA were amplified using qPCR and standard curve generated. The efficiency of each primer set were calculated using the slope of the standard curve using the primer efficiency calculator at www.finnzymes.fi/java_applets/qPCR_efficiency.html (Appendix Table 5). Primer efficiencies should be in the range of 90-110 %. The efficiency of the Mospd 3 primers (112%) and the Snai2 primers (111 %) fall out of this range. When primer efficiencies are not in the correct range this could indicate that the qPCR reaction will not be as sensitive as desired and, therefore, the quantification of gene expression may not be accurate.

Another important control for qPCR reactions in which SYBR green has been used for fluorescence detection is melting curve analysis. This is due to the fact that SYBR green binds to all double stranded DNA and, therefore, in addition to bind the specific product it will also bind to primer dimers and non-specific PCR products. This will alter the accuracy of the data obtained. To check that only specific products are being amplified a dissociation step is added at the end of the qPCR amplification and a melting curve generated. The melting curve should only show one peak indicating only the specific product has been amplified. If there are other peaks it indicates the presence of non-specific products. The melting curves for the hprt, Mospd1, Snail and Snai2 (Appendix Figures 1 and 2) qPCR reactions only show one peak indicating that these qPCR reactions were specific. The melting temperature (Tm) of the hprt, Mospd1, Snai1 and Snai2 PCR products is 77.2 ℃, 75.7 ℃, 79.5 ℃ and 75.5 ℃, respectively. The Tm for Mospd 3 was 75.3 ℃ and for Cdh11 was 75.8 ℃ (Appendix Figure 3). However, both these curves showed an additional much smaller peak at 80 ℃ indicating some non-specific amplification. The second Mospd 3 melting peak was very low so may be too small to affect the quantification significantly. However, the Cdh11 secondary peak is larger and may indicate that the primers are amplifying a non-specific product. Therefore, the quantification of gene expression using these primers may not be accurate and should be repeated with primers that only amplify Cdh11 transcripts.

Gene	Primer efficiency
Hprt	105 %
Mospd1	109 %
Mospd3	112 %
Cdh11	109 %
Snai1	104 %
Snai2	111 %
zElf1a	110 %
zMospd1	109 %

Appendix Table 5: Efficiencies of primers used for qPCR experiments. Primer efficiencies were calculated using the slope of the standard curve generated from qPCR of serial dilutions of template cDNA using the primer efficiency calculator at www.finnzymes.fi/java_applets/qPCR_efficiency.html.

A

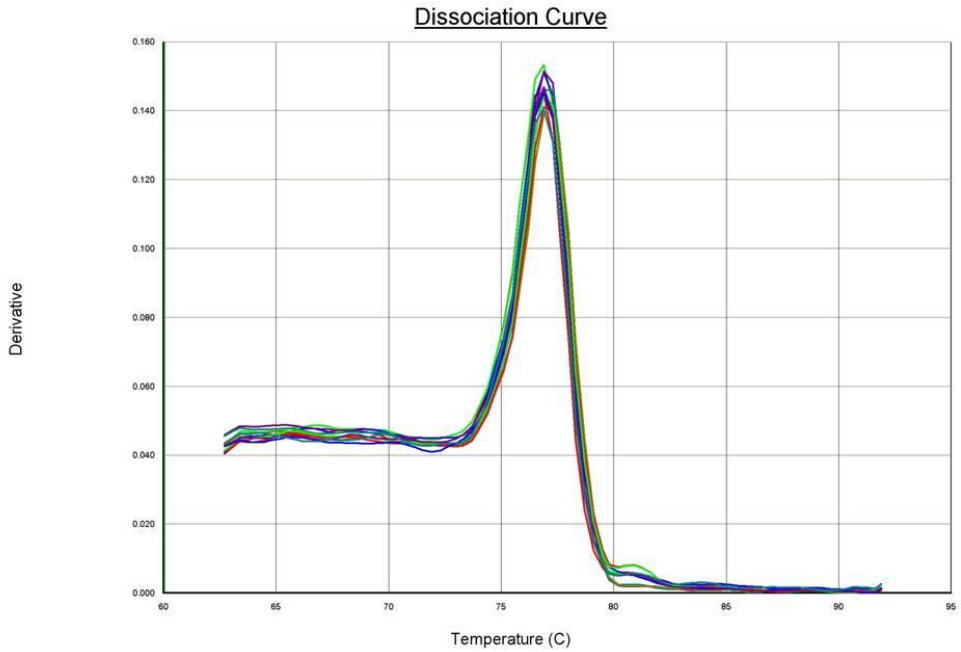

B

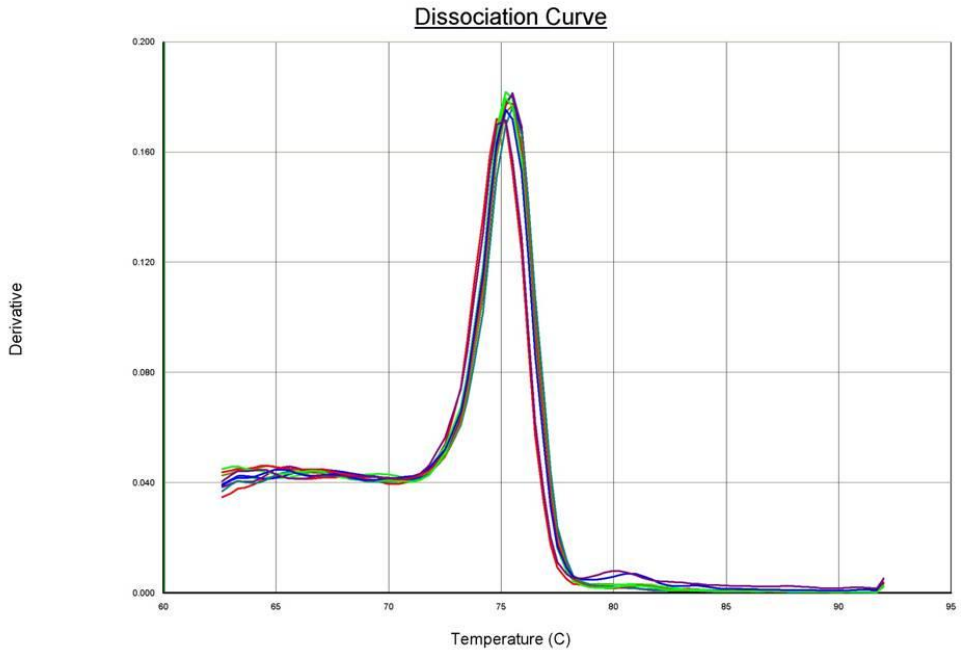

Appendix Figure 1: Melting curves representing products from the qPCR amplification using Hprt and Mospd1 primers. The different colours represent the different samples .A: The Tm for hprt is 77.2 ℃ and B: the Tm for Mospd 1 is 75.7 ℃. Both sets of melting curves only have one peak indicating that the specific product was amplified.

A

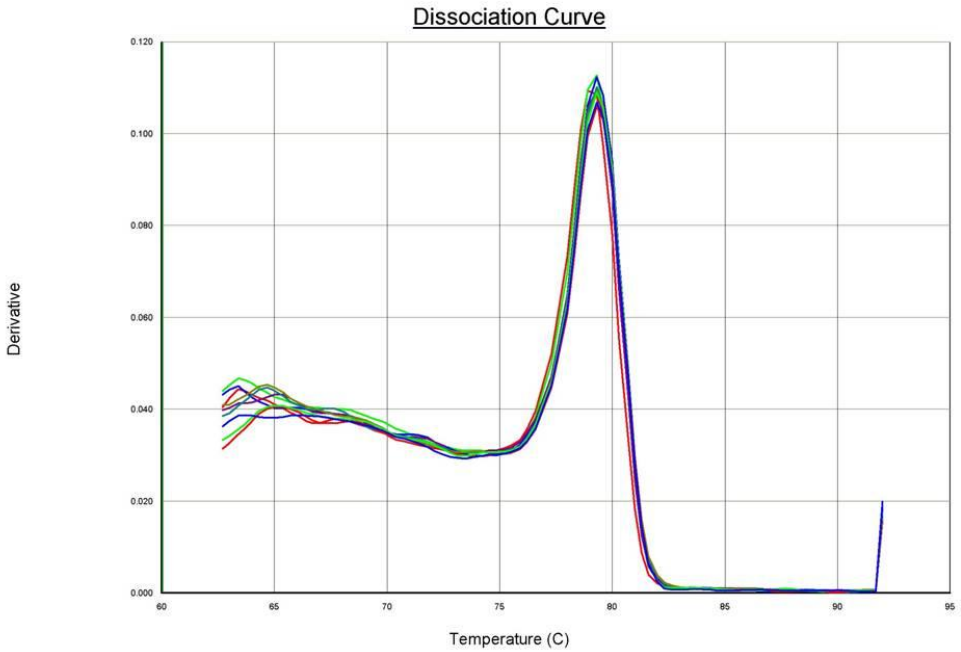

B

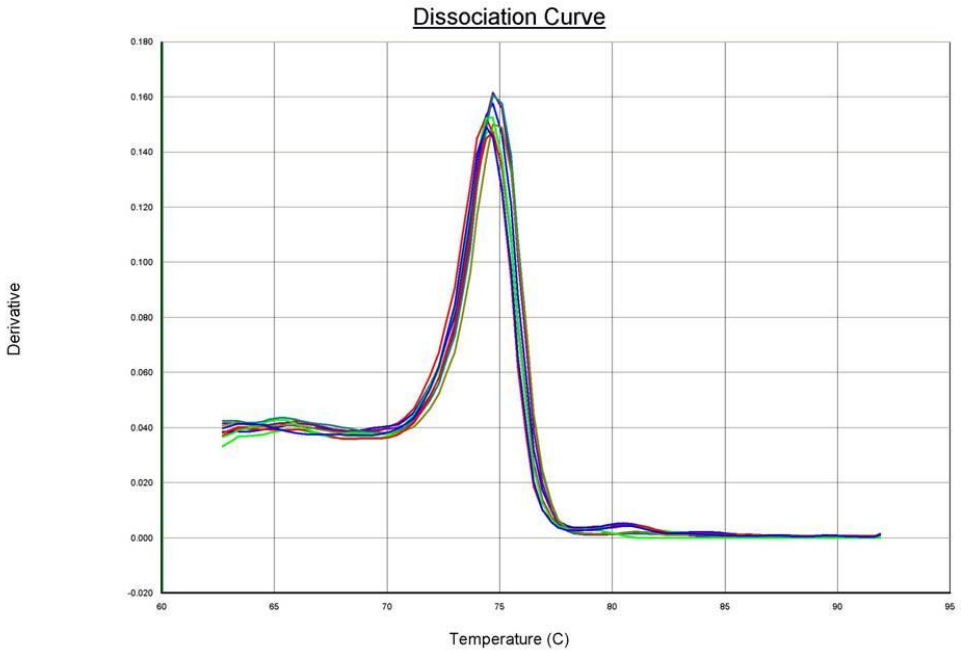

Appendix Figure 2: Melting curves representing products from the qPCR amplification using Snail and Snai2 primers. A: The Tm for Snail is 79.5 ℃ and B: the Tm for Snai2 is 75.5 ℃. Both sets of melting curves only have one peak indicating that the specific product was amplified.

A

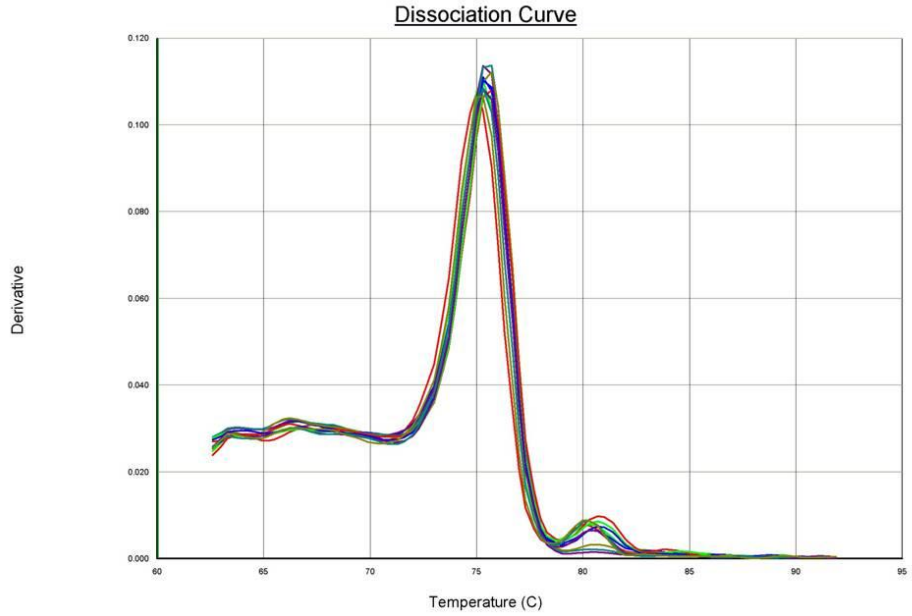

B

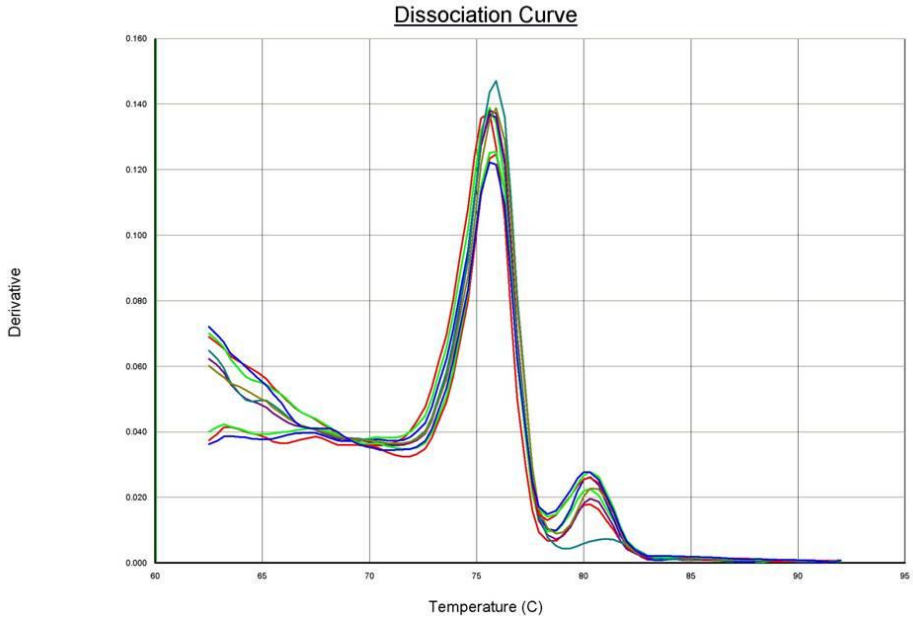

Appendix Figure 3: Melting curves representing products from the qPCR amplification using Mospd3 and Cdh11 primers. A: The Tm for Mospd3 is 75.3 ℃ and whilst there is a small peak at 80 ℃ indicating some non-specific amplification it is a very low level. B: The Tm for Cdh11 is 75.8 ℃. However, there is also a smaller peak at 80 ℃ indicating non-specific amplification in this qPCR reaction. This would decrease amplification efficiency of the specific product and the accuracy of the data. The qPCR reactions would have to be repeated using another set of primers that only showed one peak on a melting curve.

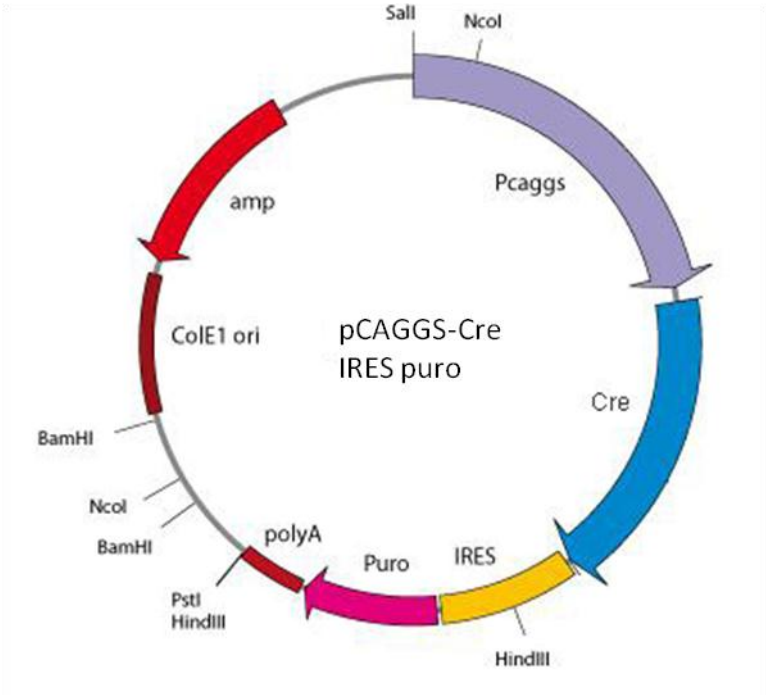

Appendix Figure 4: pCAGGS-Cre IRES puro plasmid map. Image from Katrin Buerger, PhD thesis, 2009.

.

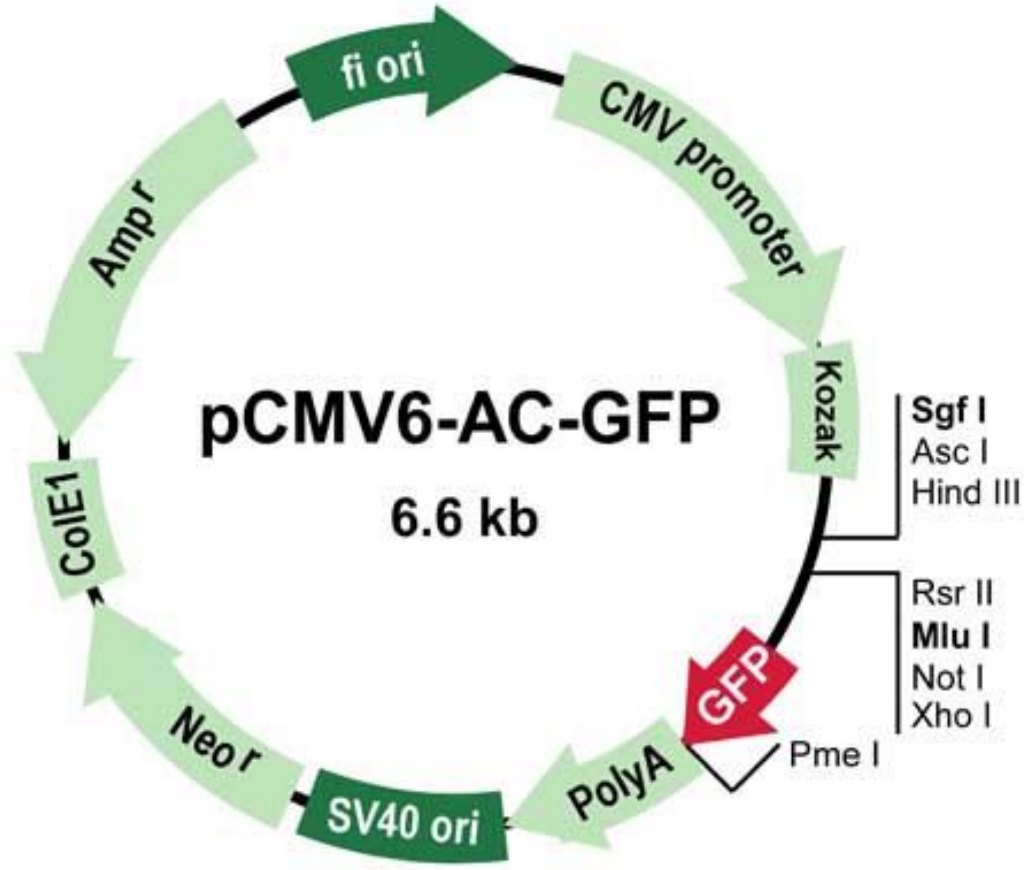

Appendix Figure 5: Plasmid map of pCMV6-AC-GFP. The plasmid obtained from Origene (USA). *Mospd 1* was cloned into the multiple cloning site. Image from www.origene.com

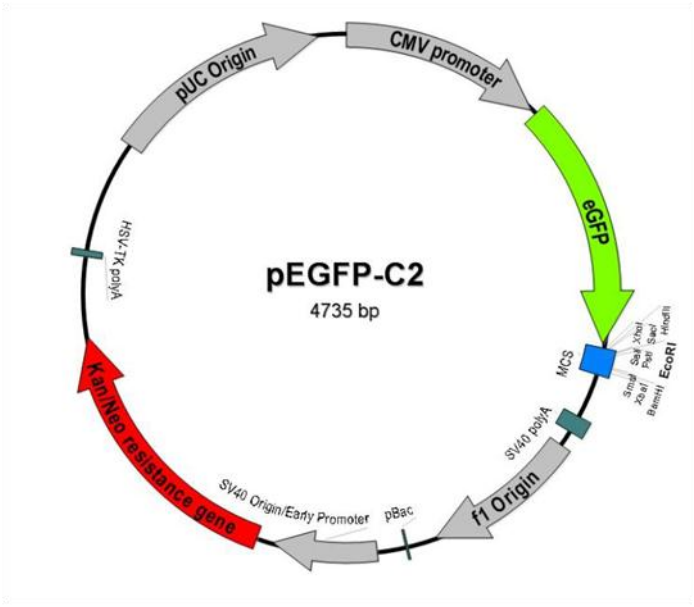

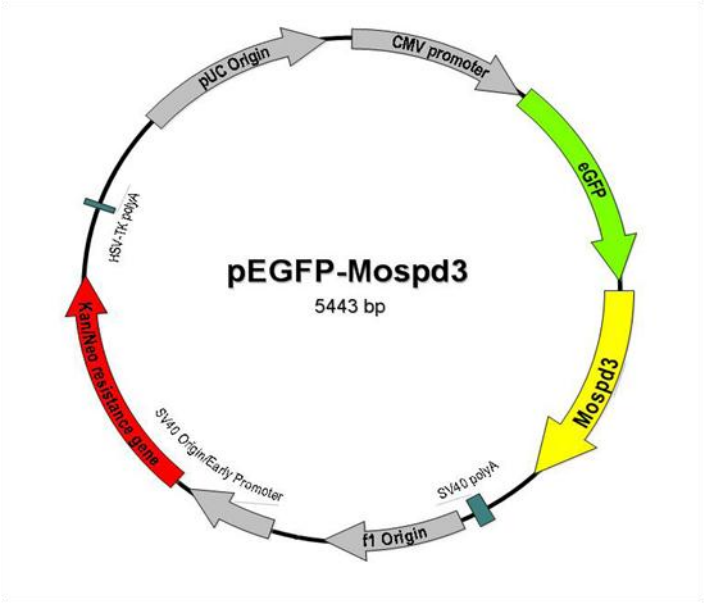

Appendix Figure 6: Plasmid maps of the pEGFP-C2 (top) and pEGFP-Mospd 3. Image from Katrin Buerger, PhD thesis, 2009.

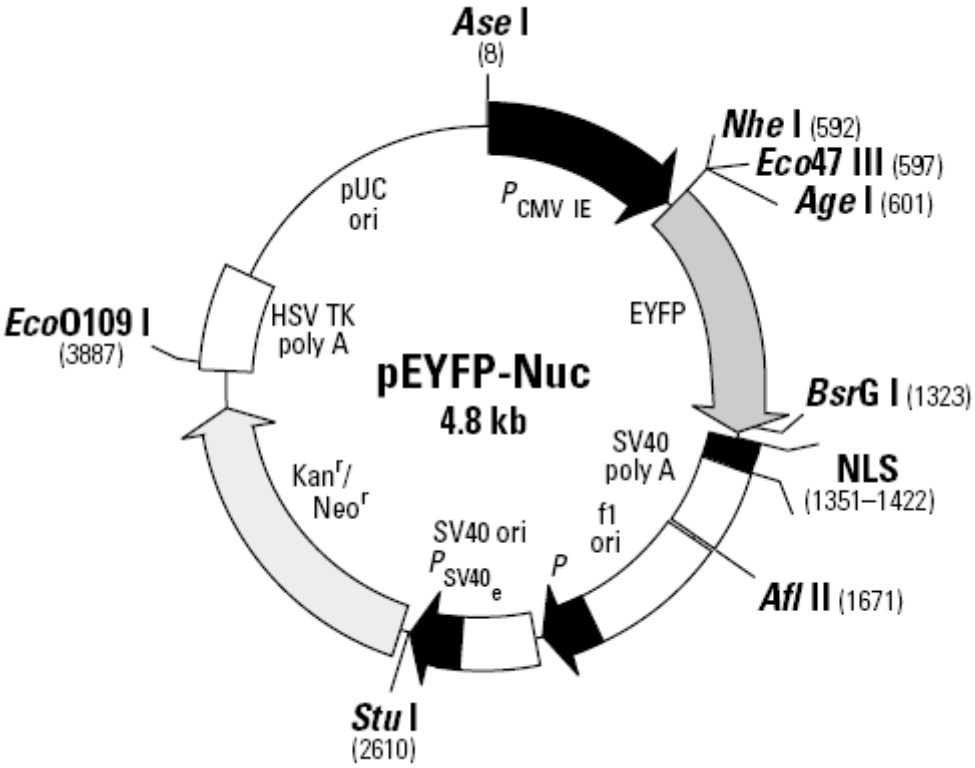

Appendix Figure 7: Plasmid map of the pEYFP-Nuc plasmid. Image from Clontech pEYFP-Nuc Vector Information datasheet.

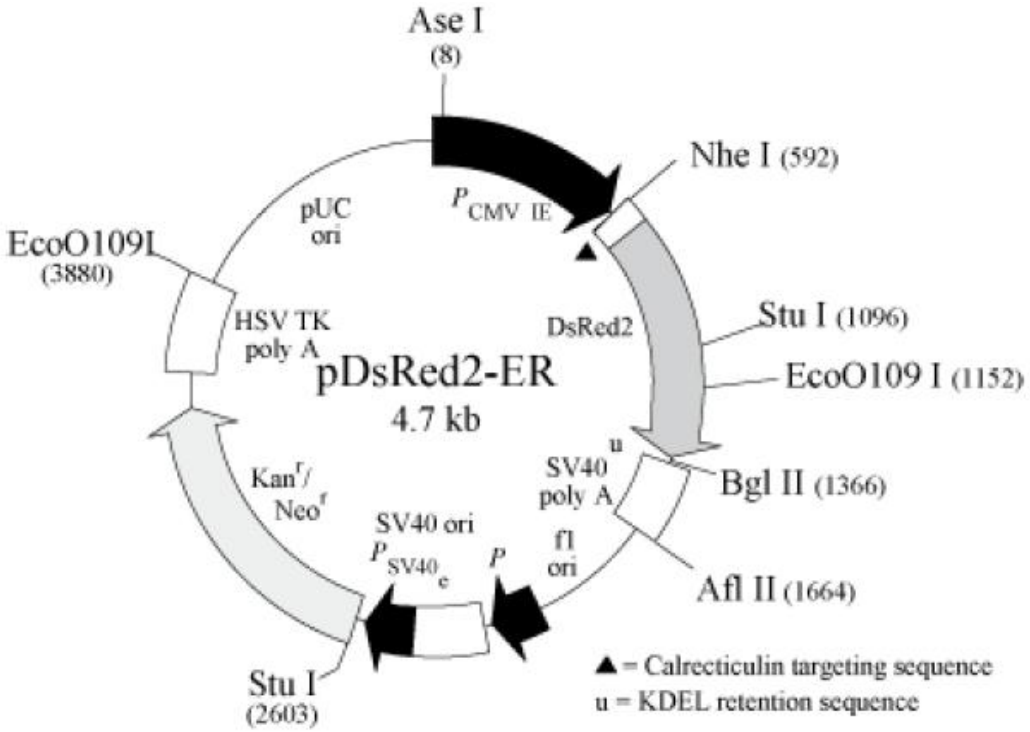

Appendix Figure 8: Plasmid map of the pDSRed2-ER plasmid. Image from Clontech pDSRed2_ER Vector Information datasheet.

Determination of the isotype of the monoclonal α-MOSPD1 and α-MOSPD3 antibodies

It is important to determine that there is only one isotype for each antibody as this determines whether the antibody is from one B cell clone and, therefore, specific to a particular epitope. The determination of the isotype of the monoclonal α –MOSPD1 and α –MOSPD3 antibodies was done by mixing the supernatant from the hybridoma cultures with coloured microparticles and allowing the mixture to flow up individual isotype test strips. After 5-10 minutes a blue band appeared in the heavy chain IgG2b window of the α-MOSPD1 test strip and in the IgG1 window for both α-MOSPD3 clones E1 and E4 (Appendix Figure 6). The α-MOSPD1 has a lambda (λ) light chain whilst both α-MOSPD3 clones have a kappa (κ) light chain. IgG1 and IgG2b isotype controls were included in all subsequent immunocytochemistry and immunohistochemistry experiments.

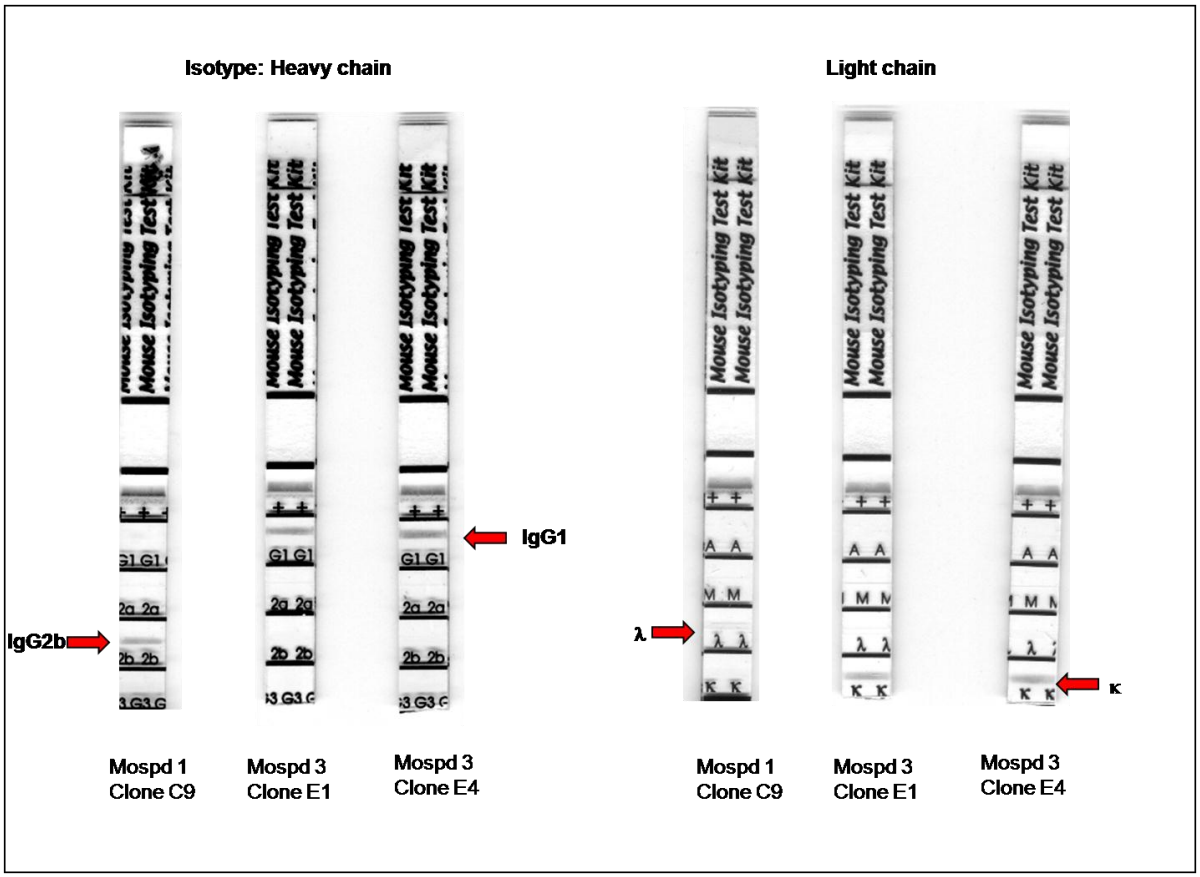

Appendix Figure 9: Isotype determination of α-MOSPD1 and α-MOSPD3 antibodies. The isotype test strips are shown with a band in the window of the isotype of each antibody. α -MOSPD1's isotype is IgG2b λ and α-MOSPD3 clones E1 and E4 isotype is IgG1 κ. ++ window of the isotype test strip shows that the supernatant/ coloured microparticle mixture had successfully diffused through the strip.

Morpholino	**Sequence**
Chordin	ATCCACAGCAGCCCCTCCATCATCC
Splice-site (MO2)	AGATAAATGTGTAGAACTCACCTTT
5 mispair for splice-site (5MP2)	AGAaAAATcTGTAcAACTgAgCTTT
Start (MO1)	GGCTCTGCTGCTGCTGCATTGGCTC
5 mispair for Start (5MP1)	GGCTgTGCTcCTcCTcCATTGGgTC

Appendix Table 6: Morpholino Sequences. Morpholinos had a 3' fluorescein tag and were obtained from GeneTools (www.GeneTools.com), resuspended in distilled water to a concentration of 1 mM and stored at room temperature in the dark.

Chordin knockdown in zebrafish

Microinjection into early zebrafish embryos can be a challenging technique. In order to ensure the technique was being performed correctly a standard positive control *chordin* morpholino was obtained from GeneTools and injected into zebrafish embryos and the embryos observed for the published *chordin* phenotype. Nasevicius and Ekker (2000) reported that when 2 ng of the *chordin* morpholino was injected into embryos a mild *chordin* phenotype, characterised by the presence of a small blood island, U-shaped somites and a tail with multiple folds, was observed. Injecting 4 ng of the morpholino resulted in the observation of a severe phenotype characterised by a larger blood island, U-shaped somites, a tail with multiple folds and a reduced head. Appendix Figure 7 shows the phenotypes observed when the *chordin* morpholino was injected into embryos in our laboratory indicating the technique was being performed correctly and a published phenotype was able to be replicated.

The embryos were assessed at 28 hpf and categorised as normal, mild *chordin* phenotype, severe *chordin* phenotype or other phenotypes, such as oedema or body axis deformed. 99 % of the non-injected control embryos were phenotypically normal with 1 % showing other phenotypes and no embryos with either a mild or severe chordin phenotype. Of the embryos injected with 2 ng of morpholino 14 % were normal, 65 % showed a mild *chordin* phenotype, 15 % showed a severe phenotype and 6 % had other phenotypes. 6 % of the 4 ng injected embryos were normal, 16 % had the mild phenotype and 69 % were severe. 9 % showed other phenotypes (Appendix Figure 8). The data was analysed using a Two way ANOVA followed by a Bonferroni post hoc test comparing non-injected, 2 ng *chordin* morpholino and 4 ng *chordin* morpholino-injected embryos to each other. Both the 2 ng and 4ng *chordin* injected embryos were statistically significant ($p<0.001$) when compared to non-injected embryos for the normal, mild and severe phenotypes. There was a statistically significant difference ($p<0.001$) in the number of mild and severe embryos observed when the 2 ng chordin and 4 ng chordin injected embryos were compared.

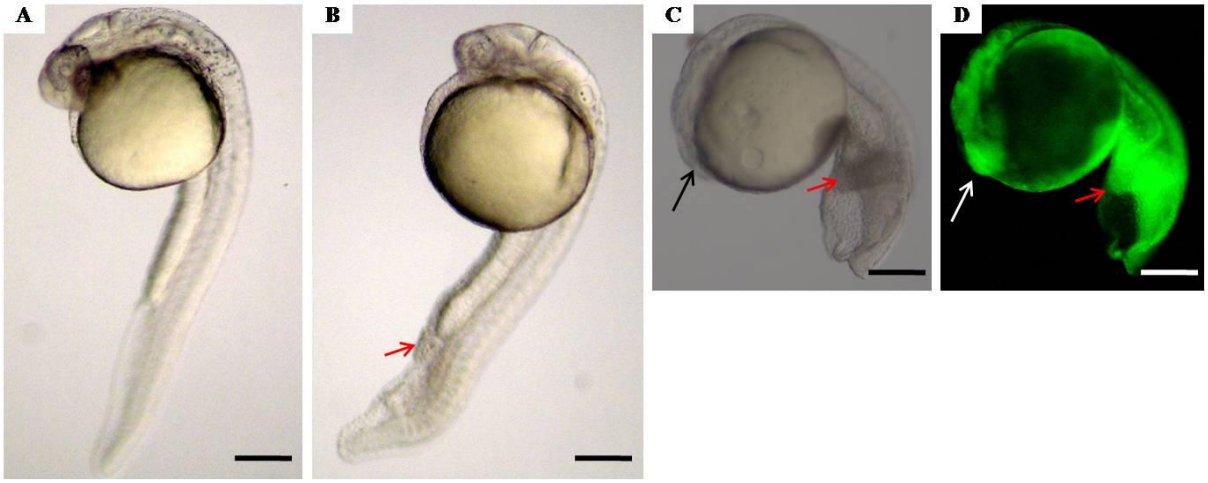

Appendix Figure 10: *Chordin* knockdown in zebrafish embryos (28 hpf). A: wild type embryo; B: weak *chordin* phenotype; C and D: severe *chordin* phenotype viewed with white light and fluorescence, respectively. The red arrows indicate blood islands; in the weak phenotype (B) the blood island is small compared to that seen in the severe phenotype (C and D). The black and white arrows indicate the reduced head in the severe phenotype zebrafish. No eye development is observed. Bars = 100 µm.

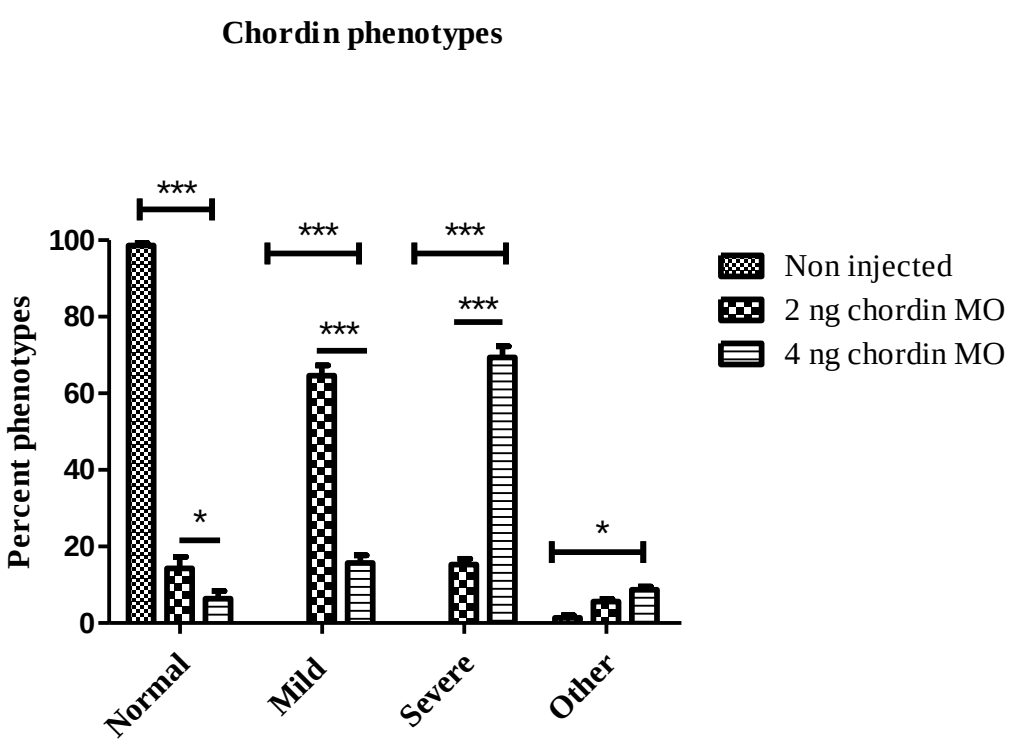

Appendix Figure 11: Percentage of embryos that displayed normal, mild, severe and other phenotypes after being injected with 2 ng and 4 ng *chordin* morpholino (MO). Two way ANOVA followed by a Bonferroni post hoc test was used to analyse the data. (* $p<0.05$; *** $p<0.001$).

This was due to the fact that there was a higher number of mild phenotype embryos in the 2 ng injected group compared to 4 ng-injected embryos and a higher number of severe phenotypes in the 4 ng embryos compared to 2 ng injected embryos. This data is similar to the Nasevicius and Ekker (2000) findings that as the dose of *chordin* morpholino is increased the severity of the phenotype increases. There was a significant difference between other non-related phenotypes observed between non injected embryos and 4 ng *chordin* MO injected embryos ($p<0.05$) possibly due to some embryos having a slightly toxic effect of the higher morpholino dose as this difference was not observed between the non-injected embryos and 2 ng *chordin* MO embryos.